Designing crystallization based-enantiomeric separation for chiral compound-forming systems in consideration of polymorphism and solvate formation

Dissertation

Zur Erlangung des akademischen Grades

Doktoringenieur

(Dr.-Ing)

von: **M.Sc. Le Minh Tam**

geboren am: 28. November 1980

in: Gialai, Vietnam

genehmigt durch die Fakultät für Verfahrens- und Systemtechnik

der Otto-von-Guericke-Universität Magdeburg

Gutachter:

Prof. Dr.-Ing. Andreas Seidel-Morgenstern

(Otto von Guericke University Magdeburg, Germany

Max Planck Institute for Dynamics of Complex Technical Systems, Germany)

Prof. Dr. Adrian Flood

(Suranaree University of Technology, Nakhon Ratchasima, Thailand)

Dr. Jan von Langermann

(University of Rostock, Institute of Chemistry, Germany)

eingereicht am: 05.11.2013

Promotionkolloquium am: 24.01.2014

ACKNOWLEDGEMENT

Abstract

Even though almost all chemical and physical properties of two enantiomers of a chiral compound are identical, each of them can show different activities in chiral environments. Therefore, purification of single enantiomers plays a vital role, in particular for pharmaceuticals. Enantioseparation is an indispensable task which gained great attention in the last decades. Among separation methods, crystallization is considered as an outstanding approach due to its low cost (compared to *e.g.* chromatography, membrane processes). However, there are just a few single enantiomers available on the market produced via crystallization up to now. This thesis contributes a systematic study of enantioseparation which focuses on the major chiral group *i.e.* compound-forming racemates considering effects of polymorphism and solvate formation.

Three model compounds were selected in this thesis, namely lactide, 3-chloromandelic acid (3ClMA) and the amino acid arginine. Since there is very limited information available about these compounds, solid phase analytical techniques such as DSC, TG-DSC, XRD and XRPD were used to characterize their solid state properties. Obtained data assert that the industrial relevant compound lactide is the "standard" compound-forming racemate while the other two compounds are more sophisticated racemates. Indeed, 3ClMA is a polymorphic system while arginine represents a hydrate forming racemate. Based on the solid properties of these compounds, solid-liquid equilibria were investigated in consideration of the equilibrating solid phases. The binary melting point and the ternary solubility phase diagrams, which are fundamentals of enantioseparation process design, have been constructed. In the solubility determination, eutectic composition variation was observed as an interesting phenomenon. Experiments proved that variation of temperatures, solvents, polymorphs, hydrates, etc. frequently leads to eutectic shifts which can be exploited to design a separation process so called "two-step" selective crystallization. This method was flexibly operated via various modes as seen throughout this thesis. The eutectic shift was exploited between melt and solution states in Chapter 7 while Chapters 8 and 9 described the realization of this technique for polymorphic and hydrate systems. Besides, the applicability of preferential crystallization was also validated for these compounds based on kinetic control. Finally, a comparison of the "two-step" selective crystallization process and kinetically controlled preferential crystallization was also carried out.

Kurzzusammenfassung

Obwohl fast alle chemischen und physikalischen Eigenschaften von Enantiomeren eines chiralen Systems identisch sind, können diese unterschiedliche Aktivitäten in einer chiralen Umgebung aufweisen. Daher ist die Aufreinigung eines Enantiomers, besonders im pharmazeutischen Bereich, besonders wichtig. Die Aufreinigung von Enantiomeren ist ein Forschungsfeld, das in den letzten Jahrzehnten mit besonderer Aufmerksamkeit verfolgt wird. Hierbei wird im Besonderen die Kristallisation als Trennverfahren eingesetzt, welches im Vergleich zu anderen Verfahren (z.B. der Chromatographie oder Membranverfahren) meist die günstigere Prozessalternative ist. Heutzutage werden jedoch nur wenige kommerziell verfügbare Enantiomere mit Kristallisationsprozessen produziert. Diese Arbeit trägt mit systematischen Arbeiten zu dem Forschungsfeld der Enantiomerenaufreinigung bei. Der Fokus ist dabei auf die in der Realität am häufigsten vorkommenden chiralen Systeme gelegt, die verbindungsbildenden racemischen Systemen, wobei auch auf Polymorphie und die Bildung von Solvaten eingegangen wird.

Für diese Arbeit wurden drei Beispielsubstanzen ausgewählt, Lactid, 3-Chlormandelsäure (3CLMA) und die Aminosäure Arginin. Da nur relativ wenige Informationen zu diesen Substanzen existieren, wurden analytische Methoden wie DSC, TG-DSC, XRD und XRPD zur Charakterisierung der Feststoffeigenschaften angewandt. Die Ergebnisse lassen die Schlussfolgerung zu, dass es sich bei dem industriell relevanten Lactid um ein „normales" verbindungsbildendes racemisches System handelt, während die beiden anderen Substanzen komplizierteres Phasenverhalten aufweisen. Bei 3ClMA und Arginin handelt es sich ebenfalls um verbindungsbildende racemische Systeme, wobei 3ClMA zusätzlich Polymorphe und Arginin Hydrate ausbildet. Mit Blick auf die Feststoffeigenschaften wurde das Fest-Flüssig Phasenverhalten dieser Substanzen untersucht. Als Ergebnis wurden binäre Schmelz- und ternäre Phasendiagramme entwickelt, die für eine Prozessentwicklung von grundlegender Bedeutung sind. Die Änderung des eutektischen Punktes wurde bei den Löslichkeitsmessungen als bemerkenswerte Eigenschaft herausgestellt. Im Verlauf dieser Arbeit wurde dieser „eutectic shift", hervorgerufen durch Temperaturänderungen, unterschiedliche Lösungsmittel und die daraus resultierenden Feststoffzuständen (Polymorphe und Hydrate), mehrfach nachgewiesen. Basierend auf dem „eutectic shift" wurden Trennverfahren, sogenannte selektive „two-step" Kristallisationsprozesse, entwickelt, welche sehr flexibel betrieben werden können. In Kapitel 7 wird beispielsweise der „eutectic shift" zwischen binärer Schmelze und Lösung ausgenutzt, während diese Technik in den Kapiteln 8 und 9 bei Systemen, die Polymorphe und Hydrate ausbilden, anderweitig angewandt wurde. Zudem wurde die Anwendbarkeit einer bevorzugten Kristallisation dieser Substanzen mit Hilfe von kinetischen Daten validiert. Zum Abschluss wurde ein Vergleich der beiden Prozessalternativen, der selektiven „two-step" Kristallisation und der kinetisch gesteuerten bevorzugten Kristallisation, für die betrachteten Stoffsysteme durchgeführt.

CONTENTS

ENANTIOMER CRYSTALLIZATION – STATE OF THE ART, GOALS AND STRUCTURE OF THESIS

Single pure enantiomers play an important role in many applications including food and agriculture industries, in particular for the production of active pharmaceutical ingredients. In principle, two enantiomers of one chiral compound can show different effects on living organisms[1–4]. Therefore enantioseparation is especially important for *e.g.* the pharmaceutical industry. Statistical overviews showed the increase of single enantiomers and the decrease of racemates in chiral drugs in the last decades. For instance, approximately 25% of chiral drugs were launched as single enantiomers between 1983 and 1986 while 58% were introduced as single enantiomers in the period 1999–2002[1]. Thus, instead of using racemates in drugs, pure enantiomers have become more preferable. Nowadays, enantiopurification plays a vital role to enhance the performances of drugs and avoid side effects on patients. Enantioselective synthesis usually consists of several steps and this routine is not always feasible to produce single enantiomers. In contrast, non selective synthesis of enantiomeric mixtures is usually an easier alternative. However, this method always needs subsequent separation steps. Innovation of enantiopurification methods, which can provide sufficient purity with high productivity and reduce production costs, is strongly motivated by both academic and industrial demand. Besides chiral chromatography, crystallization is considered as a powerful technique in enantioseparation and enantiopurification. There are many advantages of crystallization compared to other techniques. High productivities and purities are often obtained from crystallization processes. Furthermore, the products are obtained typically in solid form which is convenient for storage and transportation. Besides, crystallization processes need relative low capital investments and also allow simple operations.

However, enantioseparation via crystallization is frequently considered as one of the most difficult separation techniques due to the similarity of two enantiomers[5]. In fact, these enantiomers are identical in almost all physical and chemical properties such as melting point, solubility, nucleation, crystal growth, and reactivity[1–6]. Regarding to enantioseparation via direct crystallization, up to now, there are two main approaches involving preferential crystallization (kinetic control) and the "two-step" selective crystallization (thermodynamic control). The difference of these two methods is briefly described as follows.

First, preferential crystallization is a method based on kinetics to perform enantioseparation within the metastable zone. When selective nucleation and selective crystal growth are well controlled to obtain the desired enantiomer as crystalline solid, the counter species (counter enantiomer or racemate in the cases of conglomerate or compound-forming systems, respectively) will be retained in the mother liquors. If these processes can be stopped before the nucleation of the counter

species, very high purity of the desired enantiomer will be achieved in the solid product. Preferential crystallization is frequently applicable for conglomerate systems. Unfortunately, only 5–10% of all chiral compounds belong to this group[7]. Applicability of preferential crystallization for the major group (compound-forming systems, about 90–95% of all chiral pairs)[7] is still limited. Recently, preferential crystallization for compound-forming racemates was partially discussed by Lorenz *et al.*[8], Czapla *et al.*[9] Polenske *et al.*[10,11], Lu *et al.*[12], etc. However, up to now, there is still a lack of a systematic approach which takes the general effects of polymorphs or hydrates on performances of preferential crystallization for compound-forming systems into account.

Second, the "two-step" process is another technique which is fully based on thermodynamics. Exploiting a shift of eutectic compositions, the system can be relocated *e.g.* from a three-phase into a two-phase domain in the ternary phase diagram. Consequently, the pure enantiomer will be obtained via a simple equilibrium in this two-phase domain. Eutectic shift observation and the concept of the "two-step" process have been recently published by Kaemmerer *et al.*[13,14] and Le Minh *et al.*[15]. The eutectic shift is an interesting phenomenon and can be considered as the key step of such operations. For instance, in Kaemmerer's works, the eutectic shift was induced based on effects of temperature and/or solvent.

Preferential crystallization and the "two-step" process are two powerful techniques in enantioseparation via direct crystallization. However, there are still several limitations and uncertainties to commercialization. For instance, preferential crystallization has some drawbacks on industrial scales (*e.g.* 10–100 m^3) due to the difficulty of heat and mass transfer control. This method is also not applicable when the metastable zone widths are not sufficient. With respect to the "two-step" process, the identification of the eutectic shift is the most challenging task and usually requires a lot of experimental work. Unfortunately, this key constraint (*i.e.* the eutectic shift) is not always realized for many chiral systems under temperature and/or solvent effects.

Further development of direct crystallization techniques for enantioseparation is the main objective of this thesis. Since enantioseparation methods for conglomerate systems are well-known and pseudoracemates are rarely found, this thesis will focus on the most common compound-forming racemates (so called "true" racemates or racemic compound-forming systems). Three model compounds of compound-forming racemates are selected in this thesis including lactide, 3-chloromandelic acid and the amino acid arginine. Those compounds will represent not only normal "true" racemates but also cover other challenging aspects relating to polymorphism and hydrate formation. In the experimental part, both preferential crystallization and the "two-step" process will be applied in consideration of the relevant solid phase behaviors. To finalize appropriate crystallization design, thermodynamic and kinetic data of these three model compounds are therefore needed and will be systematically measured in this thesis.

This thesis is structured as follows:

- Chapter 1 introduces basic definitions and an overview of various available routines for enantiopurification.

- Chapter 2 provides the theoretical background of the enantiomers and the racemates. The solid state of different types of crystalline racemates will be discussed. Besides, important aspects such as polymorphism and solvate formation are also highlighted.

- Afterwards, solid-liquid equilibria (SLE) are discussed in Chapter 3 since solubility data are essential for crystallization design. Herewith, thermodynamic equilibria of chiral compounds in solvents will be examined. On the other hand, these SLE data can also be correlated by suitable thermodynamic models such as Wilson, NRTL, UNIQUAC, UNIFAC, COSMO, etc. which are briefly described in this chapter. Additionally, eutectic determination is also discussed herein.

- Chapter 4 introduces kinetic parameters which are important for crystallization process design. These aspects include metastable zone width (MSZW), induction time, etc. From the measured data, nucleation parameters such as critical radius of nucleus or critical free energy of nucleation, etc. can be estimated. Effects of additives on MSZW, crystal habit, etc. are also addressed in this chapter.

- Chapter 5 presents various enantioseparation techniques which are based on kinetic and/or thermodynamic control. Different operation modes of those methods will utilize the specification of the specific systems in the experimental part. The basis of melt selective crystallization, solution preferential crystallization and the innovative selective crystallization so called "two-step" process will be demonstrated in this chapter. A combination design between thermodynamic and kinetic crystallization is also proposed.

- Chapter 6 describes details of the experimental part. The fundamentals of three selected chiral compounds including lactide, 3-chloromandelic acid and arginine will be mentioned. Besides description of the relevant analytical methods for solid and liquid phases, experimental determination of SLE, MSZW and setup of crystallization processes will be presented in this chapter.

The next three Chapters (7–9) are the results and discussion. This part is organized in the way of increasing complexity of the studied compounds. At first, the industrial relevant compound, *i.e.* lactide, represents the "standard" case of true racemates. Afterwards, compound-forming racemates involving complex behavior such as polymorphism and solvate formation are studied with cases of 3-chloromandelic acid and the amino acid arginine.

- In Chapter 7, solid phase analysis will be carefully carried out to make sure that lactide is a chiral compound-forming system but not influenced by any special solid behavior such as polymorphism and hydrate formation. Then solid-liquid equilibria of this compound are studied to construct the binary melting point phase diagram and the ternary solubility phase diagrams. A comparison of nucleation between the enantiomer and the racemate leads to a proper selection among separation techniques. Consequently, a special design is proposed to produce the pure enantiomer(s) based on the eutectic shift between the binary and ternary phase diagrams.

- In Chapter 8, the studied compound 3-chloromandelic acid is proved to be a compound-forming system which shows polymorphic behavior. Thermodynamic and kinetic data are determined such as solubility, oiling out, association, phase diagrams, nucleation, etc. The crystallization designs are validated with both approaches, *i.e.* preferential crystallization and the "two-step" process (eutectic shifts via different polymorphs as well as solvent exchange). In this chapter, another combination based on both kinetic and thermodynamic methods is implemented for mandelic acid instead of 3-chloromandelic acid for a couple of reasons. This combination is successfully validated.

- Chapter 9 relates to arginine which is a compound-forming system forming hydrates. Similar procedures to the two previous compounds, thermodynamic and kinetic data of arginine are also determined. The separation is carried out with the selective crystallization based on the eutectic shift between different hydrates. Besides, preferential crystallization also shows high potential applicability for this system.

- Finally, the contribution and achievement of this thesis will be summarized in Chapter 10. Advantages and disadvantages of enantioseparation methods realized in this thesis will be discussed in order to generalize widely applicable separation strategies for the most abundant chiral group, *i.e.* compound-forming systems. Afterwards, the outlook will draw out future work to complement the methodology of enantioseparation via direct crystallization.

CHAPTER 1: INTRODUCTION

1.1 Chirality

A chiral molecule is defined as a molecule that has a non-superimposable mirror image. This molecule contains asymmetric atom(s), *i.e.* chiral center(s). These chiral centers are often carbon atoms which are attached to four different atoms (or groups) to form pairs of stereoisomers called enantiomers. Other chiral centers are also known such as phosphorous, sulfur, etc. Enantiomers are non-superimposable images like one's left and right hand. "Chiral" was stemmed from the term "χειϱ" which means hand from the Greek.[16] Figure 1.1 graphically demonstrates an enantiomer pair.
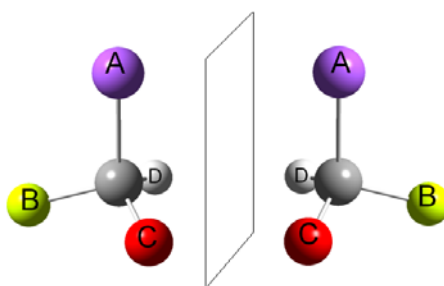
Figure 1.1: *Illustration of an enantiomer pair. Two enantiomers are mirror-images like left and right hand of one person, these molecules are non-superimpose upon each other.*

Almost all physical and chemical properties of the two enantiomers are identical in an achiral environment, such as enthalpy of fusion, melting temperature, solubility, metastable zone width, reactivity with achiral molecules, etc.[1–6] The mirror symmetry relationship of two enantiomers causes such similarity. However, they can show different effects on living organism where chiral recognition takes place[1–4]. Therefore, purification of enantiomers gains great attention in many applications, *e.g.* in pharmaceuticals (details in following paragraphs), agriculture, food products, etc.

The term "racemate" is used to indicate a mixture containing equal amounts of two enantiomers. Indeed, there are three types of crystalline racemates including conglomerate, compound-forming and pseudoracemate[7]. Details of these different types of crystalline racemates will be presented in Chapter 2. Different nomenclatures of the enantiomers are frequently used *i.e.* "R/S", "D/L" and "+/-". For organic molecules, the "R/S" configuration which is based on the order of the groups around the asymmetric carbon is usually used (Cahn–Ingold–Prelog priority rules). The "D/L" notation is often used for amino acids and other biomolecules, while the "+/-" nomenclature is designated for enantiomers based on their rotation of the plane-polarized light.[16]

1.2 History

In 1809, the discovery of plane-polarized light by Malus[17] was an important milestone in the history of development of understanding of chirality which stemmed the origins of stereochemistry. A few years later, Biot showed that the polarized light could be rotated clockwise or counterclockwise with some quartz crystals[18]. Then, he successfully extended this observation for other chiral organic substances[19].

In 1848, Pasteur found that racemic mixture of sodium ammonium tartrate tetrahydrate was composed of 50:50 of L- and D-crystals. He successfully collected selectively one population of single enantiomers from a racemic mixture using a loupe and pair of tweezers[20]. In 1866, Gernez discovered the basic principle of preferential crystallization. He successfully crystallized a single enantiomer by seeding pure enantiomer crystals into a saturated racemic solution of sodium ammonium tartrate[21]. In 1873, the term chirality was firstly used by Kelvin[22]. Then, the model of tetrahedral carbon was proposed by Le Bel (1874)[23] and van't Hoff (1875)[24]. In 1966, the convention R (for rictus) and S (for sinister) for each enantiomer was proposed by Cahn, Ingold and Prelog[25].

Methodology development for enantioseparation gained great attention in the last decades. Although there were many inventions relating to chromatography, membrane, (bio)catalyst technologies, etc., enantioseparation is still challenging particularly for industrial applications due to high investment limitation and/or low productivity of these approaches. Innovation separation techniques are, therefore, urgently required.

1.3 Chirality and pharmaceutical applications

Nowadays, for instance in the pharmaceutical industry, single enantiomers are more preferable than racemates due to a couple of reasons. As seen for many chiral pairs, one enantiomer is the active pharmaceutical ingredient (API) while the counter enantiomer can be ineffective. Propranolol is an example of which the L-enantiomer is a powerful adrenoceptor antagonist, whereas D-propranolol is not[4]. Besides, the counter enantiomers can diminish the effects of target enantiomers, *e.g.* esomeprazol[26]. That reduces the performance of drugs and may increase production cost. Furthermore, in the worst cases, counter enantiomers are even harmful, *e.g.* thalidomide, penicillamine. While one enantiomer of thalidomide has effects against morning sickness of pregnant women, the other enantiomer is a teratogen[27]. The S-enantiomer of penicillamine has antiarthritic effects but the R-enantiomer is extremely toxic[4]. Figure 1.2 highlights the interest of the APIs in the 20-year period from 1983 to 2002. Distribution of worldwide approved drugs of single enantiomers was 39% which surpassed achiral drugs (about 38%). Comparing to single enantiomers, racemates represented the minority category, at 23% of worldwide approved drugs.[1]
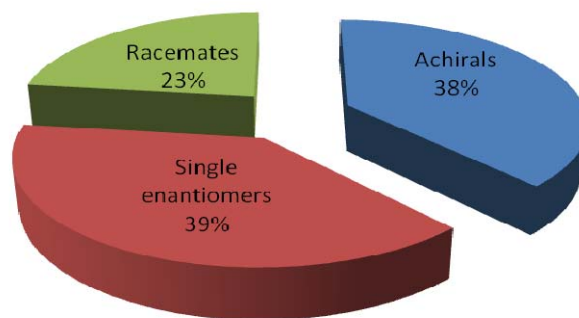
Figure 1.2: *An overview of worldwide distribution of drugs in the period from 1983 to 2002.*

In details, most chiral APIs were marketed as racemic mixtures during the 1980s. In the next decades, the chiral APIs relating to single enantiomers gradually increased. Especially, single enantiomers have been dominant in chiral drugs since 2001. Furthermore, achiral APIs were also less preferable in pharmaceuticals. This evolution was also confirmed by a publication of policy statements by the food and drug administration in 1992[1,28].

In short, using single enantiomers is an unavoidable trend in particular for pharmaceutical application. Obviously, there is clearly an urgent demand of rapid development for enantiopurification approaches which is also the motivation for this thesis. In the next part, an overview of the available techniques to produce single enantiomers will be introduced.

1.4 Access to single enantiomers

Figure 1.3 shows different methods to access single enantiomers. Among them, the major source to produce chiral molecules is the chiral pool which contains enantiopure building blocks for the target enantiomer synthesis. The chiral pool supplies "templates" for the synthesis sequences of the target enantiomers. However, existing enantiopure molecules in the chiral pool are not always available for synthesis of "new" chiral molecules. In such circumstances, an alternative is asymmetric synthesis to generate the desired chiral centers. Sometimes, chiral auxiliaries can be used in synthesis sequences. Unfortunately, those molecules are often expensive: that can diminish or even prohibit the usage of asymmetric reactions, in particular at the industrial scales. If the synthesis is carried out without any chiral molecules, that will result in equal proportion of both enantiomers in racemic mixtures. From those mixtures, additional resolution steps are needed to separate two enantiomers.[28,29]

The following comparison shows proportion of the most common approaches. Among APIs launched with a single chiral center reported for the period between 1985 and 2004, 45% of them were synthesized using molecules from the chiral pool. This approach is quite simple due to existing chiral centers in the chiral pool. In contrast, there were only about 9% of APIs synthesized via asymmetric procedures due to the cost limitation and process complexity. In those procedures, the chiral center is generated during synthesis steps. The sequence may include chemical

reactions, activities of enzymes or microorganisms. From these chiral selective pathways, the target enantiomer can be recovered selectively. This method is mainly limited by its moderate productivity and the difficulty to find the appropriate chiral selective enzymes. Nowadays, new enzymes are progressively produced by genetic technology. Finally, about 46% of drugs were produced as racemic mixtures via non-selective synthesis. This approach is simple based on classical chemical synthesis sequences. Unfortunately, non-selective synthesis always results in mixtures of two enantiomers at 50:50 percentages.[28]
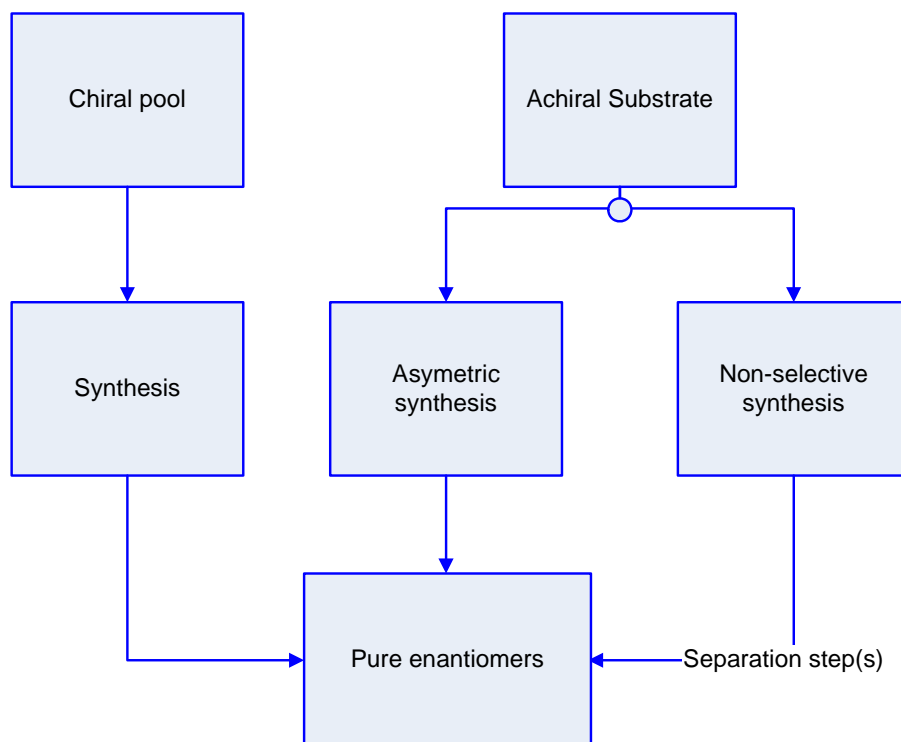
Figure 1.3: *Different routes to produce pure enantiomers. First, chiral pool is the major source to supply chiral templates for synthesis of the target enantiomers; second, asymmetric synthesis is usually an expensive approach; finally, non-selective synthesis results in racemic mixtures which are needed further resolution steps.*

Racemate resolution can be accomplished using various techniques, *e.g.* diastereomeric salt formation, kinetic resolution and chromatographic resolution, etc. Figure 1.4 summaries the most popular methods to resolve pure enantiomers from racemic or partially enantiomerically enriched mixtures.[4,5]

Among these resolution methods, crystallization of diastereomers has been more frequently applied than the other resolution methods. Chromatography was hardly used, in particular on industrial scales. The other methods (such as capillary electrophoresis, extraction, kinetic resolution, etc.) are also attractive as potential resolution methods. The following paragraphs will present an overview of these techniques.
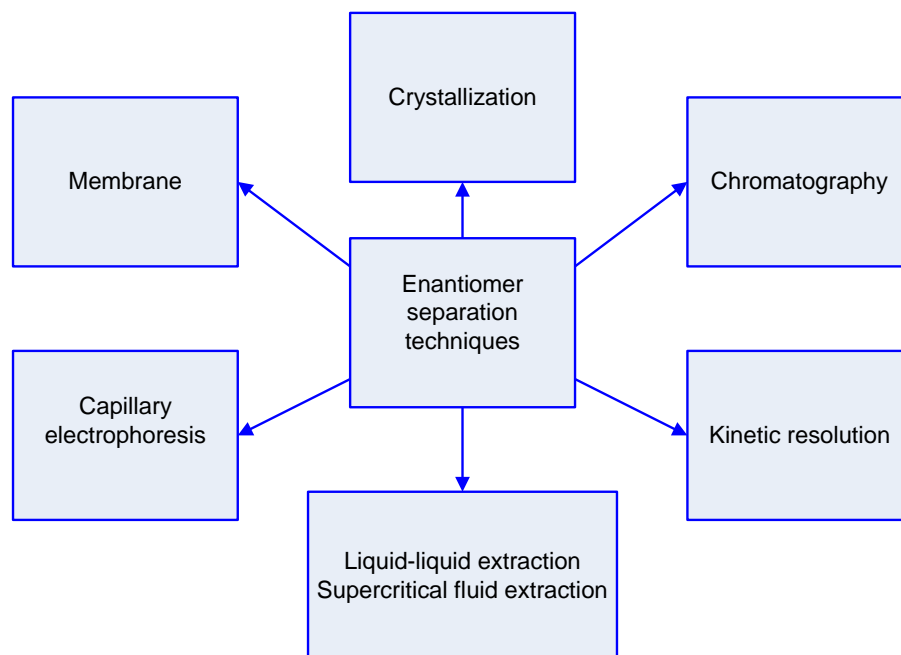
Figure 1.4: *Available methods to resolve enantiomers from racemic or enantio-enriched solutions.*

1.4.1 Resolution of a racemic mixture by crystallization

In chemical industry, crystallization is one of the oldest unit operations and a major separation and purification technique. Large quantities of organic and inorganic crystalline substances are manufactured commercially via crystallization. To purify the target enantiomers after symmetric synthesis, racemic mixtures need further separation steps of which crystallization is the most attractive because of its low cost. Figure 1.5 illustrates various modes of crystallization to perform chiral separation and/or purification.[28]

Since the mirror symmetry is a relationship between two enantiomers, enantioseparation via crystallization is considered as the most challenging separation technique comparing to the "classical" crystallization (based on different solubilities). The resolution techniques can be classified in two groups: first, the thermodynamic and/or kinetic symmetries of the chiral systems can be broken; second, these symmetries are retained.

With respect to the symmetry breaking techniques, the formation of diastereomeric salts is the most frequently used method. A chiral agent reacts with two enantiomers to form a pair of diastereomeric salts which possess different solubilities. Afterwards, a classical crystallization step can separate these diastereomeric salts and convert them to the target enantiomers.[7,28,30] Additionally, an alternative is using a chiral macrocycle in a host-guest association. The enantioselective encapsulation into this macrocycle allows us to recover the target enantiomer by a classical crystallization.[28,31,32] Furthermore, with assistance of a chiral agent, the kinetic symmetry of an enantiomer pair can be also broken. The chiral discrimination in the solid state *e.g.* conglomerate is needed. In this method, a chiral "tailor-made"

additive can be used to delay the nucleation of a single enantiomer[28,33]. As a sequence, the solid phase is the crystalline target enantiomer during a certain period of time. Afterwards, the counter enantiomer can also crystallize together with the target enantiomer, so called the simultaneous crystallization.[28,34] After that, the Ostwald's ripening is implemented by pulse heating operations at the end of the process. Consequently, the bigger crystals are composed of the enantiomer that nucleates first while the smaller crystals are composed of the second enantiomer. Both enantiomers can be separated by *e.g.* sieving.
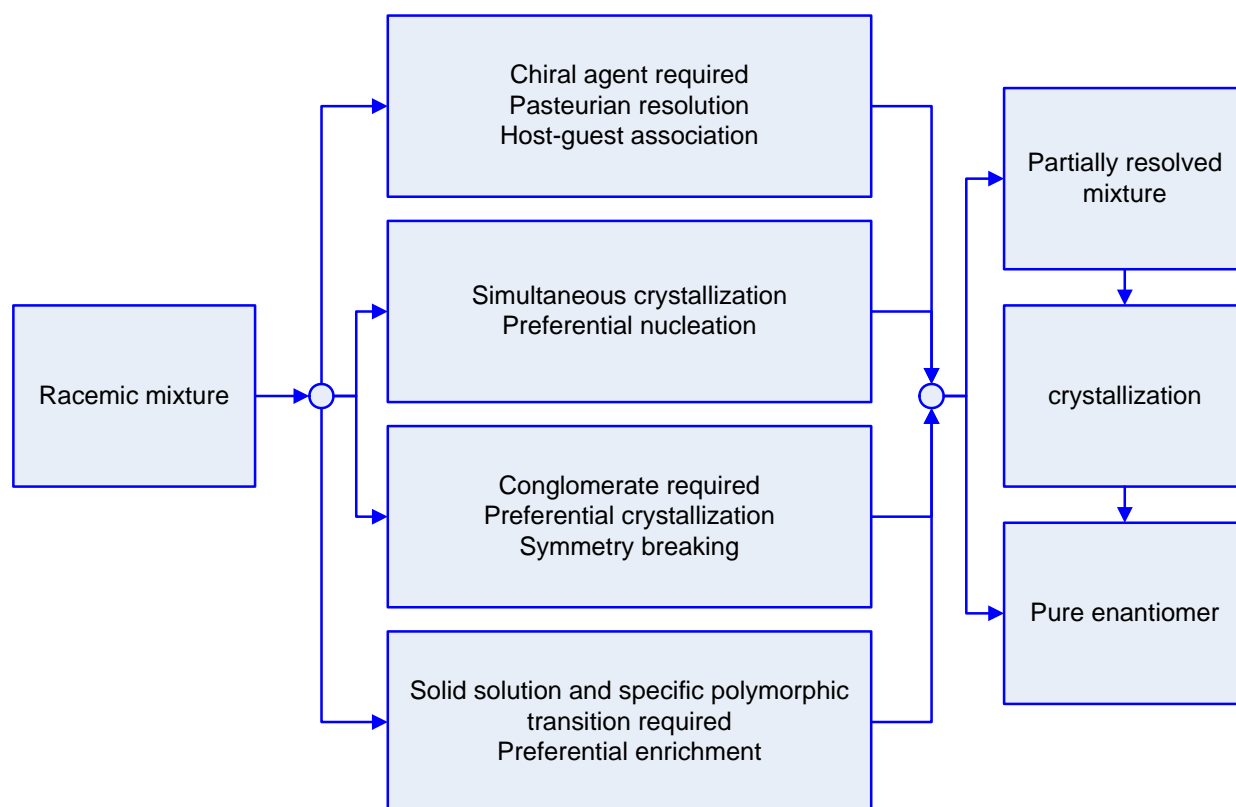
Figure 1.5: *Different routes of crystallization to produce pure enantiomers from racemic mixtures.*

On the other hand, preferential crystallization is also a powerful separation technique for enantiopurification. This technique is well understood for conglomerate systems. With respect to conglomerate systems, the preferential crystallization is the simplest method which alternatively collects enantiomers by successive crystallizations.[7,28] During the last decades, there have been attempts to apply this technique for compound-forming systems but they are still limited on lab-scale due to the challenging of kinetic control on industrial scales.[8–12] Recently, another alternative was invented based on thermodynamic control which gained preliminary successes. This method is the so called the "two-step" selective crystallization[13–15]. The key point of this method is exploiting the eutectic shift which can occurs under effects of solvent, temperature, etc. Further development of those methods will be investigated in this thesis.

When systems are fulfilled special conditions, the other crystallization approaches can also be applied for enantiopurification:

- For instance, in-situ racemization can be applied for conglomerate racemates with an assistance of suitable racemizing agents. Herewith, symmetry breaking methods can be used to resolve these racemic conglomerates. Stereoselective crystallization or preferential nucleation can be combined with racemization to resolve pure enantiomers.[28,35,36]

- Especially, deracemization is also able to produce single enantiomers. In fact, the attrition-enhanced deracemization will work with conditions of the simultaneous existence of a conglomerate in the solid phase and a fast racemization in the liquid phase. The stirring of a racemic suspension in presence of a racemizing agent and mechanical stress can ensure enantiopurification.[37,38]

- Finally, preferential enrichment can be used to resolve racemates. This method needs special conditions such as exhibiting specific polymorphic transformation and forming solid solutions with different internal order of enantiomers. In fact, solvent mediated solid-solid transformation tends to establish higher internal order. Therefore, only a single enantiomer is released into the solution, and as a sequence, the remaining solid is gradually enriched with the counter enantiomer. From this concept, successive crystallizations can be applied to obtain the target enantiomers by recovering the liquid phases.[7,28,39]

1.4.2 Other resolution methods

Besides crystallization, other methods for racemate resolution are also available. Among them, chromatography using chiral stationary phases has become one of the most powerful tools for the racemate resolution on the lab scale due to the high separation capacity per operating unit. Chiral chromatography is based on the difference of affinity of chiral compounds with the chiral stationary and mobile phases.[40,41] Besides analytical chromatography, preparative separation with simulated moving bed (SMB) chromatography is an attractive method. A SMB unit consists of switches between identical columns in order to simulate a column of infinite length. In that configuration, each enantiomer moves in opposite directions and is separated. However, due to high investment cost, chiral SMB chromatography is not often the best solution to separate racemic mixtures. It is worth to notice that chromatography and crystallization can be combined to increase the process performance as well as productivity.[42–45]

Recently, kinetic resolution is frequently used to obtain single enantiomers[46,47]. If the difference of kinetic resolution between two enantiomers in the racemic mixture is significant, one enantiomer is transformed to the desired product while the other remains unchanged and is recovered with appropriate separation methods. Obviously, the main issue of this procedure is a maximum theoretical yield of 50%. To overcome this limitation, dynamic kinetic resolution combining the resolution

step of kinetic resolution with an in-situ equilibration or in-situ racemization of the chirally labile substrate allows us to achieve a theoretical yield of 100%. The potential of a combination of preferential crystallization and enzymatic approach was also validated[48,49].

Capillary electrophoresis is one of the "youngest" separation techniques for enantioseparation but it shows potential applications. The principle of enantioseparation via a capillary electrophoresis process is based on the addition of chiral substances to running buffer solutions. High separation efficiency and easy exchanges of separation media are advantages of this method. However, low process productivity can diminish the applicability of this method on large scales.[50–52]

Up to today, chiral liquid-liquid extraction is also applied for enantioseparation[53–57]. This technique can be easily operated in a continuous countercurrent mode to fractionate the racemate into its enantiomers. However, further development of this method towards commercialization is still needed. The enantiomeric recognition is essential conditions to form selective complexes between the target enantiomer and extractors.

Membrane-based chiral resolution can be achieved using enantioselective membranes.[58–60] The enantioselective membranes act as selective barriers in the resolution process, and they selectively transport one enantiomer due to the stereospecific interaction between the enantiomer and the chiral recognition sites. That allows us to produce a permeated solution, which is enriched with one enantiomer. Different hydrogen bonding, hydrophobic, Coulombic, van der Waals interactions and steric effects between the chiral sites and membranes may cause different binding affinities.

In the above descriptions, enantioseparation via direct crystallization is the most attractive method. This thesis will focus on developing new efficient crystallization approaches which are capable to be applied for the most abundant chiral group, i.e. compound-forming racemates. In the next chapter, characteristics of different types of crystalline racemates will be discussed. Additional phenomena such as polymorphism, solvate formation are also mentioned.

CHAPTER 2: SOLID STATE OF CHIRAL COMPOUNDS AND PHASE DIAGRAMS

2.1 Solid states of chiral compounds

In the solid state, racemates can be classified into three basic categories *i.e.* conglomerate (5–10% of all chiral substances), compound-forming racemates (approximately 90–95%) and pseudoracemate systems (rare)[7]. These different types of crystalline racemates have distinctive characteristics in solid packing as well as in the phase diagrams (binary phase diagram (BPD) and ternary phase diagram (TPD)) as depicted in Figure 2.1.
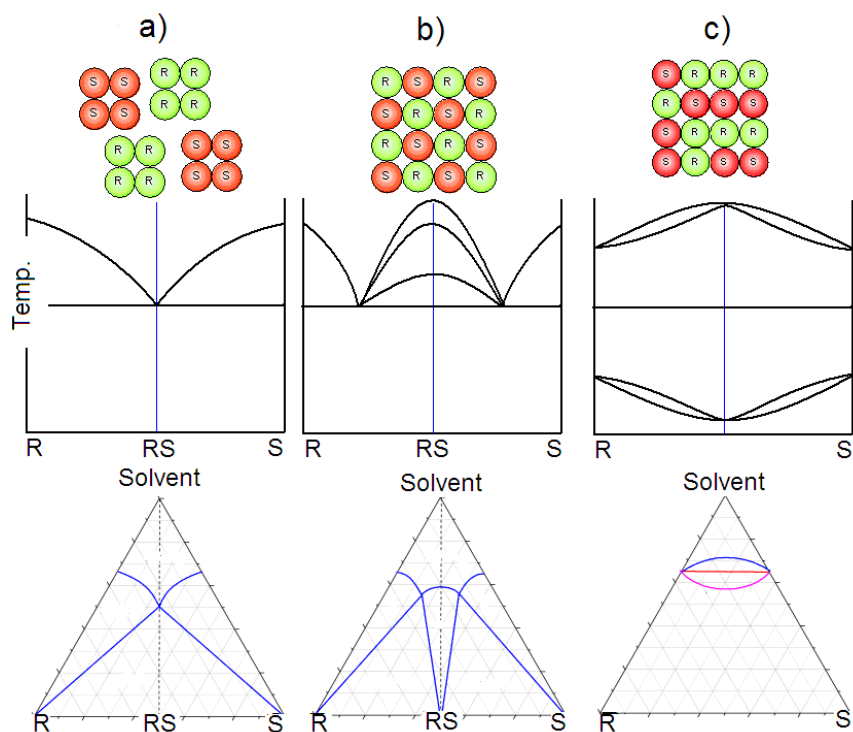
Figure 2.1: *Conglomerate, compound-forming and pseudoracemate systems are three basic types of crystalline racemates. They are distinguished from solid states to corresponding phase diagrams.*

Indeed, a conglomerate is a mechanical mixture of crystals of two enantiomers as demonstrated in Figure 2.1(a). A conglomerate can be resolve by a selectively mechanical separation. In the case of a compound-forming racemate, however, two enantiomers coexist in the same unit cell to form a new compound as seen in Figure 2.1(b). Thermodynamically, it does not possible to get enantiopure crystals from a true racemate solution at equilibrium. Finally, pseudoracemates are solid solutions of enantiomers which are further divided in three different sub-classes *i.e.* melting points of pseudoracemates can be higher, equal or lower than that of the enantiomers as plotted in Figure 2.1(c).[7]

From discrimination of crystalline racemates, there are distinguished characteristics regarding to the phase diagrams of three basic types of racemates. Conglomerates possess only one eutectic composition at 50:50 in the phase diagrams (both BPD and TPD in Figure 2.1(a)) while compound-forming systems show two symmetric eutectic points with various compositions depending on specific chiral systems. In BPD diagrams, the melting temperatures of the conglomerate racemates are always lower than that of either the pure enantiomers or any other mixture. For compound-forming systems, the constituent enantiomers can melt at higher, lower or equal temperatures comparing to the corresponding racemates (see Figure 2.1(b), the middle part). Similarly for TPDs, the solubilities of the conglomerate racemates are always maximal comparing to all other mixtures belonging to the same isotherm. This order can be changed for compound-forming systems of which solubility ratios between the racemate and enantiomer can be higher, lower or equal to unity. Finally, solid solutions have three different sub-types of which different phase diagrams are presented. The straight line (in Figure 2.1(c), middle or lower part) corresponds to an ideal solid solution which possesses an unchanged temperature during dissolution and the enthalpy of mixing equals zero. The other lines correspond to the phase diagrams which are positive or negative deviations comparing to the ideal case. These phase diagrams have no eutectic point. In solid state, the enantiomers are not in fixed positions of crystal lattice but rather than a solid solution.[7] Since pseudoracemates are rare, the next part will focus on the first two abundant chiral groups.

Various analyses have been frequently used to discriminate conglomerate and compound-forming systems:

- Solid phase analyses: Due to the difference in solid structure between conglomerate and compound-forming racemates, all the solid phase analyses can be used to discriminate types of crystalline racemates, *e.g.* single-crystal X-ray diffraction (XRD) or even X-ray powder diffraction (XRPD). Indeed, XRPD patterns of racemic mixtures and constituent enantiomers are identical in cases of conglomerates. Otherwise, the distinguished patterns can indicate compound-forming systems. The other approaches are also frequently used *e.g.* differential scanning calorimetry (DSC), Raman, infrared spectroscopy, etc.[61]

- Solubility comparison: Solubility analysis is also an approach to recognize type of chiral systems. In the case of conglomerates, enantiomers always result in minimal solubility comparing to other enantiomeric mixtures. However, solubilities of the enantiomers and the racemate of a compound-forming system can be varied depending on homogeneous and heterogeneous interactions as well as solute-solvent interactions.

The type of a crystalline racemate may depend on the temperature of the system. This behavior can occur for compounds which show compound-forming behavior above a temperature T and conglomerate behavior below this temperature.[62] On the other hand, the existence of polymorphs or hydrates is also challenging for phase

diagram construction. Obviously, these chiral systems possess more complex phase diagrams than the basic diagrams shown in Figure 2.1. In the following paragraphs, definition and characteristics of polymorphism and solvate formation are needed and briefly introduced.

2.2 Polymorphism

Polymorphism is a complex state of solid materials. "*A solid crystalline phase of a given compound resulting from the possibility of at least two different arrangements of the molecules of that compound in the solid state*"[63]. Indeed, polymorphs have different lattice structure (*i.e.* different cell packing as well as unit cell dimensions) but they are comprised from the same chemical compositions. Polymorphs show different arrangements and/or conformations of the molecules. Polymorphism can significantly change physical and chemical properties of studied compounds *e.g.* bioactivity, stability, melting, solubility, etc.[7,28,63–65]

The existence of polymorphism can have a negatively impact for the marketability of the product. Therefore, the stability of polymorphs should be taken into account. In principle, polymorphs can behave as enantiotropic or monotropic manners. These relationships possess different thermodynamic stability as depicted in Figure 2.2.
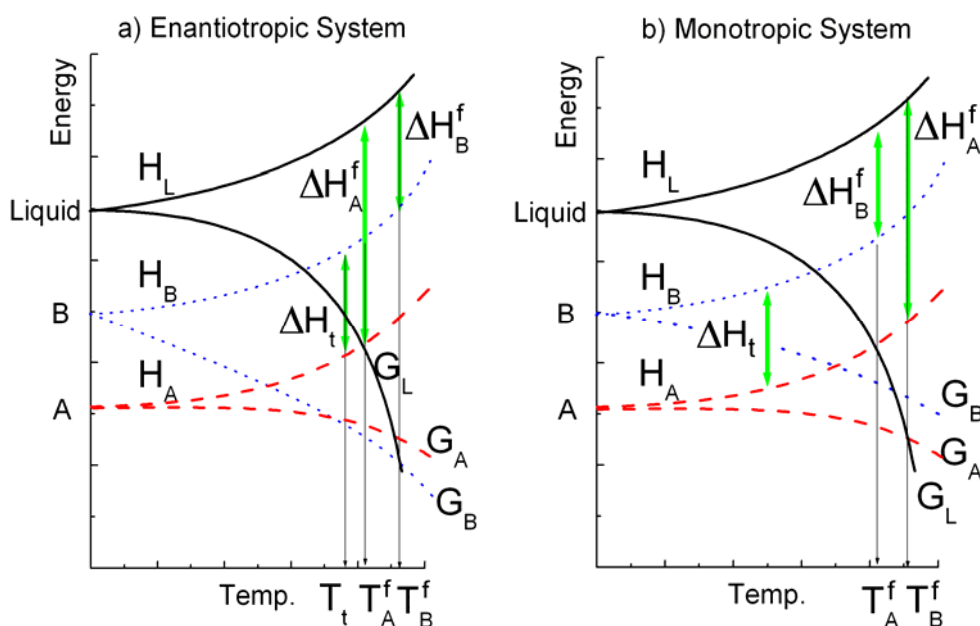
Figure 2.2: *Enantiotropic and monotropic stability. Notations: A, B and L stand for two polymorphs and liquid, respectively. Curve H_i represents enthalpy, ΔH^f_i stands for enthalpy of fusion. T^f_i is the melting temperature. ΔH_t and T_t are enthalpy of transformation and transition temperature between two polymorphs. G_i is Gibbs energy of phase i.*[66]

Enantiotropy or monotropy are two basic types of polymorphic systems. This classification based on their stability with respect to temperature and pressure. Herein, the stability of polymorphs is studied with variation of temperature (constant pressure). Figure 2.2(a) presents a case of enantiotropy. In this case, one of

the polymorphs is stable in a certain temperature range while the other polymorph is stable at different temperatures. The polymorphic conversion occurs at the transition temperature (T_t). On the other hand, Figure 2.2(b) presents a case of monotropic system. Herein, only one polymorph is stable at all temperatures below the melting point while the other polymorph(s) is unstable.[7,63,67]

Indeed, for a enantiotropic system, polymorph A is stable below the transition temperature T_t. Above this temperature, polymorph A has less free energy G_A than polymorph B does. When the temperature increases more than T_t, free energy and solubility of polymorph B becomes less than those of A. Thus polymorph B becomes more stable than polymorph A. For an enantiotropic system, a reversible transformation can be observed at a definite transition temperature (Figure 2.2(a)). On the other hand, monotropes are shown in Figure 2.2(b). The polymorph A has less free energy than the other polymorph(s) throughout the temperature range below the melting point. There is no reversible transition below the melting point since the free energy curves do not cross. The polymorph with higher free energy curve and solubility is the unstable form. Generally, heats of fusion can be used to distinguish between monotropic and enantiotropic systems. Indeed, polymorphic transformation of enantiotropes is endothermic whereas an exothermic effect is typical for monotropes.

The difference between polymorphs and habit modifications in crystals was already discussed[68]. On one hand, the different morphologies of polymorphs can be recognized by visual or microscopic observation since they are different in their solid phase structures including type of lattice, symmetry, space lattice, etc. On the other hand, changes in crystal habits are resulted from a different mechanism. The difference of relative growth rates of specific faces leads to variation of crystal habit but that does not alter the basic physical properties of the substance.

Different analytical methods to characterize polymorphs are available. Those methods are ranged from simple ones (*e.g.* melting point determination via DSC)[69–72] to complex ones (*e.g.* structural determination via XRD).[72,73] Among them, frequently used methods are known as studying the morphology of crystals by microscopy, observing changes in crystals with temperature, phase transition by thermal methods, interpreting molecular motion and chemical environment by XRPD[74] or the use of vibration spectroscopy and solid state NMR[73,75].

2.3 Solvates

The definition of solvate formation can be stated as follow. Solvent in the surrounding medium may become incorporated into the lattice of crystalline solids in specific stoichiometric ratios. These compounds are termed solvates. They are called hydrates when the solvent is water. The properties of hydrates can influence marketability of anhydrate species.[76] Pseudo-polymorphism is a term sometimes used to distinguish solvates from polymorphs. Approximately one-third of APIs are capable to form different hydrates. Depending on the desired product performance,

either the anhydrate or the hydrate forms can be selected as the final API dosage. However, an undesired phase transformation may cause unexpected changes of the physical and chemical properties of the drugs. These changes can relate to their solubility, dissolution rate, stability, particle size, and morphology[76–80], in turn, those may significantly affect the quality of the final products. The hydrate formation has gained great attention in the last decades. Some hydrate-forming compounds may convert to an amorphous form upon dehydration and some may become chemically stable[81].

CHAPTER 3: THERMODYNAMICS OF SOLID-LIQUID EQUILIBRIA

3.1 Thermodynamic equilibrium

The state of a thermodynamic system is defined by a set of thermodynamic state variables which usually include pressure, temperature, volume, internal energy, enthalpy, entropy, etc. The relationship between state variables is referred to equations of state. For a heterogeneous closed system containing m components in π phases, the whole system reaches the equilibrium state if the intensive quantities (including chemical potential μ) are identical for all π phases.[82]

$$
\begin{aligned}
T^{(1)} &= T^{(2)} = ... = T^{(\pi)} \\
P^{(1)} &= P^{(2)} = ... = P^{(\pi)} \\
\mu_1^{(1)} &= \mu_1^{(2)} = ... = \mu_1^{(\pi)} \\
\mu_2^{(1)} &= \mu_2^{(2)} = ... = \mu_2^{(\pi)} \\
&... \\
\mu_m^{(1)} &= \mu_m^{(2)} = ... = \mu_m^{(\pi)}
\end{aligned}
$$

(Equation 3.1)

In general, the total differential of the Gibbs energy is a function of pressure, temperature and composition:[82]

$$
dG = \left(\frac{\partial G}{\partial P}\right)_{T,n_i} dP + \left(\frac{\partial G}{\partial T}\right)_{P,n_i} dT + \sum_i \left(\frac{\partial G}{\partial n_i}\right)_{P,T,n_{ji}} dn_i
$$

(Equation 3.2)

$$
G(T,P) = \sum_i \mu_i n_i
$$

(Equation 3.3); $\qquad \dfrac{\Delta G}{n_i} = \Delta g_i = \Delta \mu_i \qquad$ (Equation 3.4)

At equilibrium, the general form of the phase rule is stated as the following equation[83]:

$$
F + \pi = m + n
$$

(Equation 3.5)

where: F is the number of degrees of freedom of the system, π is the number of phases at equilibrium, m is the number of components, n is the extensive variables (*e.g.* $n = 2$ when pressure and temperature are considered, or $n = 1$ for isobaric systems).

3.1.1 Solubility of single components

A solid-liquid equilibrium (SLE) is quantified by introducing fugacity[84] which relates to chemical potential by equation 3.6. With respect to temperature, the reference state is denoted as "0".

$$\Delta \mu_i = \mu_i - \mu_i^0 = RT \ln \frac{f_i}{f_i^0} \qquad \text{(Equation 3.6)}$$

The condition for the standard fugacity is freely selectable. Usually, the fugacity of the pure component at the specific system temperature and pressure is used as the standard fugacity. The fugacity can be described according to equation (Eq. 3.7) with the aid of the activity coefficient γ and the standard fugacity.

$$f_i = a_i f_i^0 = x_i \gamma_i f_i^0 \qquad \text{(Equation 3.7)}$$

The starting point for the calculation of SLE is the fugacity f. The relationship of a liquid and a solid phase of component i at equilibrium:

$$f_i^L = f_i^S \qquad \text{(Equation 3.8)}$$

Combining Eq. 3.7 and Eq. 3.8, and further re-arrangement gives

$$x_i^L \gamma_i^L f_i^{0L} = x_i^S \gamma_i^S f_i^{0S} \quad \text{(Equation 3.9);} \qquad \frac{f_i^{0L}}{f_i^{0S}} = \frac{x_i^S \gamma_i^S}{x_i^L \gamma_i^L} \qquad \text{(Equation 3.10)}$$
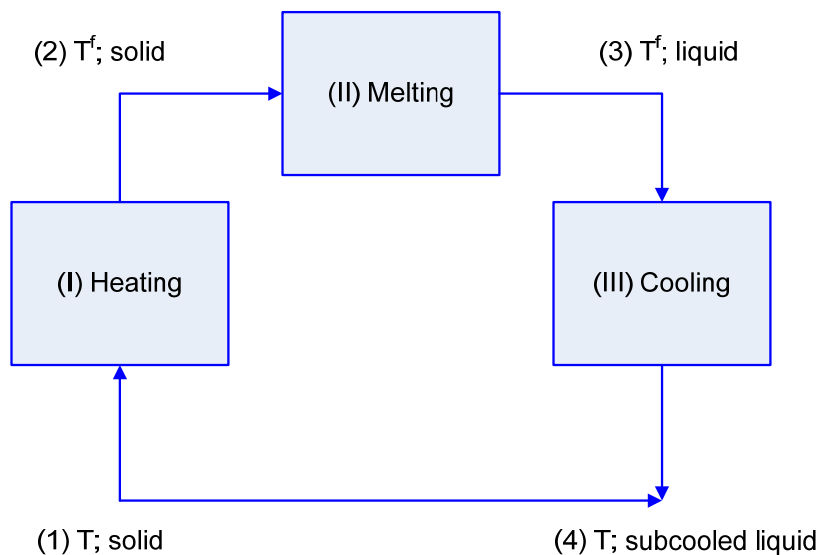
Figure 3.1: *The dissolution process (states (1) → (4)) can be alternatively presented in another pathway following steps (I) to (III). First, sample is heated form T to T^f in step (I) corresponding to states (1) and (2). Then, the sample melts at temperature T^f during step (II) (states (2) → (3)). Afterwards, melt is cooled down from temperature T^f to T in step (III) (states (3) → (4)).*[85]

The standard fugacity is needed to calculate the solubility according to equation (3.10). These values are often chosen in a sufficient manner in order to drop them out of the equation or the difference among two states can be derived. Herein, an approach using a thermodynamic cycle (Figure 3.1) involving three steps to obtain the ratio of the standard fugacity is introduced. First, the solid at state (I) is heated from temperature T up to the state (II) corresponding to its melting temperature T_f. Then, melting step at temperature T_f transfer solid material into liquid form. Finally, a cooling step (III) will reach the hypothetical state of a sub-cooled liquid.

The Gibbs enthalpy change for a transition from a pure solid to sub-cooled liquid is calculated as follows:

$$\Delta g_i = RT \ln \frac{f_i^{0L}}{f_i^{0S}} \qquad \text{(Equation 3.11)}$$

The change of the Gibbs enthalpy can also be calculated with the fundamental equation for the Gibbs enthalpy (Eq. 3.12).

$$\Delta g_i = \Delta h_i - T \Delta s_i \qquad \text{(Equation 3.12)}$$

Combining the two equations yields the ratio of the standard fugacity:

$$\ln \frac{f_i^{0L}}{f_i^{0S}} = \frac{\Delta h_i}{RT} - \frac{\Delta s_i}{R} \qquad \text{(Equation 3.13)}$$

The enthalpy can be determined from the thermodynamic cycle as shown in Figure 3.1. The enthalpy is integrated from the three steps.

$$\Delta h_i = \underbrace{\int_T^{T^f} c_{p,i}^S dT}_{I} + \underbrace{\Delta h_i^f}_{II} + \underbrace{\int_{T^f}^T c_{p,i}^L dT}_{III} \quad \text{(Eq. 3.14);} \qquad \Delta h_i = \Delta h_i^f + \int_{T^f}^T \Delta c_{p,i} dT \quad \text{(Equation 3.15)}$$

The entropy is obtained from the enthalpy:

$$\Delta s_i = \frac{\Delta h_i^f}{T^f} + \int_{T^f}^T \frac{\Delta c_{p,i}}{T^f} dT \qquad \text{(Equation 3.16)}$$

Assuming the difference in the heat capacity is a constant in the studied temperature range. Combining Eqs. 3.13, 3.15 and 3.16 will result in the following equation:

$$\ln \frac{f_i^{0L}}{f_i^{0S}} = \frac{\Delta h_i^f}{RT}\left(1 - \frac{T}{T^f}\right) - \frac{\Delta c_{p,i}\left(T^f - T\right)}{RT} + \frac{\Delta c_{p,i}}{R} \ln \frac{T^f}{T} \qquad \text{(Equation 3.17)}$$

$$\text{or:} \qquad \ln \frac{x_i^S \gamma_i^S}{x_i^L \gamma_i^L} = \frac{\Delta h_i^f}{RT}\left(1 - \frac{T}{T^f}\right) - \frac{\Delta c_{p,i}\left(T^f - T\right)}{RT} + \frac{\Delta c_{p,i}}{R} \ln \frac{T^f}{T} \qquad \text{(Equation 3.18)}$$

In general, the triple point temperature and the melting temperature deviate only slightly from each other so that in the Eq. 3.18 at the triple point the melting enthalpy can be replaced by the heat of fusion at the melting point. Two terms relating to the heat capacity difference on the right hand side of Eq. 3.18 can be eliminated due to their opposite signs and small contribution terms. With these simplifications, the phase equilibrium relation (Eq. 3.18) can thus be formulated:

$$\ln \frac{x_i^S \gamma_i^S}{x_i^L \gamma_i^L} = \frac{\Delta h_i^f}{RT}\left(1 - \frac{T}{T^f}\right) \qquad \text{(Equation 3.19)}$$

For eutectic system, the pure solid is crystallized, *i.e.* the activity coefficient and the molar fraction of the pure component in the solid phase are unity.

$$\gamma_i^S = 1; x_i^S = 1 \qquad \text{(Equation 3.20)}$$

The phase equilibrium conditions (Eq. 3.19) reduce to:

$$\ln x_i^L \gamma_i^L = -\frac{\Delta h_i^f}{RT}\left(1 - \frac{T}{T^f}\right) \qquad \text{(Equation 3.21)}$$

This equation is also called the Schröder-van Laar equation. It also shares the similarity with the equations of van't Hoff and Clausius-Clapeyron. Since melting enthalpy and temperature are commonly detectable by thermal analysis methods *e.g.* DSC, DTA, the solubility will be derived from Eq. 3.21 if activity coefficient is known. For the non-ideal solutions, activity coefficient can be estimated via a couple of models as described in part 3.2.

3.1.2 Solubility of compound-forming systems

The dissolution of a true racemate (denoted DL) can be considered as a chemical reaction:[86]

$$DL_S \longleftrightarrow D_L + L_L \qquad \text{(Equation 3.22)}$$

One can correlate the SLE of compound-forming racemates using the well-known Prigogine-Defay equation (Eq. 3.24). Details of the formulation can be seen in literature[87].

$$\ln 4\gamma_D \gamma_L x_D^l \left(1 - x_D^l\right) = \frac{\Delta h_{DL}^f}{R}\left(\frac{1}{T_{DL}^f} - \frac{1}{T}\right) \qquad \text{(Equation 3.23)}$$

$$\ln(4\gamma_D x_D^l \gamma_L x_L^l) = \frac{\Delta h_{DL}^f}{R}\left(\frac{1}{T_{DL}^f} - \frac{1}{T}\right) \qquad \text{(Equation 3.24)}$$

3.2 Activity and activity coefficient models

The activity of component *i* at a set of temperature, pressure, and composition is defined as the ratio of the fugacity of *i* in the current state and the standard state[82] as Eq. 3.25 (P^0 and x^0 are arbitrary but at specified pressure and composition). The activity coefficient of species *i* in solution γ_i is defined as the ratio of the activity *i* to some convenient measurements of the concentration of *i* which is usually expressed as mole fraction.

$$\alpha_i(T,P,x) = \frac{f_i(T,P,x)}{f_i(T,P^0,x^0)} \qquad \text{(Equation 3.25)} \qquad\qquad \gamma_i = \frac{\alpha_i}{x_i} \qquad \text{(Equation 3.26)}$$

The relation between partial molar excess Gibbs energy and activity coefficient is given by:

$$\overline{g}_i^E = RT \ln \gamma_i \qquad \text{(Equation 3.27)}$$

For an ideal solution $\overline{g}_i^E = 0$ and, therefore, $\gamma_i = 1$

Considering the partial properties given above, the equation takes the form of Gibbs/Duhem equations[82,88] which is expressed as:

$$g^E = RT \sum_i x_i \ln \gamma_i \qquad \text{(Equation 3.28)}$$
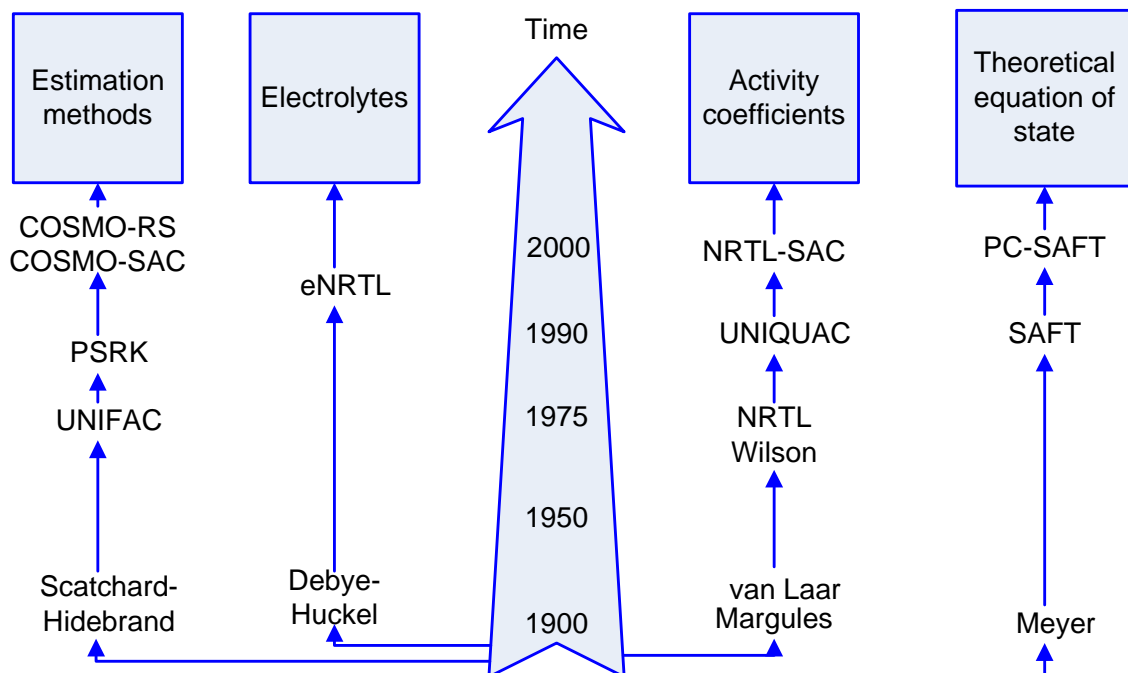
Figure 3.2: *A century overview of the most popular models for solid-liquid equilibrium determination including empirical, semi-empirical, predictive models[89].*

With respect to activity coefficient, there are a couple of models which encompass empirical, semi-empirical, predictive models as summarized in Figure 3.2. Several typical methods such as Margules, Wilson, NRTL, UNIFAC, etc. will be introduced in this chapter.

3.2.1 Margules equation

In 1895, Margules proposed a simple equation to calculate activity coefficient which is very suitable for simple binary mixtures. These mixtures usually contain molecules that are similar in size, shape and chemical nature. The one-constant form is equivalent to describe symmetrical activity coefficient curves.[82]

$$g^E = Ax_1x_2 \qquad \text{(Equation 3.29)} \qquad \lg\gamma_1 = \frac{A}{RT}x_2^2 \,;\, \lg\gamma_2 = \frac{A}{RT}x_1^2 \qquad \text{(Equation 3.30)}$$

In these equations, A is a function of temperature and may be positive or negative. Indeed, such symmetrical behavior of activity coefficient curves is rarely observed experimentally. However, a modified two-constant form is still commonly used because of its simplicity.

$$\lg\gamma_1 = x_2^2\left[\overline{A}_{12} + 2x_1\left(\overline{A}_{21-}\overline{A}_{12}\right)\right] \qquad \text{(Equation 3.31)}$$

3.2.2 van Laar equation

The van Laar equation can be used to calculate activity coefficient of binary solutions. The limit of this method is capable to apply for two components (in particular for non-polar liquids) which can be different molecular sizes but not strongly dissimilar in chemical properties. The constants of the van Laar equation are only observed by estimation from experimental data and it is not possible to directly estimate interaction of components in solution without essential assumptions.[82]

$$\frac{g^E}{RT} = \frac{2a_{12}x_1x_2q_1q_2}{x_1q_1 + x_2q_2} \quad \text{(Equation 3.32)} \qquad \ln\gamma_1 = \frac{A}{1+\dfrac{Ax_1}{Bx_2}} \,;\, \ln\gamma_2 = \frac{B}{1+\dfrac{Bx_2}{Ax_1}} \quad \text{(Equation 3.33)}$$

$$\text{where: } A = 2q_1a_{12} \text{ and } B = 2q_2a_{21} \qquad \text{(Equation 3.34)}$$

3.2.3 Wohl model

Wohl expanded the excess Gibbs energy as a power series in z_1 and z_2 which are actually the effective volumes of the two components as follows.

$$\frac{g^E}{RT(x_1q_1 + x_2q_2)} = 2a_{12}z_1z_2 + 3a_{112}z_1^2z_2 + 3a_{122}z_2^2z_1 + 4a_{1112}z_1^3z_2 +$$
$$+ 4a_{1222}z_2^3z_1 + 6a_{1112}z_1^2z_2^2 + \dots \qquad \text{(Equation 3.35)}$$

$$\text{where:} \qquad z_i = \frac{x_iq_i}{x_1q_1 + x_2q_2} \qquad \text{(Equation 3.36)}$$

The Wohl equation contains two types of parameters, *q* and *a*. Herewith, *q* is a measure of size of molecule *i* while *a* stands for interaction. The parameter a_{12} is a constant characterizing the interaction between molecule "1" and molecule "2", a_{112} represent interaction between three molecules, two of component "1" and one of component "2", and so on.[82] The ternary formulation of Wohl's model was already discussed elsewhere[90–91].

In particular, assuming $a_{12} \neq 0, a_{112} = a_{122} = ... = 0$, we have:

$$\frac{g^E}{RT} = (x_1 q_1 + x_2 q_2) 2 a_{12} z_1 z_2 = \frac{2 a_{12} x_1 q_1 x_2 q_2}{x_1 q_1 + x_2 q_2} \qquad \text{(Equation 3.37)}$$

The liquid phase activity coefficients for the Wohl expansion can be obtained from Eq. 3.37 by replacing term $\ln \gamma_i = \frac{g_i^E}{RT}$

The above models were developed on the basis of completely random mixture theory. This theory assumed species of molecules "1" and "2" in the vicinity of any molecule proportional to their mole fractions. There is a different class of excess Gibbs energy models which take into account the non-randomness characteristics, can be formulated. In fact, each molecule has a local composition that is different from bulk composition. These models assume that the ratios of species "1" to species "2" molecules surrounding any molecules are depended on the differences in size and interaction energies of the chosen molecules. Several models were constructed based on the non-randomness theory which will be introduced in the next paragraphs.

3.2.4 Wilson model

The Wilson model provides good representation of excess Gibbs energies for a variety of miscible mixtures. It is particular useful for solution of polar or associating components in non-polar solvents. The Wilson model can be expressed for a solution of *m* components.[82,92]

$$\frac{g^E}{RT} = -\sum_{i=1}^{m} \left(x_i \ln \left(\sum_{j=1}^{m} x_j \Lambda_{ij} \right) \right) \qquad \text{(Equation 3.38)}$$

$$\text{thus:} \quad \ln \gamma_k = -\ln \left(\sum_{j=1}^{m} x_j \Lambda_{kj} \right) + 1 - \sum_{i=1}^{m} \frac{x_i \Lambda_{ik}}{\sum x_j \Lambda_{ij}} \qquad \text{(Equation 3.39)}$$

There are adjustable parameters Λ_{ij}. They relate to pure component molar volume $v_{i,j}$ and to characteristic energy difference $(\lambda_{ij} - \lambda_{ii})$:

$$\Lambda_{ij} = \frac{v_j}{v_i} \exp \left[-\frac{\lambda_{ij} - \lambda_{ii}}{RT} \right] \qquad \text{(Equation 3.40)}$$

3.2.5 UNIQUAC

An extended quasichemical theory for the non-randomness of mixtures containing molecules of different sizes was proposed by Abrams. This extension was called the universal quasichemical theory, abbreviated as UNIQUAC. The excess Gibb energy g^E consists of two parts including the combinatorial part and the residual part. The combinatorial part represents the contribution of the excess enthalpy, which results from the different sizes and shapes of the molecules considered. On the other hand, the residual part is the contribution of the excess enthalpy which is caused by energetic interaction between the molecules.

$$g^E = g^E_{combinatiorial} + g^E_{residual} \qquad \text{(Equation 3.41)}$$

$$\frac{g^E_{combinatorial}}{RT} = \sum_{x=1}^{m} x_i \ln \frac{\phi_i^*}{x_i} + \frac{z}{2} \sum_{i=1}^{m} q_i x_i \ln \frac{\theta_i}{\phi_i^*} \qquad \text{(Equation 3.42)}$$

$$\frac{g^E_{residial}}{RT} = -\sum_{x=1}^{m} q_i' x_i \ln \left(\sum \theta_j' \tau_{ji} \right) \qquad \text{(Equation 3.43)}$$

Segment volume fraction ϕ_i^* and area fractions θ and θ' are given by

$$\phi_i^* = \frac{r_i x_i}{\sum r_j x_j} \;;\; \theta_i = \frac{q_i x_i}{\sum q_j x_j} \;;\; \theta_i' = \frac{q_i x_i}{\sum q_j x_j} \qquad \text{(Equation 3.44)}$$

The coordination number z is usually set to 10. The activity coefficient is calculated with the following equations:

$$\ln \gamma_i = \ln \gamma_i^C + \ln \gamma_i^R \qquad \text{(Equation 3.45)}$$

$$\ln \gamma_i^C = \ln \frac{\phi_i}{x_i} + \frac{z}{2} q_i \ln \frac{\theta_i}{\phi_i} + l_i - \frac{\phi_i}{x_i} \sum_j x_j l_j \qquad \text{(Equation 3.46)}$$

$$\text{where: } l_i = \frac{z}{2}(r_i - q_i) - (r_i - 1); r_i = \sum_k \nu_k R_k ; q_i = \sum_k \nu_k Q_k \qquad \text{(Equation 3.47)}$$

$$\text{and} \quad \ln \gamma_i^R = \sum_k \left(\nu_k^{(i)} \left[\ln \Gamma_k - \ln \Gamma_k^{(i)} \right] \right) \qquad \text{(Equation 3.48)}$$

$$\ln \Gamma_k = Q_k \left[1 - \ln \left(\sum \theta_m \Psi_{mk} \right) - \sum \left(\frac{\theta_m \Psi_{km}}{\sum \theta_n \Psi_{nm}} \right) \right] \qquad \text{(Equation 3.49)}$$

In those equations, k is subgroup; R_k and Q_k are group contribution factors, depending on the subgroup. These factors depend respectively on the van der Waals volume and area. ψ_{mk} is the main-group interaction parameter and x_i is the mole fraction of subgroup m in the solution.[82,93–95]

3.2.6 NRTL model

The <u>n</u>on-<u>r</u>andom <u>t</u>wo <u>l</u>iquids (NRTL) is also based on the concept of the local composition. This concept was firstly described by Renon[96]. Unlike Wilson's equation, however, it is applicable for both partial miscible and completely miscible systems. The NRTL equation for excess Gibb energy is given:

$$\frac{g^E}{RT} = \sum_{i=1}^{m} x_i \frac{\sum_{j=1}^{m} \tau_{ji} G_{ji} x_j}{\sum_{j=1}^{m} \tau_{ji} G_{ji}} \qquad \text{(Equation 3.50)}$$

$$\text{where: } \tau_{ji} = \frac{g_{ji} - g_{ii}}{RT} ; \ G_{ji} = \exp\left(-\alpha_{ji} \tau_{ji}\right) \qquad \text{(Equation 3.51)}$$

Neglecting third and higher order interactions terms in the NRTL description, the activity coefficients, γ_i, in a system with m components are given by:

$$\ln \gamma_i = \frac{\sum_{j=1}^{m} \tau_{ji} G_{ji} x_j}{\sum_{l=1}^{m} G_{li} x_i} + \sum_{j=1}^{m} \frac{x_j G_{ij}}{\sum_{l=1}^{m} G_{lj} x_l} \left(\tau_{ij} - \frac{\sum_{r=1}^{m} x_r \tau_{rj} G_{rj}}{\sum_{l=1}^{m} G_{lj} x_l} \right) \qquad \text{(Equation 3.52)}$$

Indeed, meaning of g_{ij} is similar to of Wilson equation. It is an energetic parameter characterizing the i-j interaction. The parameter α_{ij} relates to the non-randomness in the mixture, with $\alpha_{ij} = 0$ the mixture is completely random and the NRTL equation reduces to the Margules's equation.

For the moderate non-ideal systems, the NRTL equation offers no advantages than the simple equations of van Laar and Margules. However, for strong non-ideal mixtures, the NRTL shows good representation of experimental data in particular for partially miscible systems.

For a chiral solution containing two enantiomers and a solvent, indexes (1) and (2) stand for the enantiomers and (3) for the solvent. Thus, there are different types of interactions between these species such as between enantiomer-enantiomer denoted at "1-2" and enantiomers-solvent denoted at "1-3" or "2-3". Each pair needs three parameters (*e.g.* $\alpha_{12}, g_{12}, g_{21}$ for pair "1-2") to quantify their state in the real solution.

Two levels of the NRTL model are considered excluding and including heterochiral interactions ("2-3") that leads to the three- and six-parameter models, respectively.

3.2.7 Predictive models

The above methods are empirical or semi-empirical models which are frequently used to estimate excess Gibbs energy as well as activity coefficient of multi-component mixtures. Unfortunately, experimental solubility data are not available in many cases. Therefore, predictive models can be applied as an alternative approach. There are a couple of predictive models, *e.g.* UNIFAC[97–99], COSMO based[100–102], etc. The original UNIFAC method is based on the UNIQUAC method. The difference between these two methods is shown on the way where the van der Waals parameters are obtained.[103] Gmehling *et al.* developed a modified UNIFAC model in 1978, called the modified UNIFAC (Dortmund) model. Indeed, UNIFAC uses the van der Waals's volume and surface area to calculate the surface and volume parameters. The expressions for the activity coefficient are similar. Solvation thermodynamics is another approach to characterize molecular interactions and accounts for liquid-phase non-idealities. Solvation thermodynamic models, theoretically based on computational quantum mechanics, allow us to predict physical properties without experimental data. Conductor-like Screening Model, abbreviated as COSMO, is a potential predictive method for SLE determination. There are several derivatives of COSMO such as COSMOtherm, COSMO-RS and COSMO-SAC. The basic principle behind COSMO-based thermodynamic models is the "solvent accessible surface" of a solute molecule. Conceptually, COSMO-based models create a cavity with the exact size of a molecule within a homogeneous medium, or solvent, of a dielectric constant then place the molecule inside the cavity. COSMO-based models require input in the form of a sigma profile, which is obtained by performing quantum-mechanical calculations. Besides, new methods (*e.g.* PC-SAFT) gain great attention[104,105].

From the above models, the NRTL will be used in this thesis to estimate activity coefficients of ternary systems of two enantiomers in a specific solvent. The NRTL model allows us to quantify heretochiral and homochiral interactions of these enantiomers as well as interactions between enantiomers and the solvent based on just few experimental solubility data.

3.2.8 A simple three-parameter model for SLE

The above activity coefficient estimation methods have to use the equations of Schröder van Laar and Prigogine-Defay to correlate SLE. Therefore, thermodynamic data including enthalpy of fusion and melting temperature are needed as input parameters. In many cases, there are not available these thermodynamic data or even not measurable. Therefore, another alternative is recommended here based on a simple three-parameter model.

The variation of temperature has typically a strong impact on solubility. The classical equation describing the solid-liquid equilibrium of a component *i* is:

$$\ln\left(\frac{x_i \gamma_i}{x_i^s \gamma_i^s}\right) = -\ln\frac{f_i^0}{f_i^{0s}} = \frac{-\Delta h_{m,i}}{RT}\left(\frac{T_{m,i} - T}{T_{m,i}}\right) + \frac{\Delta c_{p,i}}{R}\left(\frac{T_{m,i} - T}{T}\right) - \frac{\Delta c_{p,i}}{R}\ln\left(\frac{T_{m,i}}{T}\right) \qquad \text{(Equation 3.53)}$$

where: x_i is the molar fraction and the γ_i and f_i^0 are the activity coefficient and standard fugacity in both liquid and solid (denoted "s") phases. $\Delta h_{m,i}$ and $T_{m,i}$ are the enthalpy of fusion and the melting temperature of component i. $\Delta c_{p,i}$ is the difference of the heat capacities of the two phases. T is the absolute temperature identical for both phases and R is the universal gas constant.

Assuming complete immiscibility in an ideal solid phase, Eq. 3.53 can be simplified and rearranged to yield the following equation:

$$\ln(x_i \gamma_i) = \left(-\Delta h_{m,i} + \Delta c_{p,i} T_{m,i}\right)\frac{1}{RT} + \frac{\Delta c_{p,i}}{R}\ln T + \frac{1}{R}\left(\frac{\Delta h_{m,i}}{T_{m,i}} - \Delta c_{p,i} - \Delta c_{p,i}\ln T_{m,i}\right) \qquad \text{(Eq. 3.54)}$$

Summarizing the different terms relating to the specific temperature effects, further expressions will provide Eq. 3.55 (details in Appendix A):

$$\ln x_i(T) = a_i\frac{1}{T} + b_i\ln(T) + c_i \qquad \text{(Equation 3.55)}$$

Eq. 3.55 offers a simple way to evaluate the temperature-dependence of solubilities. It is similar to the Grant model (1984)[106], which was suggested based on different assumptions. Apelblat also proposed this type of temperature-dependence as an empirical model (1997)[107,108]. This method has already provided good correlation for many solid-liquid systems[106–110].

3.3 Estimation of the eutectic composition in chiral systems

In general, the eutectic compositions of chiral compound-forming systems can spread in a wide range form x_{eu} = 0.5 to 1.0. For designing crystallization processes, these eutectic points play a crucial role.[7,28,111–113] The limitation of both achievable productivity and product purity from crystallization processes directly relate to the eutectic compositions. This part will represent the Klussmann's method[113] for a quick screening of the eutectic composition.

From solubilities of the enantiomer (i.e. x_R^{Enan}) and of the racemate (i.e. x_{RS}), this approach assumes that:

$$x_R^{Enan} = x_R^{Eu} \qquad \text{(Equation 3.56)}; \qquad x_R^{Eu} x_S^{Eu} = x_R^{Rac} x_S^{Rac} \qquad \text{(Equation 3.57)}$$

The later assumption was suggested in literature[86] based on equilibrium conditions. These assumptions lead to the following equation for the eutectic coordinates.

$$x_S^{Eu} = \frac{x_R^{Rac} \times x_S^{Rac}}{x_R^{Eu}} = \frac{\left(\dfrac{x_{RS}}{2}\right)^2}{x_R^{Enan}} = \frac{x_{RS}^2}{4x_R^{Enan}}$$

(Equation 3.58)

and: $\quad Eu = \left[x_R^{Eu}; x_S^{Eu}\right] = \left[x_R^{Enan}; \dfrac{x_{RS}^2}{4x_R^{Enan}}\right]$
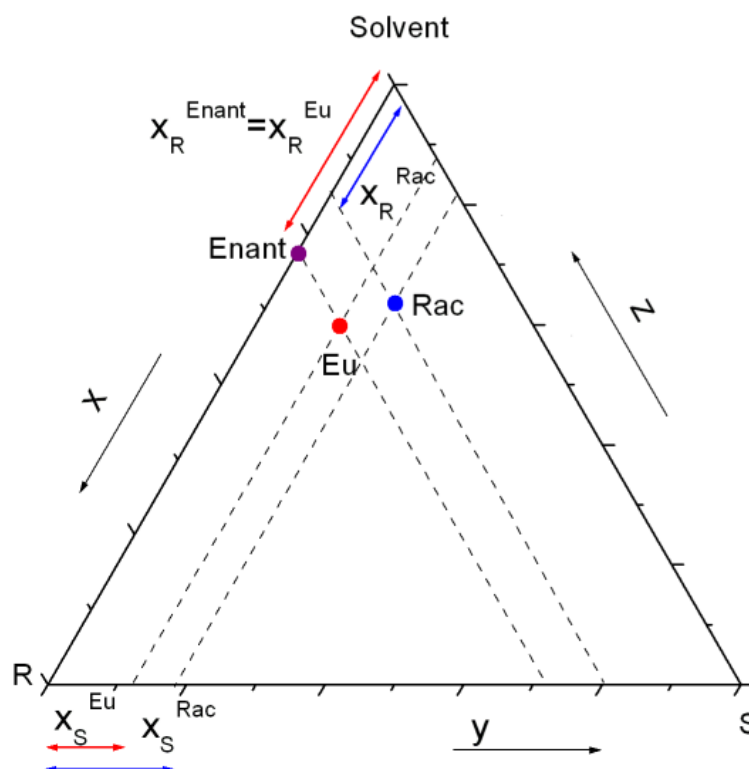
Figure 3.3: *Schematic presentation of the Klussmann's approach.*

This result can be also expressed using the enantiomeric excess (*e.e*), further arrangement leads to the eutectic composition. It is worthy to notice about the term "eutectic composition" which is frequently used throughout this thesis. In fact, a ternary system of two enantiomers and a solvent can have different types of eutectic points such as in constituent sub-binary phase diagrams between the enantiomers and the solvent but those eutectic points are not our interest. Herein, the eutectic composition will refer to enantiomeric eutectic composition in the coordination of enantiomer-enantiomer. The definition of this term can be seen in section 6.3.3.2.

$$e.e = \frac{x_R - x_S}{x_R + x_S} \times 100, \% \qquad \text{(Equation 3.59);} \qquad e.e_{Eu} = \frac{1 - \dfrac{\alpha^2}{4}}{1 + \dfrac{\alpha^2}{4}}, [-] \qquad \text{(Equation 3.60)}$$

$$\text{with: } \alpha = \frac{x_{RS}}{x_R} \qquad \text{(Equation 3.61);} \qquad x_{Eu} = \frac{1 + e.e_{Eu}}{2}, [-] \qquad \text{(Equation 3.62)}$$

From these descriptions, precise solubility determination is needed. Solubilities of single components are important initial parameters for eutectic composition estimation. Solubility determination of ternary mixtures is also needed to validate the estimation of the eutectic composition. Besides, solubility data are input parameters for activity coefficient estimation (*e.g.* via the NRTL model). Further, crystallization design is critically based on solubility data. Solubility determination will be carried out in this thesis via polythermal and/or isothermal methods. Details of these measurements will be described in section 6.3.3.

From solubility data, the van't Hoff approach[114] is frequently used to estimate enthalpy of dissolution ΔH^{diss} utilizing Eq. 3.63. From solubility data, a linear function of *ln(x)* vs. *1/T* is plotted. The slope of the obtained function contains ΔH^{diss} term.

The net enthalpy of dissolution is a sum of enthalpy of diffusion (ΔH^f) and enthalpy of mixing (ΔH^{mix}) as the relationship in Eq. 3.64[115]. The ideality of solution can be derived from these enthalpies. ΔH^{mix} is equal to zero for the ideal solution since there is no interaction between solute and solvent molecules. Thus, the value of ΔH^{diss} will be close to ΔH^f if the solution is close to ideality.

$$\ln(x) = -\frac{\Delta H^{diss}}{R}\frac{1}{T} + const.$$ (Equation 3.63)

$$\Delta H^{diss} = \Delta H^f + \Delta H^{mix}$$ (Equation 3.64)

CHAPTER 4: KINETIC ASPECTS

4.1 Nucleation

Nucleation is one of the most important phenomena not only for crystallization but also for other sciences. Many studies show that nucleation can be induced by different ways. The common ways inducing nucleation have been known such as agitation, mechanical shock, friction and extreme pressures within solutions and melts. External influences such as electric, magnetic fields, spark discharges, ultraviolet light, X-rays, γ-rays, sonic, ultrasonic irradiation, cavitations, etc. can also cause nucleation.[116–118]

In crystallization, supersaturation or subcooling degree is just a necessary condition. A supersaturated solution can retain clear for a specific period without crystallization. Herewith, the solution needs a number of nuclei which act as centers of crystallization. Nucleation may occur spontaneously or it may be induced artificially. Nucleation can be classified as primary and secondary nucleation (see Figure 4.1).[116,117]
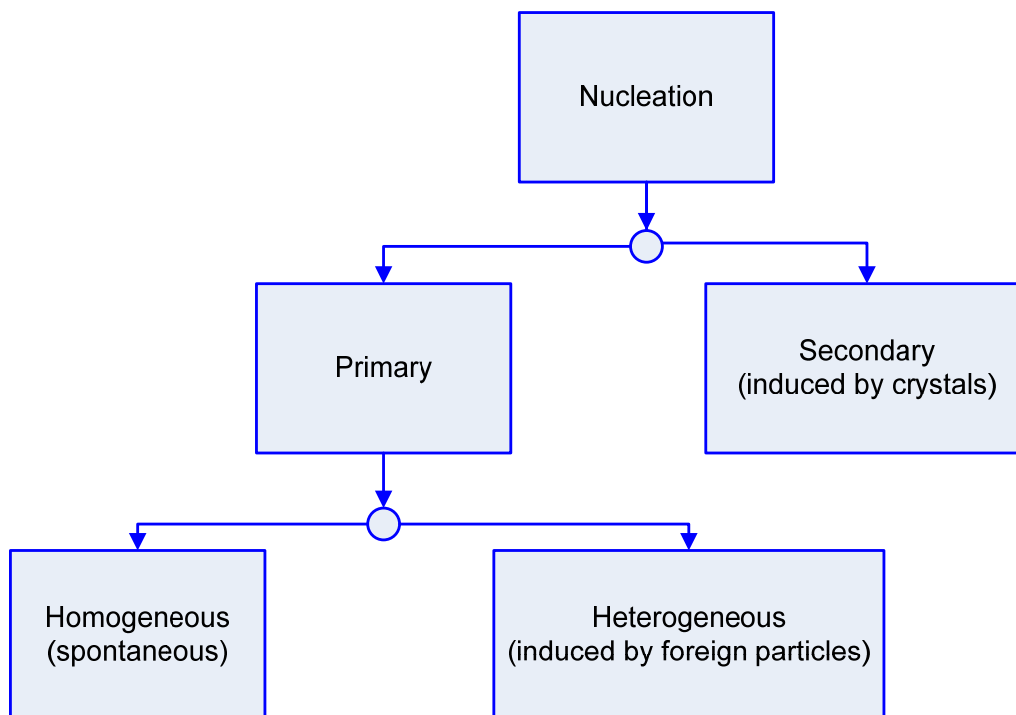

Figure 4.1: *Nucleation classification.*

4.1.1 Primary nucleation

Primary nucleation can be induced in two different manners. First, nuclei can be formed spontaneously (homogeneous nucleation) from a supersaturated solution. Second, these nuclei are induced by foreign particles, so called heterogeneous nucleation. These nucleation processes will be discriminated as follows.

4.1.1.1 Homogeneous nucleation

To form crystal nuclei, the constituent molecules will coagulate and orientate into a fixed lattice. Simultaneously, the small nuclei are also very easy to dissolve again into solution because they contain extremely high energies. These opposite tendencies result in the existence of a critical number of molecules within a "stable" nucleus. The nucleus can grow beyond a certain critical size which is called the critical radius of the nucleus. In general, a stable crystal nucleus can be comprised from about ten to several thousand molecules. In that case, it becomes stable under the average conditions of supersaturation obtaining in the bulk of the fluid. Thus, further molecular additions to the critical cluster would result in nucleation and subsequent growth of the nucleus. This concept is demonstrated in Figure 4.2.[116–118]
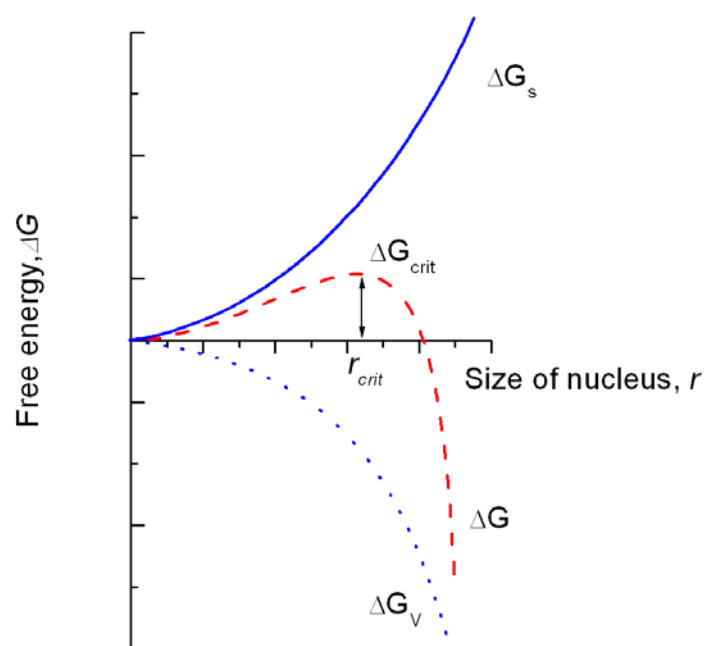
Figure 4.2: *Free energy diagram for nucleation explaining the existence of a "critical nucleus". Herein, ΔG is overall excess free energy, ΔG_s is surface excess free energy, ΔG_v is volume excess free energy.*

With respect to the classical theory of nucleation[116,118,119], the overall excess free energy between a small solid particle of solute and the solute in solution is equal to the sum of the surface excess free energy and the volume excess free energy. The simplest case is considered for a sphere of a radius r. The overall excess free energy (ΔG) is

equal to the sum of surface excess free energy (ΔG_s) and volume excess free energy (ΔG_v). Analytical equivalents are:

$$\Delta G = 4\pi r^2 \sigma + \frac{4}{3}\pi r^3 \Delta G_v \qquad \text{(Equation 4.1)}$$

where: ΔG_v is the free energy change of the transformation per unit volume; σ is the interfacial energy between the developing crystalline surface and the supersaturated solution in which the nucleus is located.

Two terms on the right-hand side of Eq. 4.1 possess opposite signs and depend differently on r. The free energy formation (ΔG) passes through a maximum (ΔG_{crit}) that corresponds to the critical nucleus (r_{crit}). For a spherical cluster, this value is obtained by maximizing Eq. 4.1, setting $\frac{d\Delta G}{dr} = 0$ with respect to r:

$$\frac{d\Delta G}{dr} = 8\pi r \sigma + 4\pi r^2 \Delta G_v = 0 \qquad \text{(Equation 4.2)}$$

Therefore, we have:

$$r_{crit} = -\frac{2\sigma}{\Delta G_v} ; \Delta G_{crit} = \frac{16\pi\sigma^3}{3(\Delta G_v)^2} = \frac{4\pi\sigma r_{crit}^2}{3} \qquad \text{(Equation 4.3)}$$

By introducing the degree of supersaturation S (Eq. 4.4), The Gibbs-Thomson relationship for a non-electrolyte is given:

$$S = \frac{C}{C*} \qquad \text{(Equation 4.4);} \qquad \ln S = \frac{2\sigma v}{kTr} \qquad \text{(Equation 4.5)}$$

Further arrangement, gives:

$$-\Delta G_v = \frac{2\sigma}{r} = \frac{kT\ln S}{v} \qquad \text{(Equation 4.6)}$$

where: v is specific volume of the solute molecule and k is the Boltzmann constant.

Combining Eqs. 4.3 and 4.6, yields ΔG_{crit} as Eq. 4.7. The radius of a spherical critical nucleus at a given supersaturation degree can be expressed as Eq. 4.8.

$$\Delta G_{crit} = \frac{16\pi\sigma^3 v^2}{3(kT\ln S)^2} \qquad \text{(Equation 4.7);} \qquad r_{crit} = \frac{2\sigma v}{kT\ln S} \qquad \text{(Equation 4.8)}$$

4.1.1.2 Heterogeneous nucleation

Heterogeneous nucleation can also be induced in a homogeneous supersaturated solution if it contacts with other phases and/or molecular species. The surfaces (of foreign phases/particles) could act as a place where the formation of clusters of a new phase is preferred. Since the old phase practically always exist in itself foreign molecules, microscopic particles, bubbles, etc., heterogeneous nucleation is much more widespread than homogeneous nucleation.[116–118]

4.1.2 Secondary nucleation

In secondary nucleation, nuclei are formed by already existing microscopic crystals. The mechanism of secondary nucleation can be counted for both attributions of collision and fluid shear. Collision is a complex process which can occur between already existing crystals with either a solid surface of the crystallizer or with other crystals themselves. Fluid shear nucleation occurs when liquid travels across a crystal at a high speed. The moving fluid sweeps away nuclei that would otherwise be incorporated into a crystal, causing the swept-away nuclei to become new crystals.

In preferential crystallization, secondary nucleation is frequently used by suitable seeding strategies together with cooling profiles.[7,28] They are decisive keys to control particle size distribution and purity of final products. Either the material to be crystallized or "strange" particles can be used as seeds. In fact, seeding is a powerful method in enantioseparation via preferential crystallization. There are various scenarios of seeding such as isothermal seeded preferential crystallization (SIPC), polythermal auto seeded preferential crystallization (AS3PC), etc. Those methods were well discussed in literature for conglomerate systems and recently for compound-forming systems.[7–12,28,120–122]
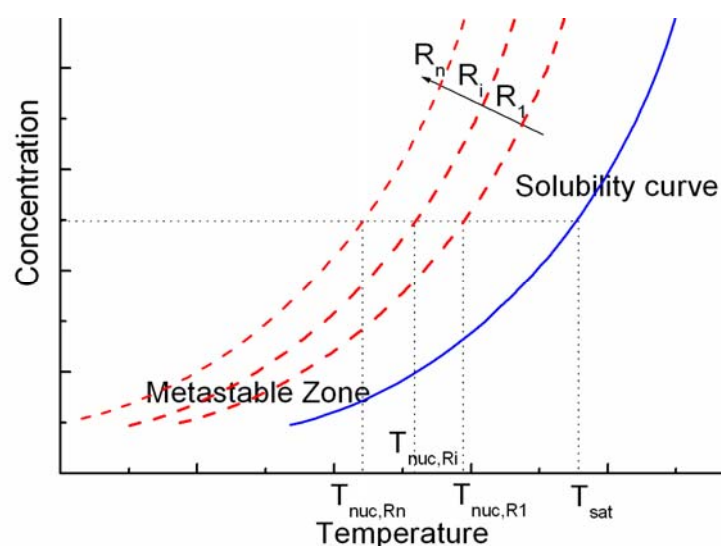
4.2 Induction time and metastable zone width

Figure 4.3: *MSZW ($\Delta T = T_{sat} - T_{nuc}$) corresponding to different cooling rates (R_i). ΔT_{max} is detectable via the Nyvlt's method.*

The induction time and the metastable zone width (MSZW) are important data for preferential crystallization design. The induction time is defined as the time elapsed from the period in which the solution achieves a supersaturated state to the first nuclei detected.[116–118,123,124] On the other hand, Nyvlt proposed a theory correlating MSZW with respect to different cooling rates[125,126]. The MSZW is estimated corresponding to the maximal subcooling ΔT_{max} as seen in Figure 4.3. ΔT_{max} stands for the subcooling corresponds to a cooling rate equal to "zero" which can be determined by an extrapolation from different cooling rates.

4.3 Effects of additives on crystallization processes

Additive-controlled crystallization has been rapidly developed in the last decades. The presence of additives in solution media can vigorously influence many decisive parameters of crystallization processes such as solubility, nucleation rate, MSZW, induction time, crystal morphology, etc.[127] Nowadays, additives are frequently used to control particle size distribution and particle morphology of desired products. That is essentially important in *e.g.* pharmaceuticals since bioactivity of drugs depending on dissolution rates which, in turn, depend on particle size and morphology. Therefore, right additive selection is important for crystallization design.

Additives are classified as two basic types *i.e.* insoluble and soluble additives.[127] Either nucleation or polymorphs of nucleated crystals can be controlled by insoluble additives which can act as templates for the nucleation process. They can promote crystallization by heterogeneous nucleation which has a lower activation energy barrier than homogeneous nucleation[66,116,127,128]. On the other hand, based on the selective adsorption effects of soluble additives, these additives can be added before or after crystallization. For chiral resolution, chiral molecules are used as additives to control enantioselective crystallization. Based on selective effects of chiral additives on two enantiomers, the nucleation and crystal growth of one species can be diminished or even stopped.[28,129,130]

CHAPTER 5: DIRECT ENANTIOSEPARATION TECHNIQUES VIA SELECTIVE AND PREFERENTIAL CRYSTALLIZATION

The concepts of various enantioseparation via direct crystallization methods applicable for the major chiral group, *i.e.* compound-forming systems will be discussed in this chapter. From the thermodynamic point of view, the classical selective crystallization is limited by the eutectic composition. That is the motivation for the development of an alternative so called the "two-step" selective crystallization which produces higher purity beyond the eutectic composition but still retains advantages of thermodynamic control. Besides selective crystallization, various operation modes of preferential crystallization (kinetic control) are also introduced. Finally, to overcome the individually intrinsic limitations of selective and preferential crystallization methods, a combination crystallization process based on both thermodynamics and kinetics is also proposed at the end of this chapter.

5.1 Selective crystallization based on phase diagrams

Selective crystallization is a classical technique based on thermodynamic concepts.[7,28] These crystallization processes are preferred in industrial production since they are operated based on equilibrium states. In principle, enantioseparation via selective crystallization can be operated via either melt or solution crystallization.

5.1.1 Melt selective crystallization

Melt crystallization is one of the oldest operations which are frequently used in chemical industry due to a couple of reasons. This technique can provide a high efficiency per separation stage which usually reaches very high purity levels, *e.g.* commonly more than 99%. Additionally, adding an auxiliary agent (*i.e.* a solvent) is not necessarily required to crystallize target compounds in melt crystallization. In this thesis, melt crystallization processes are operated based on the constraints of thermodynamics (kinetics is discussed elsewhere). The purity is usually the main target of these processes. In cases of crystallization from suspensions, crystal size distribution is also an important property of final products. Comparing melt crystallization with other separation techniques such as distillation or extraction, the energy consuming of melt crystallization is a big issue. However, the energy requirement for melt crystallization can be reduced by heat integration. Two main types of melt crystallization processes are frequently applied, *i.e.* forming crystal layers on the heat exchange wall and growing the crystals in suspension.[131]

The BPD can be constructed based on thermodynamics[28,132–136]. Figure 5.1 schematically presents the phase equilibria in the BPD.
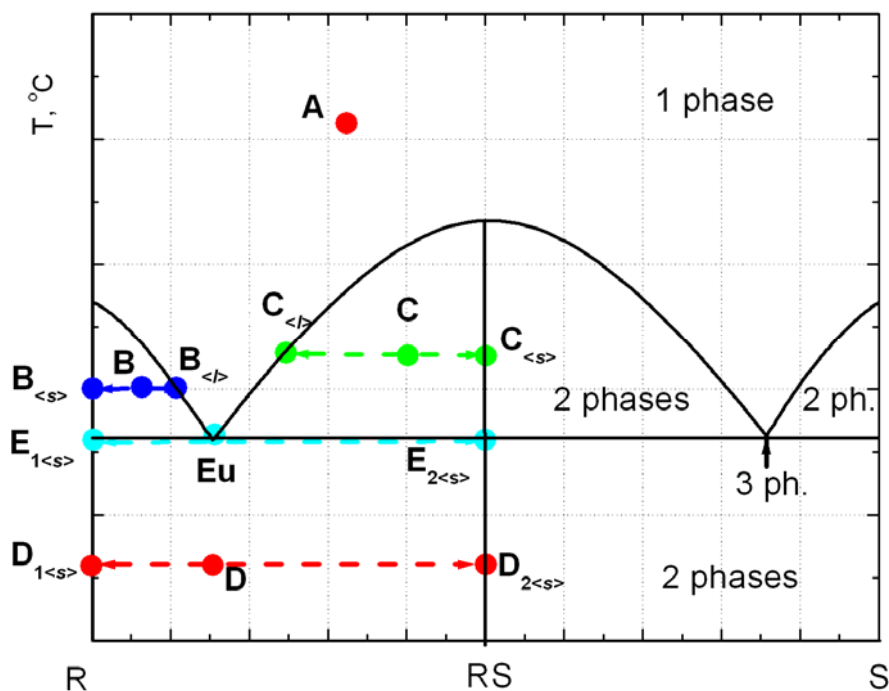
Figure 5.1: *Schematic BPD and phase equilibria of compound-forming systems. Systems from (A) to (D) represent equilibria in the different phase domains. <s> and <l> are indexes of solid and liquid phases, respectively. For instance, a system at B will establish an equilibrium between the solid phase (B<s>) and the corresponding mother liquor (B<l>). Other systems can be similarly analyzed.*

Thermodynamic equilibrium analyses of these systems in the BPD (Figure 5.1) are summarized in Table 5.1. The results are obtained by applying the Gibb's phase rule.

Table 5.1: *Phase equilibria interpretation based on BPD, applied the Gibb's phase rule.*

System	Phase	F	Equilibrium	Solid phase	Liquid phase
A	1	2	A	-	A
B	2	1	$B \longleftrightarrow B_{<l>} + B_{<s>}$	$B_{<s>}$: R	$B_{<l>}$
C	2	1	$C \longleftrightarrow C_{<l>} + C_{<s>}$	$C_{<s>}$: RS	$C_{<l>}$
Eu	3	0	$Eu_{<l>} \longleftrightarrow E_{1<s>} + E_{2<s>}$	$E_{1<s>}$: R; $E_{2<s>}$: RS	Eu
D	2	1	$D \longleftrightarrow D_{1<s>} + D_{2<s>}$	$D_{1<s>}$: R; $D_{2<s>}$: RS	-

Thus depending on the starting compositions, different solid products can be obtained as pure enantiomers, racemate or other enantiomeric mixtures. Herewith, the yield of the process can be determined. Starting with *m* (g) of an initial mixture

contains x_R^{ini} of the target enantiomer (denoted R), amount of m_1 (g) of the final product is recovered with composition of the target enantiomer x_R^{end} at the equilibrium. The yield is defined by the recovered amount of the target enantiomer over the total amount of that enantiomer in the initial mixture. This value is calculated as Eq. 5.1

$$\eta = \frac{m_1 . x_R^{end} . 100}{m . x_R^{ini}}, [\%] \qquad \text{(Equation 5.1)}$$

Based on the lever rule, the theoretical yield can be calculated from the initial composition and the eutectic composition. For the initial mixture belongs to the two-phase domain such as system **B**, the process yield will be maximal if this system is further cooled adjacent to boundary of the two- and three-phase domains. Equation 5.2 (details in Appendix B) governs the theoretical yield.

$$\eta = \frac{\left(x_R^{ini} - x_R^{Eu}\right) 100}{x_R^{ini}\left(1 - x_R^{Eu}\right)}, [\%] \qquad \text{(Equation 5.2)}$$

5.1.2 Solution crystallization

Adding a new component as a solvent to the binary compound-forming system of two enantiomers will result in the corresponding ternary system presented in the TPD as Figure 5.2(a). Similar to the binary system, equilibria in the different domains can be analyzed using the Gibb's phase rule. Basically, the TPD is composed from the one-, two- and three-phase domains as denoted in Figure 5.2(a).[7,28,137,138] To calculate the yield, two situations are considered as shown in Figure 5.2(b).[139]
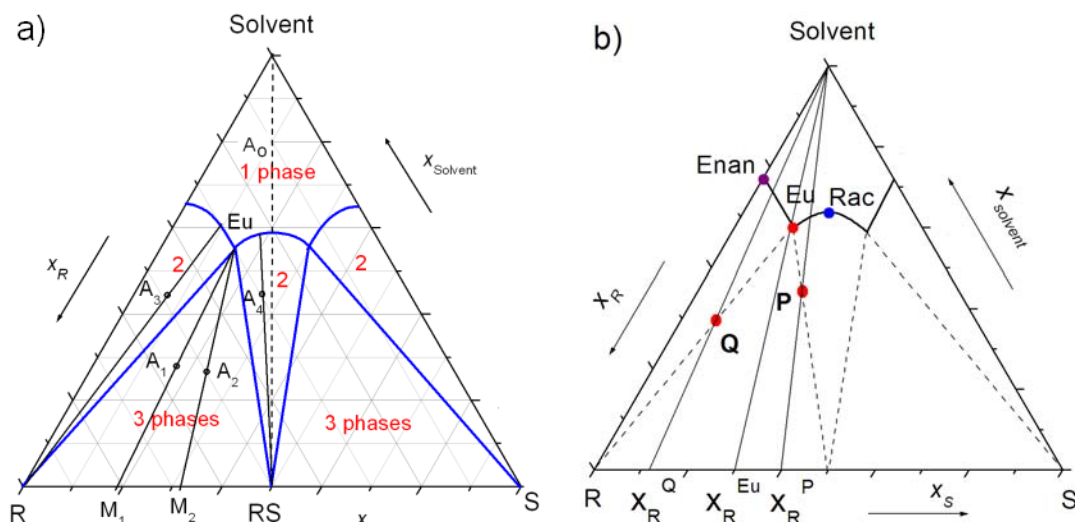

Figure 5.2: *(a) Phase equilibria based on TPD analysis. These equilibria are also the basis of the classical selective crystallization. (b) **P** and **Q** are two systems located on the boundaries of the two- and three-phase domains which result in maximal yields comparing to other arbitrary mixtures.*

As depicted in TPD (Figure 5.2(a)), one can easily obtain a eutectic liquid and an equilibrating solid mixture of the enantiomer and the racemate if the overall composition of the system belongs to the three-phase domains, *e.g.* systems A_1 and A_2. Besides, the two-phase domains are actually composed of single pure solids and their mother liquors. Indeed, systems A_3 or A_4 will result in pure species of the enantiomer or the racemate, respectively. Let consider solutions with initial compositions at **P** and **Q** at the boundary lines between the two- and three-phase domains (Figure 5.2(b)).

The theoretical process yields (η) for these systems are functions of enantiomeric excess of initial solution (*e.e₀*) and amount of the added solvent as Eqs. 5.3 and 5.4 (details in Appendix C).

$$\eta_P = \frac{50(1 + e.e_0) - x_E(1 + m_P)}{(100 - x_E)(0.5 + 0.5ee_0)} \times 100 \qquad \text{(Equation 5.3)}$$

$$\eta_Q = \frac{(1 + m_2)\left[\dfrac{(0.5 + 0.5e.e_0)100}{0.5 + 0.5e.e_0 + m_Q} - x_E\right]}{(100 - x_E)(0.5 + 0.5e.e_0)} \times 100 \qquad \text{(Equation 5.4)}$$

where: x_E-eutectic composition; $m_{P,Q}$-adding amounts of solvent.

Due to the thermodynamic limits, the composition of a slightly enantiomerically enriched solution cannot be enriched further than the eutectic composition. Therefore, the theoretically maximal purity is equal to the eutectic composition. To obtain higher purity, the "two-step" process selective crystallization is recommended. The concept of this method is illustrated as follows.

5.1.3 "Two-step" process as a modified selective crystallization exploiting the eutectic shift

Various operation modes of the "two-step" process will be examined in the experimental part. Those methods use a similar concept exploiting shifts of the eutectic compositions. This part will principally demonstrate the main ideas of the "two-step" process by using an "artificial" illustration based on a combination of two BPDs. The key constraint is that these BPDs possess two different eutectic compositions Eu_1 and Eu_2 as seen Figure 5.3. With respect to the target enantiomer, the first BPD possesses higher eutectic composition than that in the second BPD ($x_R^{Eu1} > x_R^{Eu2}$). When this constraint is fulfilled, there is an opportunity to transfer the liquid at Eu_1 into the two-phase domain of the second BPD corresponding to the eutectic Eu_2. Consequently, the target enantiomer will crystallize as a solid phase corresponding to the second BPD.
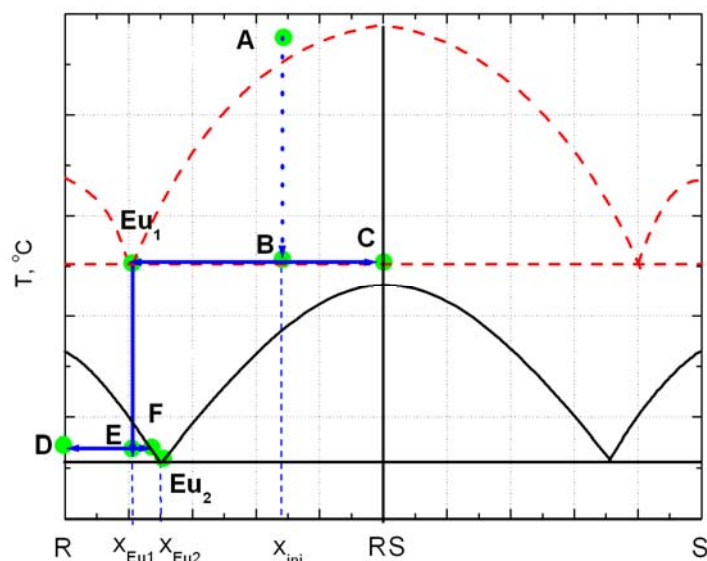
Figure 5.3: *Concept of the "two-step" process which follows A→B→Eu₁→E→D.*

Herein, we consider a system **A** as the starting point for the "two-step" process. As seen in Figure 5.3, this system is slightly enriched by the abundant enantiomer of which x_R^{ini} presents the initial enantiomeric composition. This mixture can be simply moved adjacent to position **B** in the first BPD by only one cooling step. At this state, equilibrium is established between a solid **C** (racemate) and the eutectic liquid **Eu₁**. Due to the assumption of the target enantiomeric composition of **Eu₁** is higher than that of **Eu₂**, Point **E** (formed from point **Eu₁**) can be moved to the two-phase (enantiomer and mother liquor) domain of the second BPD. After relocating this system (*i.e.* **Eu₁**) to point **E** as shown on the second BPD, the second equilibrium occurs between a mother liquid at **F** and a pure solid of enantiomer at **D**. The target enantiomer is consequently harvested and a washing step may be needed to dissolve adsorbed impurities. The total process yield is calculated as Eq. 5.5.

$$\eta_{total} = \eta_{step1} \times \eta_{step2}, [\%] \qquad \text{(Equation 5.5)}$$

Throughout this thesis, three different yields are frequently compared:

- *The experimental process yields* are calculated by Eqs. 5.1 and 5.5 for designed process under specific conditions.

- *The theoretical yields* are calculated from Eqs. 5.3, 5.4 and 5.5. This calculation is based on three assumptions: a) the same initial conditions are referred to the experimental process yields; b) mass losses in intermediate steps are equal to zero; c) systems are located on the boundary of the two- and three-phase domains, *e.g.* at points **P** and **Q** in Figure 5.2(b).

- In the optimal conditions, the initial solution **A** possesses the enantiomeric composition equal to the eutectic composition of **Eu₁**. Then, only the 2nd step is actually needed. *Thus, the maximal total yield* of whole process is equal to that of the 2nd step (Eq. 5.4).

5.2 Preferential crystallization

Comparing to selective crystallization, preferential crystallization is another approach based on kinetic control where the difference in the crystallization rates of the racemate comparing to the constituent enantiomers are exploited. This technique is also called resolution by entrainment.[7,28] Figure 5.4 demonstrates the concept of preferential crystallization to purify the enantiomer(s). We consider a supersaturated solution below solubility curve at the selected isotherm T_{cryst}. The solution belongs to the metastable zone width (MSZW). Indeed, this solution is not thermodynamically stable, but it can retain as clear supersaturated solutions for a period so called induction time.
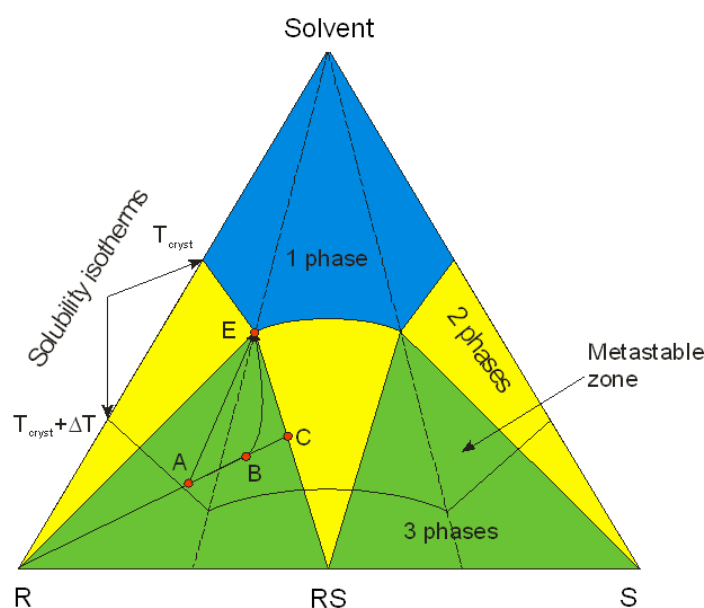

Figure 5.4: *Concept of preferential crystallization.*

Details of preferential crystallization have been discussed elsewhere[8–12,28], hereby just the main ideas are summarized in this part. The MSZW, which is graphically presented in Figure 5.4, plays an extremely important role for preferential crystallization. Considering the starting solution presented at **A,** this system is assumed to be enriched by the abundant enantiomer or a partially resolved racemic solution which can be obtained from different sources. The selective nucleation is needed. Herewith, for instance, pure seed crystals of the target enantiomer are added to crystallize this enantiomer. As long as the racemate is remained in the mother liquor, the crystallization process will produce the single enantiomer as a solid product. Simultaneously, the mother liquor moves towards direction **A→B**. Crystallization of the counter species (racemate) does not take place if the seed crystals show a selective effect. That means the degree of supersaturation is not sufficient for nucleation of the racemate. In other words, no suitable nuclei inducing crystallization of the racemate is present in the solution. Obviously, the concentration of the more abundant enantiomer in the solution decreases during crystallization process of the target enantiomer (**A→B**). In contrast, concentration of the counter species in solution is increasing that, in turn, leads to the secondary nucleation of the

racemate *e.g.* at point **B** and changes the trajectory of crystallization process towards point **E** instead of the ideal case at **C**. Thus, crystals of the single enantiomer should be collected from the solution before the entrainment of the counter species (*i.e.* racemate) occurs. Likewise, a similar approach can be applied to crystallize the racemate from the opposite direction by seeding the racemate.

Seeding strategies are decisive for the success of preferential crystallization. Based on different strategies of seeding, popular methods are frequently applied such as seeded isothermal preferential crystallization (SIPC), auto-seeded polythermic programmed preferential crystallization (AS3PC), etc. Indeed, SIPC is a simple method where seeds are added at a fixed end temperature of crystallization while auto seeding can occur during cooling profiles.[8–12,28]

5.3 An innovative combination of preferential crystallization and selective crystallization

The basis of the "two-step" process is transferring a supersaturated solution from the three-phase domain into the two-phase domain. Based on that concept, another routine can also play the similar function. This development bases on a combination between preferential crystallization and selective crystallization. First, preferential crystallization is applied to crystallize the racemate species and, as a result, to move the overall mother liquor composition to pass through the eutectic composition. Thus, preferential crystallization can be considered as an enantiomeric enrichment step for mother liquor which is analogical to the first step of the "two-step" process. As a sequence, the sub-step evaporation a calculated amount of solvent will move that enriched mother liquor into the two-phase domain. Finally, selective crystallization will be applied to this system to crystallize the pure enantiomer within this two-phase domain. The schematic presentation of this combination is presented in Figure 5.5 and the process follows the trajectory **A→B→D→R**.
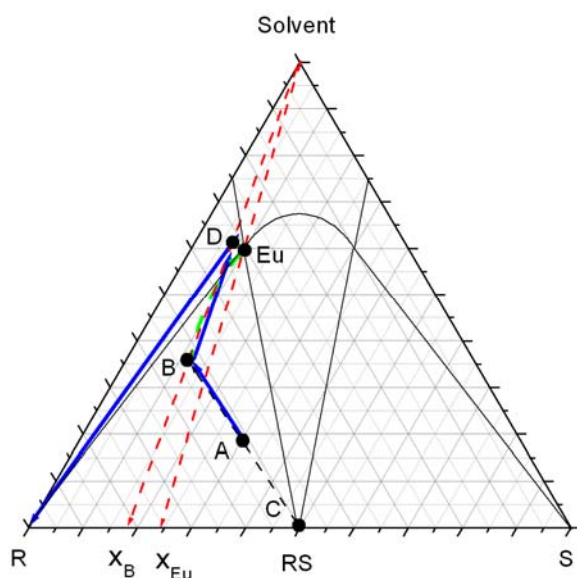

Figure 5.5: *A combination technique based on kinetic and thermodynamic operations.*

Thus, various direct crystallization techniques can be applied to perform enantioseparation for compound-forming racemates as described in this chapter. The experimental part of this thesis will validate some of the proposed methods with appropriate systems.

CHAPTER 6: EXPERIMENTAL DESCRIPTION

6.1 Introduction of three studied compound-forming racemates

Three chiral compounds are selected to validate the feasibility of enantiopurification for the most challenging and abundant chiral group, *i.e.* the compound-forming systems. These model compounds are namely lactide, 3-chloromandelic acid and arginine. The selection of those compounds is oriented towards development of general approaches which are able to apply for different scenarios of compound-forming racemates considering existence and mutual effects of different polymorphs or solvates.

6.1.1 Lactide – An industrial relevant compound

Lactide is another name of dilactide which is comprised of two molecules of lactic acid. There are two chiral centers existing in the structure of lactide which form mirror images of each other of the two enantiomers as presented in Figure 6.1. Kaemmerer *et al.* proposed that lactide is a compound-forming system[140].
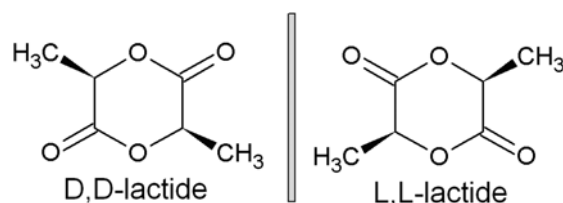

Figure 6.1: *Two enantiomers of lactide are non-superimposable mirror images of each other.*

Lactide is a precursor for polylactide (PLA) synthesis sequence. Based on renewable resources, developing sustainable and eco-efficient plastics including natural polymers, biopolymers, and synthetic polymers is the important trend of the 21st century.[141] Nowadays, the traditional existing oil-based polymers are gradually replaced by these bio-source materials. PLA is comparable to traditional plastics *e.g.* polystyrene, poly(ethylene terephthalate), etc. in both cost and performance aspects. There are plenty of applications of PLA in rigid packaging, flexible film packaging, cutlery, apparel and staple fiber, injection molded products (*e.g.* cups, bottles), etc.[142–146] In general, PLA is frequently produced via ring-opening polymerization catalyzed by a Sn(II)-based catalyst[147,148]. Additionally, PLA can be also produced by condensation polymerization directly from lactic acid. Mechanical properties of PLA depend strongly on the structure and composition of the polymer chains. Indeed, the ratios of the L- to the D-enantiomer of lactic acid can change PLA properties. The PLA comprising L-lactide only is a semi-crystalline material with the highest melting point, while PLA co-polymers with higher D-enantiomer contents exhibit lower

melting points.[149,150] Therefore purification of lactide is decisively importance for the PLA synthesis.

With respect to the precursor single lactide, this compound is widely produced by fermentation of sugar sources such as corn, sugarcane, tapioca, etc. which provide carbohydrate sources. Crude lactic acid usually contains many impurities such as acids, alcohols, esters, traces of sugars and nutrients[141,151]. However, the most challenging is the purification of the target enantiomer from the mixtures of various ratios of two enantiomers due to their mirror-symmetry relationship.

Lactide will be the first compound studied in this thesis. It represents the group of common chiral compound-forming systems which do not show any special behavior in solid state such as polymorphism or solvate formation.

6.1.2 3-chloromandelic acid (3ClMA)

The second case studied is 3ClMA, $C_8H_7ClO_3$. It is a derivative of mandelic acid. Many compounds in this family are interesting in drugs due to flexible skin penetration. That is based on their small molecular weights and sizes. This substance often presents in cosmetics, antibacterial agents, urinary excretions, etc. It is also used as an intermediate for the synthesis of other chiral molecules.[152] Pure enantiomers of 3ClMA can be produced by enzymatic sysnthesis.[153,154] However, the knowledge about 3ClMA is still limited, in particular solid phase behavior, solubility data, etc. Zhang *et al.* reported that 3ClMA is a racemic compound-forming system and the eutectic composition in the TPD (with a mixture of water and isopropanol as solvent) can be varied at different temperature.[155] Observations regarding to *e.g.* polymorphism and solid solutions have not been mentioned yet.

R- and S-enantiomers of 3ClMA are drawn as Figure 6.2. The carbon atom is a chiral center which joins to four different groups, *i.e.* hydrogen, hydroxyl, carboxyl and benzyl ring (attached to a chloro atom at the meta-position).
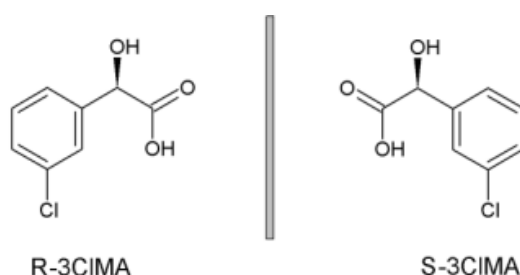

Figure 6.2: *Two enantiomers of 3ClMA.*

Besides 3ClMA, experiments also used other derivatives such as 2- and 4-chloromandelic acid (abbreviated as 2ClMA and 4ClMA). Using these derivatives arms to study the solubility behavior of this family in aqueous solution in which they show an interesting behavior so called oiling out (see details in Chapter 8). Finally,

mandelic acid is also used to validate applicability of a combination between preferential and selective crystallization.

6.1.3 Arginine

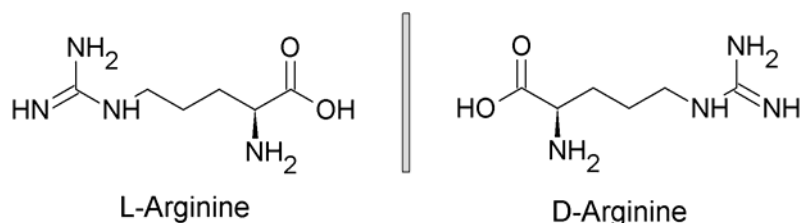Structures of enantiomers of the amino acid arginine are shown in Figure 6.3.

Figure 6.3: *Structure of enantiomers of arginine.*

Recently, arginine and its compounds with many organic, inorganic acids have been gained a great attention in the field of nonlinear optical materials. They are often used in many optical devices, *e.g.* optical switches, optical modulators and other electro-optical devices, owing to their practical applicability in the extension of the limited and fixed frequency outputs available from laser.[156–160] Arginine can be used as an additive to control crystal shape of other amino acids such as glutamic acid.[161] It is also an attractive pharmaceutical ingredient due to the different effects of two enantiomers on living organisms.[162–164] However, knowledge about several important properties of arginine is still limited, for example the formation of its hydrates has been not sufficiently understood. There is a lack of reliable solid-liquid equilibria (SLE) for designing and optimizing enantioseparation via crystallization processes. Klussmann *et al.* proposed that arginine is a conglomerate system.[165]

Large amounts of arginine can be found in protamine and histone. High concentrations of free arginine are also found in many plants including red algae, cucurbitaceae and conifer where it severs as nitrogen storage and transport form. Arginine is also able to be produced by bio- or chemical synthesis. Nowadays, the enantiomer L-arg is produced mainly by fermentation.[166,167] A small amount of it is isolated from protein hydrolysates. The enantioselective chemical or enzymatic catalysis based synthesis processes of arginine cannot be always fulfilled to produce enantiomerically pure substances. Indeed, chemical synthesis usually obtains racemic mixtures.[168] Therefore, the development of separation processes to resolve enantiomerically enriched solutions into pure enantiomers has gained high demand. With respect to partially enantiomerically enriched solutions, those can be yielded from various resources *e.g.* preparative chiral chromatography or enzymatic processes, etc.

6.2 Experimental plan

For all of the model compounds, systematic studies of both thermodynamic and kinetic aspects are carried out. These data are vital factors for rational enantiopurification design via direct crystallization. Experiments were planed as seen in Figure 6.4.
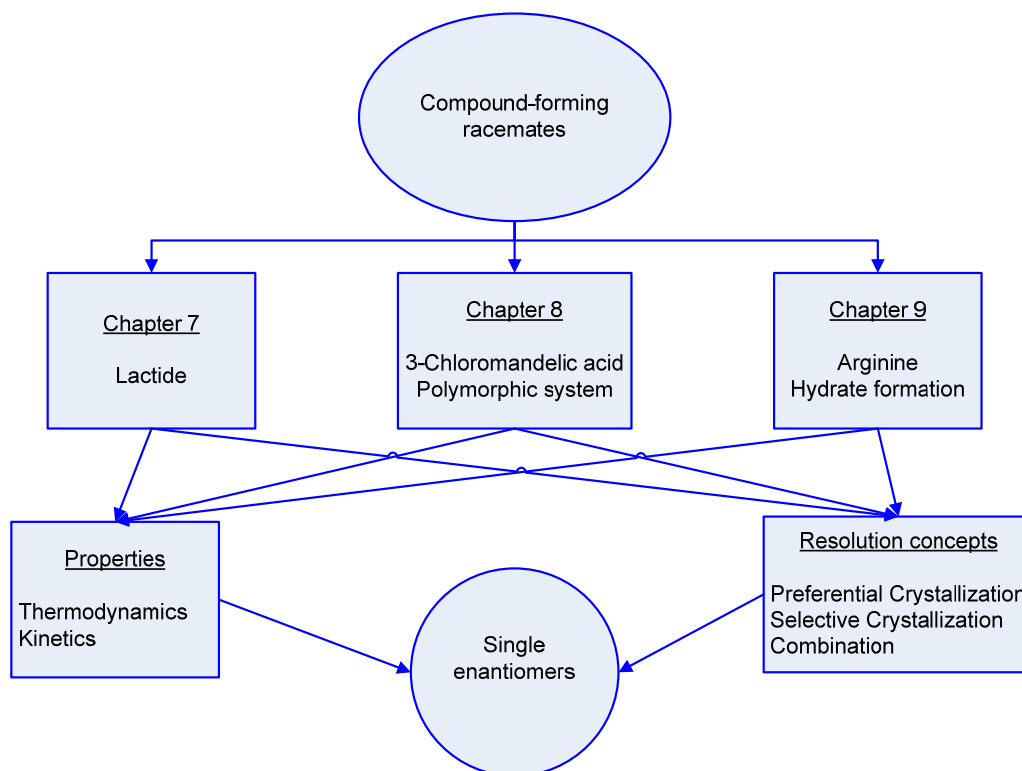

Figure 6.4: *Structure of the experimental part of the thesis.*

At first, solid phase analyses were applied to characterize the three selected systems. Lactide represents a standard compound-forming racemate while 3ClMA and arginine involve complex behavior of polymorphism and solvate formation. Based on the understanding about solid phase behavior, solid-liquid equilibria will be experimentally determined with assistance of model correlations. On the other hand, homogeneous nucleation determination was also carried out to support preferential crystallization. Finally, enantioseparation design based on different thermodynamic and kinetic operations were validated for each chiral system.

6.3 Analytical methods assist chiral characterization

In this thesis, a systematic investigation was performed for both the solid and liquid. With respect to the solid phase characterization, various techniques were frequently used including X-ray diffraction (applied for single crystals and powder form), thermal analysis and microscopic analysis. Other methods were also used such as mass spectroscopy, Raman, FBRM, etc. On the other hand, the liquid phases were followed by various analysis methods such as HPLC, optical rotation, density and refractometry measurements, turbidity observation via the Crystal16™, etc.

6.3.1 Solid phase analyses

6.3.1.1 Differential scanning calorimetry (DSC)

DSC is a powerful technique to determine solid properties such as thermodynamic properties, melting point phase diagram, polymorphism, solvate formation, etc.[169–172] Herewith, thermal analysis was performed with a DSC 131 (Setaram, France), which was regularly calibrated using standard high pure metals (indium, tin, and lead) in a medium temperature range. The measurements were carried out with a constant heating rate of 0.5 ^{o}C·min^{-1} in suitable temperature ranges (adapted for specific systems), under high pure helium (99.999%) atmosphere at 8 mL ^{o}C·min^{-1}. The substance was ground with a pestle and mortar to obtain fine powder. Amounts of 10–20 mg of samples were packed in closed aluminum crucibles of 75 μL. The measurements were executed with several samples of the same mixtures.

Coupled TG–DSC measurements (TG–DSC111, Setaram, France) allows us to determine simultaneously weight and enthalpy changes of a studied sample via specified heating programs. Measurement conditions were: 10–20 mg samples in open Al crucibles, a heating rate of 0.5 ^{o}C·min^{-1} and a Helium flow of 8 mL ^{o}C·min^{-1}. The calorimetric resolution of the instrument is 0.4 μW, the detection limit is 5–15 μW. The microbalance detection limit is 1 μg and the mass resolution is 0.4 μg.

6.3.1.2 X-ray Diffraction

X-ray powder diffraction (XRPD) is often used in solid phase determination.[73,173] The solid phases were analyzed by XRPD in an X'Pert Pro apparatus (PANanalytical GmbH, Germany). The radiation source was CuKα (λ = 1.5406 Å). Samples were measured on a Si holder and scanned from diffraction angles (2θ) of 3–40° with a resolution step size of 0.017^o and a counting time of 50 s for each step. Time-resolved XRPD was also used with the same above measuring conditions. The samples were exposed directly in ambient conditions and regularly analyzed by XRPD after planed periods.

In the experimental part, single crystals of several compounds were crystallized under suitable conditions. Then, single crystal X-ray diffraction (XRD) and structure analysis of these crystals were carried out by Dr. Hrib at Otto von Guericke University (Magdeburg).

6.3.1.3 Particle size distribution using inline and in-situ FBRM probe

The Focused Beam Reflectance Measurement (FBRM) is frequently employed to analyze inline and in real time particle size and/or particle population in liquid media.[174–177] The principle of probe is graphically presented in Figure 6.5. The FBRM probe is directly immersed in a liquid medium. A continuous beam of a monochromatic laser light is focused through the sapphire window of the probe into the medium. This beam is moved, and follows a circular path along the window

perimeter. Comparing to the high speed of movement of the beam, the particle motion in the fluid can be neglected. When the particles pass the probe window, the laser beam crosses their edges whereby the beam is reflected. The FBRM collects the backscatter and convert the received back-reflection beam into an electronic signal. In this thesis, a FBRM instrument from Mettler Toledo (S400A model) was used. This unit allows us to detect particle sizes between 0.5 microns and 2.5 mm.
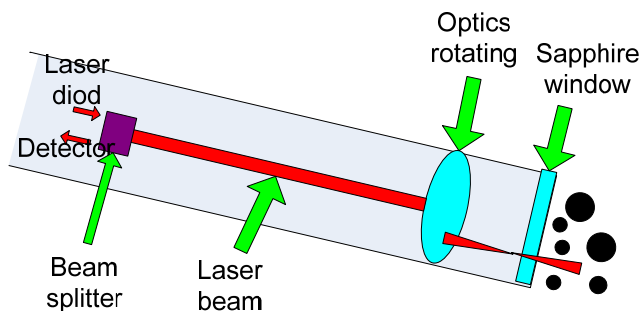
Figure 6.5: Schematic FBRM probe.

6.3.2 Liquid phase analysis

6.3.2.1 High performance liquid chromatography (HPLC)

HPLC is a frequently used as a high accuracy tool in analytical chemistry to identify and quantify interested substances in multi-component mixtures.[40,41] In this thesis, a chiral column (Chirobiotic-T; 250x4.6 mm) was used. The chiral stationary phase containing 5 μm sized particles coated with teicoplanin. The eluent was 0.7 mL·min^{-1} at a temperature 25 °C, defined diluted samples of 5 μL were injected for each measurement. For each system, a suitable calibration (Appendix D) was used to calculate concentration of the enantiomers.

6.3.2.2 Refractometry and density measurements

A Mettler Toledo refractometer model RE40 was used for the measurement of the total concentration. The light source is a light emitting diode of which beam passes through a polarized filter to obtain mono-wavelength at 589.3 nm. A high resolution optical sensor records the total reflection of the reflected light. This total reflection is converted into refractive index which relates to the total concentration of sample via a suitable calibration (Appendix D). This method has advantages due to a very short measurement time comparing to *e.g.* HPLC. Each measurement uses just few drops of a sample. Additionally, the sample temperature during measurement can be precisely controlled.

On the other hand, total concentration is also determined via density measurements. Density measurements were also performed with a density meter from Mettler Toledo (model DE40). This measurement is based on the electromagnetically induced

oscillation of a glass U-tube which is installed in the unit. A magnet is fixed to the U-tube and a transmitter induces the oscillation. This oscillation frequency will change when the glass tube is filled with a sample (gas or liquid). The vibration frequency is measured by a sensor and converted into density. The density meter does not require prior calibration of the model substance. The accuracy temperature can be adjusted before the measurements. This measurement is performed in a closed system therefore it is suitable for sensitive samples, *e.g.* easily recrystallizing solutes or volatile solvents.

6.3.2.3 Polarimetry

Optically active substances are able to rotate the plane of vibration of polarized light at a specific angle. For each substance, the specific optical rotation is a characteristic constant which can be used for its identity and purity analysis. In general, the rotation angle is a function of light frequency, sample concentration and composition as well as actual temperature. In the experimental work, a polarimeter Perkin Elmer (Model 341) is used with wavelength 680 nm and calibrations for each substance. A simplified polarimeter concept is schematically demonstrated in Figure 6.6.
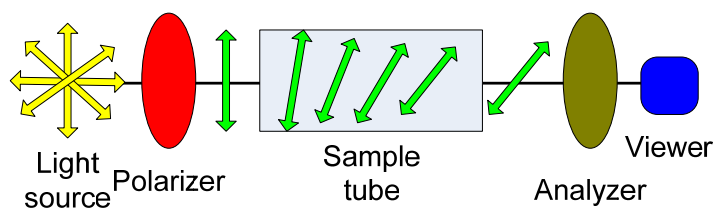

Figure 6.6: *Polarimetric measurement concept. The sample is placed in the tube (with flat glass ends). Polarized light which results from a polarizer is shone through the tube. The prism at the other end of the tube is attached to a recorder (e.g. an eye-piece) in order to measure the rotation angle.*

6.3.2.4 Turbidity observation with Crystal16™

The commercial apparatus Crystal16™ (Avantium, Netherlands) was used to monitor the turbidity of studied samples. Small samples of 1 mL scale were immersed in this apparatus. Magnetic stirrers were immersed. Temperature was controlled with the uncertainty of 0.01 °C. The results are analyzed using the Avantium's "CrystalClear" software.[178,179]

Turbidity observation was used in this thesis for multiple purposes such as determination of metastable zone width, induction time and saturation temperature of suspension. Moreover, turbidity observation also allows us to detect "oiling out" behavior since the formation of two immiscible liquids will change turbidity of the system. These experiments were carried out with closed vials of 1 mL and a stirring rate of 1200 rpm.

6.3.3 Solubility measurements

Solubility measurements were performed with both isothermal and polythermal methods[180] which gain good conclusions for all the three selected systems. Materials for solubility measurements as well as other parts of this thesis are summarized in Appendix E.

6.3.3.1 Isothermal solubility measurements

Double- or triple-wall jacketed vessels were connected to a thermostat (Lauda, Germany) and temperature was set constant. Solvents and excess amounts of solutes were placed into 5 mL closed vials which were immersed in the thermostated vessels. These samples were heated up above approximately 5 °C and kept about 60 min before finally adjusting to the target temperatures. The measured temperature ranges adapted to specific systems. These solutions were then stirred over 2–4 days with an electromagnetic device to ensure equilibrium conditions. The temperatures in the vessels were frequently checked with a Pt-100 thermometer (resolution of 0.01 °C). Subsequently, the liquid portion was separated using a syringe and a filter (PET-membrane, pore size 0.4 μm).

The weight fractions of the saturated solutions were determined using *e.g.* gravimetric method, HPLC, density or refractive measurement. For the three model compounds, these measurements are very representative and precise. As an advantage of this method, the liquid and solid samples at equilibria can be simultaneously analyzed. This advantage is very meaningful in studying complicated systems existing different polymorphs or solvates.

6.3.3.2 Polythermal solubility measurements

In this work, the commercial apparatus Crystal16™ was used to monitor turbidity and to detect saturation temperature where suspension becomes clear under suitable heating programs. Applied for sixteen unknown-samples, their saturation temperatures can be automatically and simultaneously determined. Initial materials were pre-crushed (or recrystallized) to have fine particles in order to obtain good turbidity signals. The suspensions of solutes and solvents were agitated about 6 hours before heating. Thermal programs were executed in a suitable temperature range with a constant heating rate of 0.02 °C·min^{-1}

In this thesis, the solubility is experimentally determined as weight fraction (w). Assuming that the solution of interest contains three components, *i.e.* the target enantiomer (a, [g]), the counter enantiomer (b, [g]) and solvent (c, [g]). Weight fraction of the target enantiomer (w_{enan}) is defined as Eq. 6.1. Besides, another term "enantiomeric composition" is also frequently used throughout this thesis and denoted as x. That considers only two enantiomers as mentioned in part 3.3. Since only two enantiomers are considered, the mole fraction and mass fraction are the same. Definition of x is introduced as Eq. 6.2.

$$w_{enan} = \frac{a}{a+b+c}, [-] \qquad \text{(Equation 6.1)} \qquad x_{enan} = \frac{a}{a+b}, [-] \qquad \text{(Equation 6.2)}$$

6.4 Homogeneous nucleation determination

Metastable zone widths were detected via turbidity observation using the Crystal16™. The saturated solutions were cooled down with different cooling rates of 0.01, 0.02, 0.035 and 0.05 ºC·min^{-1}. The Nyvlt's method was applied to estimate the maximal subcooling for specific saturated solutions. That correspond to the hypothetic "zero" cooling rate obtained from extrapolation of the above cooling rates. On the other hand, induction time was also determined from the Crystal16™ by measuring the period of which supersaturated solutions still retain clear under specific saturation degrees. Similar approaches applied for larger scales (vessels of 10 and 50 mL) but nucleation was detected via FBRM probe.[181,182] Magnetic stirrers were used at 350 rpm for large-scale measurements. The temperature was controlled by a thermostat Lauda and frequently checked with Pt-100.

6.5 Crystallization setup

Crystallization experiments were observed by online and offline procedures. For the online observation[183], experimental setup is shown as Figure 6.7. A crystallizer of 500 mL was agitated with a propeller (350 rpm). The filter allows us to transfer the clear mother liquor in pipeline (temperature controlled) into the polarimeter and the densitometer. These analyzers used suitable calibrations to define total concentration and enantiomeric compositions of these solutions. Then, the solutions were recycled back to the crystallizer. Simultaneously, variation of particle size distribution of the solid phase will be followed by the in-situ FBRM probe.
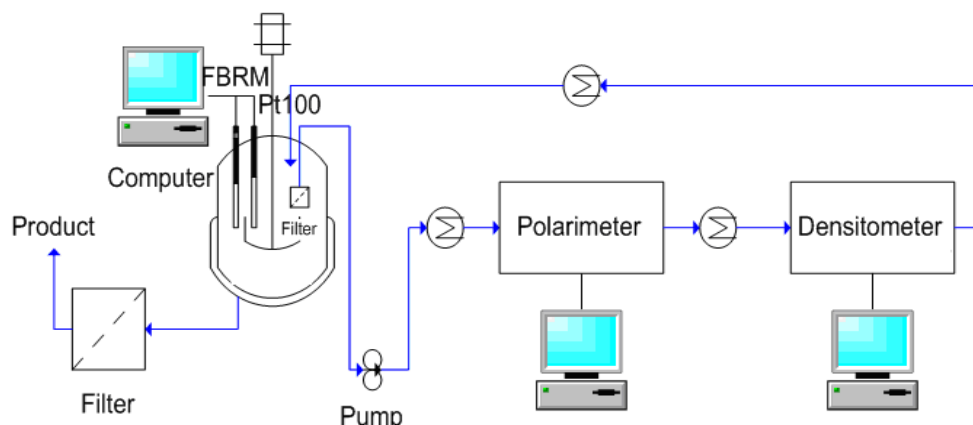

Figure 6.7: *Online monitoring of preferential crystallization via combination of polarimeter and densitometer with the in-situ FBRM probe.*

For the offline observation, the mother liquors were not connected to the above analyzers. The samples will be sampled with time schedule and measured offline with HPLC, density meter, refractometer and gravimetric method, etc.

CHAPTER 7:

LACTIDE, AN INDUSTRIAL RELEVANT CHIRAL COMPOUND

7.1 Solid phase investigation of lactide

Chiral discrimination in the solid state of racemates plays a crucial role for enantiopurification via crystallization. As mentioned in Chapter 2, there are three different crystalline racemates which need appropriate chiral crystallization techniques. Thus, determination type of racemate for the chiral lactide system can be considered as a fundamental starting point for a sustainable enantioselective crystallization process design. In this part, solid-state characteristics of lactide will be studied with various solid-phase analyses.

7.1.1 Thermodynamic properties of lactide via DSC determination

As listed in Table 7.1, the melting temperatures of the enantiomer and the racemate of lactide were determined via DSC measurements at values of 95.16 and 121.62 ^{o}C, respectively. Obviously, the phase transition from solid to melt of the enantiomer occurs significantly earlier than that of the racemate about 26.5 ^{o}C. By comparing the melting temperatures of those species, important information can be derived to classify appropriate chiral category for lactide.

Table 7.1: *Melting temperature and heat of fusion of chiral lactide species. (DSC determination with a heating rate of 0.5 ^{o}C·min^{-1}, temperature range of 30–140 ^{o}C).*

Thermodynamic properties		L,L-lactide	D,L-lactide
Melting temperature	[^{o}C]	95.16	121.62
Enthalpy of fusion	[kJ·mol^{-1}]	14.92	21.42

Indeed, these simple DSC measurements reveals that lactide does not belong to the group of conglomerate racemates due to the fact that solid of a conglomerate racemate always transforms into liquid earlier than the constituent enantiomers do. This concept contradicts observed data in Table 7.1. Thus, a hypothesis of conglomerate behavior for the lactide system can be simply rejected based on the above DSC data. However, a better understanding about proper type of the crystalline racemate of lactide is still an unknown since it can be either a compound-forming system or a solid solution. Then, X-Ray powder diffraction (XRPD) is applied for both the enantiomer and the racemate in next paragraphs.

7.1.2 Solid phase identification via XRPD measurements

The XRPD patterns of the enantiomers and the racemate of lactide are presented in Figure 7.1. Comparing XRPD patterns in Figure 7.1(a/b) and (d), the enantiomers and the racemate of lactide show totally different reflections. The pronounced reflexes of the enantiomers are found at *e.g.* 8.29, 12.92, 13.94, 16.69°, etc. while typical reflections of the racemate locate at positions of 11.25, 14.97, 21.19, 27.30°, etc. Thus, crystal structures of the enantiomers and the racemate of lactide are composited differently. In other words, the two enantiomers crystallize in the same unit cell to form a new stoichiometric compound in the crystalline racemate of lactide. Hence, lactide belongs to the well-known racemate group, *i.e.* racemic compound-forming systems. To validate this argument, the complete BPD is required.
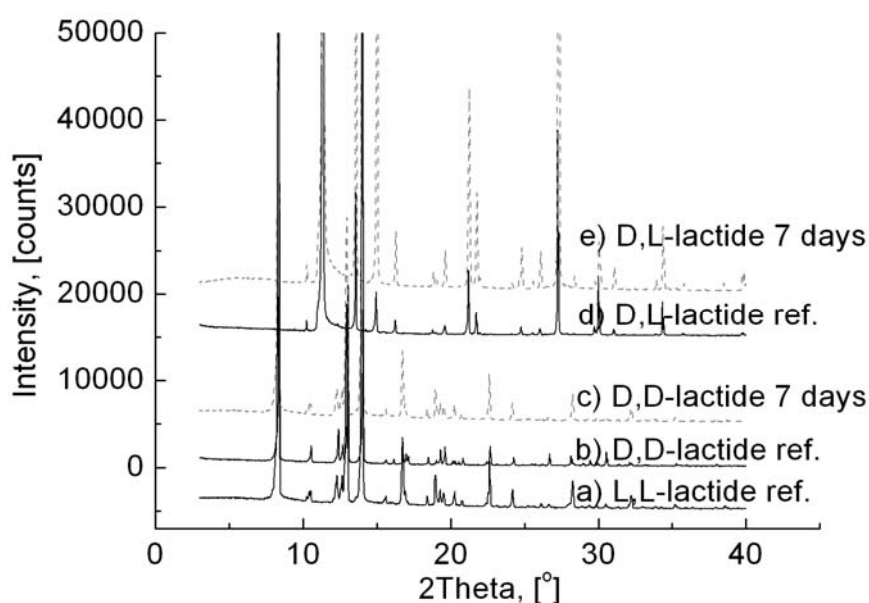
Figure 7.1: *XRPD patterns of lactide species. Patterns (a), (b) and (d) are the references of L,L-, D,D-enantiomer and D,L-lactide, respectively. (c) and (e) are XRPD patterns of samples exposed to moisture to qualify their stability.*

On the other hand, the stability of lactide species is also examined. Those crystals were directly exposed in ambient conditions in one week. Comparing patterns in Figure 7.1(c) and (e) with their corresponding references, the lactide samples contacted with moisture are relatively stable, their XRPD patterns are completely identical to the references (Figure 7.1(a/b) and (d) for the enantiomers and the racemate, respectively). In an extra work, those species were kept longer and they are quite stable within two-three months. Then, liquid layers appeared on top of vessels. In short, the hydrolytic dissociation of dimer lactide in moisture can occur with a relatively slow rate which can be considered as an advantage for lactide production.

Furthermore, lactide species are also quite stable in various media such as ethyl acetate (EA), methyl tert-butyl ether (MTBE), toluene, acetone, alcohols, etc. Solutions of enantiomeric composition about 75:25 percentages of L,L- and D,D-lactide

recrystallized from various solvents did not result in additional or new phases via XRPD determination (see Figure 7.2).
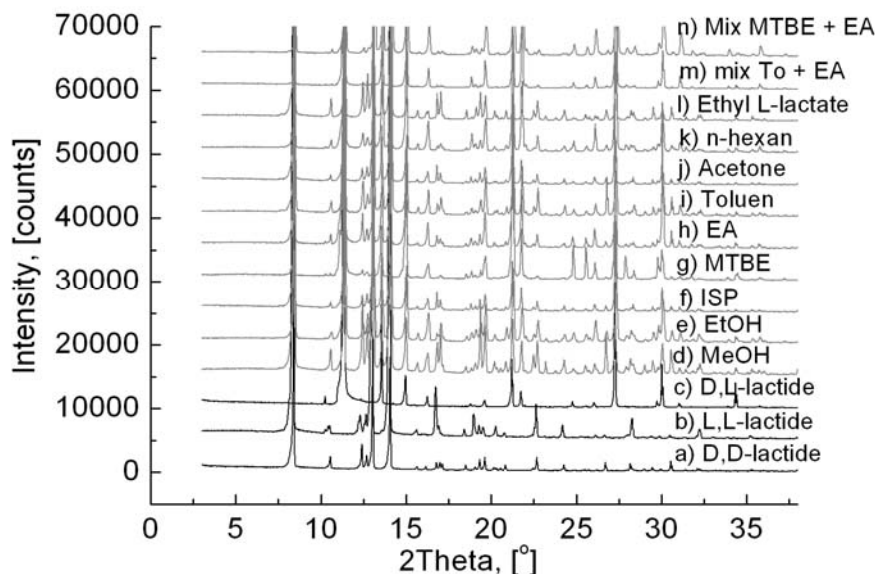

Figure 7.2: *From various solvents and solvent mixtures, recrystallized mixtures composed 75:25 percentages of L,L- and D,D-lactide show that their XRPD patterns are just overlay images of the pure enantiomer(s) and the racemate. Additional or new phases of lactide are not found.*

In principle, many chiral compounds can crystallize at different polymorphs or solvates depending on effects of temperature, media, impurity[63,64]. Herewith, information about possible existence of polymorphs or solvates can be also derived from Figure 7.2. The studied solvents included single solvents (Figure 7.2(d)–(l)) and solvent mixtures (Figure 7.2(m)–(n)). In all above solvents, those XRPD patterns perfectly match with the integrated patterns of the enantiomers and the racemate (references at Figure 7.2(a/b) and (c)). Furthermore, they are also identical to samples after DSC measurements (not shown in Figure 7.2 to avoid intricateness). Thus, under studied conditions, neither polymorph nor solvate was detected for lactide species.

7.1.3 Binary melting point phase diagram (BPD) of lactide

Similar to DSC measurements applied for single components, known-composition mixtures were prepared by dissolving different fractions of the two enantiomers in EA. Those mixtures were then recrystallized, dried and crushed to fine particles. Afterwards, DSC measurements were performed with these powder mixtures (a heating rate of 0.5 °C·min^{-1}). The BPD was constructed from various compositions of these binary enantiomeric mixtures and the results are presented in Figure 7.3.
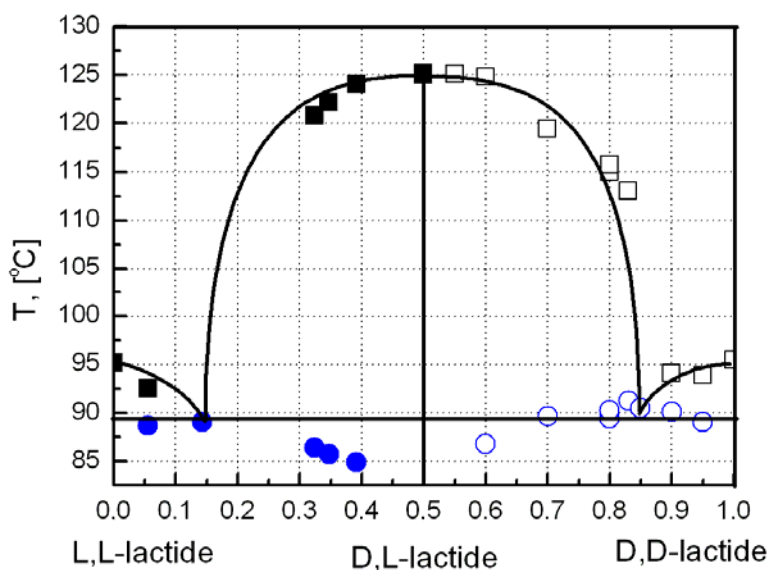
Figure 7.3: *The BPD of lactide shows a typical symmetric shape of a compound-forming racemate. Full dot and rectangular symbols represent DSC measurements. Open symbols were cited from literature[140]. The vicinity of racemate may form partial solid solutions but that will be not discussed here since crystallization design will just focus on the enantiomer side of this BPD.*

The obtained symmetric shape of the BPD around the racemate axis shows a good agreement of DSC determinations applying for both the L,L- and the D,D-enantiomers. Small deviation between the L,L- and the D,D-enantiomer sides may relate to the different impurities involved in the initial materials. However, this small deviation is still sufficient to derive the most important information of the BPD about type of crystalline racemate. Summarizing all results from X-ray diffraction, DSC measurements and the obtained BPD, lactide is a compound-forming system, *i.e.* the most challenging crystalline racemates to perform enantioseparation via direct crystallization. This conclusion gains good agreement with literature[140].

Two eutectic points, which have compositions at $x_{L,L}^{Eu}$ = 0.16 and 0.84, are detected in the BPD. Because of the symmetry relationship, only one eutectic point on the side of the target enantiomer is needed. Herewith, the eutectic composition at $x_{L,L}^{Eu}$ = 0.84 is considered for crystallization design in part 7.4.2.

7.1.4 Summary of the solid properties of the chiral lactide system

Systematic investigation proved that lactide belongs to the compound-forming systems. All the results of DSC, XRPD and the BPD gained a good agreement for this conclusion. In melt state, the eutectic composition at $x_{L,L}^{Eu}$ = 0.84 is taken into account for crystallization design. Lactide is such a good starting system in the systematic approach for enantiopurification of compound-forming racemates. This example represents the "standard" compound-forming system due to the fact that it is not

affected by polymorphism or solvate formation (a minority part in vicinity of the racemic axis is out of interest). The additional phenomena will be introduced via other model compounds in next chapters, *i.e.* 3-chloromandelic acid (a polymorphic system, Chapter 8) and the amino acid arginine (a solvate forming system, Chapter 9).

7.2 Solid-liquid equilibria (SLE) of lactide in solutions

In this part, solvents are added into binary mixtures of L,L- and D,D-lactide to study behavior of the corresponding TPDs. Although the shape of isotherms in the TPDs is basically similar to that of the BPD with two symmetric eutectic compositions around the racemic axis, presence of solvent(s) will change the internal interactions of chiral systems including solvent-solute, homochiral and heterochiral interactions[184,185]. The interaction variation can establish a new equilibrium with a new eutectic composition which may differ from that of melt equilibrium between only two enantiomers. That can result in shifts of the enantiomeric eutectic compositions. Studying eutectic shift behavior is also a major objective throughout this thesis. As described in Chapter 5, shifts of the eutectic compositions will support an innovating enantioselective crystallization approach based on thermodynamic control. One operation mode of this technique will be introduced in the end of this chapter. For that purpose, solubilities and the eutectic compositions of lactide in various media (single solvents and solvent mixtures) are needed.

7.2.1 SLE of lactide in single solvents

Single solvents (*e.g.* toluene, acetone, alcohols and a chiral solvent) are used to study SLE of lactide. In all constructed TPDs, the eutectic compositions are especially focused. Interactions of lactide species with different solvents are estimated via enthalpies of dissolution using the van't Hoff approach (Eq. 3.63).

7.2.1.1 SLE of lactide/toluene system

In Figure 7.4(a), pronounced deviations between experimental and ideal solubilities indicate non-ideal behavior of lactide solutions with toluene as solvent. Significantly lower solubilities of lactide species compared to those of the corresponding ideal cases are observed. The ideal cases were calculated from the equations of Schröder-van Laar (Eq. 3.21) and Prigogine Defay (Eq. 3.24). Based on determined solubility curves of the single lactide species as functions of temperature, the van't Hoff analysis was applied to estimate the enthalpies of dissolutions (ΔH^{diss}) as seen in Figure 7.5. Herein, ΔH^{diss} of the enantiomer and the racemate were found at +22.69 and +25.12 kJ·mol^{-1}, respectively. These values are significantly higher than the enthalpies of fusion ΔH^f (Table 7.1) for both the enantiomer and the racemate. According to Eq. 3.64, the difference between ΔH^{diss} and ΔH^f is equal to the enthalpy of mixing ΔH^{mix} which shows interactions of constituent components in solutions. The observed difference in Figure 7.4 apparently indicates non-ideality of those solutions. Comparing these ΔH^{diss}, higher solubilities of the enantiomer than those of

the racemate are expected due to less energy needed for the dissolution process of the enantiomer since these dissolution processes are endothermic. In fact, solubility of the enantiomer is approximately double than that of the racemate in the studied temperature range.
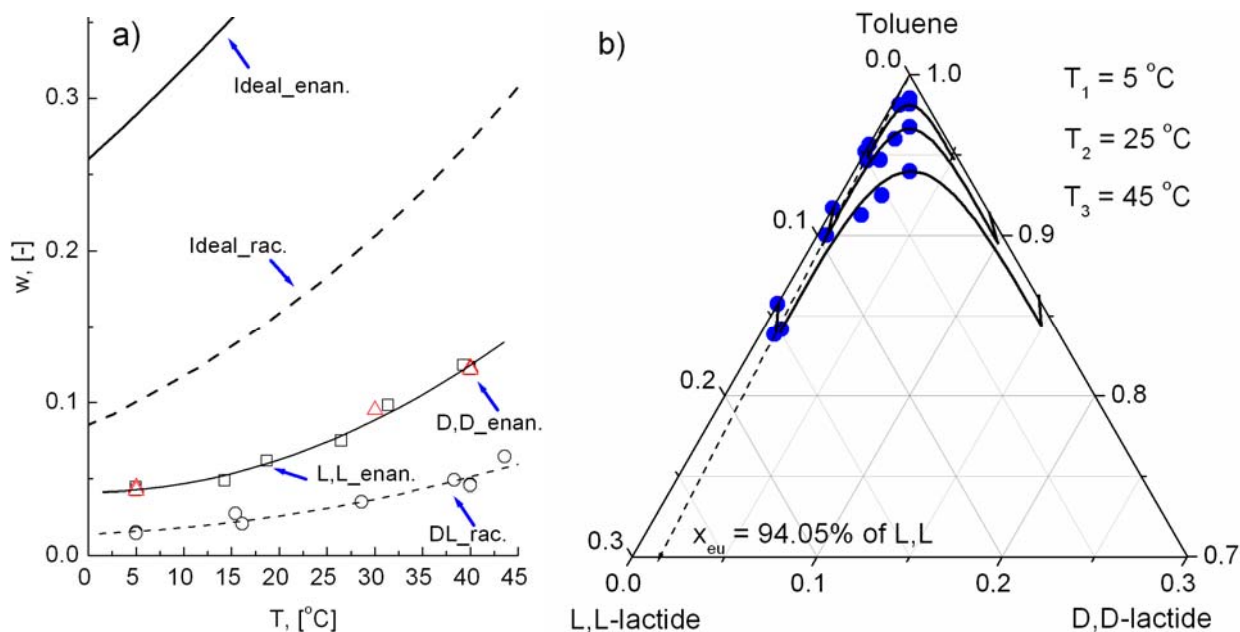

Figure 7.4: *(a) Binary solubility of lactide species in toluene, the ideal cases were calculated from the Schröder-van Laar (Eq. 3.21) and Prigogine Defay equation (Eq. 3.24); (b) TPD of lactide in toluene (zoomed in 30% area). Lines guide to the eyes.*
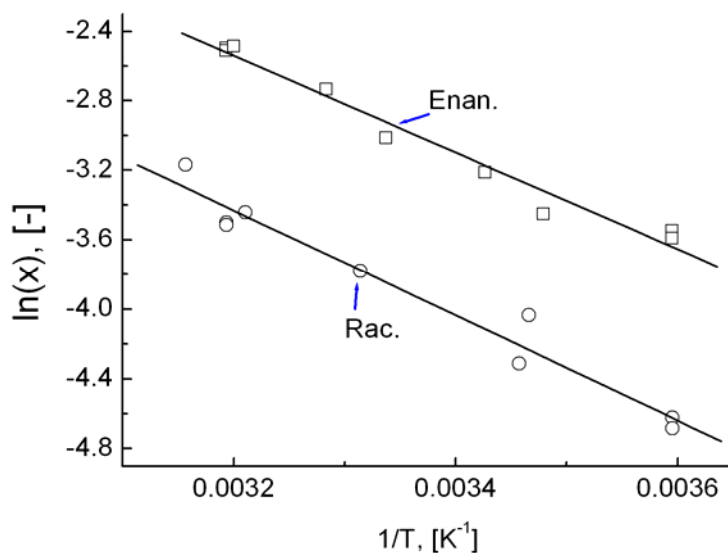
Figure 7.5: *The van't Hoff analysis applying for dissolution of the enantiomer and the racemate of lactide in toluene. The slope of linear relation (1/T vs. ln(x)) relates to enthalpy of dissolution ΔH^{diss}.*

On the other hand, as expected, solubilities of both the L,L- and D,D-enantiomers (represented by open triangle and open square symbols in Figure 7.4(a)) draw identical solubility curves of those species in toluene. In fact, toluene is an achiral solvent and therefore mutual interactions between this solvent and two enantiomers should be equal. Therefore, the symmetric isothermal solubility curves in the TPD are inferred. In Figure 7.4(b), isotherms were plotted at three temperatures 5, 25 and 45 °C. In fact, the isotherms were constructed from binary and ternary solubility measurements on the side of L,L-enantiomer, the other side was mirrored around the racemic axis.

Based on the Klussmann's approach[113] (Eqs. 3.60–3.62), an approximation of the eutectic composition can be calculated from the solubility ratios of the racemate and the enantiomers as discussed in Chapter 3. Alpha (α) is introduced (Eq. 3.61) and calculated at three temperatures as seen in Table 7.2.

Table 7.2: *The eutectic compositions of lactide in toluene at different temperatures, estimation via the Klussmann's approach is compared to experimental determination).*

Temp., [°C]	w.100, [-]		α, [-]	x_{L,L_cal}^{Eu}, [-]	x_{L,L_exp}^{Eu}, [-]
	Enan.	Rac.	Eq. 3.61	Eq. 3.62	
5	4.25	1.57	0.37	0.96	0.93
25	7.33	3.03	0.41	0.95	0.94
45	14.41	5.77	0.40	0.96	0.94

In Figure 7.4(a), solubility curves of the enantiomer and the racemate are not parallel in the studied temperature range. In principle, the solubility ratio alpha (α) should be also varied as expected. In Table 7.2, the eutectic compositions calculated from the Klussmann's approach slightly oscillate around 0.96. However, this variation is insignificant and negligible. The eutectic compositions based on the Klussmann's calculation appear to be unchanged. On the other hand, experiments show temperature-independent eutectic composition of lactide in toluene. Experimental values were found at x_{L,L_exp}^{Eu} = 0.94 in the temperature range between 5 and 45 °C. The difference of the enantiomeric eutectic compositions between experimental determination and estimation is about 2%. Because of simplicity of the Klussmann's equation, it is very useful in screening preliminary values of the eutectic compositions which can act as assistance for the fine eutectic composition determination. Additionally, the eutectic compositions between the BPD ($x_{L,L}^{Eu,BPD}$ = 0.84) and the TPD ($x_{L,L}^{Eu,TPD}$ = 0.94, experimental determination) are remarkably different which should be sufficient for an enantiopurification process exploiting the eutectic shift technique.

7.2.1.2 SLE of lactide in isopropanol (iPrOH) and acetone

Two solvents iPrOH and acetone result in absolutely different solubilities of lactide species. For instance at 20 °C, the solubilities of the enantiomer and the racemate in acetone are significantly higher than those in iPrOH about 40 and 20% (w/w) as seen in Figure 7.6(a), respectively. Lactide/iPrOH system shows pronounced non-ideal behavior as plotted in Figure 7.6(b) while lactide/acetone system appears close to the ideal solutions as depicted in Figure 7.6(c).
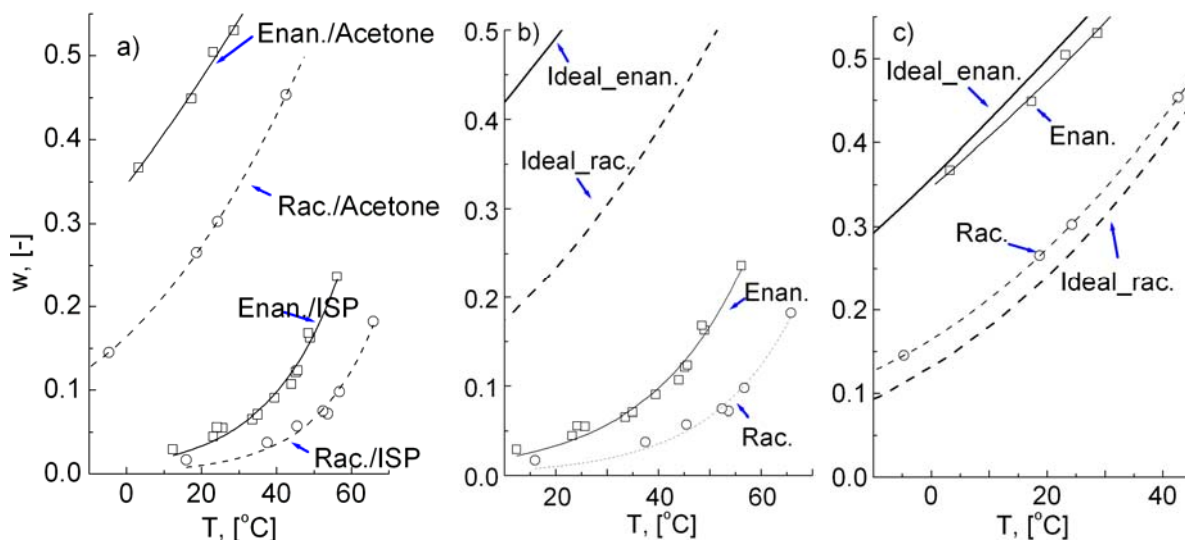
Figure 7.6: *Binary solubility of lactide species: (a) Comparison between two solvents iPrOH and acetone, (b) and (c) for the cases of iPrOH and acetone, respectively.*

In Figure 7.6(b) with iPrOH as solvent, the ideal solubility curves of both the enantiomer and the racemate are located significantly above those of the real solutions. That relates to the enthalpies of dissolution of the enantiomer and the racemate which were respectively calculated at values of +38.12 and +49.29 kJ·mol⁻¹ via the van't Hoff method. In contrast, the dissolution enthalpies in the case of acetone were found significantly lower values of +13.96 and +14.46 kJ·mol⁻¹ for the enantiomer and the racemate, respectively. Due to relative small energies needed for dissolution, both the enantiomer and the racemate result in very high solubilities in acetone. Furthermore, solubilities of the enantiomer are higher than those of the racemate.

Figure 7.6(c) shows SLE of lactide species in acetone. The solubility of the enantiomer appears rather ideal which means the homochiral interactions between the enantiomers do not strongly influence equilibrium state. However, interestingly, the solubilities of the racemate are even higher than its ideal state. That must relate to the influence of heterochiral interactions. Indeed, the heterochiral interaction energy of enantiomers is significant enough to compensate dissociation energy. The details need more quantities which will be not discussed here.

From solubilities of single components, the eutectic compositions can be derived using again the Klussmann's approach, similar to the case of lactide/toluene system. Table 7.3 summaries those values in comparison to experimental determination.

Table 7.3: *The eutectic compositions of lactide in two selected solvents, calculation versus experimental determination.*

T, [°C]	x^{Eu}_{L,L_cal} , [-]	x^{Eu}_{L,L_exp} , [-]
	IPA	
25	0.97	0.94
35	0.97	0.93
45	0.96	0.93
	Acetone	
0	0.92	0.95
10	0.92	0.94

As seen in Table 7.3, the variation of the eutectic compositions between experimental and estimated values in the cases of iPrOH and acetone are about 3.2 and 2.3%. The Klussmann's approach again shows potential applicability in screening of the eutectic compositions.
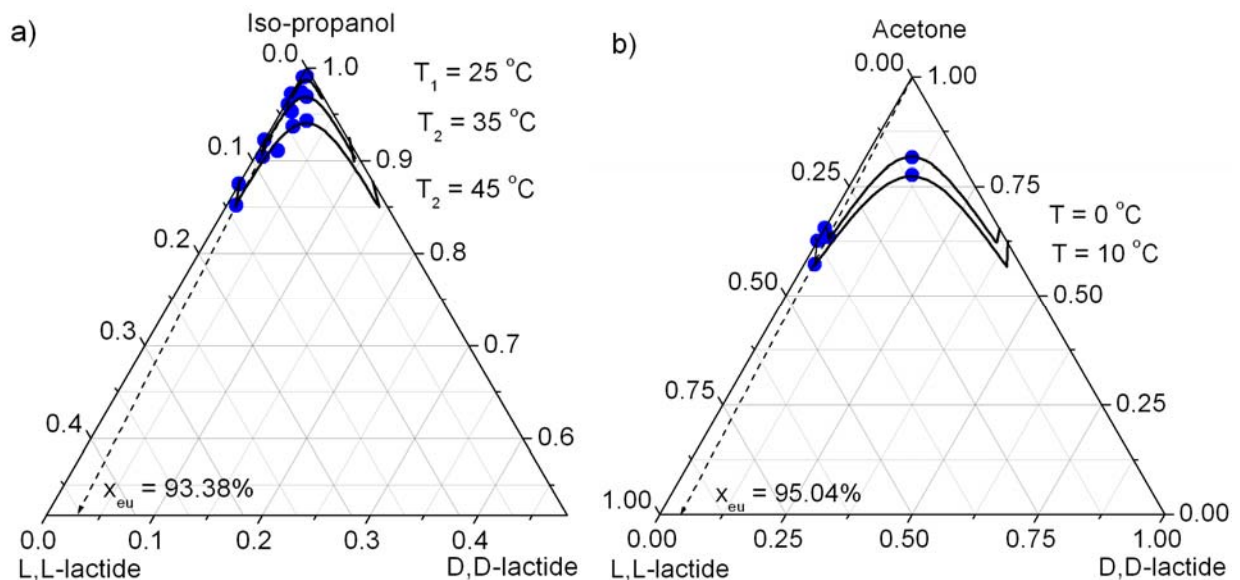
Figure 7.7: *The TPDs of lactide in two selected solvents: (a) lactide/iPrOH (scale of 50%) and (b) lactide/acetone systems.*

The TPDs of lactide in these solvents are represented in Figure 7.7. A clear trend is observed for both solvents that the eutectic compositions retain constant versus temperature (also see Table 7.3). As shown in Figure 7.6(b), even though solubility ratios of the enantiomer and the racemate in iPrOH are slightly different but the eutectic composition still does not change. Indeed, the eutectic composition in this solvent was found at $x_{L,L}^{Eu}$ = 0.93. Nevertheless, solubility curves of lactide species in acetone are rather parallel as depicted in Figure 7.6(c). Therefore, the eutectic composition is unchanged as expected. The eutectic composition in this case retains at $x_{L,L}^{Eu}$ = 0.95, higher than the previous cases about 2%.

7.2.1.3 SLE of lactide in ethyl L-lactate

Ethyl L-lactate is a chiral solvent which is composed from L-lactic acid. The aim of using this solvent is recognizing different chiral interactions between D,D- and L,L-enantiomer with this chiral solvent. If interaction difference is significant enough, the symmetry relationship of the lactide system can be broken to produce an asymmetric TPD.

However, as seen in Figure 7.8(a), both the D,D- and L,L-enantiomers result in the same solubility in this chiral solvent. Thus, interactions between each enantiomer and the chiral solvent are almost identical. The enthalpies of dissolutions of the D,D- and L,L-enantiomer are quite similar at +15.89 and +16.65 kJ·mol^{-1}. Consequently, the symmetric TPD is retained in which the eutectic composition is unchanged at $x_{L,L}^{Eu}$ = 0.95 comparing to 0.94 of an estimation using the Klussmann's equation. Recently, several chiral solvents were investigated and the same behavior was seen in literature. Both enantiomers yield the same solubilities in a chiral environment, for instance cases of N-methylephedrine[186] and mandelic acid[187].
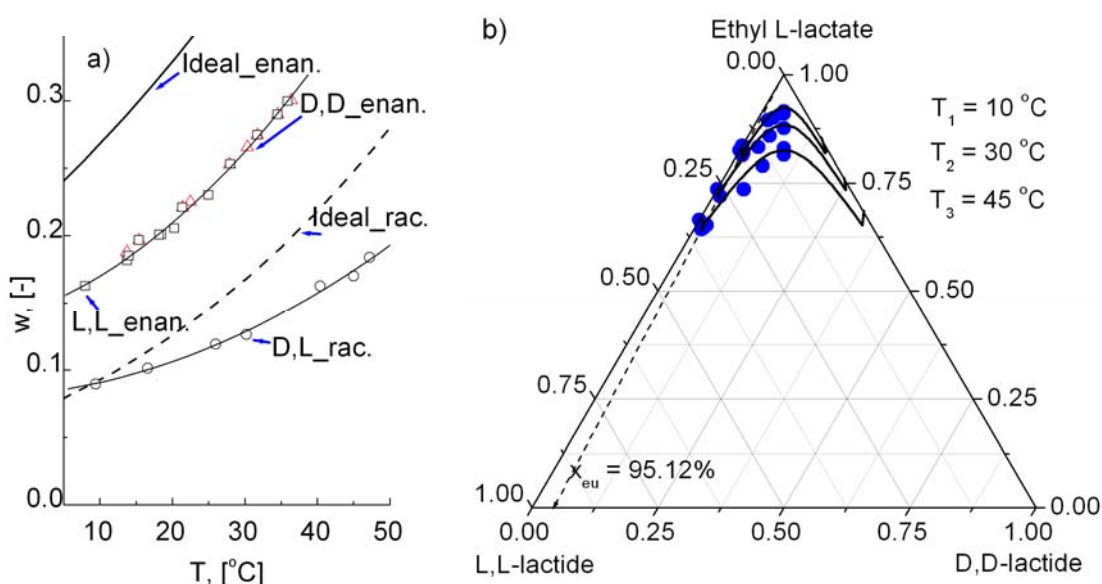
Figure 7.8: *A chiral solvent ethyl L-lactate is used in SLE investigation for lactide system.*

Interestingly, the solubilities of racemate appear close to ideal even though the enantiomers still clearly deviate from the ideal case. That tendency is quite clear at low temperature, but the difference is getting bigger at elevated temperature (see Figure 7.8(a)). Ethyl L-lactate is one more example which shows strong impacts of the heterochiral interactions in dissolution of lactide.

In short, the above solvents retain temperature-independent eutectic composition. In next paragraphs, the other single solvents will be used to expose an interesting phenomenon of lactide. In these solvents, the eutectic composition can be influenced by varying temperature (so called temperature effects) or exchanging solvents (so called solvent effects).

7.2.1.4 SLE of lactide in ethanol (EtOH)

Since ethanol is also a product in production line of lactide via fermentation processes, it is a preferred solvent for crystallization steps. Similar to the previous cases, non-ideality SLE behavior of lactide/EtOH system shifts solubility curves far from the ideal curves. Both the enantiomer and the racemate of lactide strongly deviate from the ideal cases due to their relatively large enthalpies of dissolutions at +33.09 and +37.08 kJ·mol^{-1}, respectively. Their solubilities are found at a moderate range which are not so high such solubilities in the cases of lactide in acetone or ethyl L-lactate but also not too low such those in the case of toluene.
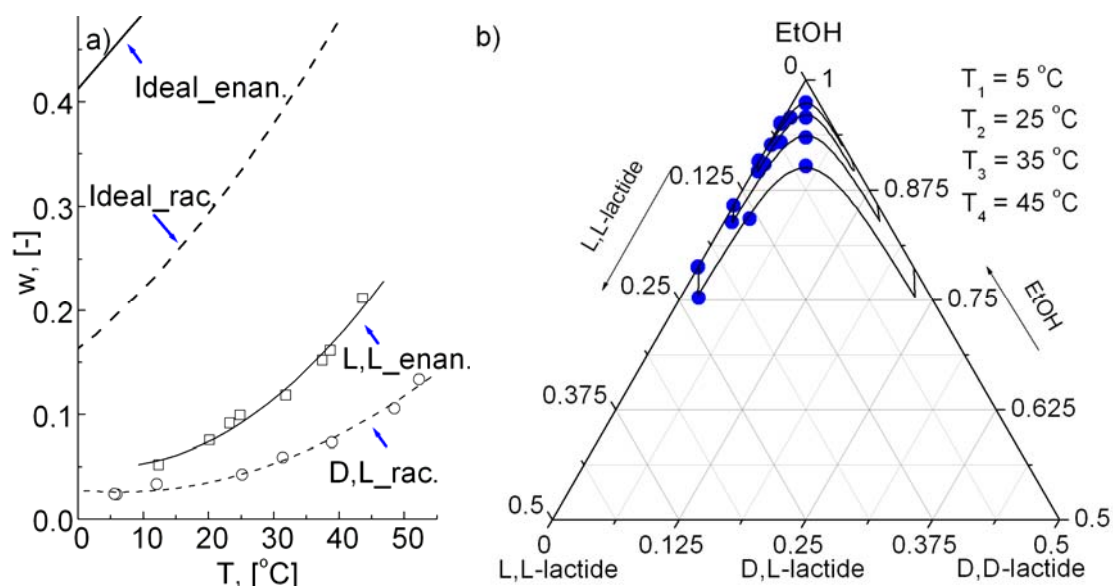
Figure 7.9: *Ethanol as solvent for SLE investigation of lactide system. This system shows the eutectic composition shift with respects to temperature. TPD is partially presented in a scale of 50%.*

A clear trend was seen form Figure 7.9(a) that solubility curves of the enantiomer and the racemate are increasing with different slopes in the investigated temperature range. In principle, that will change alpha values with respect to temperatures and lead to eutectic shifts based on the Klussmann's approach. In fact, the eutectic

compositions relatively change as plotted at four selected temperatures in Figure 7.9(b). Details are shown in Table 7.4.

Table 7.4: *The eutectic compositions of lactide in EtOH vary with temperatures.*

Temp., [°C]	w.100, [-]		x^{Eu}_{L,L_cal}, [-]	x^{Eu}_{L,L_exp}, [-]
	Enan.	Rac.		
5	4.9	2.5	0.94	0.97
25	9.1	4.2	0.95	0.95
35	14.2	6.5	0.95	0.94
45	21.2	9.7	0.95	0.93

Evidently, ethanol is a special solvent which can differently interact with two enantiomers at different temperatures. Thus, homochiral and heterochiral interactions of the enantiomers as well as interactions between the enantiomers and the solvent are influenced by temperature. That leads to the eutectic shifts under temperature effects.

7.2.1.5 SLE of lactide in ethyl acetate (EA)

EA is selected as a special solvent to study quantitatively homochiral and heterochiral interactions of the enantiomers as well as between solutes and solvent. This part will present both experimental and model correlation solubility of lactide. The experimental determination of SLE of lactide in EA was carried out in a temperature range from 10 to 45 °C and SLE was simulated with the NRTL model.
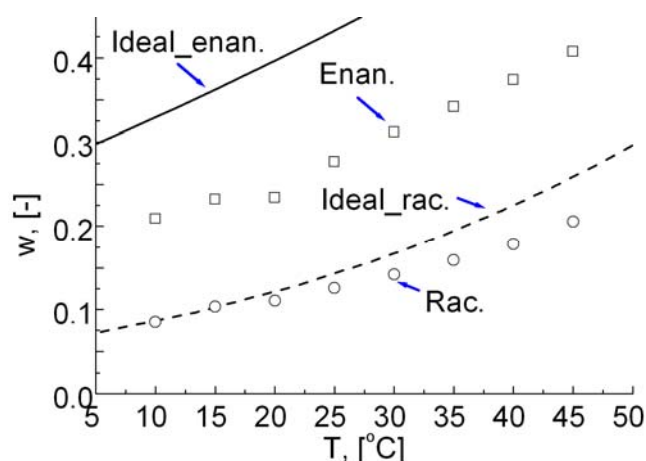
Figure 7.10: *Binary solubility of lactide species in EA. Open square, circle symbols represent solubility of the L,L- and D,L-lactide, respectively. Solid line and dashed curves were calculated from the equations of Schröder-van Laar and Prigogine Defay, respectively.*

The solubilities of lactide are shown in Figures 7.10. The solubilities of the L,L-lactide and D,L-lactide in EA increase almost linearly with temperature (Figure 7.10, square and circle symbols). A pronounced deviation of solubility from the ideal case is observed for the enantiomer (solid line in Figure 7.10). Interestingly, the solubility of the racemate is apparently close to ideal (dashed line in Figure 7.10).

Details of interactions are studied utilizing the local composition g^E NRTL model.

The NRTL model expresses the activity coefficient as a function of solution composition and temperature. In a first step, ideal solubilities (all activity coefficients set to unity) were computed using Eqs. 3.21 and 3.24 and the calorimetric values of the enantiomers and the racemate. The calorimetric data required for the modeling were obtained via DSC measurements (Table 7.1). Thus the NRTL model (Eq. 3.52) was firstly parameterized using the experimental values of the pure enantiomer in EA and the 3-parameter NRTL model. Herewith, heterochiral enantiomer-enantiomer interactions, denoted '1-2', were treated as ideal to estimate enantiomer-solvent interactions. Afterwards, the obtained parameters for the enantiomer-solvent interactions, denoted '1-3', were kept constant and enantiomer-enantiomer interactions were parameterized using the experimental solubility data of the racemate in solution (Table 7.5) and the 6-parameter NRTL model.

Table 7.5: *The parameter sets (1) and (2) for 3- and 6-parameter models of lactide in EA.*

Parameter set	α_{12}, [-]	Δg_{12}, [J·mol^{-1}]	Δg_{21}, [J·mol^{-1}]	α_{13}, [-]	Δg_{13}, [J·mol^{-1}]	Δg_{31}, [J·mol^{-1}]
1	0	0	0	4.117e-1	2.351e4	1.348e3
2	6.865e-9	5.515e5	-5.40e5	4.117e-1	2.351e4	1.348e3

The parameterization of solute-solvent interactions using the NRTL model allows us to fit the solubility curve through several experimental data points (Figure 7.11(a), solid line), (Table 7.5, set 1).

The usage of the same parameter set for the racemate results in a poor agreement with experimental data (Figure 7.11(a), thin dashed line). This simple test reveals pronounced heterochiral enantiomer-enantiomer interactions. Quantification and model parameterization in consideration of heterochiral interactions via the 6-parameter NRTL model (Table 7.5, set 2) yields a significant improvement comparing with experimental data (Figure 7.11(b)). Thus, the solubility of the racemate is not ideal, but the heterochiral enantiomer-enantiomer interactions compensate almost completely for the enantiomer-solvent interactions and render the solubility to appear as ideal.
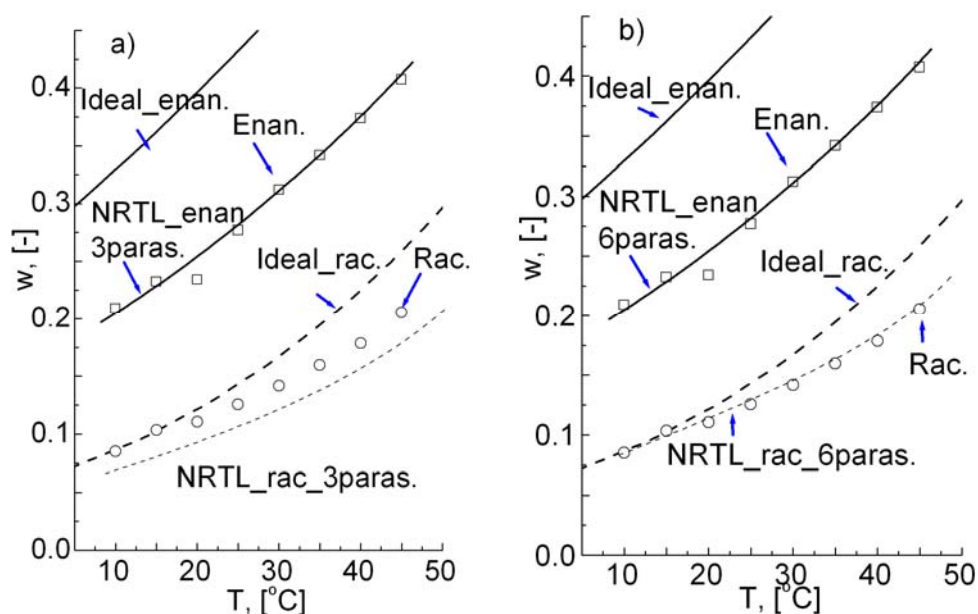
Figure 7.11: *Binary solubility of lactide species and simulation results utilizing different parameter sets: (a) the 3-parameter and (b) the 6-parameter NRTL model.*

The TPD is presented in Figure 7.12. The shape of isotherm curves in the TPD agrees with the results of DSC, XRPD, BPD that lactide is a compound-forming racemate. Figure 7.12 reveals a satisfying agreement of experimental data (symbols) and model prediction. At elevated temperatures, however, deviations are found in the vicinity of the eutectic composition. It can be observed, that the branch of the solubility isotherm of the enantiomer deviates significantly with increasing temperature. The opposite effect is observed from the experimental data. The results gain a good agreement with literature[140].
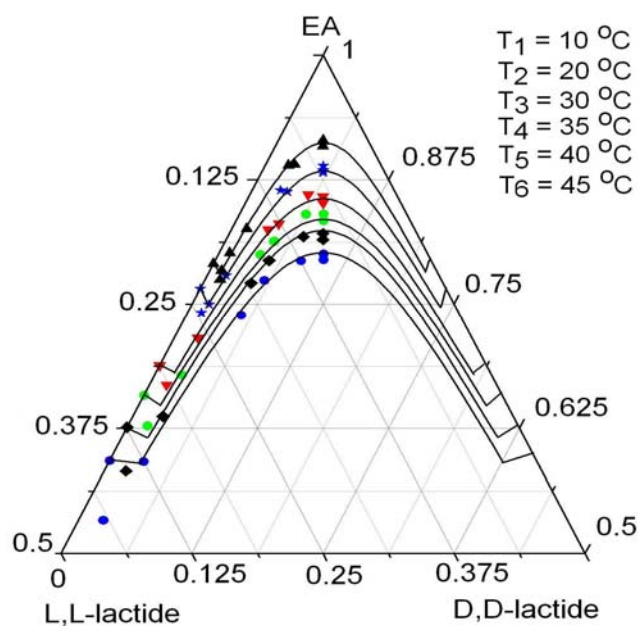
Figure 7.12: *TPD of lactide/EA system between 10 and 45 ᵒC. Zoomed in 50 % of TPD.*

With respect to eutectic composition determination, the intersections of the two branches of the solubility isotherms in Figure 7.12 for all temperatures were listed as Table 7.6. The Klussmann's method was again used to estimate the eutectic compositions. The eutectic compositions were experimentally defined at $x_{L,L}^{Eu}$ from 0.95 to 0.90 over the temperature range studied from 10 to 45 °C. On the other hand, the estimation of the eutectic composition in solution by the Klussmann's approach yielded the eutectic compositions which deviate from the experimental data. The SLE correlation based on the NRTL model results in close data to experimental determination. The presented thermodynamic SLE model allows rather accurate representation of the binary solubilities using 6 parameters. The estimation of the temperature-dependent eutectic composition in solution using 6 parameter set significantly improved in comparison to the Klussmann's model. High accuracy of the NRTL model for chiral systems has been examined in literature[186–190]. The prediction of the TPD on the basis of binary solubility data obtained a satisfying agreement. The retaining deviations between model and experimental data at elevated temperatures may originate from experimental uncertainties or model insufficiencies, which can currently not be specified in more detailed.

Table 7.6: *The eutectic compositions of lactide/EA system via different determinations.*

T, [°C]	Eutectic composition, $x_{L,L}^{Eu}$ [-]		
	Klussmann	NRTL	Exp.
10	0.96	0.93	0.91
15	0.95	0.93	0.95
20	0.94	0.94	0.94
25	0.95	0.95	0.93
30	0.95	0.94	0.92
35	0.94	0.93	0.91
40	0.94	0.93	0.90
45	0.94	0.93	0.90
melt	-	0.85	0.84

The eutectic composition change is an interesting phenomenon which was found here for both ethanol and EA. In principle, increasing number of components can vary the interactions of system and may establish different eutectic compositions. In

the next paragraph, a quaternary system is introduced in which one co-solvent is added into lactide/EA system.

7.2.2 Quaternary phase diagram – SLE in various mixture compositions of EA:MTBE

As seen in the previous part, lactide species dissolve quite well in EA as solvent. In contrast, preliminary measurements showed extremely low solubility of lactide in methyl tert-butyl ether (MTBE). In this part, mixtures of these two solvents EA and MTBE are used for further SLE investigation. In Figure 7.13, obviously, MTBE acts as an anti-solvent for lactide solution based EA solvent. Both solubility surfaces possess negative slopes when increasing MTBE amounts. Hence, MTBE can be used for an anti-solvent crystallization which is an attractive technique as described in literature[191–194].

As presented in Figure 7.13, temperature variation results in parallel solubility curves of the enantiomer and the racemate at each solvent composition. Due to parallel solubility curves, solubility ratios between the racemate and the enantiomer retain at constants for each solvent composition. Therefore, the enantiomeric eutectic composition does not change with respect to temperature as seen in Table 7.7.
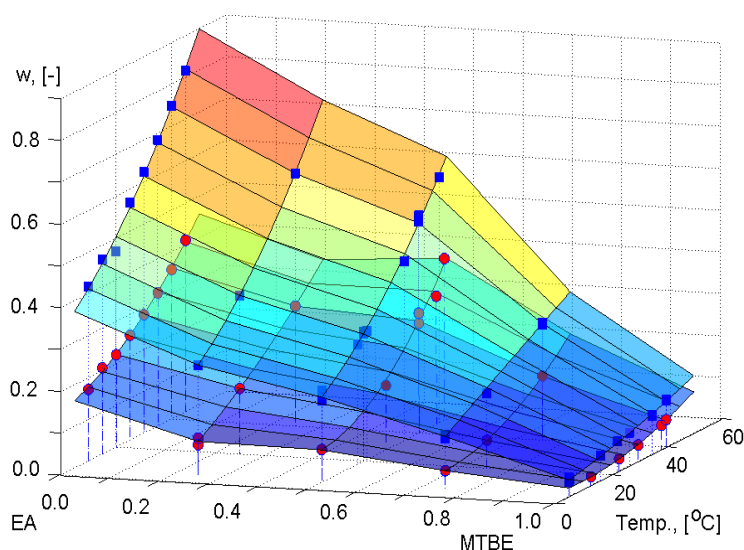
Figure 7.13: *Solubilities of lactide species in coordination of temperature and the solvent composition EA/MTBE. Square and circle symbols correspond to the enantiomer and the racemate, respectively. Surfaces guide to the eyes.*
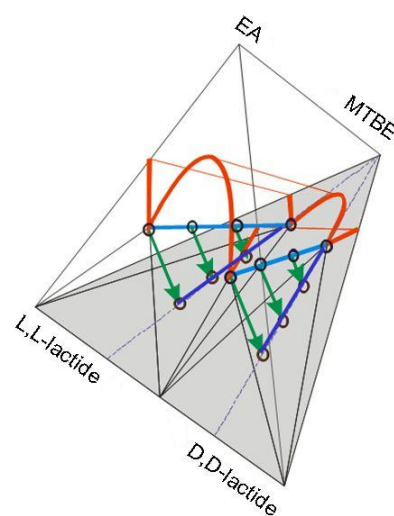
Figure 7.14: *Schematically presentation of the quaternary phase diagram of lactide in solvent mixtures (EA/ MTBE).*

The quaternary solubility phase diagram is schematically represented in Figure 7.14. This figure is helpful in a systematic view but rather difficult for further usage. A simplification was done by projecting each of selected solvent compositions in the separated TPDs which are plotted in Figure 7.15.
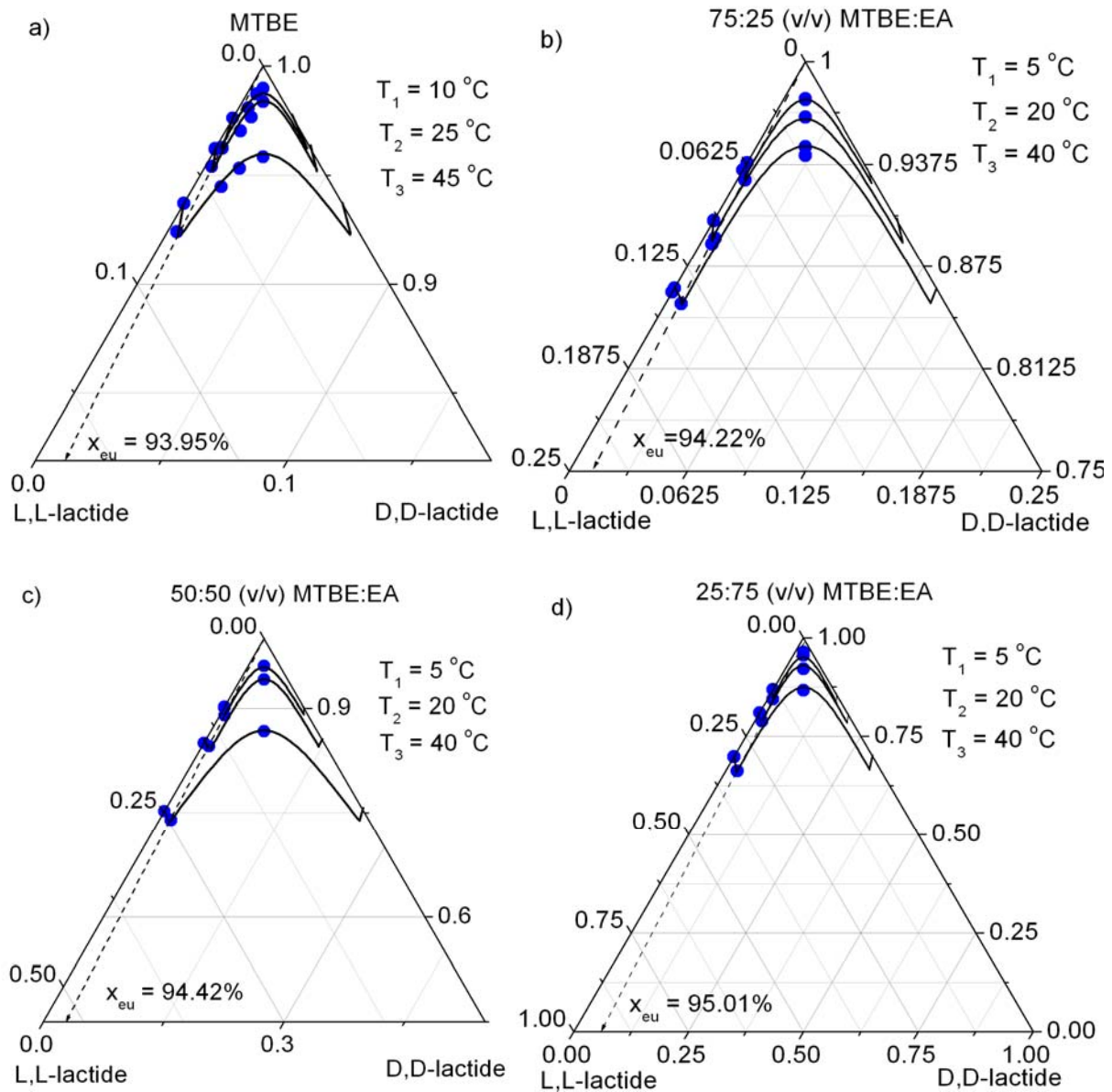
Figure 7.15: *Individual TPDs of lactide in different solvent mixtures of EA and MTBE.*

Table 7.7: *The eutectic compositions at different solvent compositions of EA and MTBE.*

EA:MTBE (v/v)	x_{L,L_cal}^{Eu} ,[-]	x_{L,L_exp}^{Eu} ,[-]
75:25	0.98	0.95
50:50	0.98	0.94
25:75	0.98	0.94
0:100	0.95	0.93

In principle, adding one more solvent to form quaternary system can vary internal interactions of the chiral solution. That may lead to establish a new equilibrium which possesses also a new eutectic composition. However, EA/MTBE mixtures did not show this behavior. From Table 7.7 and Figure 7.15, an important conclusion can be derived that the eutectic composition of lactide system in solvent mixtures of EA/MTBE is temperature- and solvent-independent. Just only the case of pure MTBE as solvent is relatively different and the rest solvents show negligible deviations around 94%.

7.2.3 Summary of SLE lactide

In all solubility measurements, the residual solid phases of lactide from solubility measurements were analyzed by XRPD. The results show that all samples have the same XRPD patterns as the initial materials, thus no new or additional phase exists. This indicates that lactide crystals are stable and no decomposition or solvate formation took place during the solubility experiments. Polymorphism was also not found for this system under the studied conditions. The shape of all isotherm curves in the TPDs reveals that lactide is a racemic compound-forming system. In several cases such as EtOH and EA, the eutectic compositions are effected by temperature and solvent. That variation was found $x_{L,L}^{Eu}$ from 0.90 to 0.97 (as highlighted in Table 7.8) which significantly differ to the eutectic composition of melt state ($x_{L,L}^{Eu}$ = 0.84).

Table 7.8: *Summary eutectic compositions of lactide system in various solvents.*

Solvent	Temperature range, [°C]	$x_{L,L}^{Eu}$, [-]
Toluene	5–45	0.94
Isopropanol	25–45	0.93
Acetone	5–35	0.95
Ethyl L-lactate	10–45	0.95
Ethanol	5–45	0.93–0.97 (*e.g.* 0.95 at 25 °C)
Ethyl acetate	10–45	0.90–0.95
MTBE : Ethyl acetate		
25 : 75	5–40	0.95
50 : 50	5–40	0.94
75 : 25	5–40	0.94
100:0	10–45	0.93

7.3 MSZW and morphology of lactide in EA

Data of MSZW are essential kinetic parameters for crystallization design. MSZW determination is one of the most time-consuming tasks. In this part, MSZW and crystal morphology of lactide species will be studied.

7.3.1 MSZW determination via the Nyvlt's method

Besides effects of *e.g.* volume of crystallizer, stirring rate, additive, etc. cooling rate is one of the most important factors which can alter nucleation. Different cooling rates lead to different nucleation temperatures with the same solutions under the same other conditions. Therefore, Nyvlt developed a model that considered a "zero" cooling rate to detect the metastable zone limit. In this work, various cooling rates including 0.01, 0.05, 0.1 and 0.2 ^{o}C·min^{-1} were applied to saturated solutions of lactide in EA. All experiments were performed with the Crystal16™, repeated 5–7 times to take average values. An extrapolation of nucleation temperatures versus cooling rates allows detecting nucleation temperature at the "zero" cooling rate. Figure 7.16(a) and (b) show the nucleation of L,L- and D,L-lactide at different cooling rates, respectively.
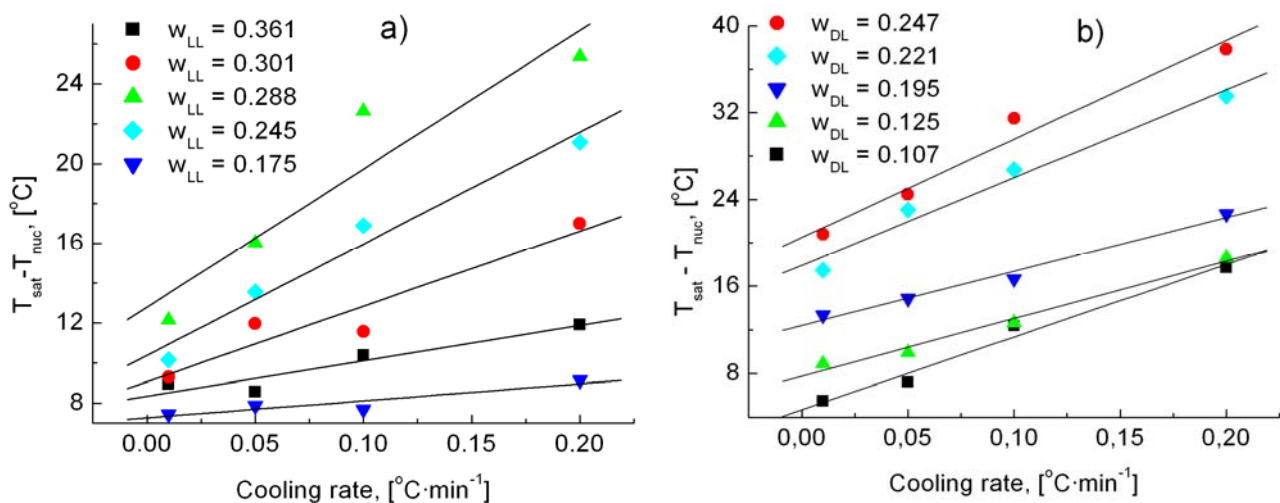
Figure 7.16: *Estimation nucleation temperature at the "zero" cooling rate via the Nyvlt's method.*

From nucleation temperatures corresponding to the "zero" cooling rate, difference between saturation and nucleation temperatures are defined as $\Delta T_{max} = T_{sat} - T_{nuc}$. Those values are plotted as functions of temperature as Figure 7.17.
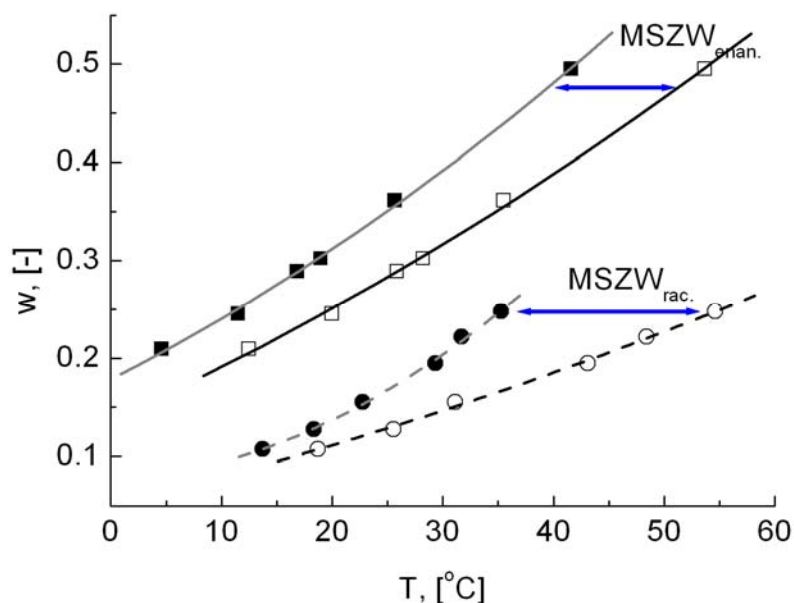
Figure 7.17: *Solubility and MSZW of lactide species in EA. Rectangular and circle symbols stand for the enantiomer and the racemate; open and full symbols for solubility and metastable zone limit.*

Obviously, MSZW of the racemate is narrower than that of the enantiomer at temperatures lower than about 34 °C. This is obviously a drawback to produce the pure enantiomers via kinetically preferential crystallization. The reason is during crystallization of the target enantiomer, the racemate can easily contaminate the solid product of the target single enantiomer (entrainment effects). Therefore, these MSZWs indicate disadvantages of applicability of preferential crystallization for the enantiomers of lactide in EA. This gains a good agreement with results from the TPDs for these studied solvents above in which extended solubility lines (metastable solubility) belong to the three-phase domains. That is not favorable conditions for preferential crystallization comparing to cases of the metastable solubility curves belong to the two-phase domains.

In short, the data from MSZWs do not support for preferential crystallization to separate the single enantiomers. The other alternative based on thermodynamics is recommended for the lactide system. All the eutectic shifts were found in parts 7.1 and 7.2 will supports for a special technique so called the "two-step" process to purify the single enantiomers.

7.3.2 The critical parameters of primary nucleation

To have further understanding about primary nucleation of lactide species, quantification of nucleation parameters is estimated utilizing MSZW data. The basis of this model was already introduced in Chapter 4.

Herein, the objective parameters of nucleation including interfacial energy σ (Eq. 4.5), critical free energy of formation ΔG_{crit} (Eq. 4.7), and radius of critical nucleus r_{crit} (Eq. 4.8) will be evaluated at different temperatures (T) and degrees of supersaturation (S). The results are shown in Table 7.9.

Table 7.9: *Quantification of homogeneous primary nucleation parameters lactide in EA.*

T	S	σ	r_{crit}	ΔG_{crit}
[°C]	[-]	[J·m^{-2}]	[nm]	[mJ·m^{-3}]
		Enantiomer		
12.52	2.89	3.54.10^{-3}	0.615	0.562
20.44	2.93	3.69.10^{-3}	0.623	0.600
25.81	2.97	3.80.10^{-3}	0.630	0.634
28.27	2.99	3.86.10^{-3}	0.635	0.654
35.53	3.01	3.98.10^{-3}	0.639	0.682
53.79	3.22	4.46.10^{-3}	0.677	0.857
		Racemate		
18.72	2.14	2.61.10^{-3}	0.442	0.214
25.53	2.58	3.31.10^{-3}	0.549	0.418
31.1	2.76	3.61.10^{-3}	0.588	0.525
43.08	3.69	4.83.10^{-3}	0.756	1.159
48.38	4.16	5.36.10^{-3}	0.825	1.530
54.59	4.52	5.78.10^{-3}	0.874	1.850

From those data, one can compare nucleation abilities of the enantiomer and the racemate. The free energy of formation for critical nuclei of the enantiomer just slightly increases with respect to temperature while that significantly increases for the racemate. A comparison is graphically presented in Figure 7.18.
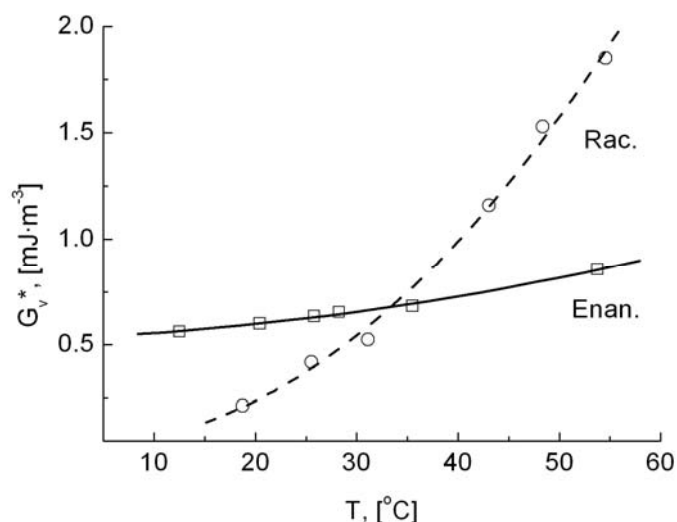
Figure 7.18: *Critical free energies of formation for homogeneous nucleation of the enantiomer and the racemate in EA as solvent. There is an intersection point at about 34 ºC where nucleation priority of the enantiomer and the racemate changes.*

Evidently, at temperatures higher than 34 ºC, the enantiomer is easier to form nucleus than the racemate does. Thus, this temperature range is preferred to obtain pure enantiomer by preferential crystallization. Nevertheless, EA is a strongly volatile solvent so that the crystallization process should be operated at lower temperatures. However, in such conditions, the racemate can simultaneously crystallize together with the enantiomer. Consequently, preferential crystallization is not recommended for purification of this system.

7.3.3 Crystal morphology

Typical crystal morphologies of lactide are introduced as Figure 7.19. Crystallized from EA, the racemate shows cubic shape while the enantiomer usually obtained as rod-like shape. In other solvents, the morphologies of those crystals are strongly changed. For instance the enantiomer crystallizes as very thin needle-like shape in ethyl L-lactate.
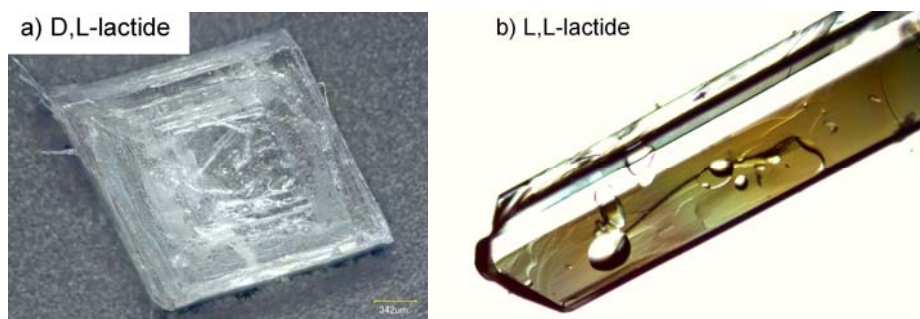
Figure 7.19: *Crystal morphologies of (a) the racemate and (b) the enantiomer of lactide recrystallized from EA as solvent. From saturated solutions at 35 ºC, temperature was kept at 25 ºC in one week to obtain these single crystals.*

7.4 Design of separation process

Since applicability of preferential crystallization is limited by the MSZW of the racemate as discussed above, this part will focus on developing enantioseparation methods for the lactide system based on thermodynamic approaches. From data of SLE in the previous sections, two purification techniques will be validated in this part considering different purity levels of final products. Depending on different applications, final products of lactide can be accepted at a moderate level or high purities. For instance, polylactide (PLA) is recently used to produce bioplastic bags of which the mechanical and physical properties are strongly influenced by ratios of the L,L- and D,D-enantiomers in polymer chains. An optimal ratio of these enantiomers for a specific product will be considered in terms of degradation time, physical and mechanical properties of PLA, and economic aspects as well. Nevertheless, in other special applications such as surgical blades, medical knives, threads, etc. high performance PLA resins require significantly higher purity of the single enantiomer(s).

Two assumptions are necessarily noticed here for the following process design. *(i) The studied solutions are assumed to be composed of the two enantiomers and a solvent.* In fact, lactide is normally produced in fermentation processes. Purification lactide from other products *e.g.* glutamic acid, citric acid, etc. is not an issue due to the solubility difference of these materials. The most challenging is separation of two enantiomers from each other because of their symmetry relationship. Therefore, the initial solution of a process design below is considered as the last state of purification sequence which contains only two enantiomers and a solvent. *(ii) Furthermore, asymmetrically enantiomeric mixtures are assumed for the initial solution.* That means the initial solution is already (even slightly) enriched in the target enantiomer. In fact, lactide mixtures can be enriched in one enantiomer via enzymatic reactions, or via subsequent steps after chemical reactions such as chiral chromatography, selective membrane, etc.

7.4.1 Option 1

Crystallization can be used to produce lactide with a moderate purity level. This option is critically limited by the enantiomeric eutectic compositions. For further applications needed higher purity, this technique can be considered as a chiral enrichment step.

7.4.1.1 The concept of method

The principle of this technique bases on equilibria in the three-phase domain of a TPD. Starting with an enantiomerically enriched solution, one can reach the purity at the eutectic composition via only one simple classical crystallization step. The process is schematically depicted in Figure 7.20.
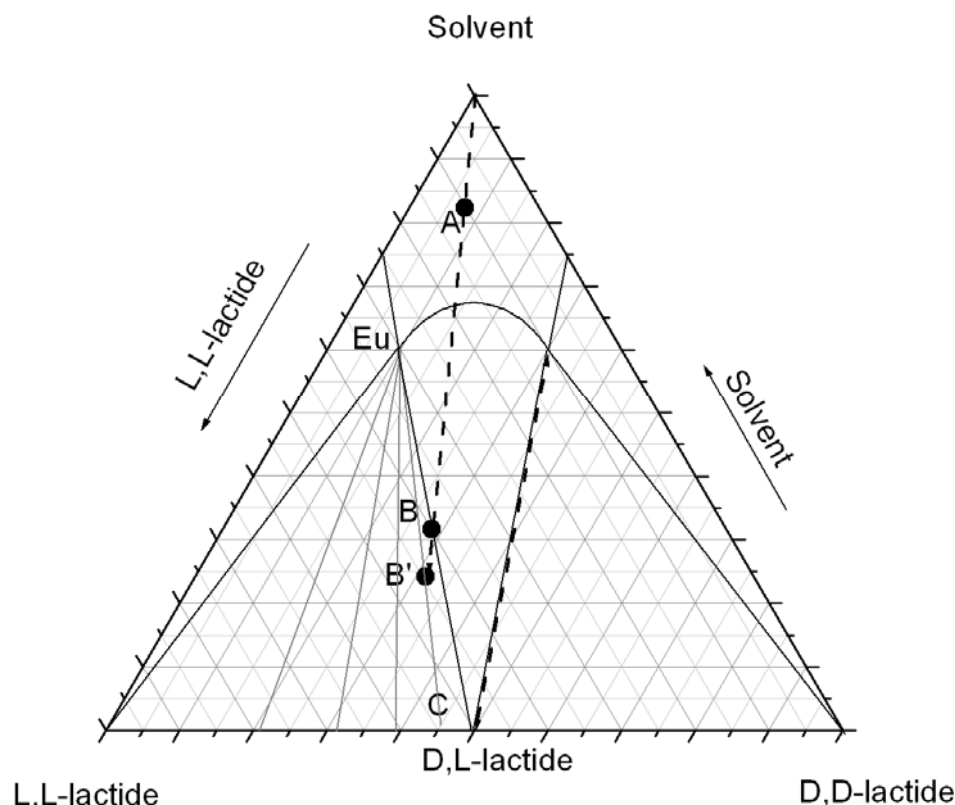
Figure 7.20: *Schematic illustration of enrichment technique towards eutectic composition.*

Initial composition **A** is considered as a slightly enantiomerically enriched solution with respect to the target enantiomer. To perform crystallization, concentration of the solution **A** needs to be higher than that of its saturated solution. Thus, the solvent evaporation will move the mother liquor composition along **AB** line and relocate the overall composition into the three-phase region (*e.g.* point **B'**). In principle, all compositions in this three-phase region will result in similar equilibria between the mother liquor at the eutectic composition **Eu** and corresponding solid mixtures with different ratios of the enantiomer and the racemate. In this case, our target is not the solid phase but the eutectic liquid which possesses an enantiomeric composition higher than that of the initial solution **A**. In principle, the point **B** on the boundary of the two- and three-phase domains is more preferable than arbitrary points **B'** in the three-phase domain due to following reasons. First, the residual solid obtained from point **B** in this process is the pure racemate at **C** which can be later used directly at racemate form as a by-product or a feed for the production of the counter-enantiomer. Second, the equilibrating mother liquor at **Eu** will be obtained at a maximal amount if the overall composition is placed at point **B** (comparing to other points in the extended line **AB**) based on the lever rule. After establishing the thermodynamic equilibrium, solid-liquid phase separation can be done via *e.g.* filtration, decanting, etc. While the residual solid can be returned to the feed stream, the target product is obtained as the liquid fraction. Consequently, the absolute volatilization of solvent will yield a solid product of which purity is equal to the eutectic composition.

In the next paragraph, this technique will be experimentally validated with ethanol as solvent. Using this solvent gains several advantages *e.g.* ethanol is also produced simultaneously in fermentation processes and lactide is quite stable in this solvent at the studied temperature range. As seen in Table 7.4, the TPD of lactide in ethanol shows the eutectic composition of $x_{L,L}^{Eu}$ = 0.95 at 25 °C. That means by applying this method, purity of the final product can reach to 95%.

7.4.1.2 Experiment validation of the "Option 1" with ethanol as solvent

A preliminary experiment was carried out with L,L-lactide to check dissolution rate of lactide in ethanol. A suspension of 35% (w/w) of L,L-lactide in EtOH was used in this measurement. Temperature was kept constant at 25 °C, system was agitated with a stirring rate of 350 rpm. The dissolution rate is relatively fast and the system reaches equilibrium after about 2 days as depicted in Figure 7.21. This time interval will be used for the next experiment to ensure the equilibrium conditions.
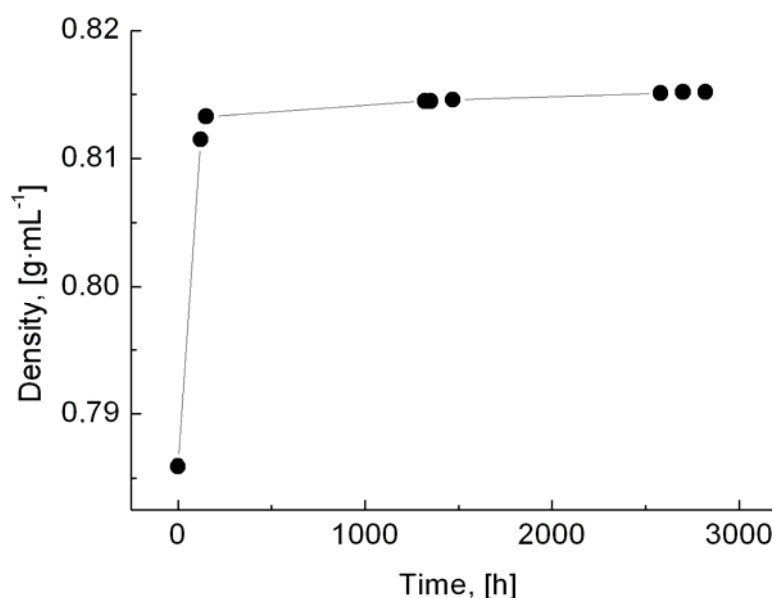
Figure 7.21: *Dissolution rate of L,L-lactide in ethanol at 25 ^{o}C.*

Calculated amounts of D,L-lactide and L,L-lactide were mixed to obtain a mixture of 70 g (60% L,L-enantiomer). This solid mixture was placed into a 500 mL reactor. Solvent ethanol was added into the reactor to obtain 336.52 g suspension. The system was agitated and kept at isothermal condition (25 °C). The suspension was agitated 2 days to ensure the equilibrium state. Solid-liquid separation was quickly done using a Buchner funnel. After evaporating the solvent, 24.45 g solid was obtained with purity of 95% L,L-lactide (HPLC analysis). The process yield is obtained from this experiment at 34% (Eq. 5.1) while the optimal case is found at 70.0% using theoretical calculation from Eq. 5.3. This process was graphically depicted in the TPD as Figure 7.22. The quantitative input and output of the above process are summarized in Table 7.10.

Table 7.10: *Validation of chiral purification based on phase equilibria in the TPD.*

Initial conditions		
m_solution	[g]	336.52
w	[-]	0.19
$x_{L,L}^{ini}$	[-]	0.60
T	[°C]	25
Time	[days]	2
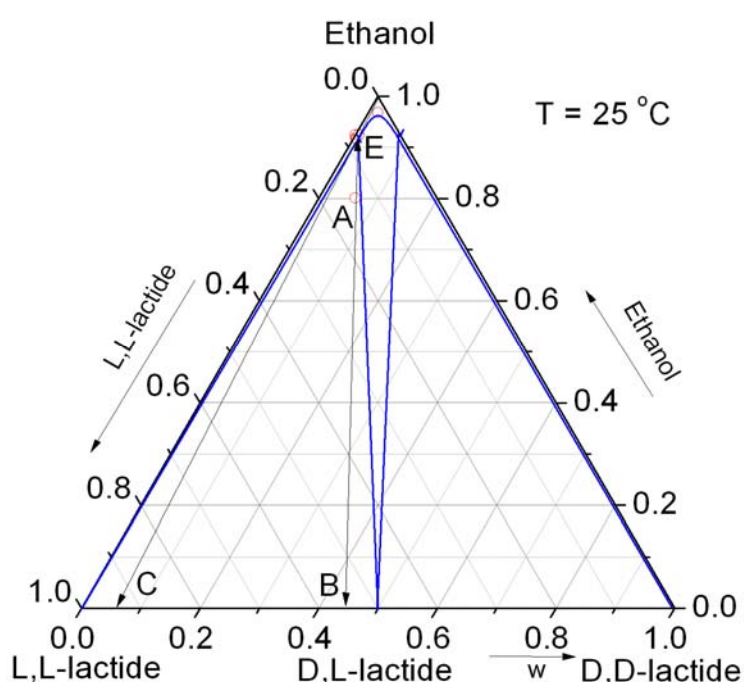
Figure 7.22: *Experiment validation for production of lactide with a moderate purity level. **A** is starting solution. **B** and **Eu** are the equilibrating solid and corresponding mother liquor at the eutectic composition. Solid product is obtained at **C** after total volatilizing EtOH from the eutectic liquid.*

In short, a demonstration of the single enantiomer lactide purification with a moderate purity level was successfully carried out with a case study of EtOH as solvent. Besides, the other solvents and solvent mixtures investigated in the previous part are feasible to achieve purities from 90% to 97% of the single enantiomer with the same method. Solvent selection is also depending on economic constraints and ability of combination one solvent in a sequence of production lines. In general, this simple technique is extremely helpful in the cases of the target chiral compounds possess high eutectic compositions. For instance, many systems show very high eutectic compositions *e.g.* serine (x_{Enan}^{Eu} = 0.99)[165,195], malic acid (x_{Enan}^{Eu} = 0.99)[196]. Back to

the eutectic compositions of lactide in different solvents, that is unfeasible to have higher purity of final products than the eutectic compositions via the described method. Therefore, an advance approach is recommended as follows.

7.4.2 Option 2 – A "two-step" process exploiting a shift of the eutectic compositions between solution and melt states

7.4.2.1 The concept of process

Recently, it was found that the eutectic composition of a chiral pair in a solvent can be changed under effects of temperature, *e.g.* as reported for methionine by Kaemmerer *et. al*[140]. Afterwards, Zhang *et al.*[155] and Le Minh *et al.*[197] also found an similar behavior for racemic compound-forming system of 3-chloromandelic acid. Based on shifts of the eutectic composition, a new concept of enantioseparation was recently proposed as described in literature[13–15]. Hereby, a so called the "two-step" process crystallization is capable to purify the target enantiomer from partially (even slightly) enantiomerically enriched solutions. Further developing this technique is strongly oriented throughout this thesis to generalize a widely applicable method, which is flexible and robust for the most common compound-forming racemates. This part will demonstrate a combination of crystallization processes based on difference of the eutectic compositions between solution state and melt state. The principle of this method is illustrated in Figure 7.23. The key of this development is that the BPD possesses a different eutectic composition (either lower or higher, herein a lower eutectic composition will be examined) than that of the TPD.

Step 1: Enrichment towards the eutectic composition via a classical crystallization step in TPD

The "first-step" is actually a classical selective crystallization which was already described in the previous paragraph (Option 1). By this way, it can be considered as an enrichment step under the guidance of the TPDs.

From a partially enantiomerically enriched solution, the "first-step" enriches the overall composition of the liquid up to the eutectic compositions. These compositions can vary from 0.90 to 0.97 of L,L-enantiomer as seen in Table 7.8. After equilibrating, solid and liquid phases are quickly separated by appropriate methods. Then, a sub-step volatilization is performed to obtain a solid mixture from this eutectic liquid. The process follows the pathway $A \rightarrow Eu_1 \rightarrow C$ as demonstrated in Figure 7.23.

Step 2: Exploiting eutectic shift by combining the TPD with the BPD

The feed-material for the "second-step" is the solid mixture obtained from volatilization of the eutectic liquid from step 1 (C). The essential condition is reminded that the eutectic composition in the TPD (Eu_1) muss be higher than that of the eutectic composition in the BPD (Eu_2). In principle, all melt crystallization techniques *e.g.* suspension melt crystallization, layer melt crystallization, etc. can be applied for this step. The overall composition C is now relocated at point D within

the two-phase domain of the BPD (Figure 7.23, lower part) by temperature adjustment. The equilibrium from **D** will result in the pure enantiomer solid at **E** and mother liquor at **F**. Point **D'** in vicinity of the boundary line is preferred due to the maximal yield of the recovered solid. Solid-liquid melt separation sub-step is required to obtain the pure enantiomer. A separation step can be carried out with centrifuges, wash columns, etc. On the other hand, the mother liquor at **Eu₂** can be recycled to *e.g.* feed-stream of the "first-step".
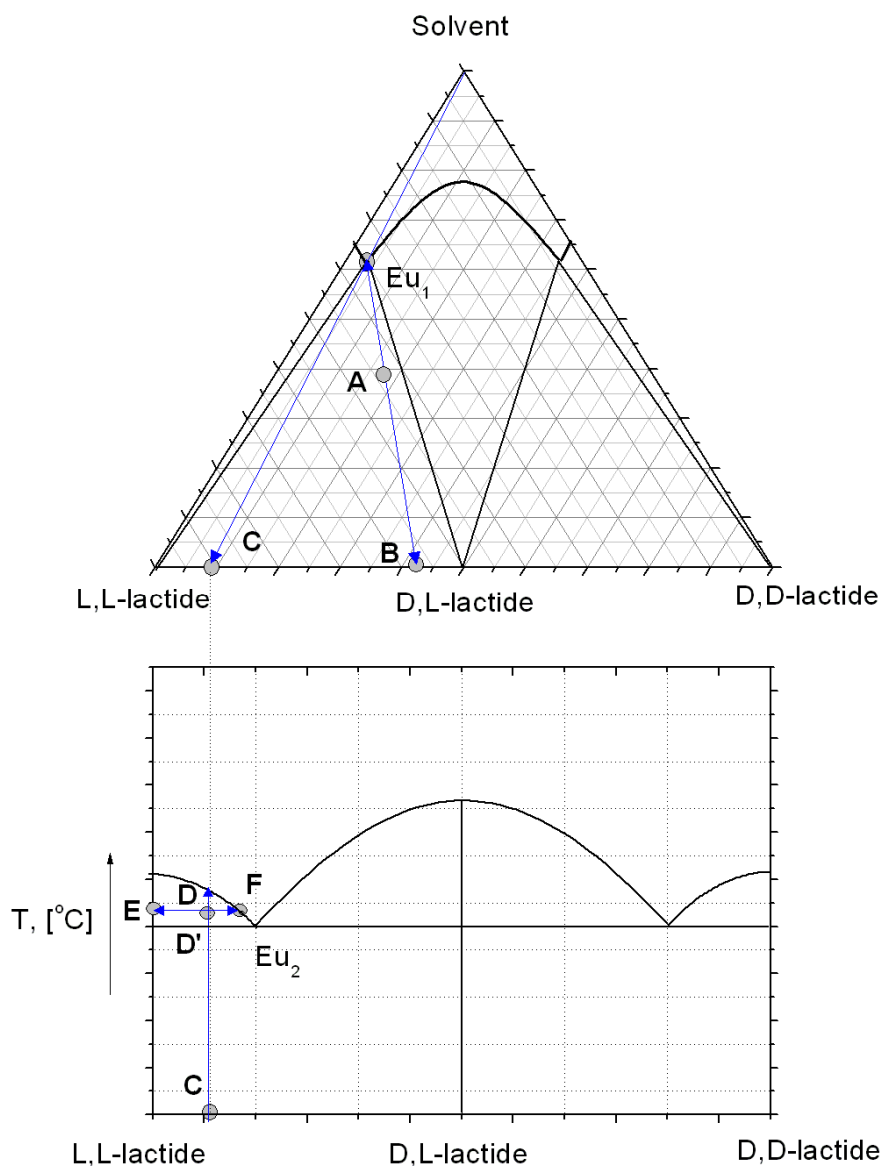
Figure 7.23: *A combination of the TPD and the BPD for an enantioselective crystallization.*

This technique shows advantages in purification the enantiomer(s) of lactide. First, this method bases on thermodynamic control which is preferred in particular for the industrial scales. Due to symmetry relationship, this technique is able to apply for production of both enantiomers. Furthermore, by-products including the racemate, slightly enantiomerically enriched solid mixtures and the enriched mother liquor can be recycled into the feed-stream of the process.

7.4.2.2 Experimental validation

The "two-step" process is experimentally validated with the following example to produce pure L,L-enantiomer of dilactide. The experimental procedure is depicted in Scheme 7.1. The BPD and TPD can be seen at Figures 7.3 and 7.9, respectively.
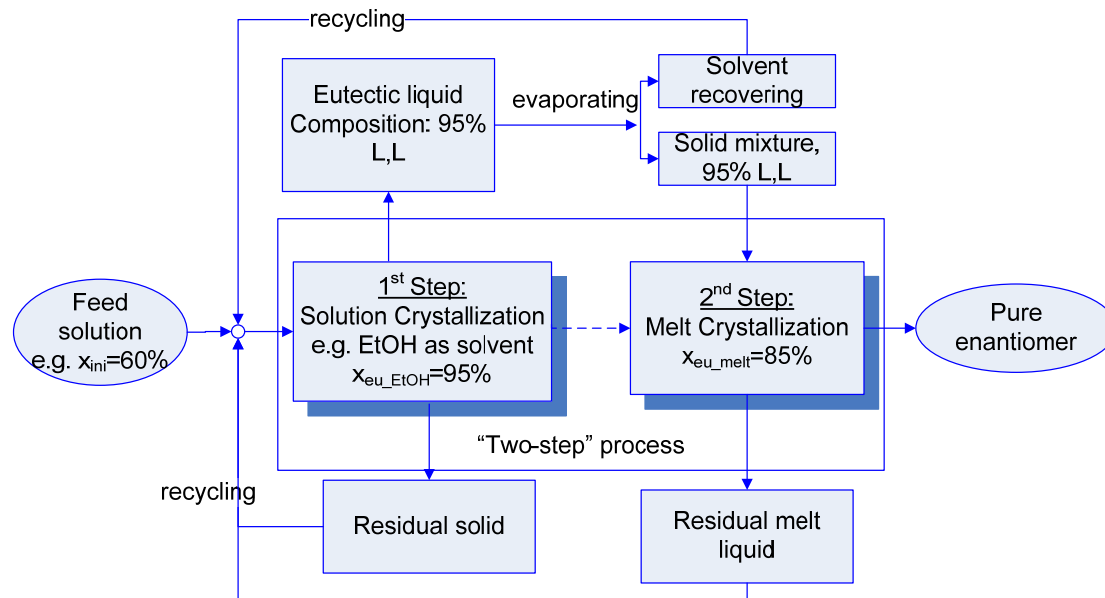
Scheme 7.1: *Experimental validation of the "two-step" process for enantiopurification of lactide.*

The solid mixture was prepared with the same composition to the final product of the process "Option 1". Amount of 25.45 g mixture containing 95.8% L,L-lactide was placed in a "cooling finger" melt crystallizer of 20 mL. Temperature was controlled by two thermostats (one for the "cooling finger" and another for the melt crystallizer). The system was held at an isothermal condition at 110 °C under well agitated condition using a magnetic stirrer. Clear melt was kept for 180 min to ensure dissolution of even the smallest particles. Then the system was cooled down to 95 °C. The temperature in the "cooling finger" was set at 93 °C. The crystallization took place within 3 days. The "cooling finger" was carefully taken out to obtain the adherent crystals on the "cooling finger" surface. HPLC analysis detected the purity of the product at extremely high level, *i.e.* no trace of D,D-enantiomer was found.

Since the system is operated at high temperature, the product attaching on the surface of the "cooling finger" is visible but attempt to quantify amount of product is challenging. The melt can quickly recrystallize during taking the "cooling finger" out of the crystallizer. Using Eq. 5.2, the theoretical yield of the melt process is obtained at 72.4%. Therefore, the total yield of whole process is estimated at 50.7% (Eq. 5.3). *In the optimal case, the initial solution has composition of **Eu**$_1$ (e.g. resulted from fermentation or chromatographic processes) and process yield will be equal to that of the 2nd step at 72.4%.*

In general, there are a couple of solvents which possess significantly different eutectic compositions to melt state as seen in Table 7.8. Therefore, they can be potential alternative solvents for ethanol in similar processes to produce single enantiomer(s) of lactide. Besides the case of lactide, there are a couple of examples which show eutectic shift behavior between melt and solution states such as malic acid[196], 3-chloromandelic acid[197], etc. Thus, high applicability of this method is expected to resolve partially enantiomerically enriched solutions.

7.5 Conclusions

- Lactide belongs to compound-forming systems since all results from either the solid phase characterization including XRPD, DSC, or the shapes of the BPD, the TPD gain a good agreement. Furthermore, lactide does not show any additional or new crystalline phase in all studied conditions. Thus, lactide represents the "standard" case of compound-forming racemates which is not affected by polymorphism or solvate formation.

- SLE measurements of lactide were carried out in consideration effects of temperature and solvent. In melt state, the BPD possesses the eutectic composition at $x_{L,L}^{Eu}$ = 0.84. The presence of solvents significantly changes internal interactions which can establish different the eutectic compositions to that of the melt state. In studied solvents and solvent mixtures, the eutectic compositions can vary in a quite large range of $x_{L,L}^{Eu}$ from 0.90 to 0.97.

- MSZWs of lactide species were measured via the Nyvlt's method. Eventually, preferential crystallization is not an efficient approach to separate the pure enantiomer(s) of lactide. The racemate can easily contaminate the target enantiomer during preferential crystallization processes. Another alternative based on thermodynamics is recommended.

- Variation of the eutectic composition leads to a special design so called the "two-step" process which is able to produce the pure enantiomer(s) of lactide from a slightly enantiomerically enriched solution. This combination exploits the eutectic shift between the melt and the solution states which can reach to the maximal yield of about 72%. If a moderate purity level meets requirement, a single step will be sufficient to reach the purity equal to the eutectic compositions (*i.e.* ~90–97%).

CHAPTER 8:

POLYMORPHIC CHIRAL SYSTEM 3-CHLOROMANDELIC ACID

In the previous chapter, a simple chiral compound as the "standard" case of chiral compound-forming systems was introduced, *i.e.* the chiral lactide system. Sophisticated racemates will be considered in this chapter. Studying effects of polymorphism on compound-forming racemates and appropriate resolution methods are the main objectives of this chapter, proved with a case study of 3-chloro mandelic acid (3ClMA).

8.1 Polymorphs and binary melting point phase diagram (BPD) of 3ClMA

The goal of this section is characterization the solid phase of 3ClMA species as a compound-forming racemate affected by different polymorphs. On that basis, the BPD will be constructed in consideration of relevant equilibrating phases. First of all, the discrimination of these polymorphs is performed via the following analyses.

8.1.1 Polymorphic recognition of 3ClMA via DSC and XRPD analyses

First, five consecutive DSC cycles were performed with a sample of the enantiomer to evaluate the possibility of polymorph existence. The results are shown in Figure 8.1(a)–(e). There is a significant difference between the first and the second DSC curves relating to different phases of the same material, *i.e.* different polymorphs. The explanation is based on Ostwald's theory[198]. Crystallization of a polymorphic compound from a melt (or solution) tends to yield crystals which can firstly exist in metastable forms. Therefore, the material obtained from a fast cooling cycle (from melt liquid obtained at the end of the previous cycle) should be the metastable polymorph. In the melting profiles, an endothermic effect is found at 91.99 $^{\circ}$C (the 2nd DSC curve, see Figure 8.1(b)) for the melting of the metastable enantiomer (namely R_2) while the stable form R_1 shows a melting effect at 103.21 $^{\circ}$C (the 1st DSC cycle, see Figure 8.1(a)). On the other hand, the XRPD patterns of the metastable enantiomer R_2 obviously differs from the stable one R_1 (Figure 8.2(a) and (b)). This evidence emphasizes the existence of polymorphs in the case of the enantiomer of 3ClMA. Likewise, two forms of the racemate are found. In Figure 8.1(f)–(j), the metastable RS_2 of the racemate possesses clearly distinguished melting profiles from the stable RS_1. The quantitative thermal properties of those forms are summarized in Table 8.1. Additionally, a phase transition from RS_2 to RS_1 occurring around 115 $^{\circ}$C (a small exothermic effect in Figure 8.1(g)) reveals the enantiotropic relationship of these polymorphs.
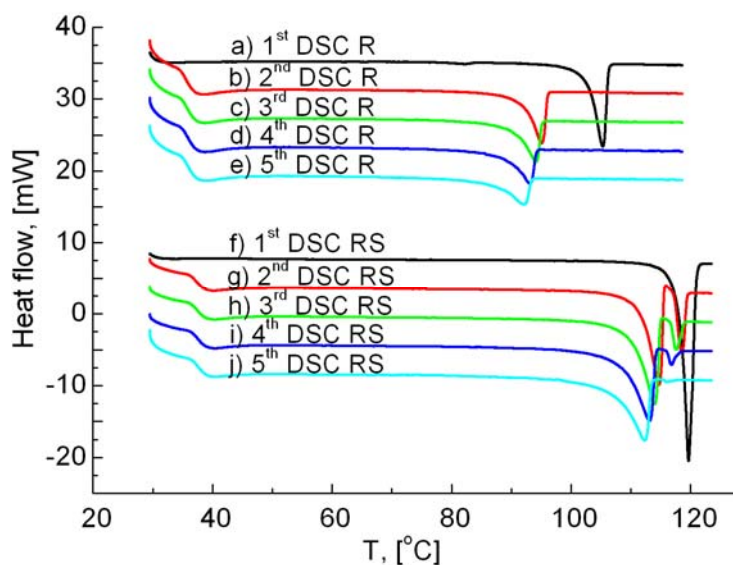
Figure 8.1: *DSC analyses of the enantiomer (a)–(e) and the racemate (f)–(j). Experiments were consecutively repeated 5 heating-cooling cycles[199] with the same sample of the enantiomer (and the racemate) to validate the existence and stability of polymorphic 3ClMA species. Heating rate was used at a value of 0.5 °C·min⁻¹, temperature range from 30 to 130 °C.*

Information about decomposition could be also obtained from Figure 8.1. The melting profiles clearly show that the melting temperatures gradually decrease from the 2nd cycle to the last one due to the possible enrichment of decomposition products after each DSC cycle. That could be seen by comparing Figure 8.1 from (b) to (e) for the enantiomer and Figure 8.1 from (g) to (j) for the racemate. Hereby, the 2nd DSC cycle delivers the "purest" metastable form among the rest four heating-cooling DSC cycles. Thus, just the second cycle can be used to evaluate the melting effects of the metastable forms. Additionally, DSC coupled with TG (thermogravimetry) detected the mass loss during each melting-cooling cycle. This loss is relatively small (about 0.3%).

Table 8.1: *Melting temperature and heat of fusion of the 3ClMA polymorphs.*

Compound	T^f, [°C]		ΔH^f, [kJ·mol⁻¹]	
	Stable form	Metastable form	Stable form	Metastable form
Enantiomer	103.21	91.99	22.55	14.62
Racemate	117.59	111.54	27.92	17.77

As expected, these polymorphs of 3ClMA possess completely different XRPD patterns. Distinguished reflections of the metastable and the stable forms of the enantiomer can be seen at positions of 10.6, 12.9, 18.3, 21.0 and 31.9°, etc in Figure

8.2(a) and (b), respectively. Likewise, the racemate polymorphs can be recognized by comparing reflections at 13.2, 14.1, 16.3, 18.23, 26.2 and 31.9°, etc in Figure 8.2(c) and (d). Thus, together with the DSC analysis in previous paragraphs, the XRPD patterns in Figure 8.2 confirmed the existence of those polymorphs.
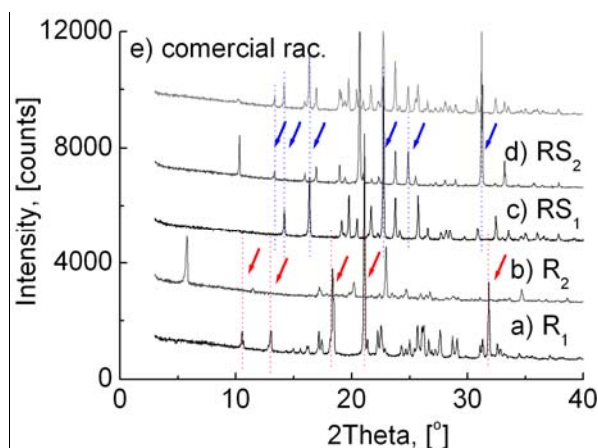
Figure 8.2: *Stable and metastable forms of the enantiomer (R₁ and R₂) and the racemate (RS₁ and RS₂).*
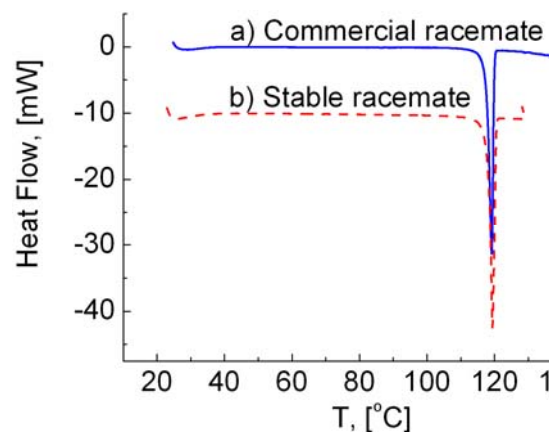
Figure 8.3: *DSC comparison of the commercial sample and the pure stable racemate RS₁.*

It is worthy to notice that the commercial racemate contains two polymorphic forms. That can be seen by comparing XRPD patterns of the stable form (Figure 8.2(c)) and an original sample of Alfa Aesar (Figure 8.2(e)). An additional phase appearing in Figure 8.2(e) is exactly identical to the metastable phase of the racemate as Figure 8.2(d). Thus, the XRPD pattern of the commercial sample is just an overlay-image of two different patterns which represent two polymorphs of the racemate. Fortunately, a small amount of the metastable phase does not violently influence the commercial sample since DSC results of the stable phase RS₁ and the commercial sample are identical as shown in Figure 8.3.

8.1.2 Polymorphic transformation of 3ClMA under ambient conditions and in solution

Time-resolved XRPD[200] were used to study the stability of these polymorphs under ambient conditions. In the case of the enantiomer, Figure 8.4 presents the transformation of the metastable into the stable polymorph within a period of two-three months. In principle, the metastable form R₂ will gradually transform into the stable form R₁. In fact, the metastable form R₂ which was recrystallized from the melt is quite stable within two-three months under ambient conditions (Figure 8.4(b)–(f)). However, new reflexes appear at 18.3, 21.0 and 31.9°, etc. They are formed after three months (see Figure 8.4(g)) that indicated the formation of the stable phase R₁ (compared to the reference R₁ in Figure 8.4(a)). This observation illustrates the progressively polymorphic transformation of the polymorphs of the enantiomer under ambient conditions.
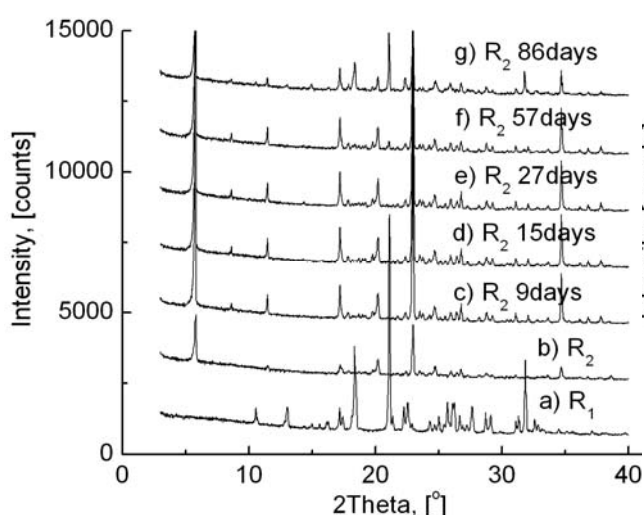
Figure 8.4: *Time-resolved XRPD (enantiomer).*   **Figure 8.5**: *Time-resolved XRPD (racemate).*
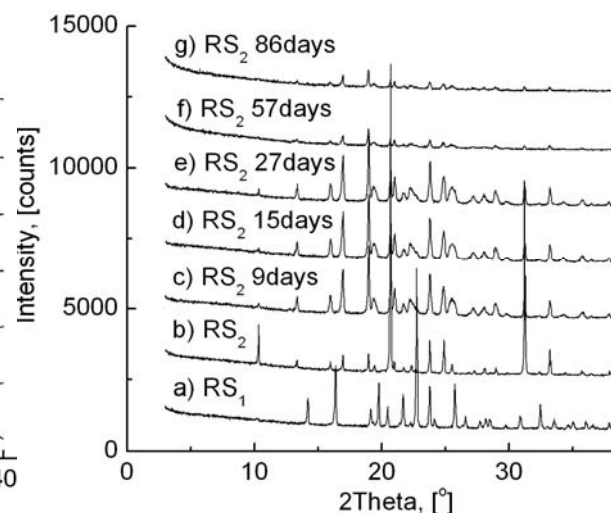
Likewise, Figure 8.5 explains the transformation process of the polymorphs of the racemate. All samples in Figure 8.5(b)–(g) show the same reflections without any new or additional phase. Thus, the metastable racemate RS_2 is "stable" at least 3 months under ambient conditions.

Additionally, the transformation of the polymorphs of 3ClMA was also studied in aqueous solutions to study the solvent effects. Indeed, the transformation process is relative simple for the enantiomer whereas it is more complicated in the case of the racemate. The XRPD results show that the enantiomer is always found as the stable phase R_1. In contrast, depending on different conditions, both the metastable RS_2 and the stable RS_1 of the racemate can be formed. For further investigation, we will focus on polymorphic transformation of the racemate in water. Results are present in Figure 8.6.
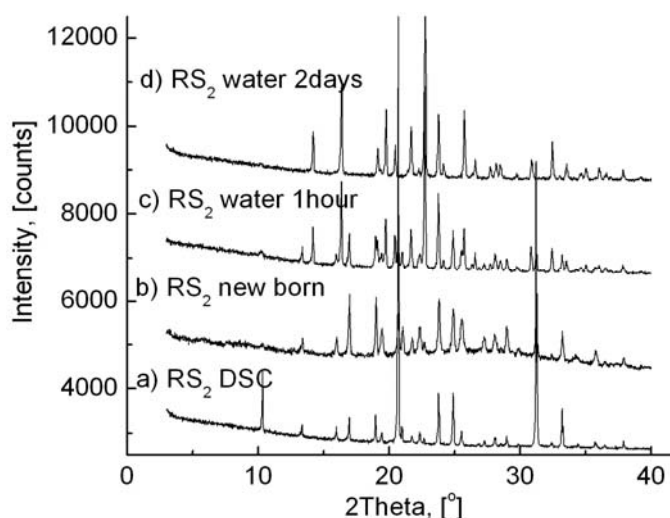
Figure 8.6: *Polymorphic transformation of the racemate species in aqueous solution. Sample (b) is identical with the metastable phase RS_2 as seen in sample (a). Then, the polymorphic transformation completes within 2 days (sample (d)).*

These experiments were carried out with saturated solutions of the racemate in water at 50 °C. Then, the sample was recrystallized at 35 °C and kept for different periods of time. At first, "new-born" crystals are obtained in the first few minutes (Figure 8.6(b)) that shows the same structure to the metastable form RS_2 (Figure 8.6(a)). These crystals will be remained shorter than 1 hour then they tend to transform into the stable phase (Figure 8.6(c)). Afterwards, the metastable phase RS_2 completely vanishes after 2 days (Figure 8.6(d)). This observation illustrates that the metastable polymorph RS_2 of the racemate 3ClMA is able to perform a solvent-mediated transformation into the stable one RS_1 within a relatively short time.

8.1.3 Single crystal structures of 3ClMA stable forms

Due to the difficulty of growing metastable forms as single crystals, hereby, only stable forms of the enantiomer and the racemate were successfully isolated and examined with XRD measurements. Crystal structures of the enantiomer and the racemate of 3ClMA are presented in Figure 8.7. Details are shown in Table 8.2.
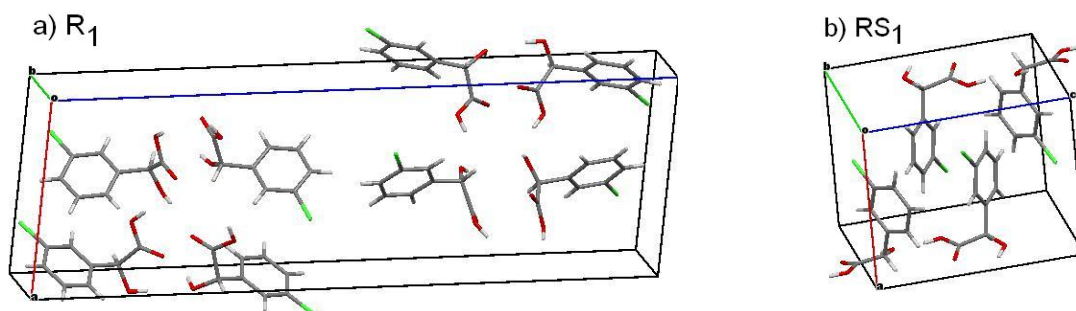
Figure 8.7: *Single crystals of the stable forms of 3ClMA species.*

Evidently, crystal structures of the enantiomer and the racemate are totally different. Even though both of them belong to monoclinic crystal systems, the enantiomer has symmetry of space group $P2_12_12_1$ while the racemate shows P21/c symmetry. Cell dimensions of these crystals are clearly distinguished. Furthermore, the unit volume of the enantiomer is two times larger than the racemate. The number of molecules in a unit cell of the enantiomer and the racemate are found at 8 and 4, respectively.

Thus, X-ray diffraction data provides important information about type of the chiral 3ClMA system. Obviously, the crystallography of the enantiomer and the racemate of 3ClMA show different crystal structures between the enantiomer and the racemate. Thus, chiral 3ClMA is clearly a compound-forming system. This conclusion will be validated via the other measurements of the BPD, solubility, the TPDs, etc. in next sections.

Table 8.2: *Refinements of single crystal structures of the enantiomer and the racemate.*

Property	Unit	The enantiomer	The racemate
Crystal system	[-]	monoclinic	monoclinic
Space group	[-]	$P2_12_12_1$	P21/c
Unit cell dimensions	a, [Å]	9.87	8.66
	b, [Å]	5.43	8.93
	c, [Å]	30.65	10.78
	α, [°]	90	90
	β, [°]	95.26	90.34
	γ, [°]	90	90
Z	[#]	8	4
Unit cell volume	[Å³]	1637.4	834.2

8.1.4 Binary melting point phase diagram (BPD)

The BPD of the polymorphic system 3ClMA will be constructed in this part. DSC technique is applied again to various compositions of the enantiomer and the racemate. First, only the stable equilibria are considered. Then, the metastable equilibria will be measured later. The melting temperature and enthalpy of fusion of the enantiomer, the racemate and the eutectic composition for the stable forms are tabulated in Table 8.3.

Table 8.3: *Melting temperature and heat of fusion of the enantiomer, the racemate and the eutectic composition of 3ClMA. All data are reported for the stable forms.*

Composition	T^f, [°C]		ΔH^f, [kJ·mol⁻¹]	
	Literature[155]	Present work	Literature[155]	Present work
R_1	105.6	103.21	26.24	22.55
RS_1	117.2	117.95	27.98	27.92
Eutectic	99.6	95.18	25.84	18.62

Similar to the lactide system in Chapter 7, these thermal properties in Table 8.3 clearly indicate that 3ClMA is a compound-forming system. The BPD will show two symmetric eutectic compositions around the racemic axis. The same measurement conditions are further applied for other mixture compositions. In Figure 8.8, DSC profiles are presented for samples of various enantiomeric compositions. The DSC curves show 3 single sharp peaks at x_R = 1.0, 0.89 and 0.50 corresponding to melting of the enantiomer, the eutectic mixture and the racemate.
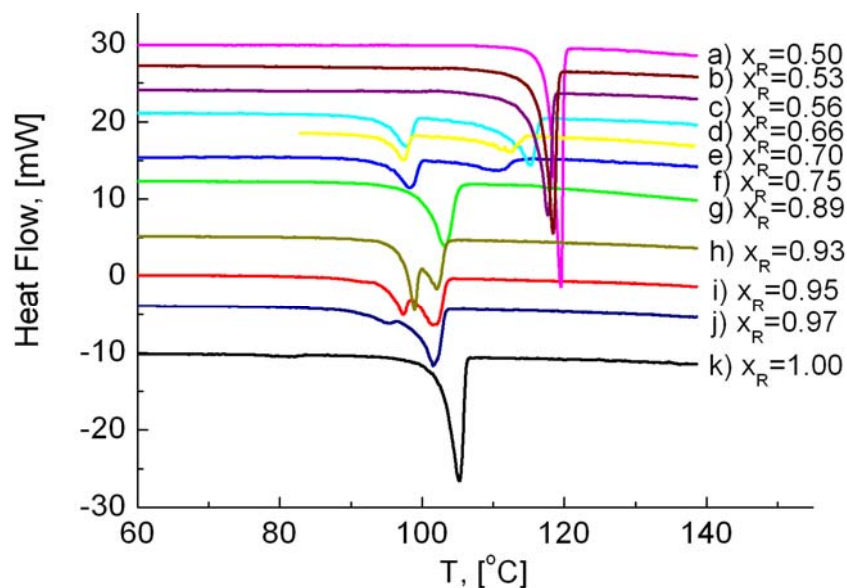
Figure 8.8: *Melting profiles of various enantiomeric compositions of 3ClMA via DSC measurements (a heating rate of 0.5 ºC·min⁻¹; 15–20 mg samples; closed crucibles of 75 µL).*

The calorimetric properties of these compositions are similar to literature[155]. However, there is a slight difference between the eutectic point found in the present work (x_R^{Eu} = 0.89; T_{eu} = 95.18 ºC) and literature data (x_R^{Eu} = 0.87; T_{eu} = 99.6 ºC)[155]. The difference of applied heating rates could lead to this deviation (0.5 ºC·min⁻¹ in the present work and 2 ºC·min⁻¹ in literature[155]). The other mixtures (composed from the eutectic composition–the pure enantiomer or the eutectic composition–the racemate) showed a melting domain consisting two peaks, *i.e.* the eutectic fusion and the subsequent dissolution effects. The eutectic temperature is found at approximately 95 ºC. Besides, the eutectic effects could be very small or even invisible when the enaniomeric mixtures are close to the enantiomer or the racemate axes.

To validate the eutectic composition, the Tamman's plot[201] is applied to define the eutectic composition and to evaluate the possibility of solid solutions of 3ClMA. In Figure 8.9, the melting enthalpy of the eutectic amount in various enantiomeric mixtures is plotted as a first order function versus composition. The eutectic composition is found at $x_R^{Eu<I>}$ = 0.89 which is actually the intersection point of two straight lines drawn from the melting enthalpies of the eutectic effects. Moreover, the extrapolated lines will show possible boundaries of partial miscibility at ΔH_{eu}^f = 0. Actually, these points are seen at x_R approximately 1.0 and 0.5. Thus, solid solution does not exist in this case.
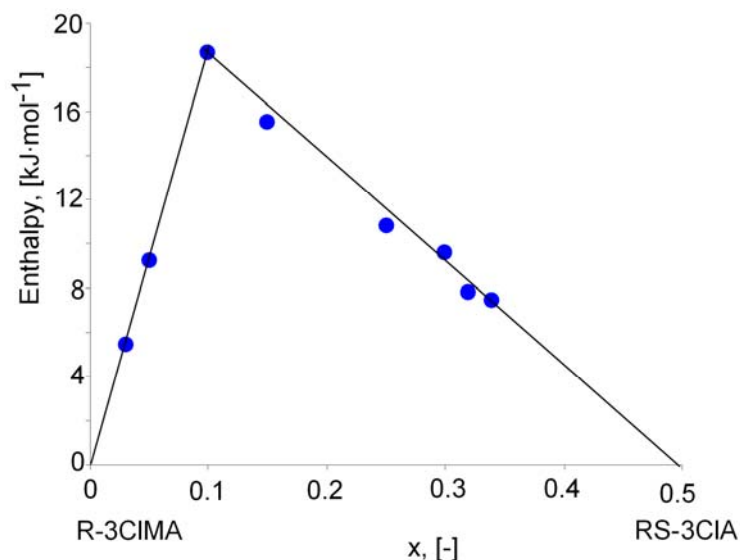
Figure 8.9: *Enthalpy of fusion is a function of enantiomeric composition via Tamman's plot.*

Consequently, DSC measurements were also applied for the metastable forms and their mixtures of which the results are presented in Table 8.4. Practically, there were drawbacks to generate and isolate metastable forms. Hereby, just some experiments were successfully carried out. The eutectic point of the metastable diagram is experimentally defined at $x_R^{Eu<II>} = 0.84$ and $T_{eu<II>} = 81.52$ °C.

Table 8.4: *Melting temperature of metastable equilibria. n.d.-not detected.*

Composition	Melting Temperature	
x_R, [-]	T_m, [°C]	T_{eu}, [°C]
1.00	91.99	–
0.97	91.06	81.16
0.95	n.d.	80.05
0.92	86.17	n.d.
0.85	–	81.52
0.65	n.d.	81.05
0.60	107.50	81.10
0.52	112.02	n.d.
0.50	111.54	–

Integrating all DSC results of both the stable and metastable forms, the complete BPD is obtained as Figure 8.10. As expected, a symmetric diagram is observed around the racemic axis. A new 1:1 compound is formed in the solid state from the S- and R-enantiomers. Obviously, the shape of the BPD confirmed that 3ClMA is a compound-forming system besides DSC, XRD, XRPD data. This conclusion gained a good agreement with literature[155]. Nonetheless, neither polymorphism nor solid solutions were mentioned in literature[155].

Furthermore, the extended lines of the stable liquidus will intersect with the metastable phase diagram at Eu$_{<III>}$ ($x_R^{Eu<III>}$ = 0.82; $T_{Eu<III>}$ = 85.3 °C) and Eu$_{<IV>}$ ($x_R^{Eu<IV>}$ = 0.94; $T_{Eu<IV>}$ = 88.5 °C) as depicted in Figure 8.10. Besides, there are two other eutectic points for the stable and the metastable equilibria as mentioned above including Eu$_{<I>}$ ($x_R^{Eu<I>}$ = 0.89; $T_{Eu<I>}$ = 95.2 °C) and Eu$_{<II>}$ ($x_R^{Eu<II>}$ = 0.84; $T_{Eu<II>}$ = 81.5 °C), respectively. These conclusions prove the complexity of the polymorphic system 3ClMA. However, this can also provide more opportunities to exploit desired equilibria between the metastable and the stable forms (under suitable conditions) which could help to apply the "two-step" process to purify single enantiomers.
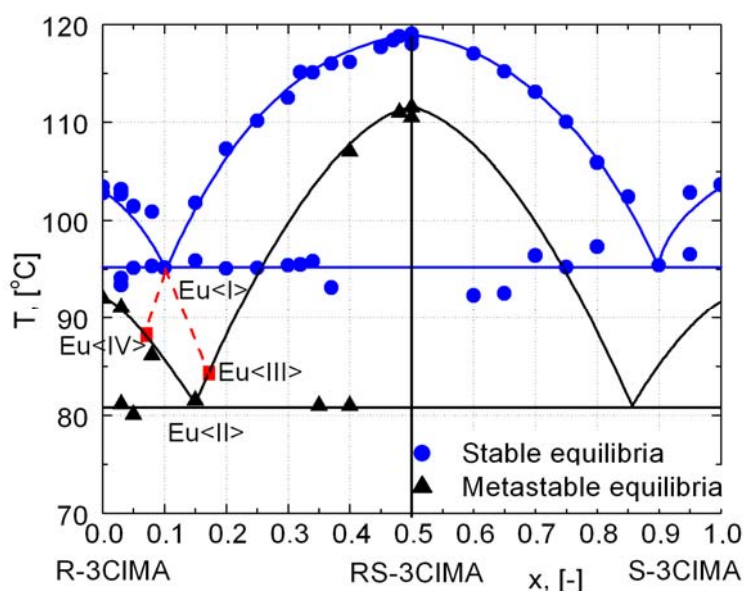
Figure 8.10: *Full BPD of the polymorphic system 3ClMA is determined via DSC measurements. All stable and metastable equilibria are plotted that leads to formation of 4 possibilities of eutectic compositions from Eu$_{<I>}$ to Eu$_{<IV>}$.*

8.1.5 Summary of solid state of the polymorphic 3ClMA system

- All data from thermal analysis DSC and X-ray diffraction assert that 3ClMA is a polymorphic system. Metastable forms are found for both the enantiomer and the racemate species. The polymorphic 3ClMA system results in a relatively complicated BPD which shows compound-forming properties for both the stable and metastable equilibria. In short, 3ClMA is the second case (besides the lactide

system) of the compound-forming racemate group which have influence of sophisticated behaviors such as polymorphism.

- The eutectic compositions in the BPD are of special interest. Two branches of the liquidus lines on the sides of the enantiomer and the racemate in the BPD intersect at compositions of $x_R^{Eu<I>} = 0.89$ and $x_R^{Eu<II>} = 0.84$ for the stable and the metastable equilibria, respectively. Additionally, other intersections between the stable and metastable forms of the enantiomer and the racemate or the reversed case result in two more eutectic compositions. Those values are found at $x_R^{Eu<III>} = 0.82$ and $x_R^{Eu<IV>} = 0.94$ as plotted in Figure 8.10.

8.2 Solid-liquid equilibria (SLE) of 3ClMA in various solvents

Similar to lactide system, SLE of 3ClMA in various media are the fundamentals for separation processes. Comparing to the lactide system, SLE of 3ClMA is more complicated due to the existence of various polymorphs. Besides polymorphism, SLE of 3ClMA are also influenced by special behaviors such as oiling out, association, etc. which will be also studied in this chapter.

8.2.1 Solid phase behavior of 3ClMA in various solvents

Various solvents were used in SLE determination including water, toluene, mixtures of toluene/EA, toluene/alcohols. Herewith, the enantiomer, the racemate and several enantiomeric mixtures were recrystallized in the above solvents (solvent mixtures) at the same conditions to SLE measurements in next parts. Then, these recrystallized solids were quickly separated out of their mother liquors and examined by XRPD measurements. Since the case of water was already discussed, this part will focus on the residual solids of 3ClMA species in toluene-based solutions.
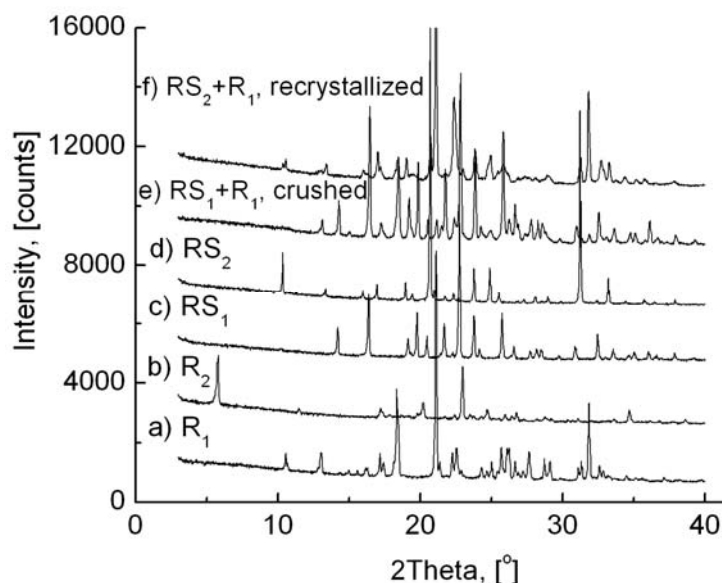
Figure 8.11: *Equilibrating solids of 3ClMA species in SLE determination with toluene and solvent mixtures.*

In the case of pure toluene as solvent, the equilibrating solids depend on polymorphic forms used at the initial materials. Toluene acts as a solvent which is able to prohibit the polymorphic transformation of the 3ClMA species. Individually, the residual solids of both the enantiomer and the racemate retain the same forms with the initial materials. Indeed, SLE measurements performed with separately recrystallized enantiomer or racemate in toluene will obtain the metastable forms R_2 or RS_2 as presented in Figure 8.11(b) or (d). Those species are found identical to the initial metastable forms during SLE. Otherwise, starting with stable pure solids (mechanical crushed, but not recrystallized), the residual solids after equilibria will retain the same stable forms as R_1 or RS_1 as shown in Figure 8.11(a) or (c). That is also correct for mixtures of R_1 and RS_1 (Figure 8.11(e)) in which the crushed materials of samples containing simultaneously the enantiomer and the racemate retain as stable forms at equilibrium in toluene. Interestingly, the sample containing simultaneously both the enantiomer and the racemate in toluene will recrystallize the enantiomer as stable form R_1 but the racemate as metastable form RS_2 (Figure 8.11(f)).

Based on toluene, other solvents were added to form solvent mixtures. Those agents including alcohols (methanol, ethanol, iso-propanol, n-butanol), ethyl acetate. SLE determination for these solvent mixtures were just performed with fine-crushed particles (not recrystallized) of the enantiomer, the racemate and their mixtures. These suspensions were kept in 2 days to examine the residual solids. The XRPD of these samples showed the stable forms of 3ClMA species (similar to Figure 8.11(e)). These solvents and solvent mixtures will be detailed in the next part.

8.2.2 Effects of polymorphism on solubility

Figure 8.12 shows dissolution rate at 25°C of the commercial racemate. Usually a dissolution curve has the shape of a logarithm function. Nevertheless, in the case of the commercial racemate sample, a different behavior was found due to effects of polymorphs.
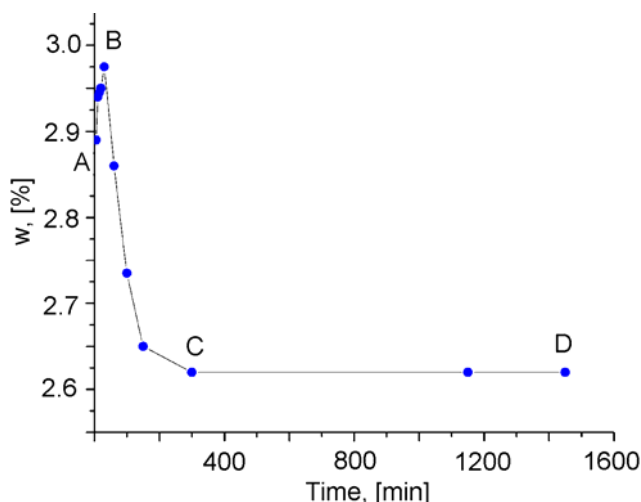
Figure 8.12: *Effects of polymorphs to dissolution process of the racemate 3ClMA in water. Experiment was carried out at 25 °C. The commercial racemate was directly used without any purification step.*

The initial commercial racemate is a mixture of two polymorphs as mentioned in part 8.1.1. A suspension of this racemate in water (w = 0.05, [-]) was well-agitated at 25 °C. In the first period **AB** (approximately first 30 min in Figure 8.12), both forms dissolve into water and the total concentration reach a maximum value (corresponding to point **B**). Since only one of polymorphs can be thermodynamically stable under given conditions, the metastable form spontaneously converts to the stable one during the time reaching to equilibrium state. The dissolution process under the influence of polymorphic transformation follows path **BC** (approximately from 30 to 300 min in Figure 8.12). Finally, the equilibrium is established after approximately 5 h (line **CD**). The saturated solution has a concentration of w = 0.026. Similar dissolution processes, which are affected by polymorphs or solvates, were also reported in literature.[63]
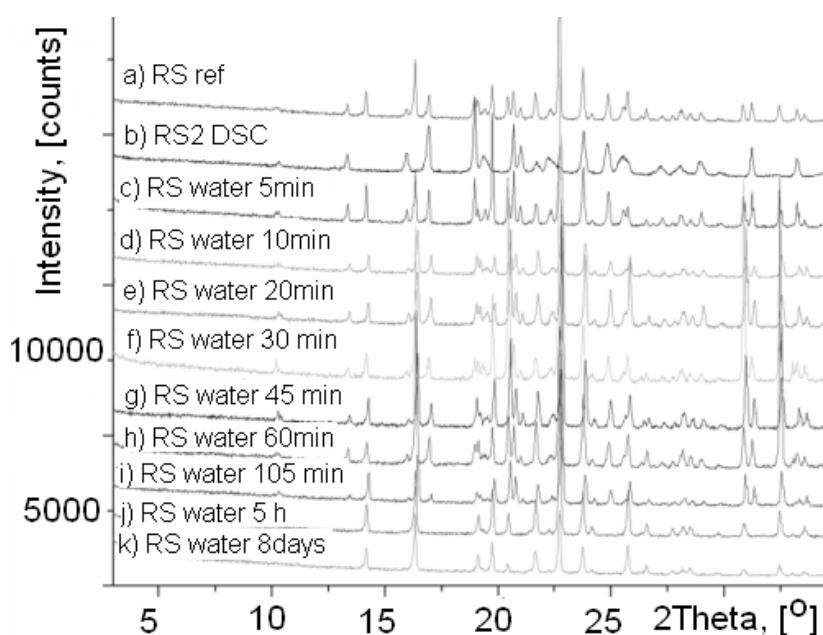
Figure 8.13: *Polymorphic transformation of the racemate.*

In Figure 8.13, the phase transformation was confirmed by XRPD measurements with the corresponding residual solids. The solid samples between 5 and 30 min (see Figure 8.13(c)–(f)) contain two phases, *i.e.* RS_1 and RS_2, according to the continuous dissolution processes of these polymorphs into water. Other solid samples (between 30 and 105 minutes) contain 2 phases as well, but amount of the less stable phase is getting smaller in comparison to the stable one (Figure 8.13(f)–(i)). The metastable phase RS_2 completely vanishes after 5 hours as Figure 8.13(j). This sample retains the same structure after 8 days as Figure 8.13(k). This observation illustrates that the metastable polymorph of the racemate 3ClMA is able to perform (solvent-mediated) transformation into the stable form in a relatively short period.

8.2.3 SLE of 3ClMA in various solvents

SLE of 3ClMA in toluene will be determined in this part. Then, various solvent mixtures of toluene and alcohols, ethyl acetate are also studied. Finally, water is the last case studied of this part.

8.2.3.1 Binary and ternary solubility in toluene

Figure 8.14(a) presents solubility of 3ClMA in toluene. Herewith, both the enantiomer and the racemate are used as the stable forms. The initial materials were crushed to fine powder and directly used for solubility measurements with the polythermal method via the Crystal16™. Since there was no recrystallization, those species retained as stable forms as described above.
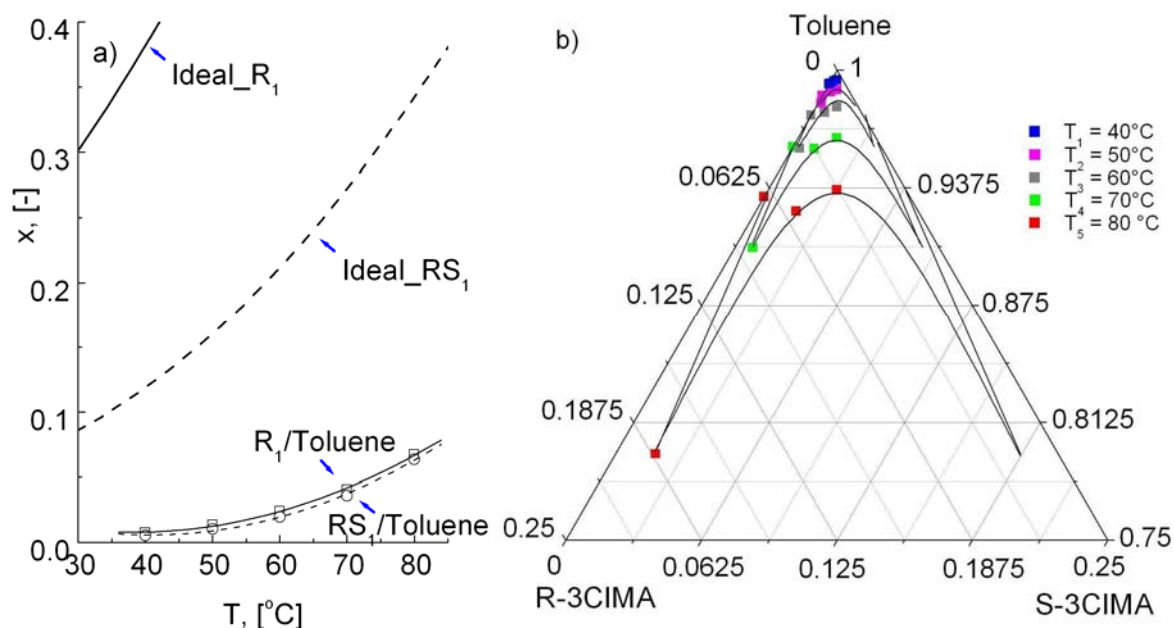
Figure 8.14: *(a) Binary solubility of 3ClMA in toluene; (b) zoomed TPD in an area of 25%.*

Obviously, 3ClMA species dissolve poorly in toluene since their solubilities were determined as significantly low values even at elevated temperatures (Figure 8.14(a)). The explanation is based on the structures of those substances which are not able to form hydrogen bonds between 3ClMA species and toluene. Furthermore, 3ClMA is a strong polar solute while toluene is a non-polar solvent. Therefore, solubilities of 3ClMA species in toluene are very low as observed.

Even though the solubility of the enantiomer is higher than the racemate, both of them are significantly lower than the ideal cases as seen in Figure 8.14(a). This simple comparison indicates the strong non-ideal solutions of 3ClMA species in toluene. This behavior was again confirmed by the estimation of the enthalpy of dissolution via the van't Hoff method. Those values were found for the enantiomer and the racemate at +51.27 and +58.42 kJ·mol^{-1}, respectively.

On the basis of binary solubility, the TPD of 3ClMA in toluene was further constructed with contribution of other enantiomeric mixtures. The TPD was drawn in the conventional equilateral triangular shape (Figure 8.14(b)). The shape of isothermal solubility curves again confirms that 3ClMA is a racemic compound-forming system. Especially, the eutectic compositions retain unchanged at x_R^{Eu} = 0.91

over the temperature range between 5 and 50 °C while a calculation via the Klussmann's approach (Eqs. 3.60 – 3.62) is found at x_R^{Eu} = 0.93.

8.2.3.2 Modification of toluene-based solvents with alcohols

Due to the limited solubility of 3ClMA in toluene as described above, various alcohols were used to modify the solubility of 3ClMA. Those alcohols were selected based on an idea of increasing size of alkyl groups. Four common alcohols were used including methanol (MeOH), ethanol (EtOH), iso-propanol (iPrOH) and n-butanol (ButOH). Although these co-solvents were used with a small amount of 5% (w/w), they significantly increased solubility of 3ClMA species as seen in Figure 8.15. Sizes of the alkyl groups of alcohols strongly influence to the solvent structures of the modified solvents. These mono-alcohols have two parts, *i.e.* hydrophobic hydrocarbon chains and a hydrophilic group (–OH). Modifying toluene by alcohols can improve ability of hydrogen bond formation between solutes and solvent mixtures, therefore increasing solubility. These modified solvents result in completely different enthalpies of dissolution as seen in Table 8.5. Both the enantiomer and the racemate species increase the solubility following the priority: MeOH>EtOH>iPrOH>ButOH.
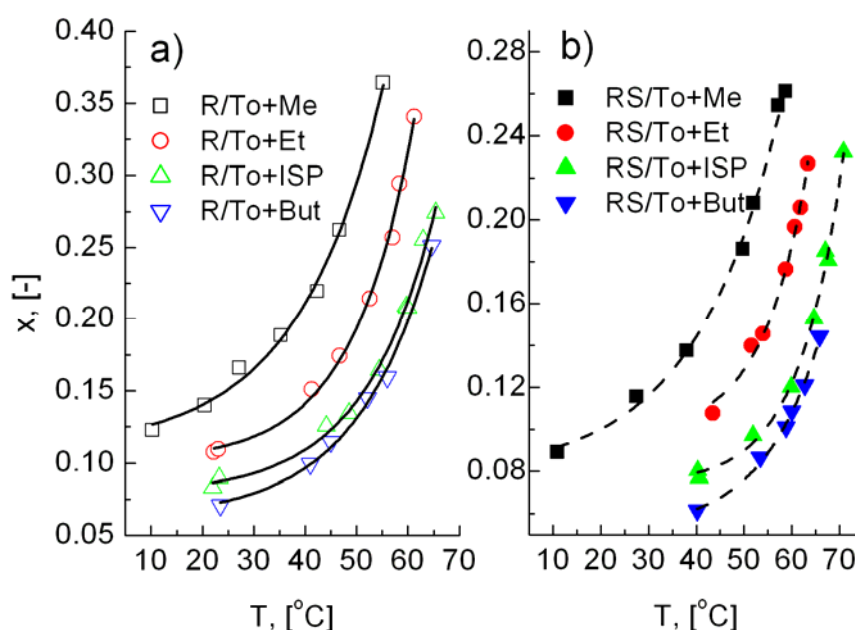
Figure 8.15: *SLE in solvent mixtures of 95:5% (w/w) toluene/alcohols.*

In short, small amounts of alcohols are able to increase significantly solubility of the 3ClMA species in toluene-based solvents. Thus, these alcohols can be further used as assistant agents in crystallization process due to their ability in tuning solubility of 3ClMA species in toluene. Additionally, the calculated eutectic compositions in these solvent mixtures are rather similar to the case of pure toluene as solvent. The calculated eutectic compositions appear to be temperature- and solvent-composition independent. Those values are found around $x_{R\_cal}^{Eu}$ = 0.93. Further investigation for

the TPDs of those solvent mixtures seems to be not necessarily since the results are expected to be similar to the pure toluene as solvent.

Table 8.5: *Enthalpy of dissolution and estimated eutectic composition of 3ClMA in toluene-based solvents modified with various alcohols.*

Solvents	ΔH_{R1}^{diss}, [kJ·mol⁻¹]	ΔH_{RS1}^{diss}, [kJ·mol⁻¹]	$x_{R\_cal}^{Eu}$, [-]
Toluene + MeOH	20.35	24.60	0.93
Toluene + EtOH	21.68	29.25	0.93
Toluene + iPrOH	22.91	31.21	0.92
Toluene + ButOH	26.33	34.36	0.93
Toluene	51.27	58.42	0.93

8.2.3.3 Effects of ethyl acetate (EA) to SLE of the 3ClMA/toluene system

EA is also able to enhance solubility of 3ClMA species similar to cases of the above alcohols. Herewith, a solvent mixture containing 80:20% (w/w) toluene and EA improves significantly solubility of both the enantiomer and the racemate of 3ClMA as depicted in Figure 8.16.
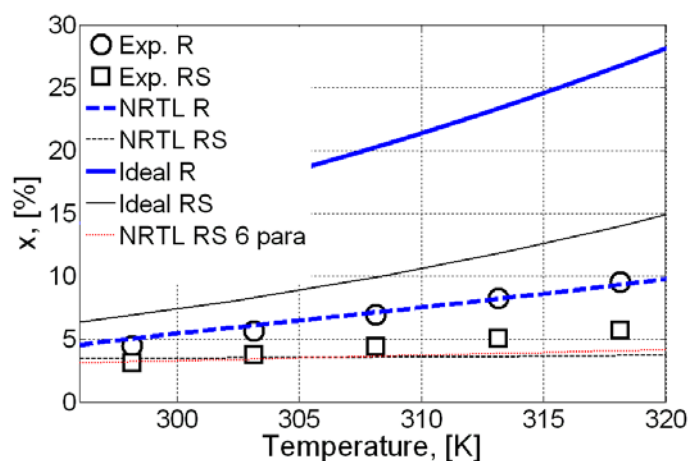
Figure 8.16: *A mixture of toluene/EA (80:20 w/w) as an alternative solvent. Symbols stand for experimental solubility data of the enantiomers (o) and the racemate (□). Lines present model correlations.*

Over the studied temperature range, solubility curves of both the enantiomer and the racemate of 3ClMA increase with temperature but both of them are strongly deviated from the ideal solutions. The deviation indicates non-ideal behavior of those real solutions. The solubility ratio of the enantiomer and the racemate retains nearly constant thus the eutectic composition is expected unchanged.

Furthermore, interactions quantification was carried out for the dissolution of 3ClMA in the solvent mixture toluene/EA (80:20 w/w). The obtained three-parameter model (Table 8.6, set 1) provided high accuracy for the enantiomer but it does not fit well for the racemate, especially at elevated temperatures (Figure 8.16, bold and thin dashed lines, respectively). Quantification and model parameterization for six-parameters (Table 8.6, set 2) yields similar results (Figure 8.16, dotted line). Thus, the computational attempts to fit the model directly to the whole experimental data set considering heterochiral interactions did not result in a more favorable fit to the solubility curve of the dissolution process of the racemate in the solvent mixture. Thus, interactions of solvent and solute are dominating dissolution process. Heterochiral and homochiral interactions between the enantiomers are negligible.

Table 8.6: *NRTL model parameter sets. Set 1 and 2 are used for the three and six parameter models describing the SLE process of 3ClMA in a solvent mixture toluene/EA (80:20 w/w).*

Parameter set	α_{12}, [-]	Δg_{12}, [J·mol^{-1}]	Δg_{21}, [J·mol^{-1}]	α_{13}, [-]	Δg_{13}, [J·mol^{-1}]	Δg_{31}, [J·mol^{-1}]
1	0	0	0	0.6033	1.1095e6	0.7205e6
2	0.00680	0.5965	-1.1260	0.6033	1.1095e6	0.7205e6

The TPD of 3ClMA in this solvent mixture was determined from the obtained three-parameter NRTL models (Table 8.6, set 1). Results are graphically presented in Figure 8.17.
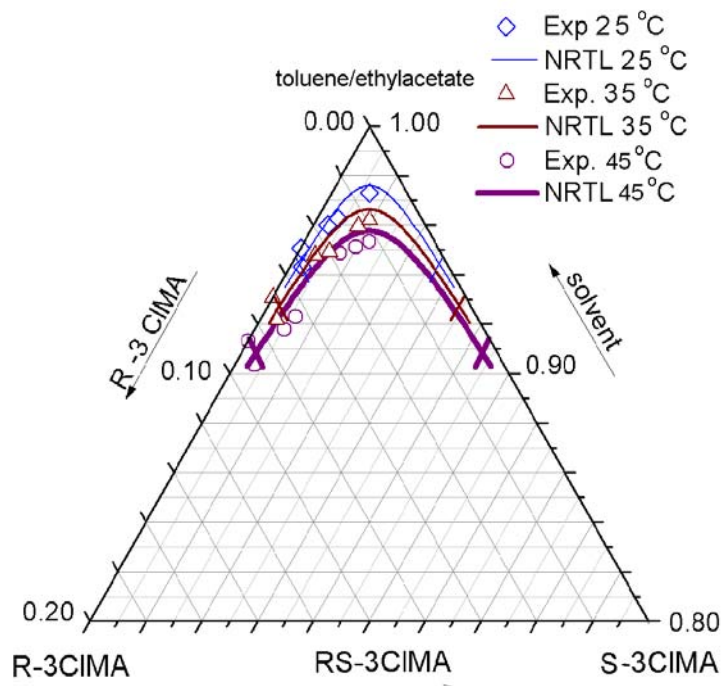
Figure 8.17: *The TPD of 3ClMA in Toluene/EA (80:20 w/w).*

Obviously, the NRTL results (lines) come close to experimental ternary solubility data (symbols). The slopes of isotherm curves should be discussed here. Generally, the extended solubility lines (so called metastable solubility curves) play an important role in preferential crystallization. Therefore, the slopes of isotherms are especially interesting. In the case of the toluene/EA mixture (Figure 8.17), the isotherms show similar slopes between 25 and 45 °C. The metastable solubility curves cross the two-phase regions, which can be attractive for preferential crystallization.

Figure 8.17 reveals a satisfying agreement of the eutectic compositions between measured data and the model prediction. The intersections of the two branches of the solubility isotherms in the TPD give the eutectic composition in the chiral system at specific temperatures. The NRTL model predicts remarkably accurate the eutectic composition in the solvent mixture. It yields the eutectic composition at x_R^{Eu} = 0.93, while experimental values were measured at x_R^{Eu} = 0.92. Both the experimental and model determination found that the eutectic composition is temperature-independent in the studied temperature ranges. Additionally, in Chapter 7, the NRTL model precisely predicted the TPD for the case of lactide. In short, the NRTL model is capable to study SLE of many chiral systems as reported in literature[186–190] as well as these two model compounds in this thesis.

8.2.3.4 SLE of 3ClMA in water

a) Special solubility behavior of the enantiomer of 3ClMA in water

SLE of the enantiomers of x-ClMA (x – stands for 2, 3 and 4) derivatives in water are relative similar. First, following analysis is carried out for a case studied of 3ClMA. Figure 8.18(a) shows an "inflection" point at about 35 °C on solubility curve of the enantiomer of 3ClMA in water. Obviously, this solubility curve can be divided into two parts. At the temperatures lower than 35 °C, solubilities slightly increase with temperature similar to the other solvents or mixture solvents described above. However, significantly high solubilities are observed at elevated temperatures. These tendencies establish solubility curve of R-3ClMA as an "S"-shape. The observation indicates two different types of solutions corresponding two different temperature ranges which need further investigation to understand these complicated behaviors. Besides 3ClMA, analogical observations were also found for other derivatives, *i.e.* 2- and 4-chloromandelic acid (abbreviated 2ClMA and 4ClMA) as plotted in Figure 8.18(a). Interestingly, the enantiomers of 3ClMA and 4ClMA yield identical solubilities which are higher than those of 2ClMA. Thus, chloro-group located at the octo- or para-positions in benzyl ring will not alter solubility of chloromandelic acid derivatives. Due to similarity tendency of these curves, the SLE of these derivatives of chloromandelic acid are influenced by the same mechanism.

Hereby, 3ClMA is selected to further study the special solubility behavior. To explain this SLE behavior, a systematic approach is applied for both the solid and the liquid phases. On one hand, this behavior can be related to solid-phase variation such as polymorphic transformation, solvate or solid solution formation. On the other hand,

that can be resulted from the change in the liquid phase. The major effects will be proven as follows.

Suspensions of the enantiomer 3ClMA and water were kept longer than 2 days at various temperatures from 5 to 60 °C. The residual solids of these measurements at two temperature regions were carefully checked with XRPD analysis. The results show that all the solid phases retain the same to the initial phase of the stable enantiomer. That means the special SLE behavior did not cause from solid-phase variation. Consequently, the only possibility relates to the liquid phase. The further attempts relating to the liquid phase found that the special SLE of the enantiomer in water is strongly influenced by two effects, *i.e.* "oiling out" and "association".

"Oiling out" behavior

First of all, "oiling out" behavior of the enantiomer can be observed using a special experiment setup based on turbidity observation (measured with the Crystal16™). The results are shown in Figure 8.19. Four heating-cooling cycles are applied for a clear solution of the enantiomer of 3ClMA in water. The concentration of this solution is w = 0.20 (w/w). The turbidity results from those cycles are quite similar. At elevated temperatures, the second liquid phase is formed and mixed with previous liquid phase. Therefore, variation of turbidity relating to these progressive events is captured by the turbidity sensor inside the Crystal16™. This phenomenon is also recently reported as a so called "oiling out"[202–205]. Herewith, Figure 8.18(b) schematically presents thermodynamic equilibrium of an "oiling out" system. There is a special domain in which a total composition at **A** will establish equilibrium of two liquids **L**B and **L**c. Consequently, this phenomenon leads to extreme high solubility of the enantiomer 3ClMA at elevated temperatures.
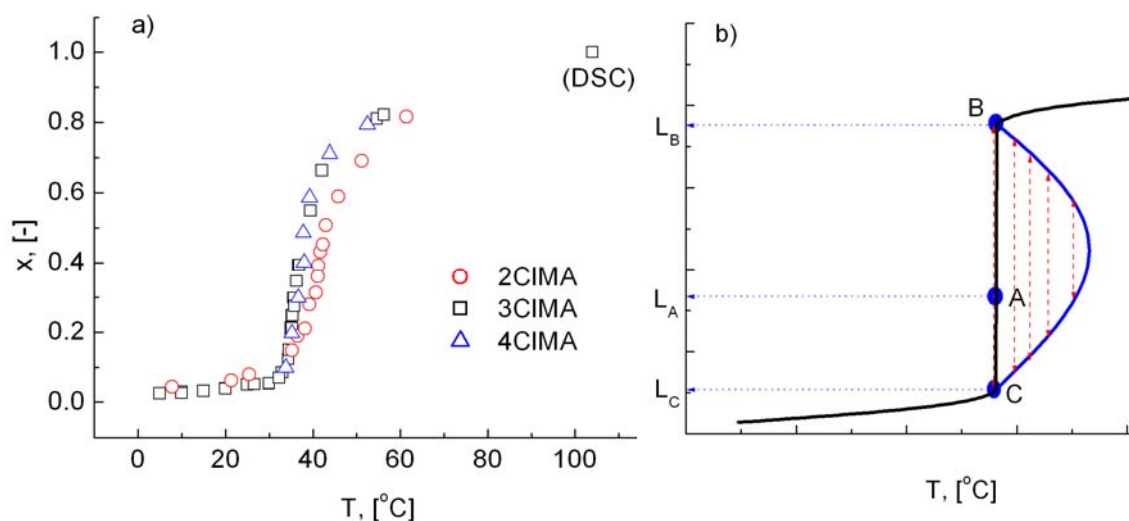
Figure 8.18: *(a) Solubility curves of the enantiomers of 2-, 3-, and 4ClMA in water show a special behavior with inflection points. (b) A hypothesis of "oiling out" is proposed[201,202].*

Afterwards, additional experiments were carried out for the same above solutions from the Crystal16™ measurements. Those samples were heated to 50 °C and stirred by magnetic stirrers as seen in the experimental set up in Figure 8.19. At elevated temperatures, the second liquid phase appears but its optic properties are very similar to normal water (difficult observation by naked eyes). The "oiling out" phase can be hardly seen in Figure 8.20 (inside marked areas).
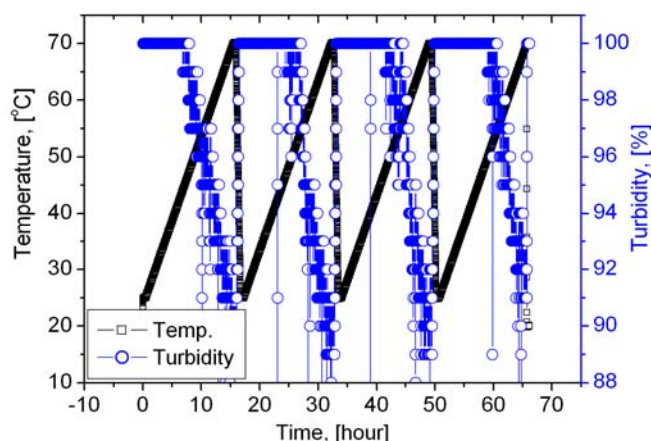
Figure 8.19: *Turbidity observation of "oiling out" occurring at elevated temperatures of R-3ClMA.*
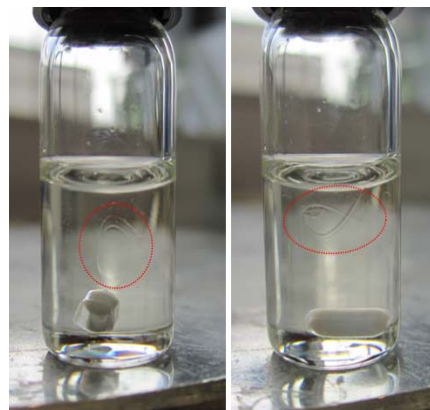
Figure 8.20: *"Oiling out" visibility*

Association-deassociation of the enantiomer 3ClMA

Besides "oiling out", SLE of the enantiomer in water is also affected by another mechanism so called association-deassociation. First of all, a clear aqueous solution of the enantiomer (w = 0.02, [-]) was examined by HPLC analysis coupled with a mass spectroscope (MS). From MS results, this solution was composed from a mixture of two different forms of R-3ClMA, *i.e.* "monomer" (M ≈ 185) and "dimer" (M ≈ 371). The results are shown (Figure 8.21).
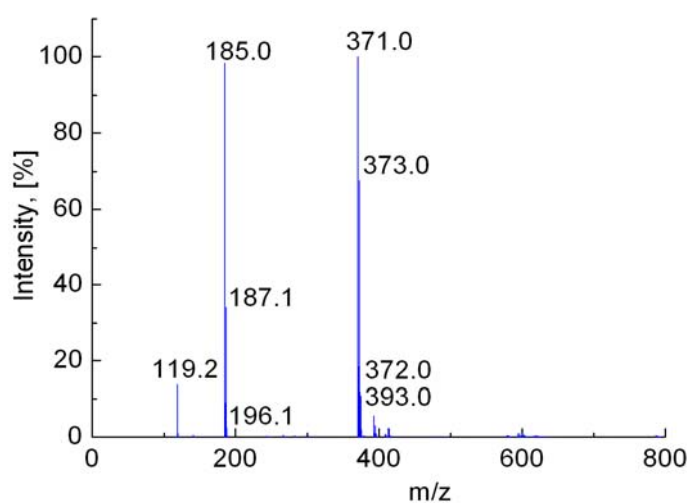
Figure 8.21: *Mixture of "dimer" and "monomer" of R-3ClMA.*

There is equilibrium between the "dimer" and "monomer" forms of R-3ClMA which is expressed as Eq. 8.1. Thermodynamically, the "dimer" form is preferable at lower temperatures while increasing temperature will move the equilibrium to produce "monomer", *i.e.* free 3CLMA acid. Therefore, that will increase the [H⁺] along with temperature as depicted in Figure 8.22.

$$R_{2<L>} \leftrightarrow R_{<L>} + R_{<L>} \qquad \text{(Equation 8.1)}$$
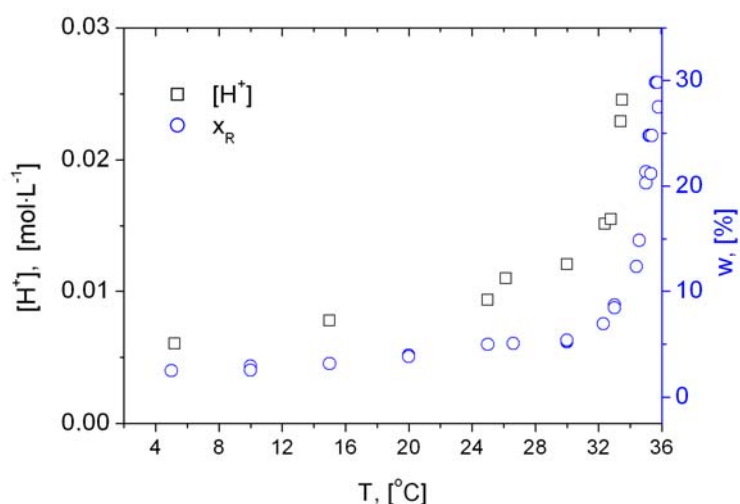
Figure 8.22: *A suspension of R-3ClMA in water is gradually heated and stirred (immersed Pt-100 and pH probes). Increasing [H⁺] values vs. temperatures might relate to de-association tendency where "dimer" of R-3ClMA transforms to "monomer" forms.*

Herewith, Raman shifts are used to derive mechanism of association and de-association. Figure 8.23 records Raman spectra of R-3ClMA with respect to temperature in toluene (a) and water (b).
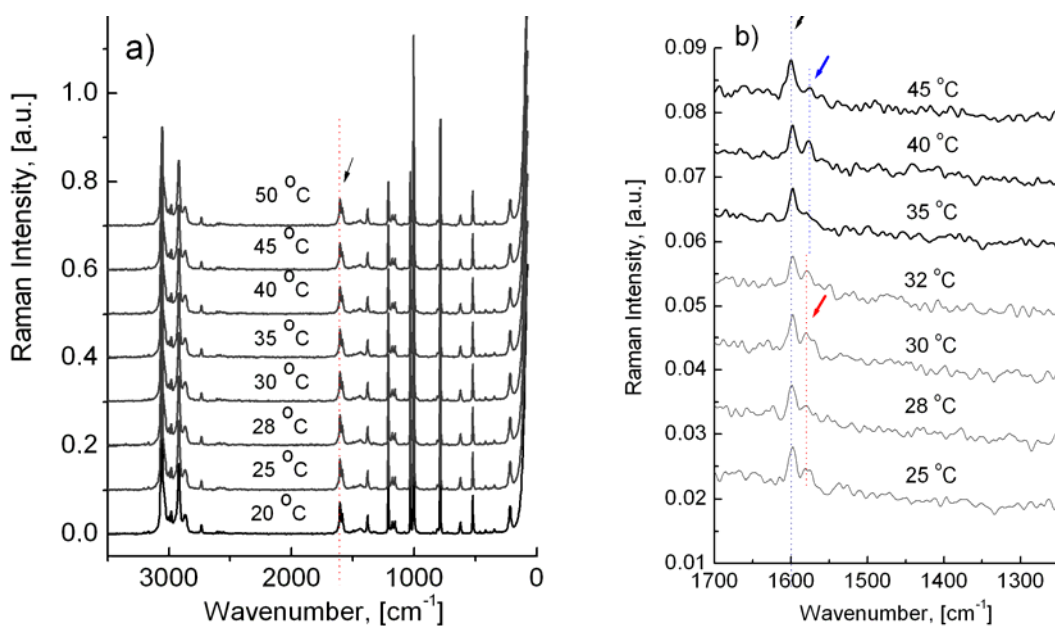
Figure 8.23: *Raman spectra of R-3ClMA in (a)-toluene and (b)-water.*

Indeed, Raman spectra are identical for all solutions of R-3ClMA in toluene over the temperature range from 20 to 50 °C. That means the solution structure of R-3ClMA in toluene is retained in the whole temperature range. In contrast, Figure 8.23(b) shows Raman's shift at 1557 and 1560 cm^{-1}. Those positions relate to vibration of –C=O in carboxyl group[206,207]. The mechanism can be proposed as follows.

At low temperatures, two molecules of R-3ClMA can form "dimer" via hydrogen bonds as illustrated in Figure 8.24. Increasing temperature will diminish the hydrogen bonds to form "monomer" and increasing system entropy. Indeed, association has been frequently seen for many systems as reported in literature.[207–209] Nevertheless, this hypothesis for 3ClMA actually needs further work to have deeper understanding about this complicated behavior.
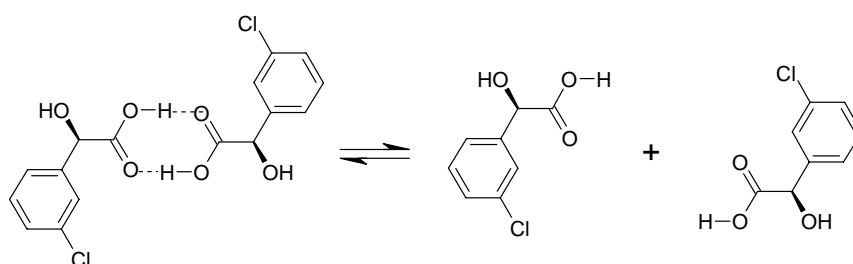
Figure 8.24: *Proposed mechanism of association-deassociation of the R-3ClMA in water[207].*

b) The TPD of 3ClMA in water

In water as solvent, only the TPDs for stable forms will be constructed in this part to reduce the complexity of this polymorphic system 3ClMA. Solubilities are measured by three different techniques (gravimetry, HPLC and refractometry) of which results are in a good agreement.

As described above, solution states of 3ClMA are different at low and high temperatures. To simplify, Figure 8.25(a) presents the solubility curves of the pure substances at temperatures lower than 35 °C. In the studied temperature range, the solubility of racemate is almost linear. Solubility of the enantiomer is more sensitive to temperature changes. However, both of them significantly differ to the ideal cases.

The TPD of 3ClMA as water solvent is drawn in the conventional equilateral triangular shape (see Figure 8.25(b)). The isothermal solubility curves show that 3ClMA is a racemic compound-forming system. The NRTL model describes pronounced accuracy SLE of 3ClMA in both case binary and ternary solubility diagram with 3 parameters as Table 8.7. Therefore, the hetero- and homochiral interactions of the enantiomers can be neglected in the aqueous solution of 3ClMA. Similar to the case of toluene/EA, the slopes of the isotherm curves here are also favorable for preferential crystallization technique to separate the pure enantiomers.
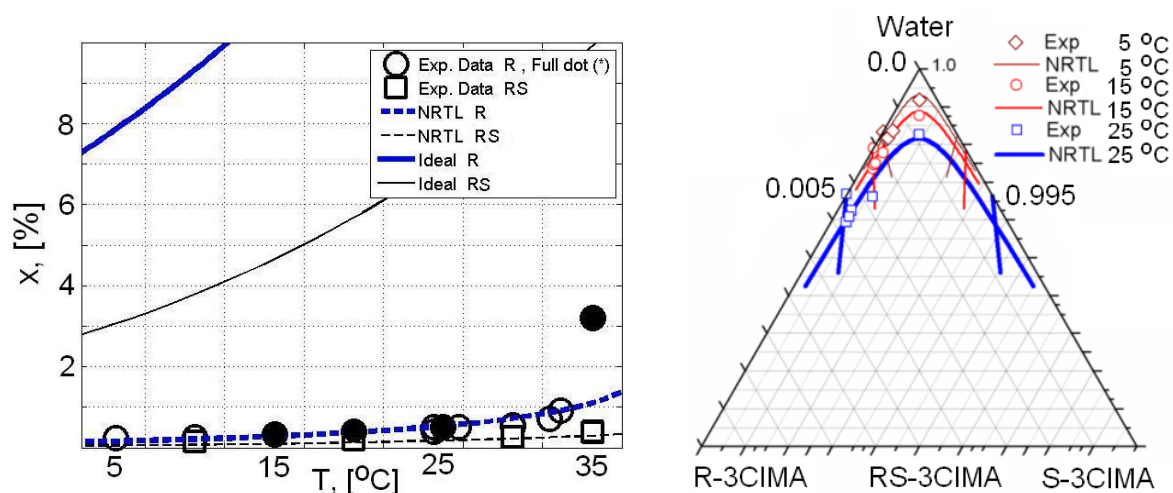
Figure 8.25: *(a) Binary solubility 3ClMA in water at moderate temperatures.*[197]*

Figure 8.25: *(b) TPD of 3ClMA species at moderate temperatures*

Table 8.7: *NRTL model parameters, assuming ideal heterochiral behavior $\Delta g_{12} = \Delta g_{21} = 0$.*

Parameters of NRTL model		
α_{13}, [-]	Δg_{13}, [J·mol⁻¹]	Δg_{31}, [J·mol⁻¹]
0.7269	-2.2581e6	3.6191e3

Indeed, the eutectic compositions in the TPDs were predicted remarkable accurately via the NRTL model for both solvents, *i.e.* a mixture of toluene/EA and water. The results are summarized in Table 8.8.

Table 8.8: *Eutectic composition determination in TPDs. (*) and (**) correspond to eutectic compositions Eu₁ and Eu₂ which will be used in experimental validation part of the proposed "two-step" process.*

T, [°C]	Toluene/EA (80:20 w/w)				T, [°C]	Water			
	w,[-]		x_R^{Eu}, [-]			w, [-]		x_R^{Eu}, [-]	
	Exp.	NRTL	Exp.	NRTL		Exp.	NRTL	Exp.	NRTL
25 (*)	0.082	0.087	0.91	0.92	5	0.027	0.031	0.89	0.89
35	0.137	0.138	0.92	0.92	15	0.039	0.038	0.89	0.89
45	0.186	0.173	0.92	0.93	25 (**)	0.061	0.064	0.89	0.89

At elevated temperatures, solubility of the enantiomer dramatically increases due to "oiling out" and de-association while the racemate slightly increase as a linear function. Moderate solubilities are found at lower temperatures, while vigorous increase of solubilites is observed above temperatures of the inflection point. This behavior leads to the variation of the eutectic composition of the enantiomeric 3ClMA system. In the temperature range lower than the inflection point, the eutectic composition change might be neglected. However, it significantly differs at higher temperatures. The full TPD is presented in Figure 8.26 of which the eutectic compositions change from x_R^{Eu} = 0.91 to 0.84 over the temperature range between 5 and 50 °C. Thus, 3ClMA system was proved that the eutectic compositions are varied under temperature effects (*e.g.* in water, between 5 and 50 °C) or solvent effects (*e.g.* between the mixture toluene/EA and water).
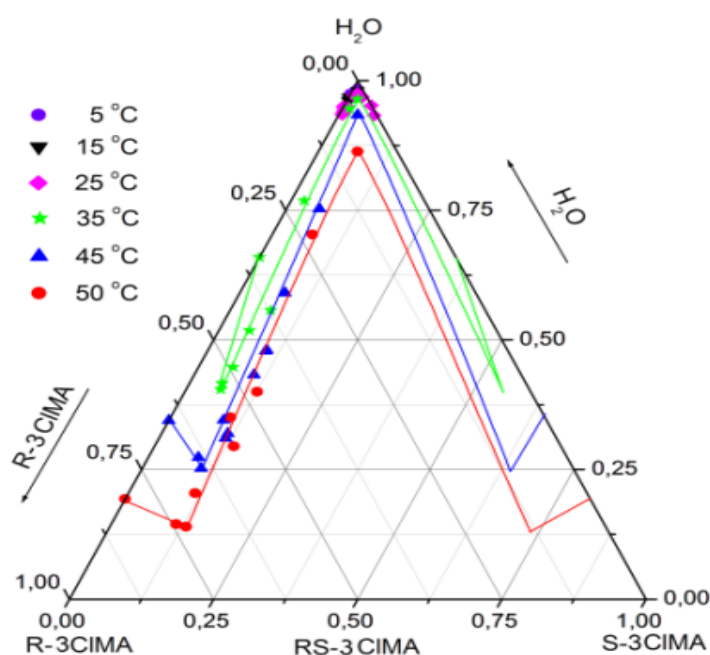
Figure 8.26: *TPD of 3ClMA in water. Lines guide to the eyes.*[197]

8.2.3.5 Summary for SLE of 3ClMA in solutions

SLE of 3ClMA in various solvents and solvent mixtures show the analogous shapes between the solubility isotherms in the TPDs and the liquidus curves in the BPD. The similarity confirms that the chiral 3ClMA belongs to the racemic compound-forming systems. Since 3ClMA is a polymorphic system, appropriate conditions to obtain "right" polymorphs have been carefully studied. From SLE determination of 3ClMA in various solvents, the eutectic compositions are obtained and recorded in Table 8.9.

Further work will develop efficient approaches to separate the R-enantiomers of 3ClMA using the acquired knowledge of the TPDs and polymorphism as described in the next section.

Table 8.9: *Summary of the eutectic compositions of 3ClMA system in different solvent(s).*

Solvent(s)	T, [°C]	x_R^{Eu}, [-]
Toluene	30–80 °C	0.91
Toluene/EA	25–45 °C	0.92
Water	5–50 °C	0.91–0.84

8.3 Resolution design via various crystallization techniques

As proved above, 3ClMA is a racemic compound-forming system including polymorphism that is a challenge for enantioseparation via crystallization. In this section, efficiency of both techniques (the "two-step" selective and preferential crystallization) will be examined for this system.

8.3.1 The concept of the "two-step" process exploiting the eutectic shift

The concept of the "two-step" process is graphically depicted in Figure 8.27. Two isotherms (T_1 and T_2) with two enantiomeric eutectic compositions (denoted as **Eu₁** and **Eu₂**) are considered in which the R-enantiomer portion of **Eu₁** is higher than that of **Eu₂**. The first step is actually an enantiomeric enrichment in the liquid phase. Starting point of process is the system at **A** of which the composition belongs to the three-phase domain of the isotherm T_1 (see Figure 8.27). Point **A** can be an arbitrary system in the three-phase domain. It will establish an equilibrium between the eutectically composed liquor at point **C** (*i.e.* target product of this step) and a specific residual solid mixture of the enantiomer and the racemate at point **B**. Thus, the purity of R-3ClMA increases from the initial value x_R^A to x_R^{Eu1} (at **C**) via a simple classical crystallization step. As a sequence, a phase separation step is needed to obtain solution **C**. Solvent exchange is the next step in order to locate the overall composition of solution **C** into the two-phase domain of the second isotherm T_2, *e.g.* at point **D**. This placing step is applicable only if the chiral system fulfills the following condition $x_R^{Eu1} > x_R^{Eu2}$. The pure target product R-3ClMA will be obtained as a crystalline phase from the equilibrium of system **D**.
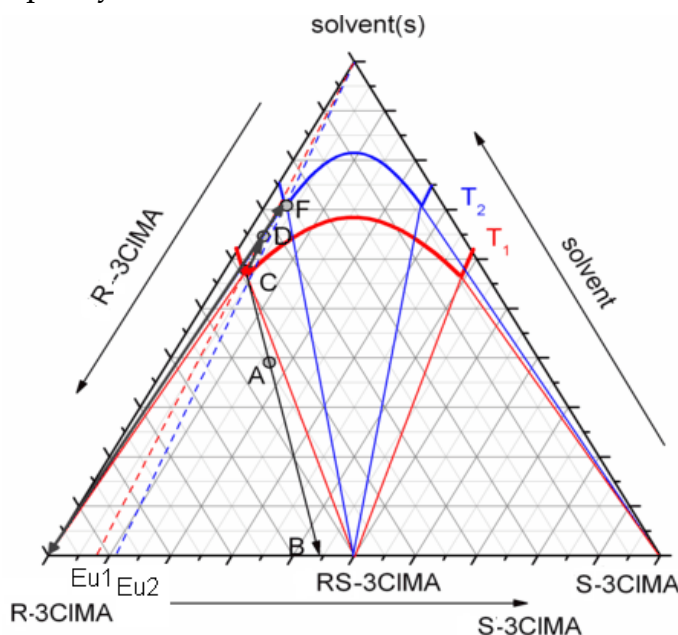
Figure 8.27: *The "two-step" process for 3ClMA.*

8.3.1.1 Validation of the "two-step" process with the eutectic shift via solvent exchange

As described in the SLE determination part 8.2, the eutectic compositions of 3ClMA can be varied in different solvents. In this work, a mixture of toluene/EA (80/20 w/w) and water are two selected solvents to validate the "two-step" process under solvent effects. Isotherms were selected at $T_1 = T_2 = 25$ °C. The determined SLE showed a shift of the eutectic compositions of 3ClMA in these two solvents (all solid phases are the stable forms R_1 and RS_1). Particularly at 25 °C, the eutectic point **Eu₁** in the solvent mixture possesses the enantiomeric composition of $x_R^{Eu1} = 0.91$ while the eutectic point **Eu₂** in water (at 25 °C) shows the composition of $x_R^{Eu2} = 0.89$. Applying those data in the "two-step" process, the experimental validation results are summarized in Table 8.10.

Table 8.10: *The "two-step" selective crystallization process using via solvent exchange.*

Step	Starting solutions			Equilibrium phases			
				Solid		Liquid	
	m, [g]	x_R, [-]	w, [-]	m, [g]	x_R, [-]	m, [g]	x_R, [-]
1	75.91	0.74	0.14	6.15	0.56	47.15	0.92
2	47.56	0.91	0.08	0.95	0.99	42.54	0.89

First, an amount of 11.30 g initial solid mixture (enantiomeric composition x_R of 0.74 of the R-enantiomer) was added to the solvent mixture to obtain 75.91 g solution (total concentration of w = 0.14). This system belongs to the three-phase domain of the first isotherm which possesses a eutectic composition at x_R^{Eu1} (see Table 8.10). The "first" equilibrium was established at 25 °C after 3 days (checked with density measurements). An amount of 47.15 g of the eutectically composed liquid ($x_R = 0.91$ of the R-3ClMA, HPLC analysis) and 6.15 g of a residual solid mixture (containing $x_R = 0.56$, Figure 8.29(b)) were obtained. Totally evaporating solvent mixture obtained 3.82 g solid (containing $x_R = 0.91$ of the R-3ClMA). The yield of this step is calculated by Eq. 5.1 at 41.6%.

Consecutively, the second isotherm corresponding to the eutectic composition x_R^{Eu2} was exploited. An amount of water was added to the above solid (3.82 g) to obtain 47.56 g of a suspension (w = 0.08). The system was again kept at 25 °C in 3 days under well-stirred conditions. The "second" equilibrium yielded 0.95 g solid of the target enantiomer (Figure 8.29(c)) with a purity of $x_R = 0.99$ of the R-3ClMA (HPLC analysis). The corresponding mother liquor showed the eutectic composition in water ($x_R = 0.89$ of the R-3ClMA, HPLC analysis). Thus, the overall composition was located on the boundary of the two- and three-phase regions. The yield of the "second" step was 27.3%. Comparing the mass of the final product and the total mass

of initial solid mixture, the total yield was obtained as 11.4% while to the theoretical yield of 13.5%. Herein, the calculation used Eqs. 5.3, 5.4 and 5.5 for each step and the overall process, respectively. The experimental yields of each step and the overall process are plotted in Figure 8.28.
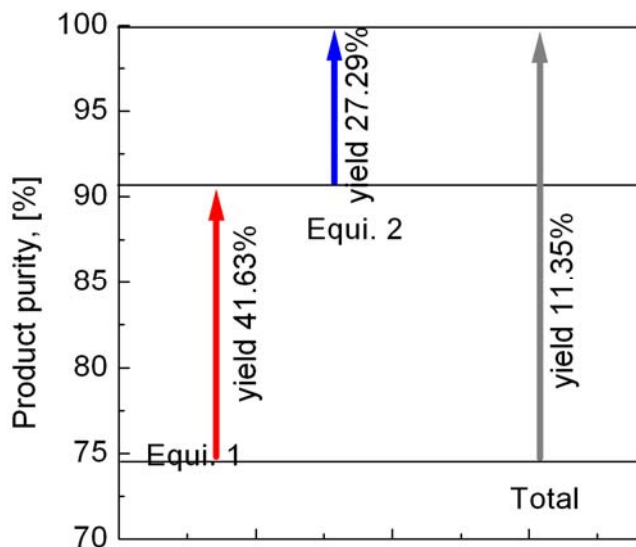
Figure 8.28: *Yields of each step and the whole enantiopurification process.*

Evidently, the total yield was relatively small. However, this value can be increased by optimizing the process configuration such as reducing the mass loss in intermediate steps, decreasing the residual solid in 1st step by alternating another optimized starting point. If the initial mixture locates at the first eutectic composition then the total yield can reach a value of 27.3%. Searching other conditions, which can provide significant differences of the eutectic compositions, is also a solution to improve the process efficiency. Besides, the by-products of residual solid in the 1st step or mother liquor in the 2nd step can be recycled due to their partial enrichment of the target enantiomer.
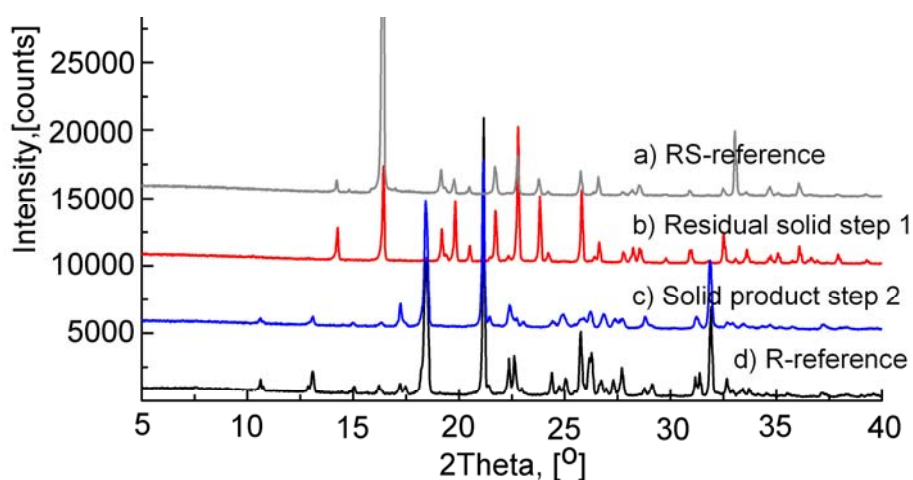
Figure 8.29: *XRPD patterns of the solid products from the "two-step" process.*

Figure 8.29 shows the XRPD patterns of the equilibrium solid phases obtained from the "two-step" selective crystallization process. Residual solid from the 1st step is a mixture of the racemate and a very small amount of the enantiomer (compared patterns (a) and (b)). The solid product of the 2nd step shows the same phase to the reference enantiomer (compared patterns (c) and (d)).

8.3.1.2 Validation of the "two-step" process using the eutectic shift via polymorphic effects

3ClMA is a polymorphic system as proved in part 8.1. As seen in the BPD (Figure 8.10), there are 4 different eutectic compositions which are composed from various polymorphs. That leads to opportunities to exploit the eutectic shift technique. The main issue is finding the suitable conditions to crystallize the 3ClMA species as the desired phases. It is worthy to remind that both enantiomer and racemate can be recrystallized as the stable forms R_1 and RS_1 in water. However, in toluene, a mixture containing simultaneously the enantiomer and the racemate of 3ClMA can recrystallize in a different manner, *i.e.* R_1 and RS_2. In fact, the enantiomeric eutectic compositions of 3ClMA in water (at 25 °C) and toluene (recrystallized) were measured at x_R^{Eu} = 0.89 and 0.82, respectively. These values will be used in Scheme 8.1. Herein, a process is designed to prove the feasibility of enantioseparation via the "two-step" selective crystallization. The concept is based on the shifts of the eutectic compositions which are resulted from various polymorphs.

Water was used in the first step. An amount of 118 g of an enriched solution with the enantiomeric composition x_R^{ini} = 0.62 was placed in the first crystallizer under well-agitated conditions at 25 °C. After 2 days, the equilibrium established between the residual solid mixture (R_1 + RS_1) and the eutectic mother liquid at **Eu₁** (x_R^{Eu1} = 0.89). From this solution, 5.5 g solid mixture of R_1 and RS_1 (89% of R-3ClMA) was obtained by an evaporating step. This solid product was transferred to the 2nd crystallizer as depicted in Scheme 8.1.

In the second step, toluene was alternatively used. Toluene was added in the 2nd crystallizer together with the previous solid mixture to obtain 50 g of solution (concentration of w = 0.11). This suspension is completely dissolved at high temperature and whole system then was kept at 70 °C. The second isotherm was exploited with the eutectic composition **Eu₂** of x_R^{Eu2} = 0.82. In principle, the solid product obtained from this step should be the pure enantiomer. However, HPLC analysis showed the purity of 98.8%. The contamination came from filtration where mother liquor was adsorbed onto the surface of crystals. The yield of this process reaches a value of 15.9% while the theoretical value at the same initial compositions (using Eqs. 5.3, 5.4 and 5.5) is 25.1%. The optimal case will obtain the yield of 45.5% if the initial solution is pre-enriched up to $x_R^{ini} = x_R^{Eu1}$ = 0.89.
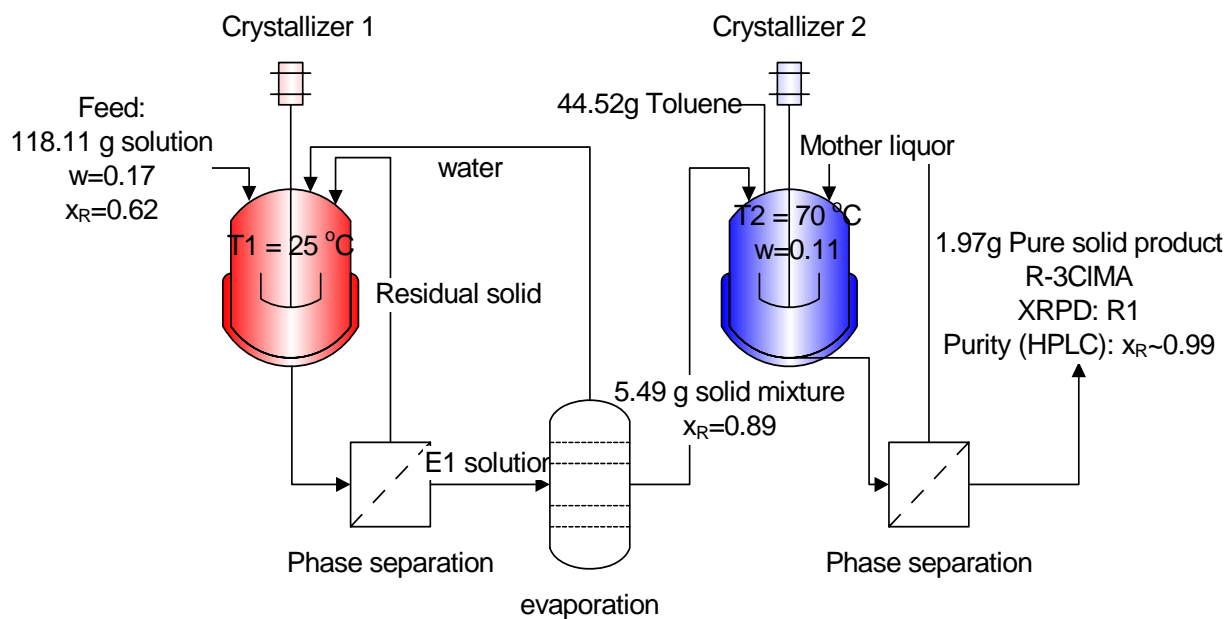
Scheme 8.1: *Applying "two-step" process for polymorphic system 3ClMA.*

Throughout the above demonstrations, evidently, the "two-step" process is quite flexible for enantioseparation. Exploiting the eutectic shift technique has been demonstrated in this part relating to solvent and polymorphic effects. Additionally, exploiting the eutectic shift under temperature effects (*e.g.* the case of water at low and high temperatures) is also a potential application. The efficiency of the above thermodynamic designs will be compared to kinetically controlled enantioseparation technique (preferential crystallization) as follows.

8.3.2 Applicability of preferential crystallization for 3ClMA system

8.3.2.1 Induction time of 3ClMA species

Attempts to measure the MSWZ of 3ClMA in water was not successful with the Crystal16™ due to the extremely large MSZW of those species. The saturated solutions of the enantiomer and the racemate at 30 °C did not crystallize even if they were cooled down to –5 °C (water as solvent). Then, an alternative which measured the induction time with respect to degrees of supersaturation was carried out. Results are shown in Figure 8.30.

In fact, only the induction time of racemate was recorded while nucleation of the enantiomer was not detectable since the supersaturation solutions of the enantiomer retained clear for such a long period (more than 2 days, longer than the operation time of crystallization processes in the next section). Due to the relationship between induction time and MSZW, it can be stated that MSZW of the enantiomer is much larger than that of the racemate. In principle, that is a disadvantage in purification of the single enantiomer(s) since the racemate species is easily able to nucleate and contaminate the final products. Nevertheless, MSWZs of both the enantiomer and the racemate are relative large (more than 30 °C). Hence, attempts to apply preferential

crystallization for enantiopurification of 3ClMA system are carried out in the next part with expectation that these MSZWs are still sufficient for preferential crystallization.
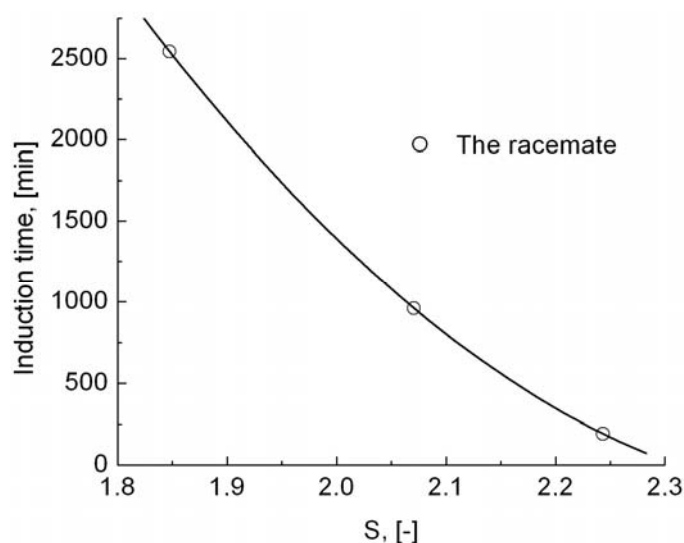
Figure 8.30: *Induction time of the racemate as a function of degree of supersaturation. Induction time of the enantiomer was not detectable due to extremely large of MSZWs.*

8.3.2.2 Preferential crystallization of 3ClMA/water system

Kinetic enantioseparation was carried out with four SIPC[7,28] experimental runs. All experiments were performed in a double jacket crystallizer 500 mL with a propeller (350 rpm) for the same initial solutions. The initial solutions were saturated solutions at 30 °C. The concentration of these initial solutions and the enantiomeric composition were set at $w_{ini} = 0.10$ and $x_R^{ini} = 0.80$, respectively. The objective of these experiments is investigation of the effects of amounts of seed and degrees of supersaturation on the performance of preferential crystallization. The seed was used as fine-crushed powder of the stable form of the enantiomer R[1]. Main results are compared in Table 8.11.

Table 8.11: *Preferential crystallization of 3ClMA is carried out under different conditions. Resolution time refers to the first crystallization period where only the target enantiomer crystallizes.*

Run	$T_{crys.}$, [°C]	m_{seed}, [mg]	Yield, [%]	Resolution Time, [min]
(a)	25	0	26.9	53
(b)	25	50	28.5	35
(c)	25	100	33.8	54
(d)	20	0	53.2	19
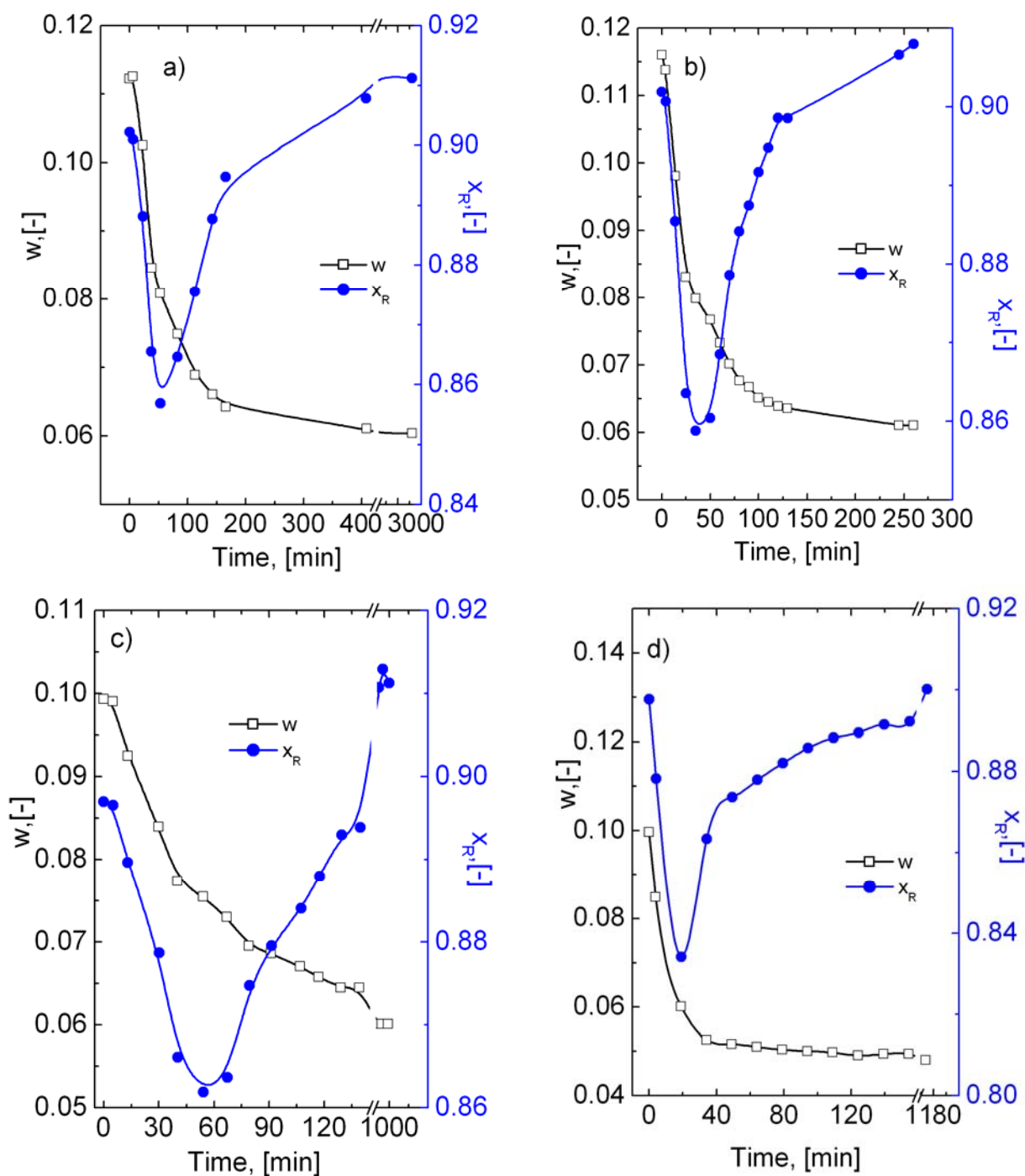
Figure 8.31: *Various SIPC operations were applied for the system 3ClMA/water to produce the pure enantiomer. Operating conditions and relevant results of samples (a)–(d) were summarized in Table 8.11.*

Figure 8.31 graphically presents the crystallization processes of 4 runs from (a) to (d). In all sub-figures, crystallization processes occur with decreasing of total concentrations of liquid phases due to the mass transfer from the liquid phase into the solid phase. In the first periods, only the target enantiomer crystallizes that leads

to decrease of the composition of the crystallized enantiomer in the mother liquors (see x_R curves). Afterwards, the secondary nucleation of the racemate will lead to the contamination of final products by the counter-species racemate and increase again x_R curves. To pursue high enantiomeric purity, these processes were stopped before nucleation of the "contaminator" racemate. Hereby, that period is called "resolution time" and listed in Table 8.11 for four experimental runs.

Amounts of seed significantly influence to crystallization of 3ClMA. Samples (a) and (b) correspond to cases of 0 and 50 mg of seed used for the same initial solutions. Results show that using seed can improve performance of preferential crystallization processes. With presence of the homochiral seed, the system does not need to consume much energy for secondary nucleation of the target enantiomer comparing to primary nucleation without seed. Therefore, the introduced-seed will selectively control whole processes. In run (a) without introduced-seed, the crystallization time for the enantiomer is much longer than that of the seeded-experiment run (b), respectively at 53 and 35 minutes. The yield of run (b) is slightly higher than run (a) about 1.5%. The reason could relate to just a small amount of seed used (only 50 mg). Case (c) used double amount of seed (100 mg) which controls better the crystallization of the enantiomer. The crystallization of the enantiomer lasts longer (about 54 minutes) while the counter-specie racemate is still remained in mother liquor. Thus, the yield of this process increases about 7% comparing to run (a).

Furthermore, degrees of supersaturation also strongly impact to crystallization process of 3ClMA (compare run (d) with the other runs). With the same initial solutions, samples (a)–(c) were performed crystallization at 25 °C while sample (d) was cooled at lower temperature 20 °C. The nucleation of the racemate of sample (d) occurs after 19 minutes and the yield increases more than run (a) about 26%, details can be seen in Table 8.11.

8.3.2.3 Enantiopurification via a combination of preferential crystallization and selective crystallization

This part will present another technique based on both kinetic and thermodynamic control. Mandelic acid (MA) was used instead of 3ClMA due to advantages of the metastable zone widths of those species. Available information in literature about MA/water system was reffered[210]. The concept of combination has been shown in Chapter 5. The main idea is using preferential crystallization to crystallize the racemate species first. As a sequence, the mother liquor composition from this crystallization process may be moved over the eutectic composition depending on delay of secondary nucleation of the enantiomer. Afterwards, evaporating a calculated solvent amount will relocate the total composition into the two-phase domain. The next step is applying the classical selective crystallization to obtain pure enantiomer as an end product.

Table 8.12: *Summary of the combined process to produce the pure enantiomer S-MA.*

		Initial conditions			Final results			
	m_0	199,44	[g]	Mother liquor	147.81	[g]	$x_S = 0.75$	[-]
Step 1	w_0	0.31	[-]	Residual	37.9	[g]	$x_S = 0.51$	[-]
	x_S^0	0.64	[-]	Solid				
Step 2	x_S^0	0.75	[-]	Final Solid	3.5	[g]	$x_S > 0.99$	[-]

Experimental validation conditions were summarized in Table 8.12. The AS3PC process was performed as depicted in Figure 8.32. The solution was completely dissolved even fine particles at 35 ℃ in 2 hours. The whole system was cooled down with two cooling cycles (rates of –1.5 and –0,5 ℃·min^{-1} for the first and the second cooling cycles, respectively). Two Pt-100 sensors were properly installed: one was directly immersed in the thermostat and another was fixed in the crystallizer. The temperature variation of the sensor in the crystallizer is especially interesting as seen in Figure 8.32(a).
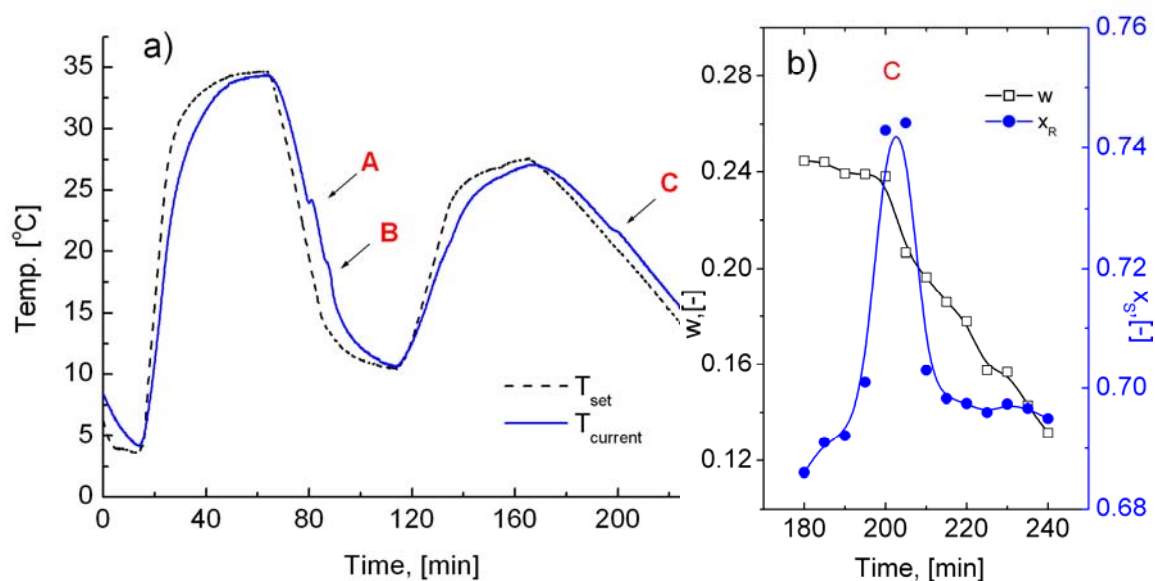
Figure 8.32: *AS3PC of MA in water. Point A: auto nucleation of the racemate; Points B and C are secondary nucleation of the enantiomer in the first and the second cooling cycles.*

Herewith, related events during the crystallization process can be derived from the temperature profiles. Let compare the set-temperature in thermostat and current-temperature in the crystallizer as denoted in Figure 8.32(a). In the first cooling cycle from the saturated solution at 35 ℃, there are two heat events at **A** and **B** corresponding to the nucleation of the MA species. In fact, the nucleation of MA species is exothermic process. The heat generating from nucleation compensates to the cooled-temperature curve resulting two kink points at **A** and **B**. Indeed, primary

nucleation of the RS-MA occurs at point **A**. Further cooling leads to secondary nucleation of S-MA at point **B**. Nucleation of MA already discussed in details elsewhere[210]. Afterwards, whole system was heated again to dissolve the enantiomer species as smaller crystals. Then, this system was cooled again with a slower cooling rate at –0.5 °C·min⁻¹. The crystallization process of the pure racemate was progressively occurring. Up to point **C**, the counter-species enantiomer again crystallized that was indicated by the event at **C**. Therefore, the process should be stopped before point **C** to avoid the entrainment of the enantiomer. This experiment was repeated one more time and the liquid phase was analyzed by HPLC. Results are partly shown for the second cooling cycle. Variation of the total concentration and enantiomeric composition of this period is presented in Figure 8.32(b).

From the AS3PC process above, mother liquor was obtained with the enantiomeric composition (x_S = 0.75) being higher than that of the eutectic composition (x_S^{Eu} = 0.7)[210]. That means the enrichment step was successfully moving the mother liquor not only reaching to the eutectic composition but also relocating the mother liquor directly into the two-phase domain corresponding to the isotherm at 20 °C (point **B** in Figure 8.33(a)). The second step was consecutive with the obtained mother liquor. The system was kept at 20 °C in two days to reach equilibrium in the two-phase region (no stirring to obtain large crystals). Whole process is presented in Figure 8.33(a) as the pathway **A→B→S-MA**. Then, single crystals of the enantiomer were obtained as Figure 8.33(b) with purity more than 99% (no trace of the counter enantiomer was found under HPLC analysis).
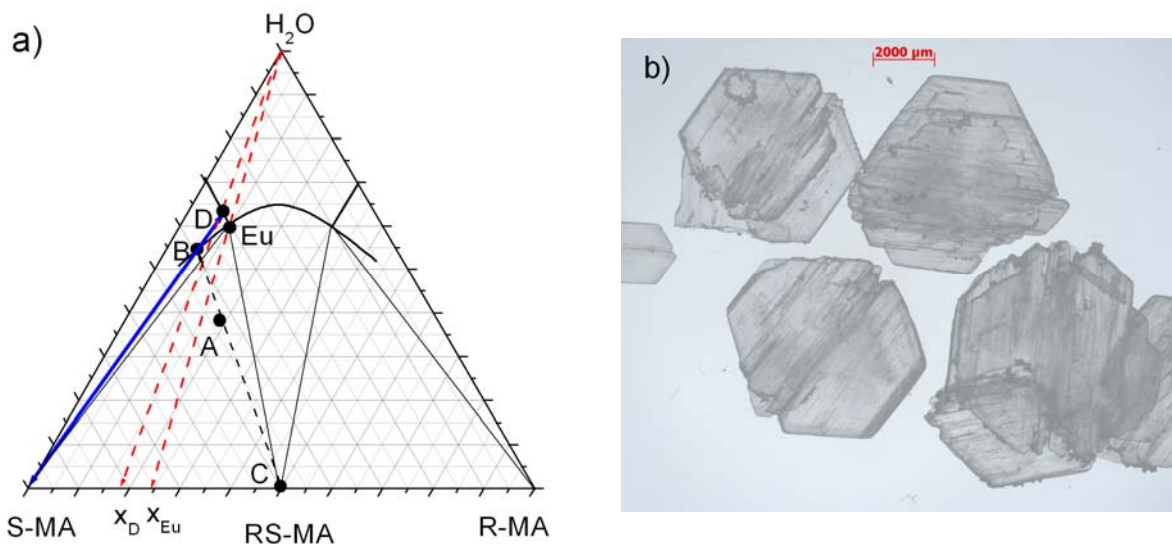
Figure 8.33: *(a) Combination process based on preferential and selective crystallization, validated with MA/water system; Process follows the trajectory **A→B→S-MA**; (b) Single crystals of S-MA obtained from the combination process.*

The experimental yield of whole process is obtained at 8.9%. That value is relatively low due to the mass loss during filtration and washing step. The theoretical yield corresponds to these condition is 23.4%. Similar to the previous cases, the optimal

conditions will improve process yield up to a value of 28.9%. This value corresponds to the composition of initial solution at $x_R^{ini} = x_R^{step1\_end} = 0.75$.

8.4 Conclusions

This chapter contributes to further development of the enantiopurification methodology for the major chiral group, *i.e.* compound-forming systems. The selected compound 3-chloromandelic acid (3ClMA) has been proven to be a compound-forming system via multiple pieces of evidence. All data from X-ray diffraction, DSC and solubility studies highly support this conclusion. Furthermore, 3ClMA was also found as a polymorphic system which increases complexity of the studied compound-forming system. The stability of the metastable polymorphs has been studied under ambient conditions as well as in different solvents. Under ambient conditions, the observed metastable modifications are stable in several months. Otherwise, solvent effects on polymorphic transformation are more complicated, in particular for the racemate.

The completed melting point phase diagram (BPD) was successfully constructed for the polymorphic compound-forming system 3ClMA with DSC measurements supported by XRPD. In the BPD, four eutectic compositions have been addressed. Two of them belong to stable and metastable equilibria while the other are originated from mixtures of the stable-metastable forms. However, finding suitable conditions to establish desired phase and, therefore, correct eutectic compositions is a challenging task. Additionally, 3ClMA did not form solid-solutions.

Solid-liquid equilibria of 3ClMA species in various media were systematically investigated in this chapter. The TPDs were constructed in consideration of relevant solid phases. The eutectic compositions were found to be varied with respect to temperature, solvent, polymorphic effects. This behavior is useful for potential application of the "two-step" selective crystallization technique. Moreover, the enantiomers of 3ClMA and other derivatives shows special behavior so called "oiling out" and association which strongly impact to the SLE results. The values of the eutectic compositions (x_R^{Eu}) in the TPD with water can vary from 0.91 to 0.84 in the temperature range between 5 and 50 °C. Besides, the alternative solvent toluene acts as an agent prohibiting polymorphic transformation. SLE of 3ClMA were also studied with toluene-based solvents modified by ethyl acetate and various alcohols.

Based on the achieved thermodynamic knowledge, efficient approaches to separate the target enantiomer have been successful experimentally validated. The eutectic shifts relating to solvent and polymorphic effects were utilized to prove the feasibility of the "two-step" selective crystallization processes. The experimental yields of the processes were found about 11–16% which can be increased by reducing the mass losses during intermediate steps up to 14–25%. The process efficiency can be improved by an optimization of initial solution compositions, mass losses in intermediate steps. Nevertheless, kinetic crystallization (preferential crystallization) is also applicable for enantiopurification which shows higher process yields

comparing to selective crystallization. Indeed, the yields were found in a range 27–53% depending on specific conditions. Amounts of seed play a vital role in kinetic process control. Furthermore, increasing degree of supersaturation can also significantly improve efficiency of the kinetic enantioseparation process.

Further development based on a combination between kinetic and thermodynamic crystallization was realized for mandelic acid/water system due to their advantages of the relevant MSZWs. In fact, this can be considered as a variant of the "two-step" process but based on half of kinetic and half of thermodynamic control. Experiment was successfully proven the feasibility of this process with a process yield about 9%. In fact, the performance of this process can be improved up to a yield of 29% in optimal conditions. This development could be a potential application for enantioseparation on large scales due to its simplicity and semi-thermodynamic operation.

CHAPTER 9:

SOLVATE FORMING SYSTEM - THE AMINO ACID ARGININE AS A CASE STUDY

Besides polymorphism, solvate formation is another complex behavior that can dramatically change properties of chiral systems. The objective of this chapter is investigation effects of hydrate formation on performance of enantioseparation for compound-forming systems. Those aspects will be examined in a frame of a representative compound, *i.e.* the amino acid arginine.

9.1 Characterization of the solid phases of arginine

Solid phase analytical methods including XRD, XRPD, TG-DSC will be again used to evaluate the possibility of hydrate formation for arginine species in aqueous solutions in consideration of solvent composition and temperature effects.

9.1.1 Arginine – A hydrate forming system

The recrystallized form of the enantiomer of arginine (L-arg) from aqueous solution possesses a different crystal structure comparing to that of the initial anhydrous enantiomer (distinguished XRPD patterns in Figure 9.1(a) and (b)). This observation in general can be explained by the possibilities of hydrate formation or by various polymorphs. Therefore the recrystallized phase was further analyzed with TG-DSC. The results are shown in Figure 9.2(a). According to the TG curve, the total weight change is ~15.2%, which approximates two water molecules in the structure (a theoretical value of 17.1%). The small deviation is probably due to a slight dehydration which could take place during the drying process. Thus, it can be stated that the enantiomer crystallizes as a dihydrate L-arg·$2H_2O$ (abbreviated L·$2H_2O$) from aqueous solution in the temperature range 5–60 °C. Endothermic effects observed in the DSC curve reveal that the dehydration process occurs in several steps over the measured temperature range (Figure 9.2(a)). The dehydrated material was analyzed again with XRPD which shows the same reflections as the initial anhydrous L-arg (Figure 9.1(a)). This double-check is necessary to ensure that the dehydration was completed but did not decompose the main carbon chain of arginine. Besides, the crystallized enantiomer of arginine was also reported as dihydrate[156,157] which gains a good agreement with the present work.
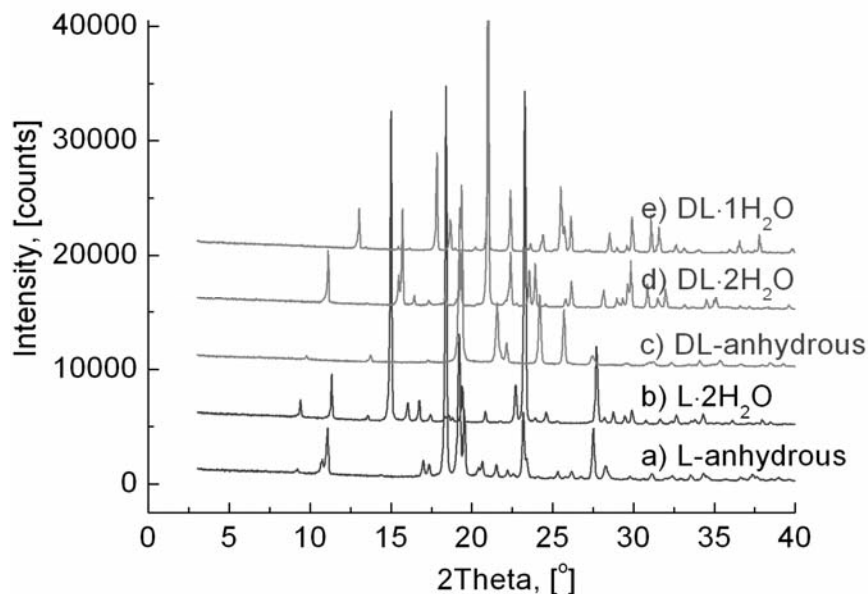
Figure 9.1: *XRPD patterns of various hydrates and anhydrous phases of arginine.*

Similar to the enantiomer, the same procedure was also applied for the racemate. The recrystallized racemate of arginine (DL-arg) was found as two different hydrates, a dihydrate and a monohydrate (abbreviated DL·2H$_2$O and DL·1H$_2$O).
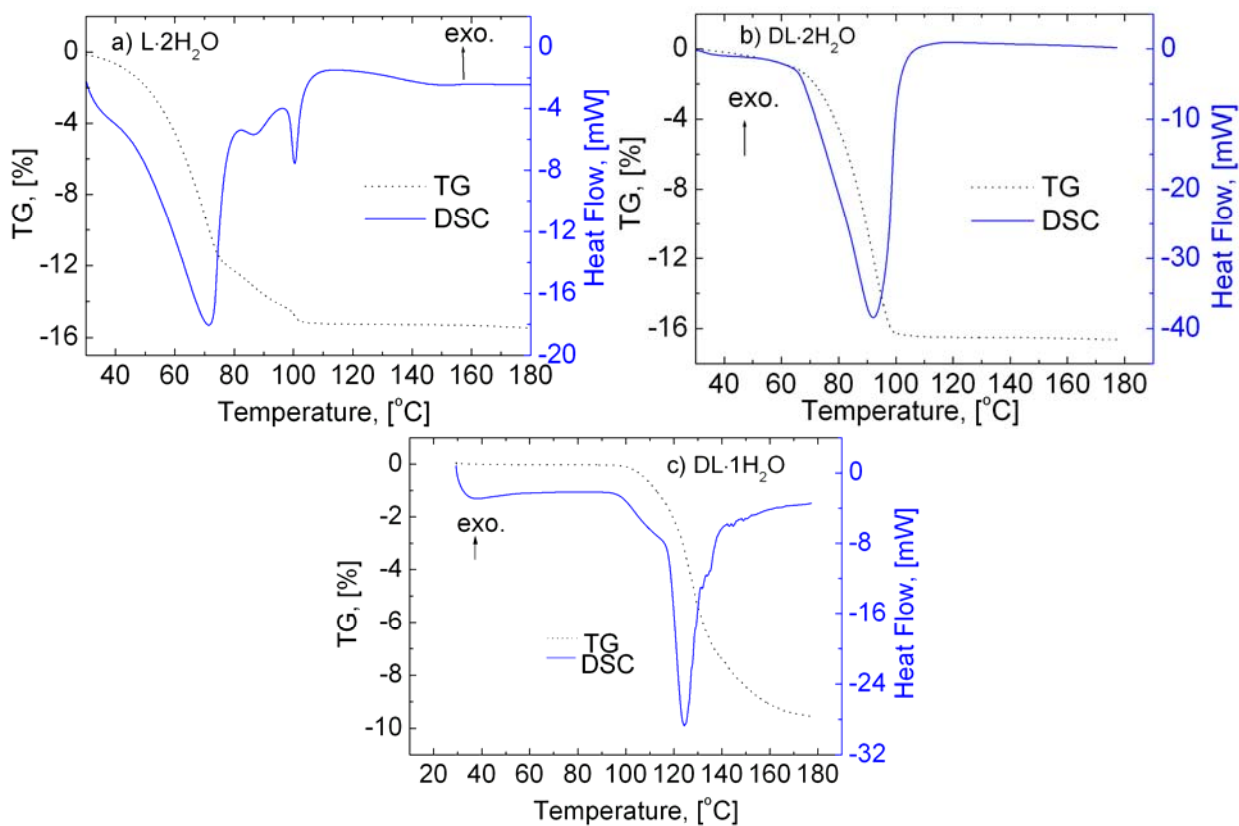
Figure 9.2: *TG-DSC results of various hydrates of arginine: (a) L·2H$_2$O, (b) DL·2H$_2$O and (c) DL·1H$_2$O.*

Their XRPD patterns are presented in Figure 9.1(d) and (e). As expected, those XRPD patterns show completely different reflections comparing to that of the anhydrous racemate (Figure 9.1(c)). Identification of hydrates was again performed with TG-DSC (Figures 9.2(b) and (c)). The total weight losses in TG curves were found at values of 16.6 and 9.5%, approximating well to two and one molecules of water in the crystalline racemates.

In Figure 9.1, the samples (a) and (c) show distinguished XRPD patterns between anhydrate species the enantiomer and the racemate that assesses chiral arginine belonging to compound-forming systems. In contrast, this observation disagrees with the conclusion of Klussmann *et al.* who stated arginine is a conglomerate system[165]. Therefore, additional evidence such as phase diagrams is needed to confirm appropriate type of racemate for arginine.

In aqueous solution, the enantiomer of arginine always crystallizes as the dihydrate form. However, the racemate can exist as di- or monohydrate depending on temperature and solvent compositions. Hence, the temperature-dependence of the hydrate formation of the racemate is studied in details. Figure 9.3(a) and (b) show that between 5 and 10 ºC, the racemate crystallizes as the dihydrate form in pure water. At higher temperatures, the monohydrate is formed (Figure 9.3(c)–(f)). In principle, DL·2H$_2$O is less thermodynamically stable than DL·1H$_2$O at high temperatures. The dihydrate-monohydrate transformation takes place at temperatures between 10 and 15 ºC. Furthermore, in solvent mixtures of water and ethanol (EtOH), the racemate always crystallizes as the monohydrate in the whole studied temperature range from 5 to 70 ºC (their XRPD patterns not shown in Figure 9.3 to avoid intricateness). Details of the transformation between DL·2H$_2$O and DL·1H$_2$O will not be discussed here. For further comparison, single crystals of hydrates are examined with XRD in the next section.
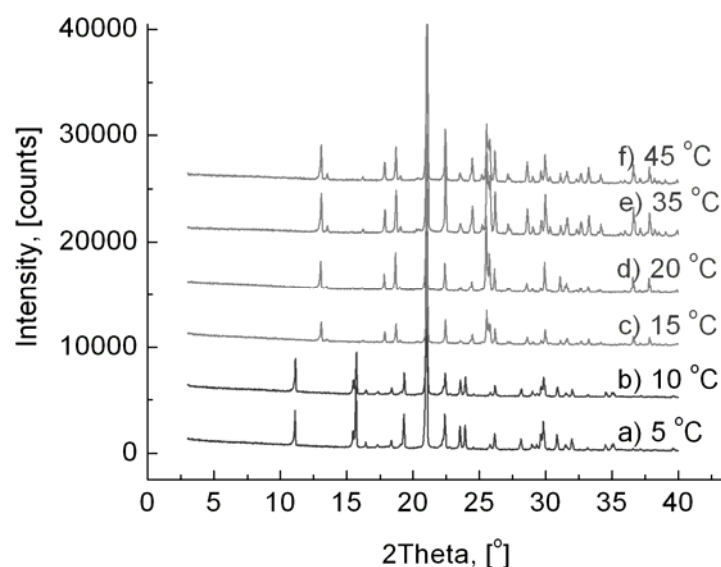
Figure 9.3: *XRPD patterns of hydrates of racemate arginine recrystallized from water at different temperatures (compared to the reference patterns in Figure 9.1).*

9.1.2 Single crystal structures of hydrates

This chapter focuses on crystallization of arginine species from aqueous solutions. In these conditions, the anhydrates will be not directly produced but rather their corresponding hydrate forms. However, hydrate–anhydrate transformation is not an issue as already well-described in several publications[211–213]. Herewith, the structures of two main compounds relating to crystallization processes, *i.e.* single crystals of L·2H$_2$O and DL·1H$_2$O, are presented in Figure 9.4.
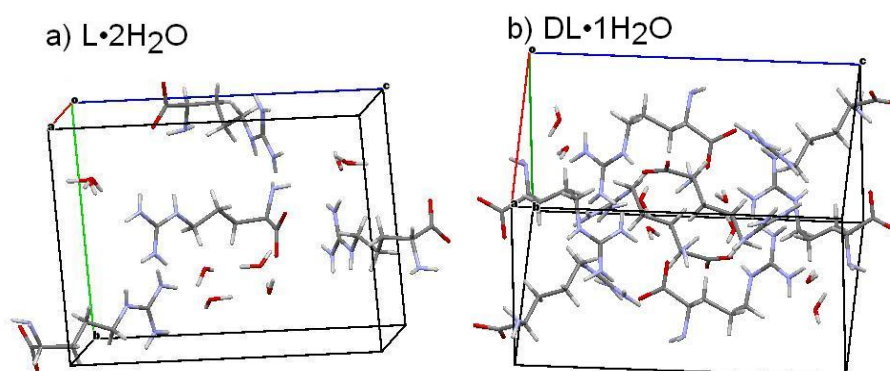
Figure 9.4: *Single crystal structures of the hydrates of arginine species.*

From these structures, crystal structure refinements are summarized in Table 9.1.

Table 9.1: *Single crystal properties of hydrate arginine species.*

Property		L·2H$_2$O	DL·1H$_2$O
Crystal system	[-]	Orthorhombic	Orthorhombic
Space group	[-]	P2$_1$2$_1$2$_1$	Pbca
	a, [Å]	5.62	11.44
	b, [Å]	11.78	9.94
	c, [Å]	15.49	15.95
Unit cell dimensions	α, [°]	90	90
	β, [°]	90	90
	γ, [°]	90	90
Z	[#]	4	8
Unit cell volume	[Å^3]	1027.1	1815.2

Obviously, the hydrates of the enantiomer (L·2H₂O) and the racemate (DL·1H₂O) possess completely different crystal structures. Even though they belong to the same orthorhombic system, but their space groups are different. The dihydrate enantiomer possesses space group type P2₁2₁2₁ while the monohydrate racemate shows type of Pbca. Unit dimensions are also distinguished. Additionally, the number of molecules in unit cells of hydrates L·2H₂O and DL·1H₂O as well as volume of these unit cells are completely different.

Even though the single crystal of DL·2H₂O as well as L-arg and DL-arg anhydrates were not measured, their XRPD pattern can be alternatively used instead of XRD data. Based on the difference of crystal structures from XRD measurements as well as XRPD patterns, all existing forms (anhydrate and hydrate) of the enantiomer are clearly distinguished from those of the racemate. The evidence assesses that conglomerate does not match to arginine system for all relevant enantiomer and racemate forms. As a result, chiral arginine was proven here to be a compound-forming system involving the formation of various hydrates. This conclusion will be confirmed by shape of TPDs in part 9.2.3. Next sections will further characterize properties of these hydrates and the effects of hydrate formation on performance of separation processes.

9.1.3 Stability of arginine under ambient conditions

Time-resolved XRPD was applied again to study the stability of the anhydrous species under ambient conditions. In these conditions anhydrates of arginine are not thermodynamically stable, thus they transform to more stable hydrates within several days. The anhydrate-hydrate transformation was captured as following analyses.
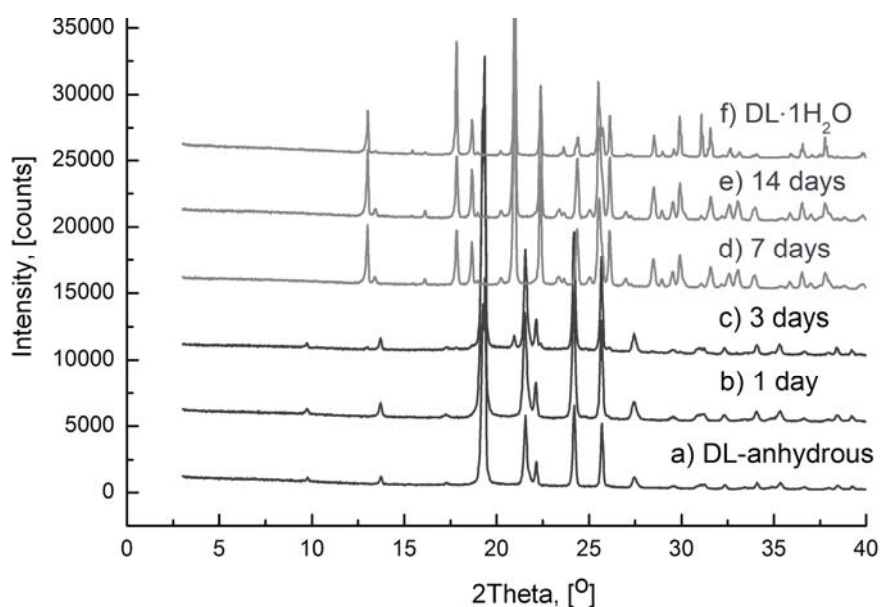
Figure 9.5: *Transformation of DL-arg anhydrous to monohydrate.*

Figure 9.5 presents the transformation tendency of anhydrous racemate within 14 days. The samples lasting from 1 to 3 days (Figure 9.5(b) and (c)) show the same XRPD patterns with the reference DL-arg anhydrous (Figure 9.5(a)). Upon the sample after 7 days (Figure 9.5(d)), new reflections in the XRPD patterns differ significantly to the anhydrate as shown in Figure 9.5(a)–(c). Indeed, X-ray diffraction pattern of the sample in Figure 9.5(d) is distinguished with the previous samples by pronounced diffraction peaks at *e.g.* 13.2, 17.9, 21.3, 22.4, 25.9°, etc. which characterize a new crystalline compound. Actually, the new reflexes are identical to the monohydrate form DL·1H$_2$O (Figure 9.5(f)). This sample afterwards retains stable (Figure 9.5(e)). Especially, under ambient conditions, dihydrate form DL·2H$_2$O was not found during this transformation process. The observation assesses that DL-arg (contacted with moisture in the air) is not thermodynamically stable and can gradually transform into monohydrate in period of one week.

On the other hand, the anhydrous of the enantiomer is more sensitive to moisture than that of the racemate. The transformation results are shown in Figure 9.6. The transformation occurs from the first day since the sample contacted with air. Comparing the initial anhydrous L-arg to the sample after 1 day, new XRPD reflexes appear at 15.0, 16.2°, etc. (compared Figure 9.6(a) and (b)) although their intensities are relatively small. Those reflexes are getting bigger after 4 days and anhydrous phase significantly reduced (compared positions at 11.5, 18.2, 19.2°, etc. in Figure 9.6(c)). Simultaneously, new reflexes at the positions of 13.3, 16.2, 24.6°, etc. also appear which are identical to the reference of L·2H$_2$O (Figure 9.6(d)). Hereby, the transformation of anhydrous enantiomer arginine into dihydrate takes place within several days under ambient conditions.
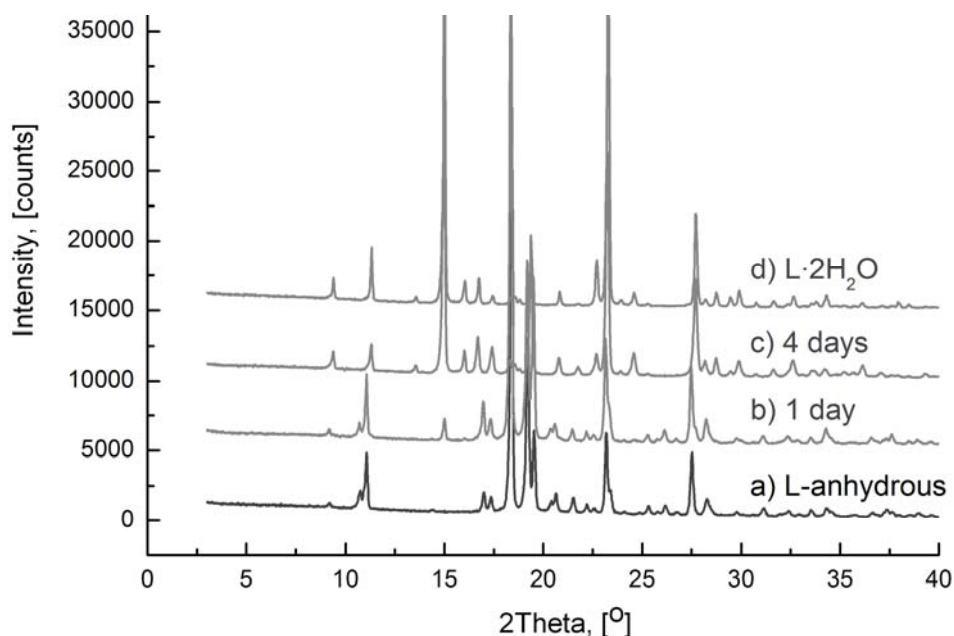
Figure 9.6: *Time-resolved XRPD measurements show the transformation of L-arg anhydrous to dihydrate.*

9.2 Solid-liquid equilibria of arginine in aqueous ethanol solutions

In this part, SLE of arginine in water are investigated. Ethanol (EtOH) will be introduced as an anti-solvent for arginine aqueous solutions. Identifying eutectic composition shifts is one of major goal of this study. SLE will be correlated with the modified three-parameter model as described in part 3.2.8.

9.2.1 Binary solubility and effects of anti-solvent ethanol

The graphical presentation of solubility of arginine in different aqueous EtOH solutions is shown in Figure 9.7. The overview of solubility of arginine species in coordination of solvent composition (EtOH/water) and temperature is presented in the upper part of Figure 9.7. Then, the lower part shows more details at four selected solvent compositions.

From Figure 9.7, three clear trends are observed and summarized as follows:

1) Solubilities of the enantiomer and the racemate are monotonically increasing functions of temperature. At first, in pure water as solvent, Figure 9.7(a) shows relative high solubilities of both the enantiomer and the racemate. For instance, the solubilities of the enantiomer and the racemate at 25 °C are w = 0.15 and 0.17, respectively. The explanation might relate to hydrogen bond formation of arginine solutions[156,157]. In solutions, arginine species are stabilized by the hydrogen bond networks with water molecules resulting in high solubilities. Besides, strong polar-polar interactions between arginine and water also play an important role.

2) EtOH acts as an anti-solvent for aqueous solutions of arginine. Increasing amounts of EtOH reduces significantly the solubilities of the enantiomer and the racemate (Figure 9.7(b)–(d)). In preliminary measurements, arginine seems to be non-dissolvable in pure EtOH. In solvent mixtures, the variation of the dielectric constant is considered as a major factor which strongly affects the solubility of arginine. From a report of Yilmaz[214], the dielectric constant of solvent mixtures composed from EtOH and water reduces along with increasing amounts of EtOH in water as shown in Figure 9.8. Thus, solvent mixtures possess as less polarity as increasing amounts of EtOH. In principle, arginine is a strong polar solute due to the fact that its structure contains a protonated amino group (NH_3^+) and deprotonated carboxylic acid group (COO^-)[159]. Due to this dipolar nature, it dissolves preferably in stronger polar solvents. In contrast, lower solubilities of arginine are expected in less polar solvents. The similar effects of EtOH were already reported for aqueous solutions of other amino acids, *e.g.* alanine, serine, valine, leucine, glycine[215] and threonine[216].

3) Variation of EtOH amounts in different aqueous solutions change the solubility ratio α between the racemate and the enantiomer (Eq. 3.61). The impact of the anti-solvent on solubility tendencies is individually different for the enantiomer and the racemate. EtOH reduces solubilities of the racemate more significant than those of the enantiomer. In pure water, solubilities of the racemate are higher than those of

the enantiomer (Figure 9.7(a)). In the solvent containing 0.30 v/v of EtOH (Figure 9.7(b)), they are found to be equal. At larger contents of EtOH, solubility curves of the racemate are located below those of the enantiomer (Figure 9.7(c) and (d) corresponding to ϕ at 0.45 and 0.65). Obviously, this leads to a change of the solubility ratio α. This value varies between ~1.14 and ~0.74 when EtOH amounts are increased from 0.00 to 0.65 volume fractions in the solvent mixtures.
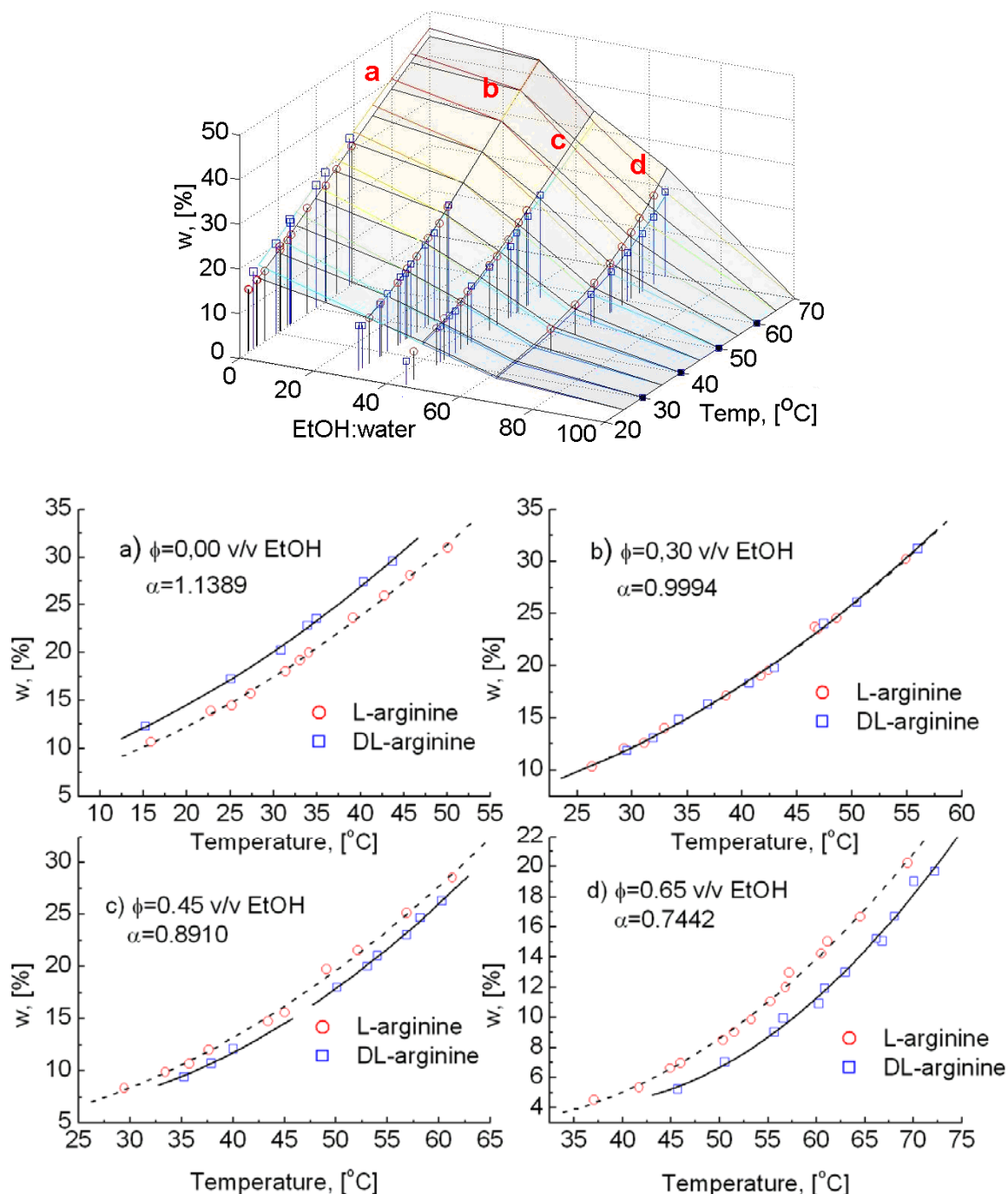
Figure 9.7: *Solubilities of the racemate and the enantiomer ($\square$,o) of arginine in various aqueous solvents. Selected solvent mixtures contain (a) 0.00, (b) 0.30, (c) 0.45, (d) 0.65 v/v of EtOH. Lines present the modified model correlation (Eq. 3.55). α is the solubility ratio of the racemate and the enantiomer (Eq. 3.61). ϕ stands for volume proportion of EtOH/water.*
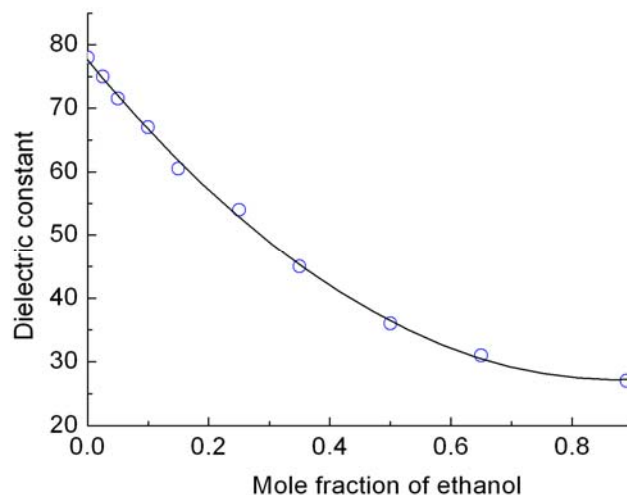
Figure 9.8: *Dielectric constant of solvent mixtures of EtOH and water.*[214]
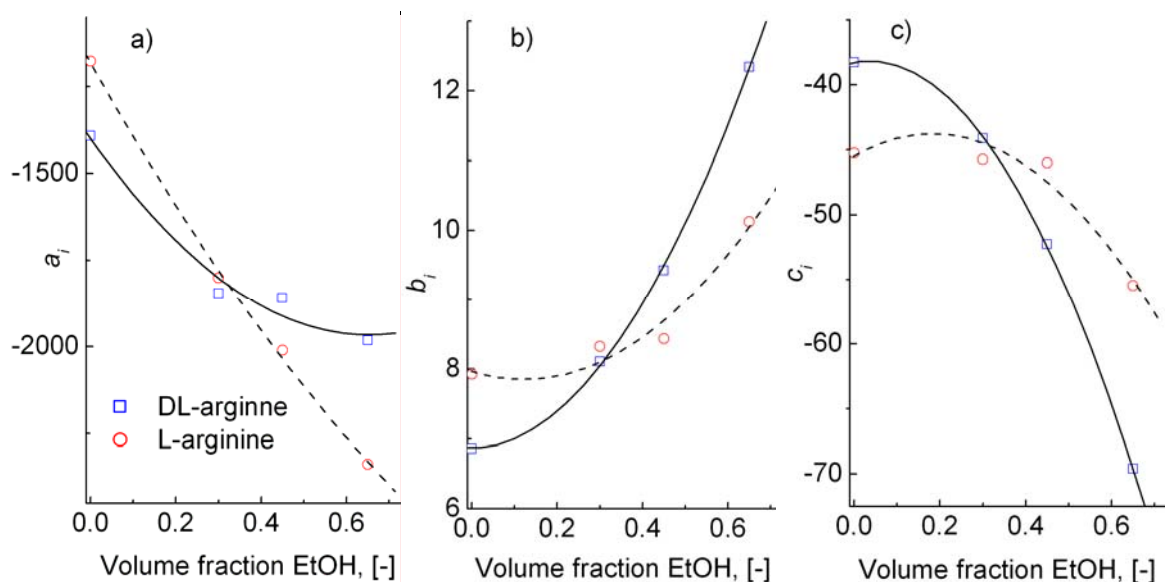
Figure 9.9: *Parameters a_i, b_i and c_i of the modified model Eq. 3.55 for the aqueous EtOH solutions of arginine. Symbols ($\square$,o) corresponding to the racemate and the enantiomer, respectively.*

The parameters of the modified three-parameter model (Eq. 3.55) were estimated from the above solubility data. The results are plotted versus solvent compositions in Figure 9.9. While b_i values are positive and increase with added EtOH amounts, a_i and c_i values are found as negative numbers of monotonically decreasing functions. To generalize for other solvent compositions, these parameters were fitted by second-order polynomial functions of volume fraction of EtOH (ϕ). The results are presented in Table 9.2.

The obtained model has been evaluated with several arbitrary experimental data. The comparison was performed with 31 measurement data involving the above "reference" solvent mixtures (ϕ = 0.00, 0.30, 0.45 and 0.65) and 2 "extra"

compositions (ϕ = 0.40 and 0.50). The details are shown in Appendix G. The overall errors between the experimental and calculated results are relatively small. In the "reference" solvents, the deviations are lower than 3.7% while this value increases up to 6.8% for "extra" solvent mixtures. Therefore, this model can be considered as a suitable approach to correlate the SLE of arginine in different solvent mixtures of EtOH and water.

Table 9.2: *Parameters a_i, b_i and c_i as functions of volume fraction EtOH (ϕ) for the racemate and the enantiomer of arginine.*

The racemate	The enantiomer
$a_{DL}(\phi)=1331.74\phi^2 -1737.29\phi -1399.30$	$a_L(\phi)= 640.66\phi^2 -2184.6\phi -1181.52$
$b_{DL}(\phi)= 12.73\phi^2 +0.11\phi +6.86$	$b_L(\phi)= 7.86\phi^2 -1.90\phi +7.97$
$c_{DL}(\phi)= -83.32\phi^2 +6.01\phi -38.28$	$c_L(\phi)= -51.59\phi^2 +18.83\phi -45.47$

From obtained binary solubility, next step is construction of full TPDs. In fact, determination the eutectic composition is one of the main objectives throughout this thesis but that usually requires significant attempts of experimental work. Herewith, the shortcut method based on the Klussmann's approach will be used again to have preliminary version of possible ranges of the eutectic compositions. This calculation will use only the solubilities of the racemate and the enantiomer. As a sequence, those results will assist fine determination of the real eutectic compositions since irrelevant ranges can be simply eliminated.

9.2.2 Eutectic composition estimation and experimental determination

The eutectic compositions are first estimated by the Klussmann's approach (Eqs. 3.60 – 3.62). The results are compared to experimental values in Table 9.3.

Table 9.3: *Eutectic compositions from calculation ($x^{Eu}_{L\_cal}$) and experimental determination ($x^{Eu}_{L\_exp}$).*

ϕ , [-]	α, [-] (see Fig. 9.7)	$x^{Eu}_{L\_cal}$, [-] (Eq. 3.62)	$x^{Eu}_{L\_exp}$, [-]	*Dev*, [%]
0.00	1.1389	0.76	0.75	0.53
0.30	0.9994	0.80	0.76	4.98
0.45	0.8910	0.83	0.78	6.78
0.65	0.7442	0.88	0.82	6.94

The estimation in pure water is relatively good with deviation from experiment of 0.53%. Increasing amounts of EtOH in solvent mixtures leads to significant deviations of the eutectic compositions between measurement and estimation. The deviation is getting bigger against added EtOH amounts, e.g. about 6.94% in the case of ϕ = 0.65. Although the Klussmann's approach is relative simple and quite helpful in rough prediction of the eutectic composition, it is not accurate enough to be further used for crystallization design for this system.

Compositions and concentrations of the eutectic points in the selected solvent mixtures are presented in Figure 9.10. Here, solubilities (w) of the eutectically composed solutions increase with temperature. However, the eutectic compositions are found to be temperature-independent in each solvent mixture. XRPD patterns of their residual solids contain mixtures of DL·1H$_2$O and L·2H$_2$O as depicted in Figure 9.11.
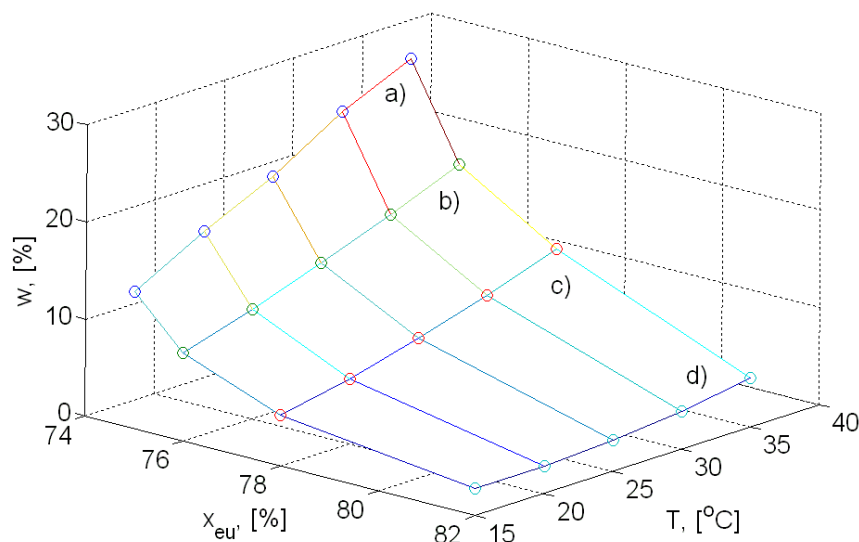
Figure 9.10: *Eutectic compositions of chiral arginine system in aqueous EtOH solutions. These eutectic compositions were determined from at least 3 or 4 measurements from various initial compositions. Curves (a) to (d) correspond to ϕ = 0.00, 0.30, 0.45 and 0.65 v/v.*

Figure 9.10 and Table 9.3 show that the variation of solvent compositions leads to shifts of the eutectic compositions. The x_L^{Eu} value is of 0.75 in pure water while this value continuously increases with added amounts of EtOH. In solutions containing ϕ = 0.30, 0.45 and 0.65, x_L^{Eu} are found as 0.76, 0.78 and 0.82, respectively. Starting from slightly enantiomerically enriched solutions, those eutectic compositions are individually not satisfying to produce high purity products (*e.g.* $x_L^{product}$ ≤ 82%) by one single crystallization step due to the thermodynamic limitation such as a demonstration in part 7.4.1. However, even higher purity of the target enantiomer can be achieved via the "two-step" process which will be validated in section 9.4.1.
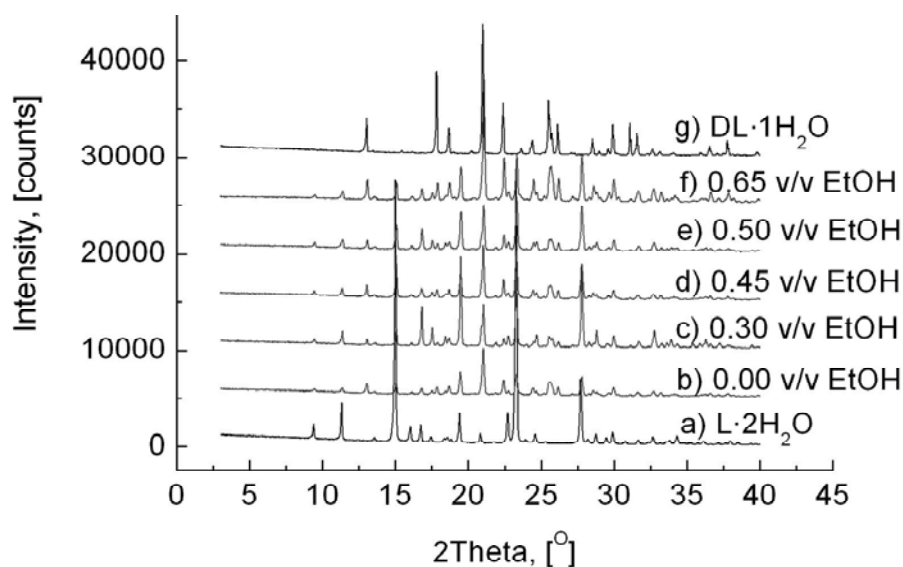
Figure 9.11: *XRPD patterns of residual solids corresponding to eutectically composed liquids: Patterns (a) and (g) are the references of L·2H₂O and DL·1H₂O, respectively. Patterns from (b)–(f) correspond to the given solvent mixtures.*

9.2.3 Ternary phase diagrams

In this part, two selected solvent compositions are focused for further SLE investigation. These two solvents include water as the first solvent and a mixture of ETOH/water (65/35 v/v) as the second one.

9.2.3.1 Full TPD of arginine in pure water

In the previous section, the preliminary eutectic compositions were estimated by the Klussmann's approach using solubility of only the enantiomer and the racemate. Then, the precise eutectic compositions were experimental determined based on the estimated values. In this part, the detailed TPD will be constructed to study behavior of the isotherms (considering also other mixtures besides only the enantiomer, the racemate and the eutectic composition) and metastable solubility curves which can provide important information for crystallization design, in particular preferential crystallization. Figure 9.12 presents the TPD of arginine in water at 5 ºC. The isotherm curve shows that solubilities of arginine at low temperature are relatively small. The extended solubility lines (*i.e.* metastable solubility curves) belong to the three-phase regions. This is not a favorite situation to perform preferential crystallization because the secondary nucleation of the counter species easily occurs during crystallization of the desired enantiomer. The effects of shape of solubility curve to preferential crystallization were already discussed elsewhere[9].
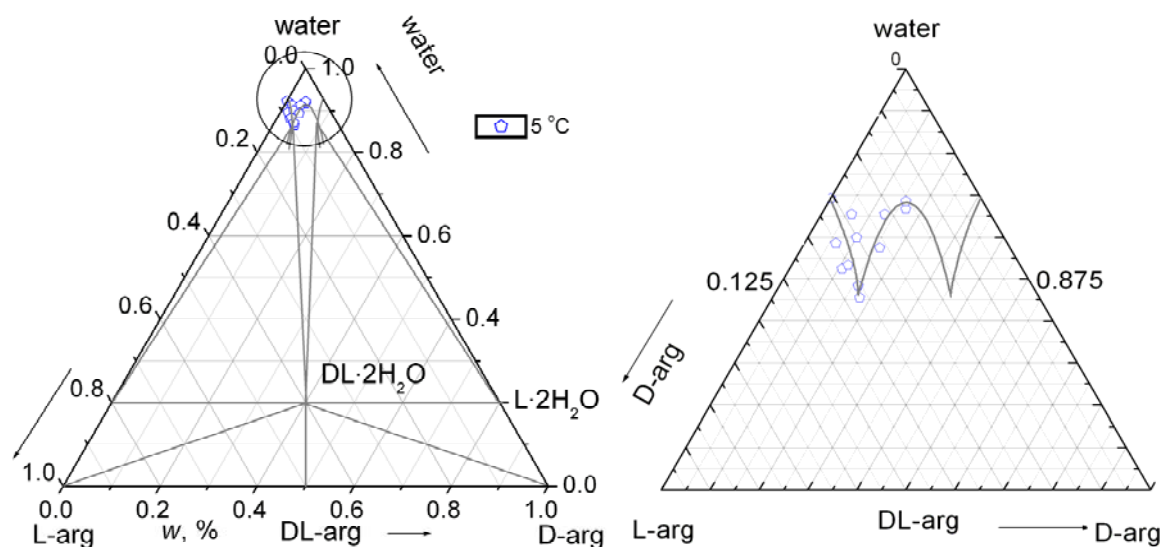
Figure 9.12: *TPD of arginine in water at 5 °C. The left part presents isotherm considering solid equilibrating phases. The metastable solubility lines belong to three-phase domain. The magnitude on the right hand side is zooming in 25% area.*

The TPD corresponding to a higher temperature range (from 15 to 45 °C) is shown in Figure 9.13. The solubility ratios of the racemate/the enantiomer do not significantly change with respect to temperatures. The isotherm curves in this case are not as steep as that in the TPD at 5 °C and the metastable solubility lines enter into the two-phase domains (Figure 9.13). Obviously, the shapes of metastable solubility curves support enantioseparation via preferential crystallization. The shape of isotherm in the TPDs confirmed again the type of crystalline racemate of arginine, *i.e.* a compound-forming system, comparing to the solid phase analysis in section 9.1.
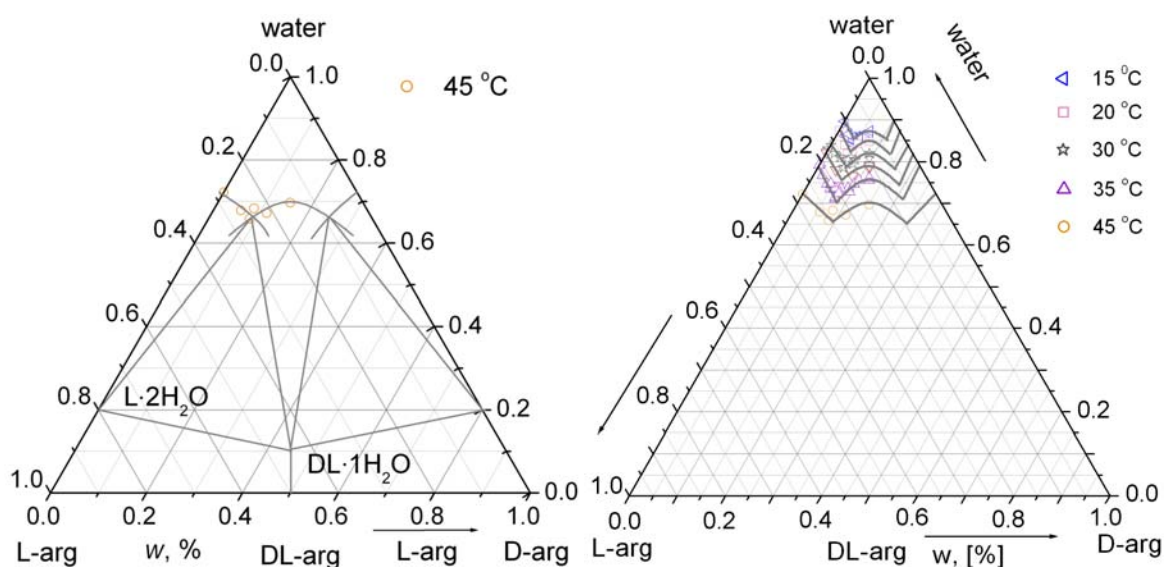
Figure 9.13: *TPD of arginine at elevated temperatures. Left side is an example of TPD at 45 °C. Right side is the simplified TPD (from 15 to 45 °C) of which all the solid phases at equilibria are identical to the case of the TPD at 45 °C.*

The eutectic composition has been briefly discussed in the previous part (9.2.2) but here will be especially studied in more details. For amino acids, the eutectic x_L^{Eu} value can be principally found in the whole range from 0 to almost 1. Effects of temperature and solvent composition to the eutectic compositions of arginine are presented in Figure 9.14. In fact, the isotherm curves from 15 to 45 °C in aqueous solution possess the eutectic x_L^{Eu} = 0.75, this number is relatively stable. Similar to the previous part of solid phase behavior, this value corresponds to the equilibrating solids of L·2H$_2$O and DL·1H$_2$O. At lower temperatures, *i.e.* at 5 °C, the eutectic composition is significant changed (*i.e.* x_L^{Eu} = 0.69) and residual solids are found as mixtures of L·2H$_2$O and DL·2H$_2$O. Besides pure water as solvent, the presence of EtOH also strongly influences the eutectic compositions, for instance a case of 65:35 (v/v) EtOH/water will also be discussed as follows.
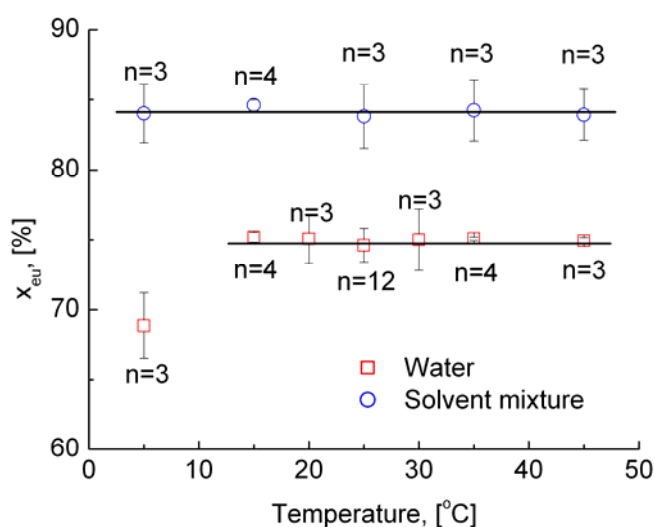
Figure 9.14: *Effects of temperature and solvent composition to eutectic composition. Amounts of EtOH in solvent mixtures can vigorously alter the eutectic compositions (herein, a mixture of 65:35 (v/v) EtOH/water is illustrated). n is the repeated measurements at each eutectic determination.*

9.2.3.2 The TPD in a solvent mixture of water and EtOH

Among solvent mixtures, a mixture of 65:35 (v/v) EtOH/water has been selected to construct the TPD. The results are shown in Figure 9.15. Compared to the previous cases, the relative positions of isotherm curves in this solvent mixture reveal that the solubilities are lower than those in pure water at the same temperatures. The metastable solubility lines belong to the three-phase domain. Hence, this mixture of EtOH/water might not be a potential solvent to perform preferential crystallization. In this solvent, the eutectic composition is x_L^{Eu} = 0.84 and does not change with respect to temperature.

Obviously, the eutectic composition (x_L^{Eu} = 0.84) is significant higher than those in pure water as solvent for both cases at low (x_L^{Eu} = 0.69) and high temperatures (x_L^{Eu} = 0.75). As mentioned in previous parts for solvent mixtures, equilibrating solids are

always found as L·2H$_2$O and DL·2H$_2$O. These achieved data can be useful for crystallization design.
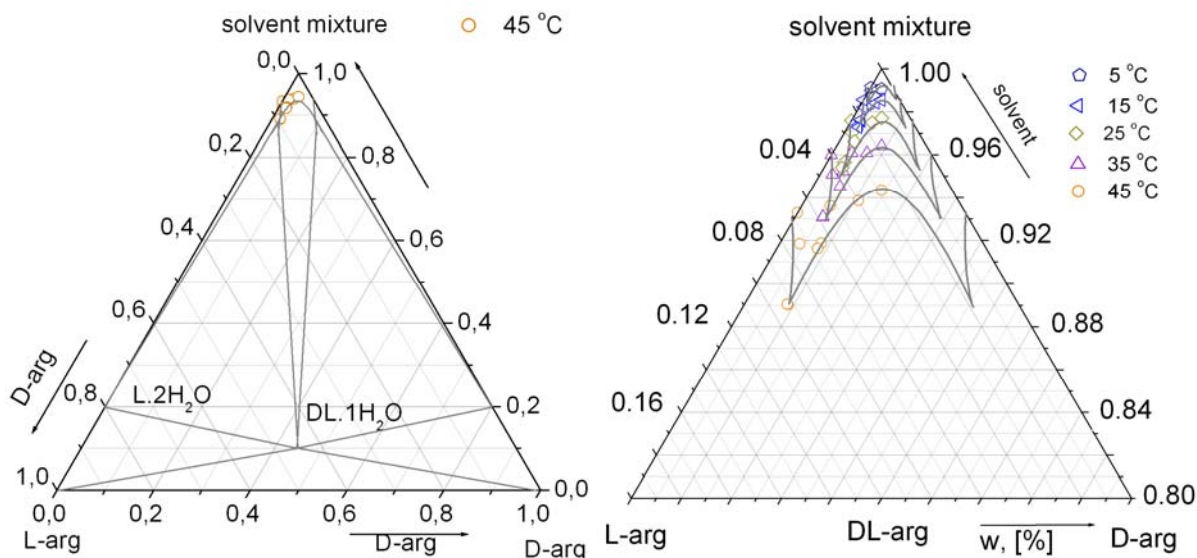
Figure 9.15: *TPD in solvent mixture of 65:35% (v/v) of EtOH/water. A detail TPD is presented for an isotherm at 45 °C on the right, the left presents isotherms from 5 to 45 °C.*

9.3 Study of crystal morphology, homogeneous nucleation and effects of additives

In this part, different hydrates of arginine will be recrystallized under suitable conditions. Afterwards, those crystals will be harvested and examined with a microscope. The effects of additives are also discussed. The metastable zone widths of both the enantiomer and the racemate will be measured in order to support preferential crystallization design.

9.3.1 Crystal morphology

Distinct habits of the crystals for the different hydrates are shown in Figure 9.16. The morphology of L·2H$_2$O resembles prismatic crystals (Figure 9.16(a)). The crystals of DL·2H$_2$O are obtained as hexagonal plates (Figure 9.16(b)) which aggregate in layers. The DL·1H$_2$O crystals are found to be elongated and plate-like crystals (Figure 9.16(c)). All of these crystals are very good transparence.
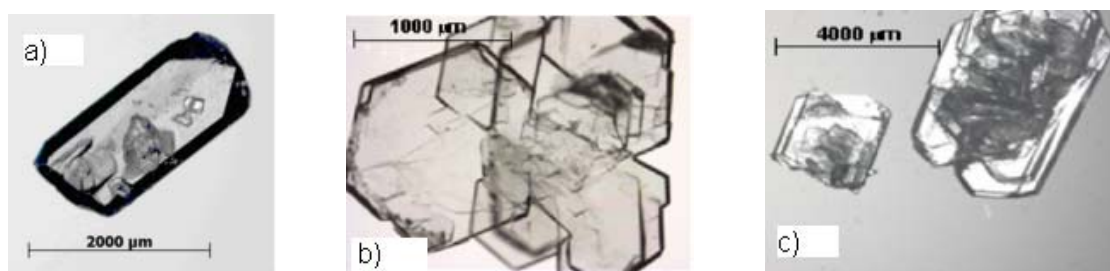
Figure 9.16: *Microscopic images of the hydrates: (a) L·2H$_2$O, (b) DL·2H$_2$O and (c) DL·1H$_2$O.*

Herewith, other L-amino acids were introduced as additives to study morphology variation of arginine species. Indeed, two additives are used including L-methionine (L-met) and L-threonine (L-thr). Saturated solutions at 35 °C, which contain 1% (w/w) of additives, were prepared. Single crystals were isothermally grown at 20 °C within 1 week. The microscopic images of these crystals are shown in Figure 9.17.

(a) L·2H$_2$O/L-met   (b) L·2H$_2$O/L-thr   (c) DL·1H$_2$O/L-met   (d) DL·1H$_2$O/L-thr
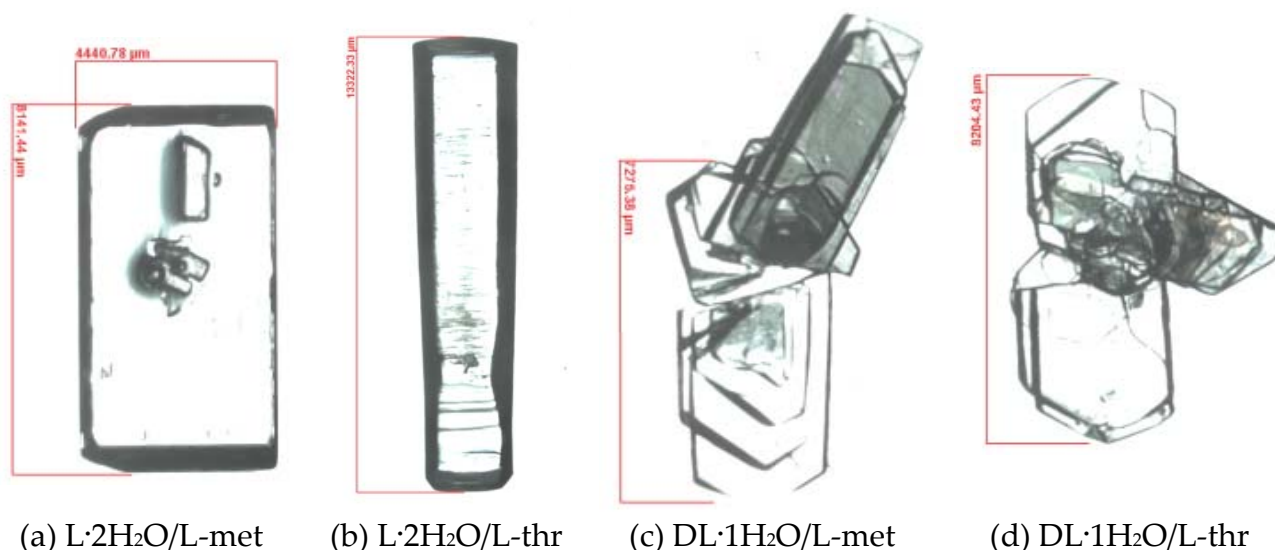
Figure 9.17: *Effects of additives L-met and L-thr on crystal morphology of arginine species.*

Obviously, additives strongly influence the crystal morphology of L·2H$_2$O. L-met supports for these crystals growing at specific crystal-faces to develop flat-plate (Figure 9.17(a)) while L-thr prefers to elongate the rod-crystals as Figure 9.17(b). Obviously, these additives are able to prohibit selective crystal-faces and modify completely different crystal morphology of the enantiomer dihydrate. However, the effects of these two additives to morphology of DL·1H$_2$O are not significant which can be compared Figure 9.17(c), (d) to Figure 9.16(c).

9.3.2 Metastable zone width (MSZW)

The heterogeneous nucleation will be investigated with pure water because this solvent will be used in the next part 9.4.2 of preferential crystallization. To detect the MSZW, three volume scales will be studied. First, lab-scale vessels of 50 mL will be used for various solutions of the enantiomer and the racemate of arginine. From these results, saturated solutions at a specific temperature will be selected to further investigate the effects of additives on the MSZWs at a scale of 1 mL exploiting the advantages of the commercial measurement unit Crystal16™ (Avantium). Finally, vials of 10 mL will be used to complement effects of volumes on MSZW of the arginine species.

9.3.2.1 Homogeneous nucleation of arginine species in pure water

The MSZW of the enantiomer and the racemate of arginine were measured via the polythermal method with thermostated vessels of 50 mL. A cooling rate of 0.05 ^{o}C·min^{-1} was applied. The onset of nucleation was detected with a FBRM probe. In a temperature range from 10 to 45 ^{o}C, ΔT_{max} of the enantiomer and the racemate were found at 8.5 and 12.8 ^{o}C as seen in Figure 9.18.
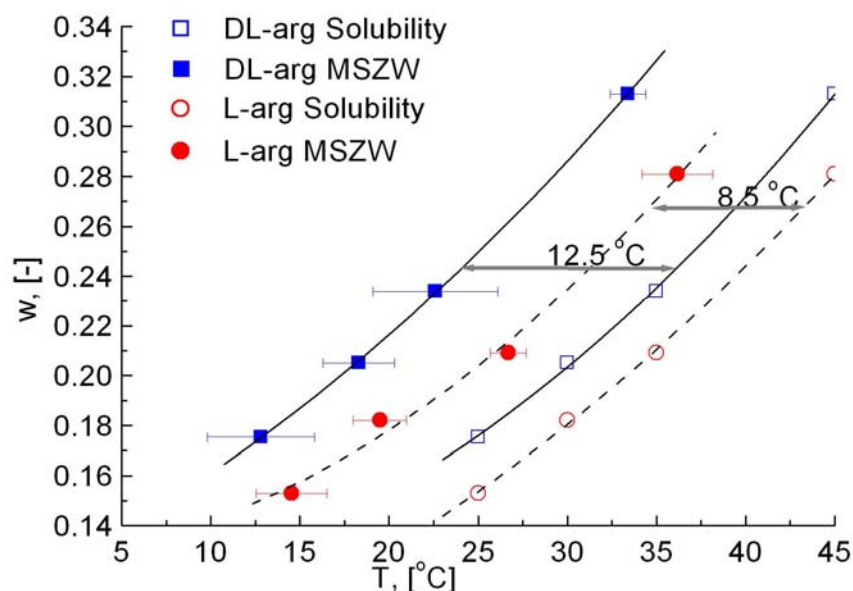
Figure 9.18: *Solubility and MSZW of arginine species. MSZW measurements were repeated 10 times, vessels of 50 mL were used. Cooling rate was 0.05 ^{o}C·min^{-1}.*

Obviously, the MSZW of the racemate is rather broader than that of the enantiomer. That can be considered as an advantage for the preferential crystallization of the enantiomer since the racemate species will be remained in a sufficient time for the crystallization process of the target enantiomer.

Even though the MSZW of the racemate is larger than that of the enantiomer, attempts to improve those MSZWs are considered to enhance efficiency of preferential crystallization. The idea is using suitable additives to enlarge the MSZWs. However, if comparison is carried out for all compositions, a huge number of repeated experiments have to be solved for each composition at different cooling rates since the Nyvlt's method will be applied here. Based on results in Figure 9.18, the metastable zone limits are quite parallel with solubility curves for both the enantiomer and the racemate. That helps to avoid the above problem by using a simpler alternative. The saturated solutions of both species at 35 ^{o}C can be represented for all other compositions. Due to the parallelism, the conclusion from these solutions can be similarly applied for other saturated solutions in the temperature range from 10 to 45 ^{o}C.

9.3.2.2 Effects of additives to the MSZWs

This part discusses effects of additives on the MSZWs of arginine species using the commercial unit Crystal16™. First of all, in general, additives can change the nucleation phase. Indeed, chiral additives can differently affect to nucleation and growth rates of the individual enantiomers.[129,130] Therefore, the nucleation phase of the racemate arginine with presence of additives L-met or L-thr should be taken into account.
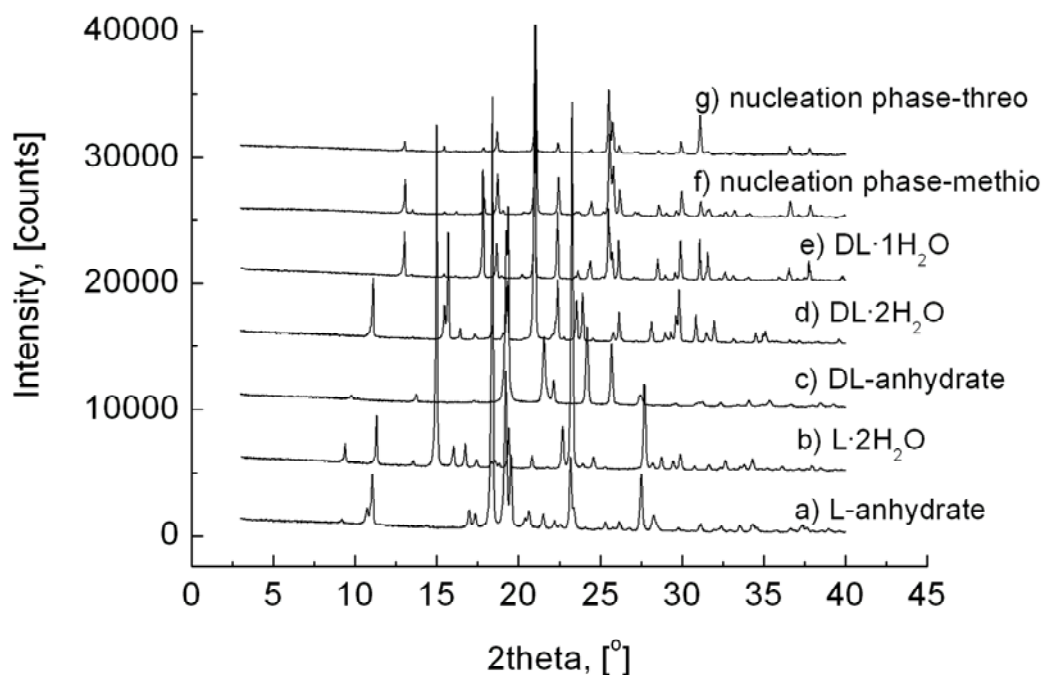
Figure 9.19: *Nucleation phase of the racemic solutions in the cases of using additives (samples (f) and (g)) are identical to the case of without additive (e). All crystallized phase are the racemate monohydrate. Samples (a) to (e) are the references.*

Preliminary experiments aimed to characterize the first solid appearing at nucleation with presence of the additives were performed. Figure 9.19 shows that XRPD patterns are identical for both cases with and without additives. Thus, using the additives does not alter the nucleation phases of arginine species.

Herewith, the MSZWs are investigated by the Nyvlt's method as mentioned above. All the points here were taken from average values of repeated experimental measurements form 50 to 150 times. The Nyvlt's extrapolation was applied to estimate the nucleation corresponding to the "zero" cooling rate from other cooling rates of 0.01, 0.02, 0.035 and 0.05 °C·min⁻¹. The same procedure was carried out for all cases with and without additives.

Figure 9.20 presents the MSZWs of both the enantiomer and the racemate which are strongly affected by the additives. Important conclusions can be derived from this figure. Obviously, the MSZW of the racemate is large than that of the enantiomer.

From the nucleation temperatures and saturation temperatures, the MSZWs of the enantiomer and the racemate are calculated at 9.8 and 13.3 ºC, respectively. Those data fit quite well with the previous conclusion from measurements of a 50 mL scale but, herein, a larger number of repeated experiments are needed for a 1 mL scale due to volume effects.

Abilities of these additives to vary individual MSZWs are especially interesting. Let make a simple comparison with a small amount of additives, *e.g.* about 3% additives. Obviously, L-met can extend the MSZW of the racemate (compare to a case of without additives) more than 8 ºC while L-thr is just able to enlarge 2 ºC. Furthermore, the MSZW of the enantiomer is not significantly affected by the additives. Indeed, L-met (also about 3%) results in almost the same MSZW to without additive cases and L-thr extends the MSZW of the enantiomer 2.5 ºC more. That leads to the conclusion of applicability of additives in kinetic nucleation of arginine species. L-met seems to be a good additive to enhance the efficiency of preferential crystallization to produce the single enantiomer. This additive is able to enlarge the MSZW of the counter species *i.e.* the racemate. Thus, L-met will support for preferential crystallization because the unexpected species, *i.e.* the racemate can be remained in the solution longer during the crystallization of the desired enantiomer. Otherwise, the additive L-thr perhaps supports for crystallization of the racemate species because it can extend the MZSW of the enantiomer more than the L-met. Even if this extension is quite small (about 2.5 ºC), it can be sufficient for a special separation.
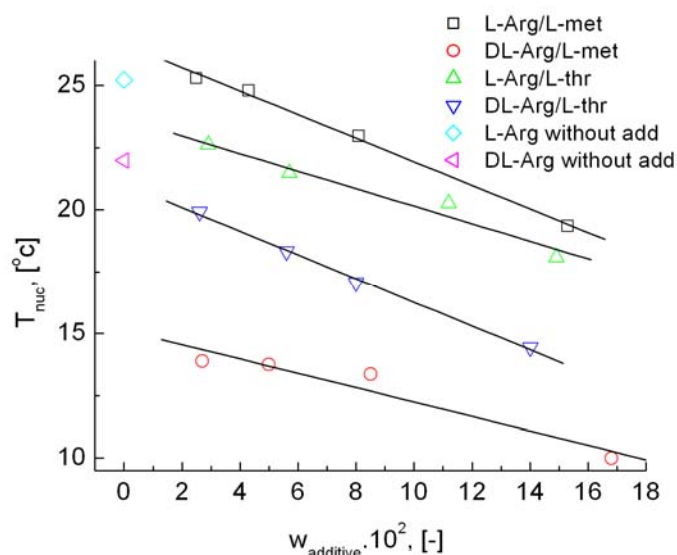
Figure 9.20: *Effects of additives to MSZWs of the enantiomer and the racemate of arginine in water.*

Back to Figure 9.20, increasing L-met and L-thr amounts shows clearly influences of these additives to the MSZWs of both the enantiomer and the racemate. The comparison for small amount additives is still applicable for the other cases as presented in Figure 9.20. However, in crystallization design, large amounts of

additives should be avoided due to the un-desired effects of the additives to other parameters such as solubility, crystal growth, decomposition, contamination, etc.

In short, L-met and L-thr are considered as good additives because they can enhance the MSZWs of both the enantiomer and the racemate. However, these two additives can vary these MSZWs in different manners. In the next section, L-met is selected for further investigation of purification the target enantiomer.

Recently, in several papers, volume effects on homogeneous nucleation have been discussed.[217–219] In the previous sections, scales of 50 and 1 mL were used to determine the MZSWs of arginine species. Next paragraph will examine the effects of different scales on the MZSWs in consideration of nucleation probability.

9.3.2.3 Volume effects on homogeneous nucleation

The nucleation was measured with saturated solutions of L-arg at 35 °C. Different volume scales including 1, 5 and 50 mL were addressed to validate volume effects on nucleation. These solutions were cooled down with a constant cooling rate of –0.05 °C·min^{-1}. Turbidity variation of small vials of 1 mL were monitored by the Crystal16™ while the bigger ones were followed by the FBRM probe (these samples were well-agitated with magnetic stirrers at a speed of 350 rpm). The "cloud" point, where first nuclei are visually detected, is recorded as the onset of nucleation. Nucleation temperature measurements were repeated to plot histogram and cumulative as shown in Figure 9.21. A comparison of volume effects on nucleation is summarized in Table 9.4.
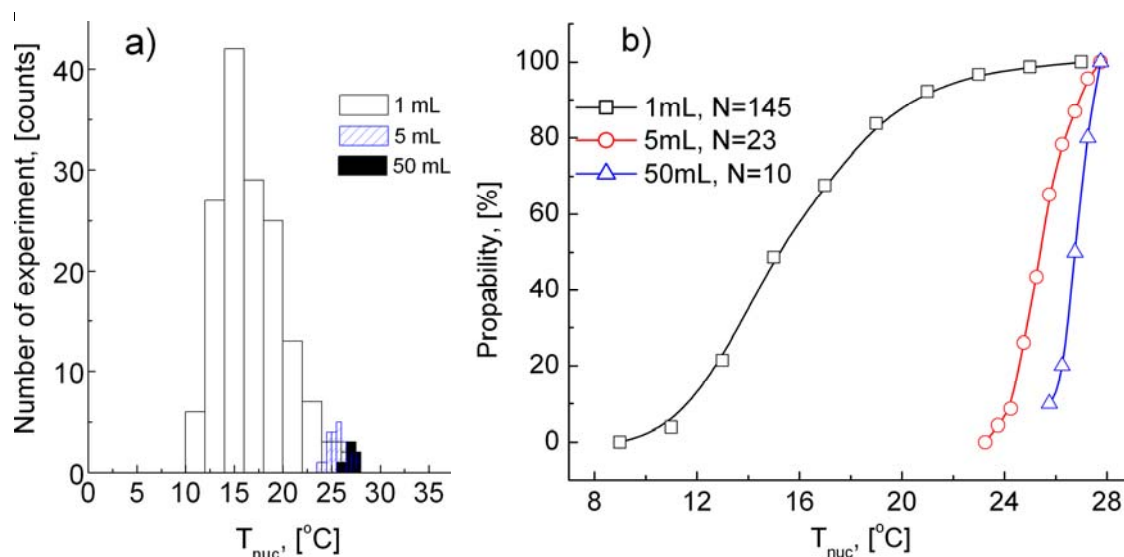
Figure 9.21: *Volume effects on nucleation of L·2H₂O.*

Obviously, volume scales show strong influence to the nucleation of L-arg. The histogram distributions are significantly scattered with the cases of small volumes and getting converged for the bigger ones. The cumulative diagrams show that *e.g.*

the scale of 50 mL just needs few of measurements to get equal information to 145 measurements of a 1 mL scale do. The reason relates to probability of nucleation depending on volume of the studied solutions. Indeed, 50 mL solution can be considered as an integration of 50 "unit volumes" of 1 mL solution. If nucleus appears in one of these "unit volumes", it will lead to nucleation for the whole system.

Table 9.4: *Representative parameters of distributions corresponding to three different volume scales.*

Volume, [mL]	Mean, [°C]	Standard dev., [-]	Repeated measurements n, [#]
1	16.65	3.31	145
5	25.67	1.03	23
50	26.94	0.65	10

9.4 Separation concepts

Based on the obtained knowledge of thermodynamics and kinetics, different crystallization approaches can be considered in this part to purify the enantiomer(s) of arginine. First, exploiting the eutectic shifts can perform the "two-step" process which was basically described in Chapter 5 and already validated with different operations as seen in Chapters 7 and 8. Herein, various possibilities of this method can be applied for arginine system based on the eutectic shifts. As seen in part 9.2, the eutectic compositions in water were found significantly different between low (*e.g.* 5 °C) and higher temperatures at x_L^{Eu} = 0.69 and 0.75, respectively. Besides, using solvent mixtures also can be a promising application via clear shifts of the eutectic compositions, *e.g.* solvent of 65/35% (v/v) EtOH/water possessing a value of the eutectic composition at x_L^{Eu} = 0.84. On the other hand, kinetically preferential crystallization (*e.g.* SIPC, AS3PC) can also be used. Preferential crystallization is strongly affected by the shape of isotherm. The TPD in water at temperatures higher than 5 °C should be favor cases for preferential crystallization. In contrast, the shapes of isotherm in water at lower temperature as well as in solvent mixtures seem to be not desirable for preferential crystallization. Nevertheless, both thermodynamic and kinetic approaches will be realized in this chapter.

9.4.1 The "two-step" process exploiting a eutectic shift relating to different hydrates

With respect to the "two-step" process, chapter 7 demonstrated the case of the eutectic shift between melt and solution, validated with an industrial relevant compound, *i.e.* lactide. A further development based on various polymorphs was examined in Chapter 8 with the case of 3-chloromandelic acid system. In this chapter,

one more variant of this method will be applied: a shift of the eutectic composition regarding to various hydrates is realized for arginine.[220] Specifications of arginine/water system at low and high temperatures are considered for this methodology development. The suggested "two-step" separation process for various hydrates is described below. The principle is based on the shift of the eutectic compositions resulting from an exchange of hydrates with respect to temperature. The trajectory $\mathbf{A} \rightarrow \mathbf{B} \rightarrow \mathbf{C} \rightarrow \mathbf{L \cdot 2H_2O}$ in Figure 9.22 illustrates the process operation.
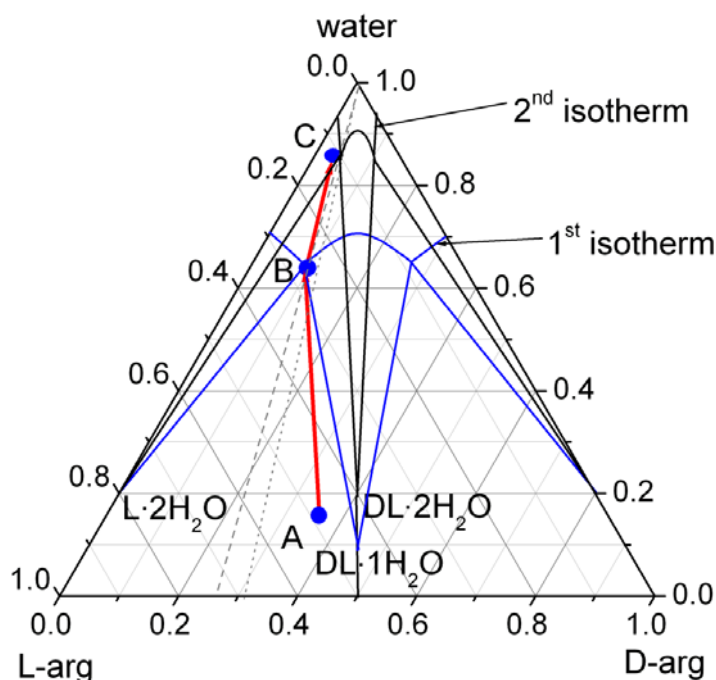
Figure 9.22: *The principle of the "two-step" selective crystallization process. The solid phases at equilibria are simplified. The dashed and dotted lines indicate the eutectic compositions of the first and second isotherms at 5 and 20 °C, respectively.*[220]

Step 1: Enrichment step exploiting the 1st isotherm at 20 °C as depicted in Figure 9.22, the relevant TPD can be seen in Figure 9.13.

In Figure 9.22, the initial solution is chosen at point **A** in the three-phase domain of the first isotherm at 20 °C. System **A** is an enantiomerically enriched solution (*e.g.* x_L^A = 0.64) which can be obtained from different sources *e.g.* chiral chromatography, chiral extraction or fermentation processes, etc. Stating with a solution represented at point **A**, a thermodynamic equilibrium is established at this temperature between the residual solid (which contains two solid phases of L·2H₂O and DL·1H₂O) and the mother liquor of the eutectic composition (point **B**, $x_L^B = x_L^{Eu1}$ = 0.75). The position of point **A** can be optimized by a better position located on the border line of the two-three phase regions, at which the residual solid will be recrystallized as the pure racemate mono-hydrate DL·1H₂O. A subsequent phase-separation step, *e.g.* filtration or decanting, is required to obtain the target eutectic solution **B** and a solid by-product. The exploitation of the first isotherm at 20 °C can be considered as an enrichment step, which improves the initial composition to the eutectic composition

(from 0.64 to 0.75 via a simple crystallization step). The residual solids (pure DL·1H₂O or a mixture of L·2H₂O and DL·1H₂O) will be recycled. The eutectically composed solution **B** is transferred to step 2.

Step 2: Placing solution **B** into the two-phase region of the 2nd isotherm (5 °C), the relevant TPD was plotted as Figure 9.12.

A calculated amount of water (based on mass balances) is added into solution **B** in order to place the overall composition into the two-phase region of the second isotherm (at 5 °C, *e.g.* point **C**). It should be noted that the composition of the target enantiomer in solution **B** (x_L^B = 0.75) obtained from the first isotherm muss be larger than that of the eutectic composition of the second isotherm (here x_L^{Eu2} = 0.69). This constraint ensures that point **C** is able to belong to the two-phase domain of the second isotherm. Hereby, a new equilibrium will be established between a solid phase of L·2H₂O and corresponding mother liquor. Herewith, selective crystallization can be used to directly obtain the desired L-enantiomer dihydrate. Further optimizing of the adjustment of solvent or/and the temperature can improve process yields. The best situation is placing point **C** on the boundary between the two- and three-phase regions of the second isotherm. Of course the residual liquor from **C**, which still contains high amounts of the target enantiomer, will be recycled. This validation is summarized in Scheme 9.1.
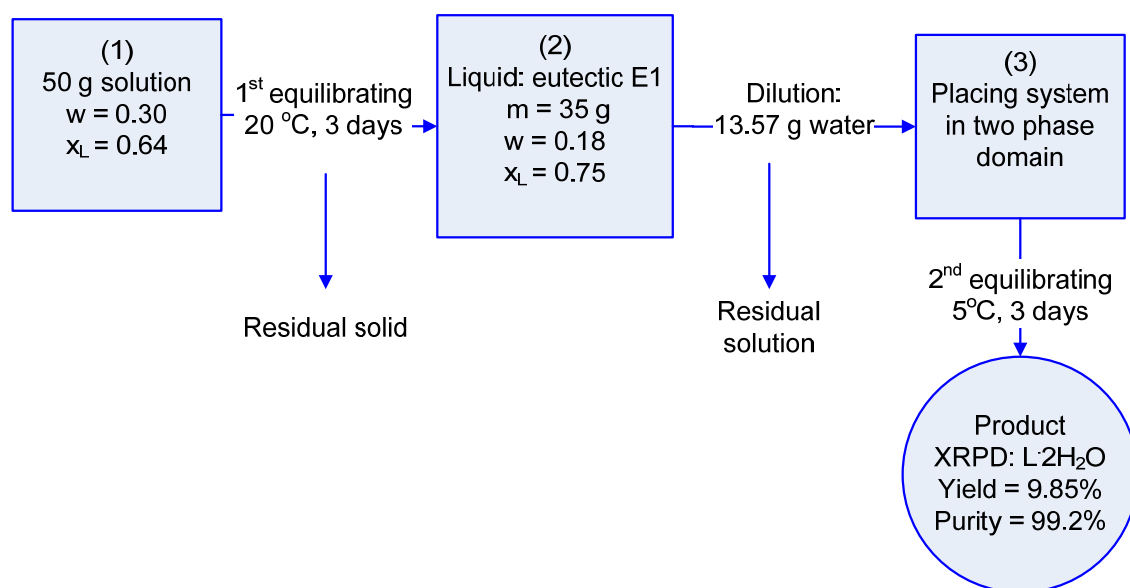
Scheme 9.1: *Experimental validation of the "two-step" process via a eutectic shift relating to different hydrates.*

For validation, the initial solution was used as a slightly enantiomerically enriched solution (x_L^{ini} = 0.64) with a concentration of w = 0.30. Starting with 50 g of this solution, an equilibrium resulted in 35 g of the eutectic solution **Eu₁**. After dilution with a calculated amount of the solvent, the second equilibrium obtained 1.13 g pure of L·2H₂O. The yield of this process is calculated from amount of recovered L-

enantiomer comparing to the total amount of L-enantiomer in the initial solution. This value is about 9.8% close to the theoretical value of 11.3%. An optimization will improve the process yield up to 43.6% when the enantiomeric composition of the initial solution is already upgraded up to $x_L^{ini} = x_L^{Eu1} = 0.75$ of the target enantiomer from suitable routines *e.g.* fermentation, chromatography, etc. The efficiency of the "two-step" process will be compared to that of preferential crystallization as follows.

9.4.2 Application of preferential crystallization techniques

Preferential crystallization will be applied in this part. The objective of this study is quantifying effects of degrees of supersaturation, initial compositions, additives, etc. on preferential crystallization. Both methods SIPC and AS3PC are examined. The experiments will be followed by offline and online analytical methods.

9.4.2.1 Offline monitoring preferential crystallization

Even though the isotherm of the TPD at 5 °C seems to be not favorable for kinetic crystallization as discussed in part 9.2.3.1, attempts to apply preferential crystallization is realized for this case. The validation will use the TPD at 5 °C corresponding to equilibrium between L·2H₂O and DL·2H₂O.

An SIPC was performed in a small double-wall jacket crystallizer of 150 mL, a stirring speed was used at 350 rpm and temperature was controlled with a thermostat (Lauda, Germany). The trajectory of the crystallization process was followed by offline HPLC and density measurements. Two experiments with the same conditions were undertaken. At first, a known-composition saturated solution at 30 °C was prepared and retained at 35 °C in 60 min before adjusting the final temperature to dissolve even the smallest particles. This solution then was cooled down to 5 °C, kept about 60 min under well-stirring condition. Afterwards a defined amount of homochiral seed L-arg, which was mechanically crushed to fine powder, was added into the crystallizer. Several samples were sampled to analyze concentration and composition of mother liquor at different time intervals. The variation of total concentration and enantiomeric composition during crystallization process was observed and the secondary nucleation of counter species *i.e.* DL·2H₂O was captured as seen in Figure 9.23. The particle size distribution of process was monitored with the FBRM probe as Figure 9.24. The second experiment was repeated at the same conditions to the previous run but without sampling steps. This experiment had been stopped before the nucleation of the racemate species. Solid and liquid fractions were quickly separated and simultaneously analyzed. Enantiomeric purity of the final product was examined using HPLC and XRPD. To reduce adsorption of the counter species in the final product, the obtained solid was washed by the mother liquor two times. HPLC was applied to evaluate the deviation between the latter and the first run. From the second experiment, the important results *e.g.* process productivity, yield, purity and the mass losses were calculated. Details are presented as follows.
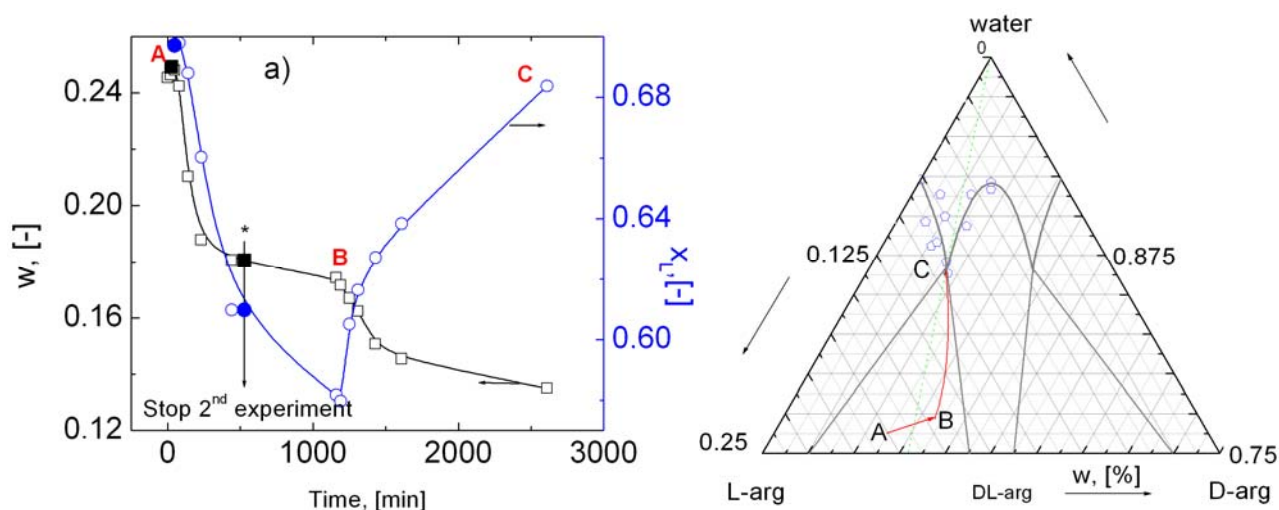
Figure 9.23: *(a) Variation of mother liquid during SIPC of L·2H₂O. (b) Trajectory in the TPD follows A→B→C. Trajectory AB corresponds to crystallization of L·2H₂O. Nucleation of DL·2H₂O occurs at B.*

Indeed, Figure 9.23 presents the variation of total mass concentration and enantiomeric composition as functions of time during the resolution a slightly enantiomerically enriched arginine solution via a SIPC. After selective seeding with L-arg crystals, the appropriate phase should preferentially crystallize for a certain period. The supersaturation degree is gradually consumed for secondary nucleation and crystal growth of the desired enantiomer after a small amount of seed (Table 9.5) is added at point **A**. The trajectory of process is followed **A→B→C**. Period **AB** corresponds to the crystallization of desired product L·2H₂O. Thus, under particular conditions and in a suitable time interval it is possible to preferentially produce crystals of just the desired enantiomer. Within this period, total concentration of solution is reducing (from w = 0.24 to 0.17). Simultaneously, the enantiomeric compositions are decreasing due to the quantitative variation of the enantiomer and the racemate (from x_L from 0.70 to 0.58). Actually, the designed enantiomer transfers from the supersaturated solution to the crystalline solid phase while undesired racemate is still remained in the mother solution. This variation is significant at the beginning. Then, it is getting slowly when system is close to point **B** (see the slopes of curves). The reason is the decreasing of supersaturated degree, *i.e.* driving force of the crystallization process.

An opposite observation of x_L variation is found in period **B** to **C**. At point **B**, the secondary nucleation of racemate starts. Thus, the D-enantiomer in solution is strongly consumed as DL·2H₂O in solid phase which leads to increasing of x_L. During **BC** period, total concentration is still reducing via mass transferring from liquid to solid phase. Finally, the final equilibrium is reached after 2 days (point **C**). The final solution of point **C** equalizes to the eutectic composition at 5 ᵒC (Table 9.5). The solid at point **C** is analyzed with XRPD which shows a mixture of L·2H₂O and DL·2H₂O.

The second experiment was stopped at a pre-defined time from the first experiment at 500 min in order to avoid nucleation of the counter species. Phase separation was

quickly done with a centrifuge filtration. As a sequence, separated solid and liquid phases were simultaneously analyzed. HPLC analysis shows a good repetition of the crystallization process comparing to the previous run. Mains results are listed in Table 9.5. The experimental yield of 32.45% is close to the calculated value of 40.96%, *i.e.* close to the case of optimized solid-liquid separation. The product purity is 98.25% of L-enantiomer since the purity of seed is 99% and mother liquor could adherent onto the product. The productivity of the process is calculated at a value of 164.5 g·Kg^{-1}·day^{-1}. The mass loss is about 20%.

Table 9.5: *The product analysis from the second run SIPC.*

Initial conditions			Product analysis		
Temp. profile	[°C]	$30 \rightarrow 5$	$m_{product}$	[g]	8.64
$m_{ini\_solution}$	[g]	150	$m_{calculated}$	[g]	10.91
w_0	[-]	0.24	Yield	[%]	32.45
x_L^0	[-]	0.70	Productivity	[g·Kg^{-1}·day^{-1}]	164.5
m_{seed}	[mg]	18	Purity	[%]	98.25

The in-situ chord length distribution of the crystals over the whole crystallization processes were recorded by the FBRM probe. Figure 9.24 shows the results of chord length particle size distribution profile of the first experiment above as functions of time.
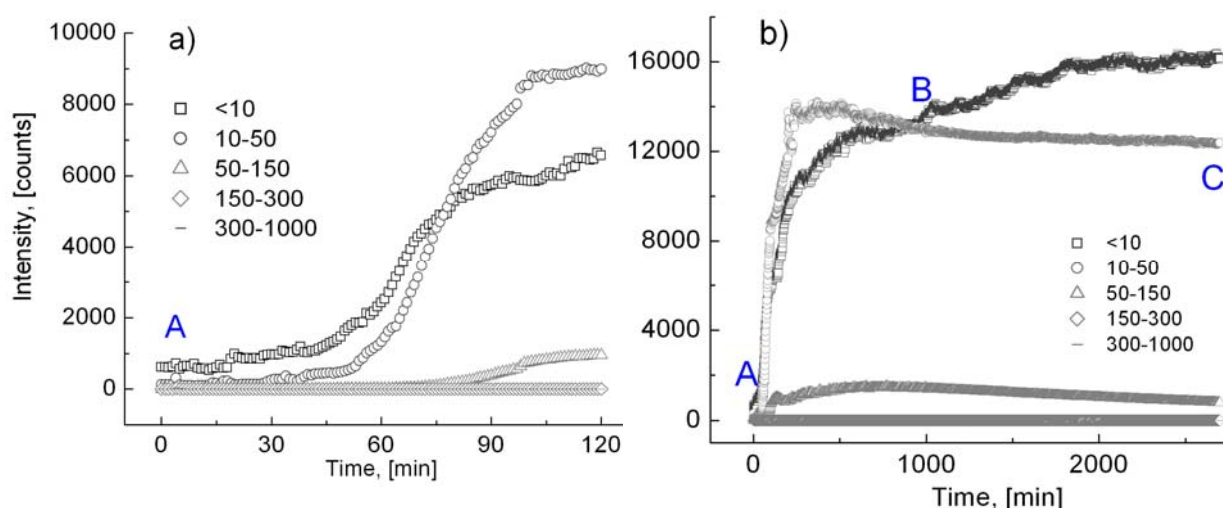
Figure 9.24: *Chord length particle size distribution (μm) using FBRM. (a) Zoom of nucleation period of L·2H$_2$O; (b) Whole crystallization process, vigorously increasing of fine counts related to nucleation.*

Secondary nucleation starts at point **A** after adding of homochiral seed L-arg into the crystallizer. In first 80 min, a number of fine particles increase vigorously (Figure 9.24(a)). The smallest fraction (<10 µm) predominantly presents in solution relating to the secondary nucleation of L·2H$_2$O. From 80 min, the bigger fraction (10–50 µm) is recorded more abundance, even fraction of 50–150 µm is progressive increasing. The observation could be explained by the dissolving of smaller particles and growing of bigger ones. At point **B** (Figure 9.24(b)), the smallest fraction (<10 µm) is again increasing corresponding to the nucleation of the counter racemate DL·2H$_2$O. The crystallization process finally reaches thermodynamic equilibrium (point **C**) after ~2 days.

In short, SIPC was successfully applied to resolve L·2H$_2$O of arginine from aqueous solution even in the worst case at 5 ^{o}C. The other isotherms would give better results because the shape of their metastable solubility lines highly supports to preferential crystallization. This simple experiment, therefore, proved the feasibility of enantiomeric separation of arginine via preferential crystallization.

9.4.2.2 Online observation of preferential crystallization

Experiments were followed by a setup as depicted in part 6.5. An amount of 500 g arginine/water solution was prepared with total concentration and enantiomeric composition at w = 0.29 and x$_L$ = 0.75, respectively. First, two experimental SIPC runs were repeated to see repeatability (SIPC 01 and 02). Obviously, almost the same trajectories of these 2 crystallization runs were observed in Figure 9.25(a). The roughness and discontinuity on these curves relates to drawback of experimental setup. In fact, arginine shows strong agglomeration and, therefore, it is very easy to block the filter (as seen in the experimental set-up part 6.5). That cumulates air bubbles in the measurement cells which lead to such discontinuity. Nevertheless, quick change the locked filter will help to follow continuously the progressive process.

Comparing runs (2) and (3) in Table 9.6, run (2) was cooled to 20 ^{o}C while run (3) was operated at lower temperature at 15 ^{o}C. Obviously, higher degree of supersaturation results in a better driving force for the crystallization process. Trajectory of the process (3) goes deeper than that of run (2) as seen in Figure 9.25(b). That means the secondary nucleation of L-arg occurs faster while nucleation of the counter species racemate can be delayed. The run (4) was applied the same conditions with run (3) but 3 times of seed L-arg was used. However, that makes the nucleation of racemate being faster. Finally, run (5) was performed with seed of the racemate. Interestingly, that did not make nucleation of L-enantiomer during first 500 min.
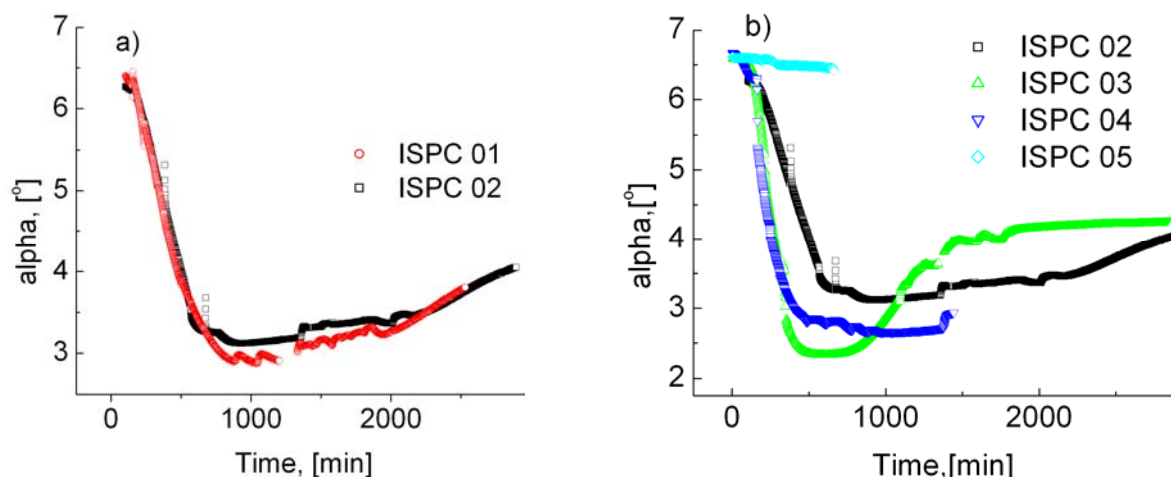
Figure 9.25: *Online monitoring SIPC with 5 experiments validated for various resolution conditions. Herein, variation of optical rotation alpha vs. time is presented; online density measurements do not shown here to avoid intricateness. Runs (1) and (2) validate repeatability of experiments under the same initial conditions. Runs (2)–(4) compare different operating conditions.*

The yield was calculated based on the obtainable amount the enantiomer over the total amount of it in the initial solution. The obtainable amount of the target enantiomer here was correlated at the moment before nucleation of the racemate as seen in Figure 9.25. From online measurements, density and optical rotation alpha values were used to calculate the total concentration and composition of the current solution inside the crystallizer. Those values show the remained amount of the target enantiomer in the current solution. In other words, the crystallized amount of the target enantiomer can be quantified. The process efficiency corresponding to different operating conditions are summarized in Table 9.6.

Table 9.6: *Summary of online monitoring SIPC for chiral arginine solutions.*

Run	Process parameters	m_{Seed}, [mg]	Yield, [%]
(1)	35 – 20 ᵒC	~200 mg L-arg	-
(2)	35 – 20 ᵒC	~200 mg L-arg	3.18
(3)	35 – 15 ᵒC	~200 mg L-arg	11.62
(4)	35 – 15 ᵒC	~600 mg L-arg	6.02
(5)	35 – 20 ᵒC	~200 mg DL-arg	-

9.5 Conclusions

This chapter has proven that arginine is a hydrate forming system. The recrystallized enantiomer from aqueous solution has been found as the dihydrate while the racemate can exist as di- or monohydrate forms depending on temperatures and solvent compositions. The suitable conditions to obtain the correct forms of arginine species as well as their stabilities have been studied. Additionally, all experimental evidence of both solid phase analysis and SLE determination gained a good agreement that arginine is a compound-forming system. Thus, besides lactide and 3-chloromandelic acid, arginine is the third case studied to complete the methodology for enantioseparation of the most abundant chiral group *i.e.* compound-forming system. As stated in the beginning of the thesis, this development aims to apply for a wide range of compound-forming system considering effects of polymorphism and solvate formation.

Ethanol acts as an anti-solvent for arginine aqueous solutions. Adding ethanol not only reduces solubilities of the enantiomer and the racemate but also change the solubility ratio of those species. Thus, the effects of the anti-solvent on the eutectic compositions in the TPDs of arginine are special interest. The TPDs exhibit different eutectic compositions *e.g.* between low and high temperatures in water, between with presence and without anti-solvent ethanol. In each of the solvent mixtures, the eutectic compositions are strongly affected by solvent compositions but temperature-independent. The selected TPDs of arginine in pure water and a specific solvent mixture were constructed in details.

Based on the SLE of arginine solutions, the 'two-step" selective crystallization technique has been applied to purify single enantiomer(s) from a partially enantiomerically enriched solution. This application exploited the specification of the eutectic shift between low and high temperatures of arginine species in pure water. Actually, this operation exchanges solid equilibrating phases between dihydrate and monohydrate of the racemate. The yield was obtained about 10%. This value can be improved by an optimized operation such as adjusting composition of the initial solutions to the fist eutectic composition which can increase the process yield up to 43.6%. Besides, exploiting eutectic shifts in cases of solvent mixtures can also be a potential application since the eutectic shifts with presence of ethanol are significant. This chapter is a successful example of which the thermodynamic "two-step" process crystallization is applied for a new feature of the eutectic shift based on different hydrates.

The MSZWs of arginine species support the development of preferential crystallization. Indeed, the MSZW of the racemate is larger than that of the enantiomer which will able to sufficiently remain the racemate in the mother liquor during crystallization of the enantiomer. Additives were also investigated to enlarge the MSZWs of arginine species. L-methionine enlarges the MSZW of the racemate more than that of the enantiomer. Those additives selectively adsorb on the preferred crystal-faces to develop crystals at certain faces.

Based on thermodynamic and kinetic data, preferential crystallization techniques have been also performed to check feasibility of enantioseparation for partially enantiomerically enriched solutions. Various operating parameters were controlled to improve performances of separation processes. Experiments were carried out with different amounts of seed, degrees of supersaturation, etc. Preferential crystallization is very suitable for enantioseparation of arginine/water system due to the advantages of the shapes of isotherm curves (preferential crystallization even worked well for the worst case of TPD at 5 °C in water). Besides, the additives show selective effects on nucleation of arginine species. The efficiency of additives for enantioseparation of arginine aqueous solution via preferential crystallization is very promising which can be considered as future work.

CHAPTER 10: CONCLUSIONS AND OUTLOOK

10.1 Conclusions

Enantioseparation is an indispensable requirement for many applications, in particular in the pharmaceutical industry. Direct crystallization is considered as the most powerful technique among the available enantioselective separation methods due to high efficiency, realization without auxiliary agents and relatively low costs. However, a number of commercial single enantiomers produced via direct crystallization pathways are still limited up to now. Therefore, rapidly developing new powerful enantioseparation methods is an urgent demand which is also the motivation of the thesis in hand. The major objective of this thesis encompassed the development of crystallization-based enantioseparation methods applicable for various compound-forming racemates considering effects of polymorphism and solvate formation. These tasks were systematically realized through three model compounds: lactide, 3-chloromandelic acid (3ClMA) and the amino acid arginine as detailed in Chapters 7, 8 and 9, respectively.

In the experimental part, lactide was the first case studied. With the assistance of solid phase analyses, namely XRPD and DSC, lactide was identified as the "standard" compound-forming system. In the crystalline racemate, two enantiomers of lactide coexist in the same unit cell and form a new stoichiometric compound. Lactide does not involve any special behavior such as polymorphism or solvate formation. This conclusion gains a good confirmation from solubility determination based on the shape of the relevant ternary phase diagrams (TPD). The solid-liquid equilibria (SLE) of lactide in several solvents and solvent mixtures were successfully investigated. The enantiomeric eutectic compositions were especially considered. In solutions, the variations of the heterochiral or/and homochiral interactions of the enantiomer-enantiomer as well as the enantiomer-solvent interactions lead to the eutectic shifts; Nevertheless, the eutectic shifts between solution and melt states were found to be more significant than cases of the above solutions. From those specifications, a "two-step" process was designed and validated exploiting the eutectic shift between the binary melting point phase diagram (BPD) and the TPD. Indeed, this operation mode allows purification single enantiomer(s) of lactide from slightly enantiomerically enriched solutions. On the other hand, based on the metastable zone width determinations of lactide, preferential crystallization is not suitable for enantiopurification of this system.

In Chapter 8, the complexity of compound-forming systems was raised by the presence of polymorphs of both the enantiomer and the racemate species. The formation and stability of polymorphs of 3ClMA under ambient conditions and in

various media were examined with proper solid-phase analyses, *e.g.* DSC, time-resolved XRPD. Afterwards, a completed BPD of this polymorphic system was constructed which shows four configurations of the eutectic compositions. These eutectic compositions are formed between the stable/metastable forms of the enantiomer/the racemate. Thus, for polymorphic chiral systems, the eutectic shifts can be established between desired polymorphs under suitable conditions. Additionally, with respect to 3ClMA system, the eutectic shifts were also found for solvent effects, *e.g.* cases of water and mixtures of toluene/EA. Variation of temperature in water also leads to the eutectic shifts since the solution structures alter relating to oiling out and association. All the eutectic shifts detected in this chapter are available to exploit the "two-step" selective crystallization process. Enantioseparation was validated for the eutectic shifts due to solvent and polymorphic effects. The yields of the demonstrated processes were relatively low due to the mass loss in intermediate steps and these processes were carried out under not optimized conditions. Furthermore, using preferential crystallization is also a suitable approach for enantioseparation of 3ClMA in aqueous solution. In comparison to the "two-step" process, the yields obtained in preferential crystallization were higher. Finally, a combination of preferential crystallization and selective crystallization was successfully realized for enantioseparation, *e.g.* mandelic acid as a case studied.

Effects of solvate formation on properties of compound-forming systems and the performances of enantioseparation processes were investigated in the Chapter 9 for arginine. Similar to the previous cases, the formation and stability of solvates have been carefully studied with various solid-phase analytical tools. The enantiomer crystallizes from aqueous solution as a dihydrate in the whole temperature range studied, while the racemate can exist as di- or monohydrate depending on temperature and solvent composition of water/ethanol mixtures. The thermodynamics of solid-liquid equilibria were investigated to construct the TPDs for the corresponding hydrate forms. The TPDs of arginine were quite complicated due to various solid phases at equilibria. Similar to the polymorphic system, the complex behavior of the hydrate arginine system gives also an opportunity to apply the "two-step" resolution process since the eutectic compositions change with respect to different hydrates as well as under influence of the anti-solvent ethanol. Validation experiments were successfully carried out. Besides thermodynamic control, Chapter 9 was also examined the applicability of different modes of preferential crystallization. Similar to the 3ClMA case, the results of these two separation techniques (*i.e.* thermodynamic and kinetic control) were compared and the same conclusions were drawn for the amino acid arginine system. Preferential crystallization provided higher process yields than the "two-step" process.

In summary, this thesis contributed several innovative crystallization-based enantioseparation processes for the major chiral group, *i.e.* compound-forming systems. That covers many aspects of compound-forming systems including sophisticated effects of polymorphism and solvate formation. The variants presented in this thesis were originated from two basic approaches, *i.e.* the thermodynamic

control (the "two-step" enantioseparation process) and kinetic control (preferential crystallization). At a certain degree of generalization, a systematic approach to perform enantioseparation starting from a slightly enantiomerically enriched solution of a compound-forming racemate is recommended as Scheme 10.1.
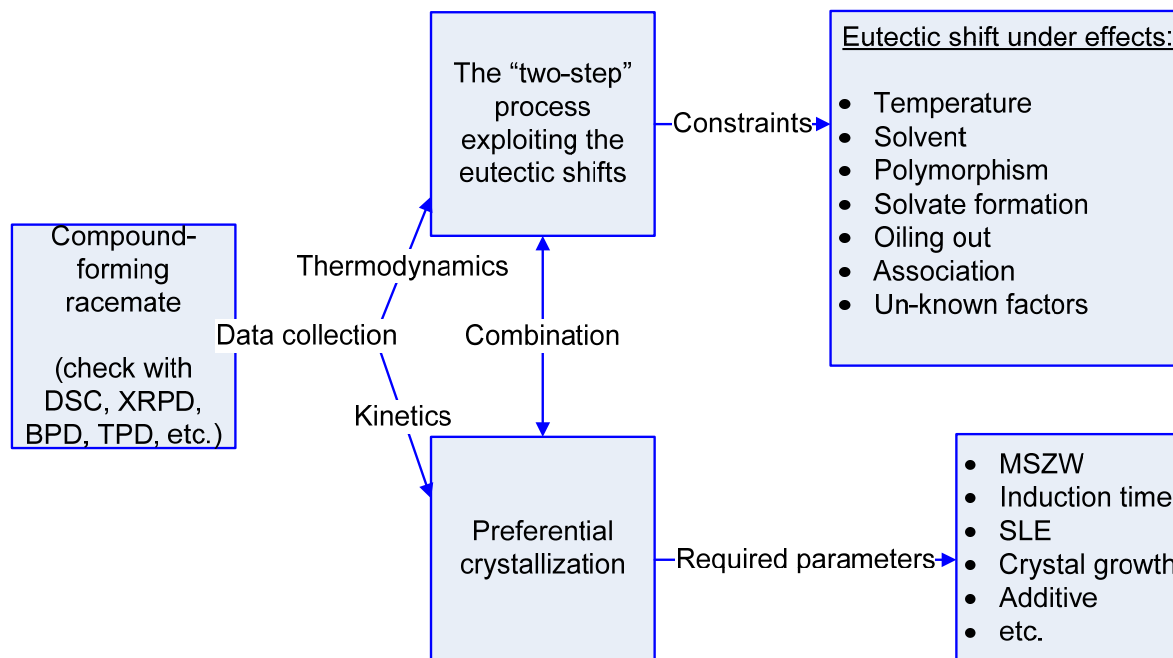
Scheme 10.1: *A general procedure to separate single enantiomers from slightly enantiomerically enriched solutions. To perform the thermodynamically controlled "two-step" processes, the key constraint is the eutectic shift. In contrast, preferential crystallization relies on kinetic parameters.*

10.2 Outlook

Based on shifting the eutectic compositions, various "two-step" processes were experimentally validated on a lab scale. Further applications should be extended to pilot plants or industrial scales. The identification of other conditions triggering eutectic shifts can be attractive future objectives.

The yields of the "two-step" processes were found to be still relatively small. Therefore, optimization is needed to enhance process performances. Cyclic variants of the "two-step" processes can be attractive subjects for future work.

Similar to the thermodynamic approach applied in this thesis, kinetically controlled preferential crystallization is very attractive. It requires optimization with respect to cooling profiles, degrees of supersaturation and seeding strategies. Cyclic operation can be eventually used to produce simultaneously both enantiomers.

Bibliography

1   Hava Caner; Efrat Groner; Liron Levy; Israel Agranat, *Trends in the development of chiral drugs*, DDT, **2004**, 9, (3), 105–110.

2   Neal M. Davies; Xiao Wei Teng, *Importance of Chirality in Drug Therapy and Pharmacy Practice: Implications for Psychiatry*, Advances in Pharmacy, **2003**, 1, (3), 242–252.

3   Tomin, J.; Zivanov-Čurlis; Popovic, D.; Glogovac, S.; Bašić, D., *Differences in local anesthetic effects of optically active isomers of local anesthetic compounds*, Biotechnol. & Biotechnol. Eq., **2006**, 20, (3), 9–14.

4   Bingyun Li; Donald T. Haynie, *chiral drug separation*, Encyclopedia of Chemical Processing, **2006**, 449–458.

5   Bhupinder Singh Sekhon, *Enantioseparation of Chiral Drugs–An Overview*, International Journal of PharmTech Research, **2010**, 2, (2), 1584–1594.

6   Rouhi, A., M., *Chiral Chemistry*, Chem. Eng. News, **2004**, 82, (24), 47–62.

7   Jean Jacques; André Collet; Samuel H. Wilen, *Enantiomers, Racemates and Resolutions*, Krieger Pub. Co., **1994**.

8   Heike Lorenz; Daniel Polenske; Andreas Seidel-Morgenstern, *Application of Preferential Crystallization to Resolve Racemic Compounds in a Hybrid Process*, Chirality, **2006**, 18, 828–840.

9   Czapla, F. H.; Elsner, M. P; Lorenz, H.; Seidel-Morgenstern, A., *Parameterization of population balance models for polythermal-auto seeded preferential crystallization of enantiomers*, Chem. Eng. Sc., **2009**, 64, (4), 753–763.

10   Daniel Polenske; Heike Lorenz; Andreas Seidel-Morgenstern, *Separation of Propranodol Hydrochloride Enantiomers by Preferential Crystallization: Thermodynamic Basis and Experimental Verification*, Crystal Growth & Design, **2007**, 7, (9), 1628–1634.

11   Polenske, D.; Levilain, G.; Lorenz, H.; Coquerel, G.; Seidel-Morgenstern, A., *Isothermal and Auto-Seeded Polythermal Preferential Crystallisation in the Mandelic Acid System*, BIWIC 14th International Workshop on Industrial Crystallisation, **2007**, 245–249.

12   Yinghong Lu; Xiujuan Wang; and Chi Bun Ching, *Application of Preferential Crystallization for Different Types of Racemic Compounds*, Ind. Eng. Chem. Res., **2009**, 48, 7266–7275.

13   Henning Kaemmerer; Heike Lorenz; Andreas Seidel-Morgenstern, *Alternatives Verfahren zur Racemattrennung verbindungsbildender Systeme mittels Kristallisation*, Chemie Ingenieur Technik, **2009**, 81, (12), 1955–1965.

14   Henning Kaemmerer; Matthew J. Jones; Heike Lorenz; Andreas Seidel-Morgenstern, *Selective crystallisation of a chiral compound-forming system – Solvent screening, SLE determination and process design*, Fluid Phase Equilibria, **2010**, 296, 192–205.

15   Tam Le Minh; Heike Lorenz; Andreas Seidel-Morgenstern, *Enantioselective Crystallization Exploiting the Shift of Eutectic Compositions in Solid-Liquid Phase Diagrams*, Chem. Eng. Technol. **2012**, 35, (6), 1003–1008.

16   Ernest Ludwig Eliel; Samuel H. Wilen; Michael P. Doyle, *Basic organic stereochemistry*, Wiley-Interscience, **2001**.

17   Malus, E. L., *Sur une propriété de la lumière réfléchie (On a property of reflected light)*, Mem. Soc. d'Arceuil, **1809**, 2, 143–158.

18   Biot, J. B., Mem. Cl. Meth. Phys. Inst. Imp. Fr, **1812**, 13, 1.

19   Biot, J. B., Bull. Soc. Philmath. Paris, **1815**, 190.

20   Pastuer, L., Ann. Chim. Phys., **1848**. 24, (3), 442.

21   Gernez, D., Compte Rendu de l'académie des sciences Paris, **1866**, 63, 843.

22   Kelvin, L., The second robert boyler lecture in J. oxford univ. Junior Scientis Club, **1894**, 18, 25.

23   Le Bel, J. A., Bull.Soc.Chim, France, **1874**, 22, 337.

24   van't Hoff, J. H., Bull. Soc. Chim. France, **1875**, 23, 295.

25   Cahn, R. S.; Ingold, C.; Prelog, V., Angewandte Chemie International Edition in English, **1966**, 5, 385–415.

26   Mansfield, P.; Henry, D.; Tonkin, A., *Single-enantiomer drugs: elegant science, disappointing effects*, Clin. Pharm., **2004**, 43, (5), 287–290.

27   Teo, SK.; Colburn, WA.; Tracewell, WG.; Kook, KA.; Stirling, DI.; Jaworsky, MS.; Scheffler, MA.; Thomas, SD.; Laskin, OL., *Clinical pharmacokinetics of thalidomide*, Clin Pharmacokinet, **2004**, 43, (5), 311–327.

28   Sakai, Kenichi; Hirayama, Noriaki; Tamura, Rui (Eds.), *In Novel Optical Resolution Technologies*, Topics in Current Chemistry 269, Springer, **2007**.

29   Collins, A. N.; Sheldrake, G. N. and Crosby, J., *Chirality in industry: the commercial manufacture and applications of optically active compounds*, Wiley, Chichester, **1992**.

30   Kozma, D., *CRC Handbook of Optical Resolutions via Diastereomeric Salt Formation*, CRC Press, Hoboken, **2001**.

31   Arnaud Grandeury; Samuel Petit; Géraldine Gouhier; Valérie Agasse; Gérard Coquerel, *Enantioseparation of 1-(p-bromopheny) ethanol by crystallization host –*

guest complexes with permethylated β-cyclodextrin: crystal structures and mechanisms of chiral recognition, Tetrahedron: Asymmetry, **2003**, 14, 2143–2152.

32   Harata, K., *Stuctural aspects of stereodifferentiation in the solid-state*, Chemical Reviews, **1998**, 98, (5), 1803–1828.

33   Lia Addadi; Ziva Berkovitch-Yellin; Isabelle Weissbuch; Jan van Mil; Linda J. W. Shimon; Meir Lahav; Leslie Leiserowitz, *Growth and Dissolution of Organic Crystals with "Tailor-Made" Inhibitors-Implications in Stereochemistry and Materials Science*, Angewandte Chemie International Edition in English, **1985**, 24, (6), 466–485.

34   David Maillard; Guntram Koller; Ewgenij Wakaresko; Sabine Gottburg-Reininger, *Process of isolation enantiomer component from enantiomer mixtures by particle-size-controlled crystallization*, patent number 20110184169, **2011**.

35   Dominik Koszelewski; Barbara Grischek; Silvia M. Glueck, Wolfgang Kroutil; Kurt Faber, *Enzymatic Racemization of Amines Catalyzed by Enantiocomplementary ω-Transaminases*, Chem. Euro. J., **2011**, 17, 378–383.

36   Ludwik Synoradzki; Halina Hajmowicz; Jerzy Wisialski; Arkadiusz; Tomasz Rowicki, *Calcium Pantothenate. Part 3. Process for the Biologically Active Enantiomer of the Same via Selective Crystallization and Racemization*, Organic Process Research & Development, **2008**, 12, 1238–1244.

37   Viedma, C., *Experimental evidence of chiral symmetry breaking in crystallization from primary nucleation*, Journal of Crystal Growth, **2004**, 261, 118–121.

38   Wim L. Noorduin; Hugo Meekes; Arno A. C. Bode; Willem J. P. van Enckevort; Bernard Kaptein; Richard M. Kellogg; Elias Vlieg, *Explanation for the Emergence of a Single Chiral Solid State during Attrition-Enhanced Ostwald Ripening: Survival of the Fittest*, Crystal Growth & Design, **2008**, 8, (5), 1675–1681.

39   Hiroki Taniguchi; Jianding Yu; Yasutomo Arai; Toshirou Yagi; Desheng Fu; Mitsuru Itoh, *In Situ Raman Scattering Study on Successive Crystallization of Bulk BaTi2O5 Glass*, Ferroelectrics, **2007**, 346, (1), 156–161.

40   Ravi Bhushan; Juergen Martens, *Amino Acids. Chromatographic Separation and Enantioresolution*, HNB Publishing, **2010**.

41   Schmidt-Traub, H.; Michael Schulte; Andreas Seidel-Morgenstern, *Preparative Chromatography*, Wiley-VCH, **2012**.

42   Gedicke, K.; Kaspereit, M.; Beckmann, W.; Budde, U.; Lorenz, H.; Seidel-Morgenstern, A., *Conceptual Design and Feasibility Study of Combining Continuous Chromatography and Crystallization for Stereoisomer Separations*, Chemical Engineering Research and Design, **2007**, 85, (7), 928–936.

43   Malte Kaspereit; Pavel Jandera; Michal Škavrada; Andreas Seidel-Morgenstern, *Impact of absorption isotherm parameters on the performance of enantioseparation using simulated moving bed chromatography*, Journal of Chromatography A, **2002**, 944, 249–262.

44   Heike Lorenz; Patrick Sheehan; Andreas Seidel-Morgenstern, *Coupling of simulated moving bed chromatography and fractional crystallisation for efficient enantioseparation*, Journal of Chromatography A, **2001**, 908, (1–2), 201–214.

45   Arvind Rajendranb; Galatea Paredesa; Marco Mazzotti, *Simulated moving bed chromatography for the separation of enantiomers*, Journal of Chromatography A, **2009**, 1216, 709–738.

46   John M. Keith; Jay F. Larrow; Eric N. Jacobsen, *Practical Considerations in Kinetic Resolution Reactions*, Adv. Synth. Catal., **2001**, 343, 5–26.

47   Andrea-Nekane R. Alba; Ramon Rios, *Kinetic Resolution: A Powerful Tool for the Synthesis of Planar-Chiral Ferrocenes, Molecules*, **2009**, 14, 4747–4757.

48   Kerstin Wuerges; Katerina Petrusˇevska-Seebach; Martin P. Elsner; Stephan Luetz, *Enzyme-Assisted Physicochemical Enantioseparation Processes Part III Overcoming Yield Limitations by Dynamic Kinetic Resolution of Asparagine Via Preferential Crystallization and Enzymatic Racemization*, Biotechnology and Bioengineering, **2009**, 104, (6), 1235–1239.

49   Petrusevska-Seebach, K., Würges, K., Seidel-Morgenstern, A., Lütz, S., Elsner, M.P., *Enzyme-assisted physicochemical enantioseparation processes - Part II: Solid-liquid equilibria, preferential crystallization, chromatography and racemization reaction*, Chemical Engineering Science, **2009**, 64, (10), 2473–2482.

50   Yoshihide Tanaka; Shigeru Terabe, *Enantiomer separation of acidic racemates by capillary electrophoresis using cationic and amphoteric β-cyclodextrins as chiral selectors*, Journal of Chromatography A, **1997**, 781, 151–160.

51   Ossicini, O.; Fanali, S., *Enantiomeric separation by electrophoretic techniques, Chromatographia*, **1997**, 45, (1), 428–432.

52   Wenzhe Lu; Richard B. Cole, *Determination of chiral pharmaceutical compounds, terbutaline, ketamine and propranolol, by on-line capillary electrophoresis – electrospray ionization mass spectrometry*, Journal of Chromatography B, **1998**, 714, 69–75.

53   Kewen Tang; Yuanyuan Chen; Kelong Huang; Jiajia Liu, *Enantioselective resolution of chiral aromatic acids by biphasic recognition chiral extraction*, Asymmetry, **2007**, 18, 2399–2408.

54   Tang, Kewen; Song, Litao; Pan, Yang; Jiang, Xinyu; Miao, Jiabing, *Enantioselective Partitioning of Racemic Ibuprofen in a Biphasic Recognition Chiral Extraction System*, Chin. J. Chem., **2010**, 28, 119–124.

55   Kewen Tang; Jianmin Yi; Kelong Huang; Guoli Zhang, *Biphasic Recognition Chiral Extraction: A Novel Method for Separation of Mandelic Acid Enantiomers*, Chirality, **2009**, 21, 390–395.

56   Boelo Schuur; Bastiaan J. V. Verkuijl; Adriaan J. Minnaard; Johannes G. de Vries; Hero J. Heeres, Ben L. Feringa, *Chiral separation by enantioselective liquid–liquid extraction*, Org. Biomol. Chem., **2011**, 9, 36–51.

57   Feipeng Jiao; Xiaoqing Chen; Xinyu Jiang, *Enantioselective Extraction of Ofloxacin Enantiomers Using Ester Alcohol L-Tartarate as Chiral Selector*, Iran. J. Chem. Chem. Eng., **2009**, 28, (1), 7–11.

58   Pravin G. Ingole; Kripal Singh; Hari C. Bajaj, *Preparation of Enantioselective Thin Film Composite Polymer Membrane for Optical Resolution of α-Amino Acids*, J Trends Chem, **2010**, 1, (1), 1–7.

59   Rui Xie; Liang-Yin Chu; Jin-Gen Deng, *Membranes and membrane processes for chiral resolution*, Chem. Soc. Rev., **2008**, 37, 1243–1263.

60   Bryajak, M.; Kozlowski, J.; Wiezorek, P.; Kafarski, P., *Enantioselective transport of amino-acid though supported chiral liquid membrane*, Journal of Membrane Science, **1993**, 85, (3) 221–228.

61   Eric Francotte; Wolfgang Lindner (Ed.), *Chirality in Drug Research*, WILEY-VCH Verlag GmbH & Co. KGaA, Weinheim, **2006**.

62   Katalin Nemák; Mária Ács; D. Kozma; E. Fogassy, *Racemic compound formation –conglomerate formation – Part 4. Optical resolution and dertermination of the melting phase of 2',6'-pipecoloxylidide and four 1-alkyl-2',6'- pipecoloxylidide*, Journal of Thermal Analysis, **1997**, 48, 691–696.

63   Harry G. Brittain, *Polymorphism in Pharmaceutical Solids*, Drug and The Pharmaceutical Science, 95, **1999**.

64   Madhu Pudipeddi; Abu T.M. Serajuddin, *Trends in Solubility of Polymorphs*, Journal of Pharmaceutical Sciences, **2005**, 94, (5), 929–939.

65   McCauley, J. A. ; Varsolona, R. J.; Levorse, D. A., *The effect of polymorphism and metastability on the characterization and isolation of two pharmaceutical compounds*, J. Phys, D: Appl. Phys., **1993**, 26, 85–89.

66   Joel Bernstein, *Polymorphism in molecular crystals*, Oxford Science Publications, **2002**.

67   Jan-Olav Henck; Maria Kuhnert-Brandstatter, *Demonstration of the Terms Enantiotropy and Monotropy in Polymorphism Research Exemplified by Flurbiprofen*, Journal of Pharmaceutical Sciences, **1999**, 88, (1), 103–108.

68   Mullin, J. W., *Crystallization (4th Edition)*, Reed Educational and Professional Publishing Ltd, **2001**.

69   Marthi, K.; Ács, M.; Pokol, G.; Tomor, K.; Eröss-Kiss, K., *DSC studies on the polymorphism and pseudopolymorphism of pharmaceutical substances*, Journal of Thermal Analysis, **1992**, 38, 1017–1025.

70   Hiroshi Takiyama; Hirobumi Suzuki; Hirohisa Uchida; Masakuni Matsuoka, *Determination of solid–liquid phase equilibria by using measured DSC curves*, Fluid Phase Equilibria, **2002**, 194–197, 1107–1117.

71   Giron, D.; Piechon, P.; Goldbronn, C.; Pfeffer, S., *Thermal analysis, microcalorimentry and combined techniques for the study of the polymorphic behaviour of a purine derivative*, Journal of the Thermal Analysis and Calorimetry, **1999**, 57, 61–73.

72   Daniel Kalnin; Pierre Lesieur; Franck Artzner; Gerard Keller; Michel Ollivon, *Systematic investigation of lard polymorphism using combined DSC and time-resolved synchrotron X-ray diffraction*, Eur. J. Lipid Sci. Technol., **2005**, 107, 594–606.

73   Yang L.; Zhou Y.; Zhu M.; Zhao L.; Wei L.; Bian Y.; *Stereochemistry and Solid-State Structure of an Intrinsically Chiral Meso-Patterned Porphyrin: Case Study by NMR and Single-Crystal X-ray Diffraction Analysis*. J Org Chem., **2013**, 78, (19), 9949–9955.

74   Milja Karjalainen; Sari Airaksinen; Jukka Rantanen; Jaakko Aaltonen; Jouko Yliruusi, *Characterization of polymorphic solic-state changes using variable temperature X-ray powder diffraction*, Journal of Pharmaceutical and Biomedical Analysis, **2005**, 39, 27–32.

75   Russell Fulwood, *Chiral analysis by NMR spectroscopy*, Durham theses, Durham University, **1992**.

76   Khankari, R. K.; Grant, D. J. W., *Pharmaceutical hydrates*, Thermochimica Acta, **1995**, 248, 61–79.

77   Sherry L. Morissettea; Oern Almarssona; Matthew L. Petersona; Julius F. Remenara; Michael J. Reada; Anthony V. Lemmoa; Steve Ellisa; Michael J. Cimab; Colin R. Gardner, *High-throughput crystallization: polymorphs, salts, co-crystals and solvates of pharmaceutical solids*, Advanced Drug Delivery Reviews, **2004**, 56, 275–300.

78   Lahav, M.; Leiserowitz, L., *The effect of solvent on crystal growth and morphology*, Chem. Eng. Sci., **2001**, 56, 2245–2253.

79   Antonio Llinàs; Jonathan C. Burley; Timothy J. Prior; Robert C. Glen; Jonathan M. Goodman, *Concomitant Hydrate Polymorphism in the Precipitation of Sparfloxacin from Aqueous Solution*, Crystal Growth & Design, **2008**, 8, (1), 114–118.

80   Simon N. Black; Murray W. Cuthbert; Ron J. Roberts; Birgitta Stensland, *Increased Chemical Purity Using a Hydrate*, Crystal Growth & Design, **2004**, 4, (3), 539–544.

81   Byrn. S. R.; Pfeiffer, R. R.; Stowell, J.G., *Solid-State Chemistry of Drugs*, SSCI, West Lafayette, IN, **1999**.

82   Prausnitz, J. M.; Lichtenthaler; R. N.; de Azevedo, E. G., *Molecular Thermodynamics of Fluid-Phase Equilibria third Edition*, PTR Prentice-Hall inc., New Jersey, **1999**.

83   Gibbs, J.W., Scientific Papers , Dover, New York, **1961**.

84   Peter Atkins; Julio de Paula Atkins, *Physical Chemistry (8th Ed.)*, W.H. Freeman, **2006**.

85   Jurgen Cmehling; Barbel Kolbe; Michael Kleiber; Jurgen Rarey, *Chemical Thermodynamics for Process Simulation*, Wiley-VCH, **2012**.

86   Morowitz, H. J., *A Mechanism for the Amplification of Fluctuations in Racemic Mixtures*, J. Theoret. Biol,**1969**, 25, 491–494.

87   Prigogine, I.; Defay, R., *Chemical Thermodynamics*, Longmans, Green and Co LTD, **1954**.

88   Stanley I. Sandler, *Chemical and Engineering Thermodynamics* - 3rd Edition, Jon Wiley & Sons, **1999**.

89   Chau-Chyun, C.; Paul, M. M., *Applied thermodynamics for process modeling*, AIChE J., **2002**, 48, (2), 194–200.

90   Steven L. Jackson, *Extension of Wohl's ternary asymmetric solution model to four and n components.* American Mineralogist, **1989**, 74, 14–17.

91   Linda L. Elkins; Timothy L. Grove, *Ternary feldspar experiments and thermodynamic models*, American Mineralogist, **1990**, 75, 544–559.

92   Sara K. Ghosh; Sawaran J. Chopra, *Activity Coefficients from the Wilson Equation*, Ind. Eng. Chem., Process Des. Dev., **1975**, 14, (3), 304–308.

93   Alvarez Juliá, J.; Barrero, C. E.; Corso, M. E.; Grande, M. C.; Marschoff, C. M, *On The Applicability of the Uniquac Method to Ternary liquid-liquid Equilibria*, The Journal of the Argentine Chemical Society, **2004**, 92, (4 /6), 81–90.

94   João A. P. Coutinho; Fernando L. P. Pessoa, *A modified extended UNIQUAC model for proteins*, Fluid Phase Equilibria, **2004**, 222–223, 127–133.

95   Brelvl, S. W., *Simple Correlations for UNIQUAC Structure Parameters*, Ind. Eng. Chem. Process Des. Dev., **1982**, 21, (3), 376–370.

96   Henri Renon; Prausnitz, D. J. M., *Estimation of Parameters for the NRTL Equation for excess Gibbs Energies of strongly nonideal liquid mixtures*, I&Ec Process Design and Development, **1969**, 8, (3), 413–419.

97   Jurgen G. Gmehling; Thomas F. Anderson; John M. Prausnltz, *Solid-Liquid Equilibria Using UNIFAC*, Ind. Eng. Chem. Fundam., **1978**, 17, (4), 269–273.

98   Isamu Nagata; Jisuo Koyabu, *Phase equilibria by effective UNIFAC group-contribution method*, Thermochimica Acta, **1981**, 48, 187–211.

99   Bent L. Larsen; Peter Rasmussen; Aage Fredenslund, *A Modified UNIFAC Group-Contribution Model for Prediction of Phase Equilibria and Heats of Mixing*, Ind. Eng. Chem. Res., **1987**, 26, 2274–2286.

100   Andreas Klamt, *Conductor-like Screening Model for Real Solvent: A New Approach to the Quantiative Calculation of Solvation Phenomena*, J. Phys. Chem., **1995**, 99, 2224–2235.

101   Andreas Klamt; Frank Eckert; Wolfgang Arlt, *COSMO-RS: An Alternative to Simulation for Calculating Thermodynamic Properties of Liquid Mixtures*, Annu. Rev. Chem. Biomol. Eng., **2010**, 1, 101–122.

102   Shu Wang; Shiang-Tai Lin; Suphat Watanasiri; Chau-Chyun Chena, *Use of GAMESS/COSMO program in support of COSMO-SAC model applications in phase equilibrium prediction calculations*, Fluid Phase Equilibria, **2009**, 276, 37–45.

103   I. Kikic; P. Aless; P. Rasmussen; A. Fredenslund, *On the Combinatorial Part of the UNIFAC and UNIQUAC Models*, The Canadian Journal of Chemical Engineering, **1980**, 58, 253–258.

104   Jan Cassens; Feelly Ruether; Kai Leonhard; Gabriele Sadowski, *Solubility calculation of pharmaceutical compounds – A priori parameter estimation using quantum-chemistry*, Fluid Phase Equilibria, **2010**, 299, 161–170.

105   Joachim Gross; Gabriele Sadowski, *Perturbed-Chain SAFT: An Equation of State Based on a Perturbation Theory for Chain Molecules*, Ind. Eng. Chem. Res., **2001**, 40, 1244–1260.

106   D.J.W. Grant; M. Mehdizadeh; AH-L. Chow; J.E. Fairbrother, *Non-linear van't Hoff solubility-temperature and their pharmaceutical interpretation*, International Journal of Pharmaceutics, **1984**, 18, 25–38.

107   Alexander Apelblat; Emanuel Manzurola, *Solubilities of o-acetylsalicylic, 4-aminosalicylic, 3,5-dinitrosalicylic, and p-toluic acid, and magnesium-DL-aspartate in water from T=(278 to 348)K*, J. Chem. Thermodynamics, **1999**, 31, 85–91.

108   Alexander Apelblat; Emanuel Manzurola, *Solubilities of L-aspartic, DL-aspartic, DL-glutamic, p-hydroxybenzoic, o-anistic, p-anisic, and itaconic acids in water from T=278K to T=345K*, J. Chem. Thermodynamics, **1997**, 29, 1527–1533.

109   Alexander Apelblat, *Solubilities of manganese, cadmium, mercury and lead acetates in water from T=278.15 K to T=340.15 K*, J. Chem. Thermodynamics, **2001**, 33, 147–153.

110   Fu-an Wang; Liu-cheng Wang; Jian-chi Song; Lei Wang; Hai-song Chen, *Solubilities of Bis(2,2,6,6-tetramethyl-4-piperidinyl) Maleate in Hexane, Heptane, Octane, m-Xylene, and Tetrahydrofuran from (253.15 to 310.15) K*, J. Chem. Eng. Data, **2004**, 49, 1539–1541.

111   Muyu Zhao; Lizhu Song; Xiaobao Fan, *The boundary theory of phase diagrams and its application*, Springer, **2009**.

112   Alan A. Smith, *Calculation of the efficiency of purification by crystallization of ideal multicomponent stereoisomeric mixtures*, Tetrahedron: Asymmetry, **1998**, 9, 2925–2937.

113   Klussmann, M.; Andrew J. P. White; Alan Armstrong; Donna G. Blackmond, *Rationalization and Prediction of Solution Enantiomeric Excess in Ternary Phase Systems*, Angew. Chem. Int. Ed., **2006**, 45, 7985–7989.

114   van't Hoff. J.H., Arch. Neerl. Sci. Exact. Natur., **1886**, 20, 239–302.

115   Michael E. Aulton, *Aulton's pharmaceutics the design and manufacture of medicines (third Edition)*, Churchill Livingstone, **2007**.

116   Nývlt, J.; Söhnel, O.; Matachová, M.; Broul, M., *The kinetics of industrial crystallization*, Elsevier, **1985**.

117   D. Kashchiev, D.; van Rosmalen, G. M., *Review: Nucleation in solutions revisited*, Cryst. Res. Technol., **2003**, 38, (7–8), 555–574.

118   Leubner, Ingo H., *Precision crystallization; theory and practice of controlling crystal size*, CRC / Taylor & Francis, **2010**.

119   Kanagadurain, R.; Durairajan, R.; Sankar, R.; Sivanesan, G. ; Elangovan, S. P.; Jayavel, R., *Determination of Metastable Zone Width, Induction Period and Interfacial Energy of a Ferroelectric Crystal - Potassium Ferrocyanide Trihydrate (KFCT)*, E-Journal of Chemistry, **2010**, 7(1), 137–142.

120   Tadashi Shiraiwa; Hideya Miyazaki; Takahiro Watanabe; Hidemoto Kurokawa, *Optical resolution by preferential crystallization of DL-methionine hydrochloride*, Chirality, 1997, 9, (1), 48–51.

121   Courvoisier, L.; Gervais, C.; Mignot, L.; Petit, M. N.; Voquerel, G., *Effect of the polymorphic form of the seeds on the preferential crystallization*, J. Phus. IV France, 2011, 11, 71–77.

122   Tadashi Shiraiwa, Mitsuhiro Nakamura, Masanobu Nobeoka, Hidemoto Kurokawa, *Racemic structure and optical resolution by preferential crystallization*, Bull. Chem. Soc. Jpn, **1987**, 60, 1465–1468.

123   Dae R. Yang; Kwang S. Lee; Ju S. Lee; Sung G. Kim; Do H. Kim; Yoo K. Bang, *Modelingof metastable zone width behavior with dynamic equation*, Ind. Eng. Chem. Res., **2007**, 6 , 8158–8165.

124   Muchová, M..; Lednický, F., *Investigation of heterogeneous nucleation using the induction time of crystallization: 1. Theory of induction time*, Polymer, **1996**, 37, (14), 3031–3036.

125   Jaroslav Nývlt, *Kinetics of Nucleation in Solutions*, Journal of Crystal Growth, **1968**, 3, (4), 377–383.

126   Jaroslav Nývlt; Rudolf Rychlý; Jaroslav Gottfried; Jiřina Wurzelová, *Metastable Zone-Width of Some Aqueous Solutions*, Journal of Crystal Growth, **1970**, 6, 151–162.

127   Keshra Sangwal, *Additives and Crystallization Processes*, John Wiley & Sons Ltd, **2007**.

128   Raluca Isopescu; Carmencita Mateescu; Mihaela Mihai; Gabriel Dabija, *The effects of organic additives on induction time and characteristics of precipitated calcium carbonate*, Chemical Engineering Research and Design, **2010**, 88, (11), 1450–1454

129   Li Li; David Lechuga-Ballesteros; Beth A. Szkudlarek; Naír Rodríguez-Hornedo, *The Effect of Additives on Glycine Crystal Growth Kinetics*, Journal of Colloid and Interface Science, **1994**, 168, 8–14.

130   Cashell, C.; Corcoran, D.; Hodnett, B. K., *Effect of the amino acid additives on the crystallization of L-Glutamic acid*, Crystal Growth & Design, **2005**, 5, (2), 593–597.

131   Gerard F. Arkenbout, *Melt crystallization technology*, Technomic Publishing CO. INC. **1995**.

132   Pella, E.; Restelli, R., *Binary Phase Diagram of the Enantiomers of Indoprofen*, Mikrochimica Acta, **1983**, I, 65–74.

133   Heike Lorenz; Dragomir Sapoundjiev; Andreas Seidel-Morgenstern, *Enantiomeric Mandelic Acid SystemMelting Point Phase Diagram and Solubility in Water*, Journal of Chemical & Engineering DATA, **2002**, 47, 1280–1284.

134   M. Luísa P. Leitão; M. Ermelinda Eusébio; Teresa M. R. Maria; J. S. Redinha, *(Solid + liquid) phase diagram for trans-1,2-cyclohexanediol enantiomer mixtures*, J. Chem. Thermodynamics, **2002**, 34, 557–568.

135   Daniel Polenske; Heike Lorenz; Andreas Seidel-Morgenstern, *The Binary Phase Diagram of Propranolol Hydrochloride and Crystallization-Based Enantioseparation*, Journal of Pharmaceutical Sciences, **2009**, 1–11.

136   Xin Wang; Xiu Juan Wang; Chi Bun Ching, *Solubility, Metastable Zone With, and Racemic Characterization of Propanolol Hydrochloride*, Chirality, **2002**, 14, 318–324.

137   Heike Lorenz; Andreas Seidel-Morgenstern, *A contribution to the mandelic acid phase diagram*, Thermochimica Acta, **2004**, 415, 55–61.

138   Heike Lorenz; Andreas Seidel-Morgenstern, *Binary and ternary phase diagrams of two enantiomers in solvent systems*, Thermochimica Acta, **2002**, 382, 129–142.

139   Alex M. Chen; Yaling Wang; Robert M. Wenslow, *Purification of Partially Resolved Enantiomeric Mixtures with the Guidance of Ternary Phase Diagram*, Organic Process Research & Development, **2008**, 12, 271–281.

140   Kaemmerer, H., *New concepts for enantioselective crystallization*, Shaker Verlag, **2012**.

141   Donald Garlotta, *A Literature Review of Poly (Lactic Acid)*, Journal of Polymers and the Environment, **2002**, 9, (2), 63–84.

142   Yodthong Baimark; Robert Molloy, *Synthesis and Characterization of Poly(L-lactide-co-ε-caprolactone) Copolymers: Effects of Stannous Octoate Initiator and Diethylene Glycol Coinitiator Concentrations*, ScienceAsia, **2004**, 30, 327–334.

143   Paul Curnow; David Kisailus; Daniel E. Morse, *Biocatalytic Synthesis of Poly(l-Lactide) by Native and Recombinant Forms of the Silicatein Enzymes*, Angew. Chem. Int. Ed., **2006**, 45, 613–616.

144   Ling Fang; Rongrong Qi; Linbo Liu; Gongwen Juan; Suangwu Huang, *Synthesis of Poly(L-lactide) via SolvothermalMethod*, International Journal of Polymer Science, **2009**, 1–7.

145   Lei Hua; Weihua Kai; JinJun Yang; Yoshio Inoue, *A new poly(L-lactide)-grafted graphite oxide composite: Facile synthesis, electrical properties and crystallization behaviors*, Polymer Degradation and Stability, **2010**, 95, 2619–2627.

146   Amnat Jarerat; Yutaka Tokiwa; Hideo Tanaka, *Microbial Poly(L-lactide)-Degrading Enzyme Induced by Amino Acids, Peptides, and Poly(L-amino Acids)*, Journal of Polymers and the Environment, **2004,** 12, (3), 139–146.

147   Adam Kowalski; Jan Libiszowski; Andrzej Duda; Stanislaw Penczek, *Polymerization of L,L-Dilactide Initiated by Tin(II) Butoxide*, Macromolecules, **2000**, 33, 1964–1971.

148   Jennifer L. Robert; Katherine B. Aubrecht, *Ring-Opening Polymerization of Lactide To Form a Biodegradable Polymer*, J. Chem. Educ., **2008**, 85, (2), 258.

149   Matthieu Jalabert; Carole Fraschini; Robert E. Prud'homme, Synthesis and Characterization of Poly(L-lactide)s and Poly(D-lactide)s of Controlled Molecular Weight, *Journal of Polymer Science: Part A: Polymer Chemistry*, **2006**, 1944–1955.

150   A. Schindler; D. Harper, *Poly (Lactic Acid). I. Stereosequence Distribution in the Polymerization of Racemic Dilactide*, Polymer Letters Edition, **1976**, 14, 729–734.

151   Larry E. Erickson; Eric Fayet; Bala Krishna Kakumanu; Lawrence C. Davis, *Lactic Acid Fermentation*, A Comprehensive Review, Carcass, *2004*.

152   Sanford S. Jenkins, *The Preparation and some Properties of the Chloromandelic Acids, their Methyl Esters and Amides*, J. Am. Chem. Soc., **1931**, 53, (6), 2341–2343.

153 Robert F. Campbell; Kevin Fitzpatrick; Tord Inghardt; Olle Karlsson; Kristina Nilsson; John E. Reilly; Larry Yet, *Enzymatic resolution of substituted mandelic acids*, Tetrahedron Letters, **2003**, 44, 5477–5481.

154 von Langermann, J.; Le Minh, T.; Lorenz, H.; Seidel-Morgenstern, *A. Kombination von Biokatalyse und Kristallisation zur Darstellung enantiomerenreiner Mandelsäurederivate*. Chemie Ingenieur Technik, 2010, 82. (1–2). 93–100.

155 Yan Zhang; Ajay Ray; Sohrab Rohani, *Measurement and prediction of phase diagrams of the enantiomeric 3-chloromandelic acid system*, Chemical Engineering Science, **2009**, 64, 192–197.

156 Tapati Mallik; Tanusree Kar; Gabriele Bocelli; Amos Musatti, *Structural and thermal characterization of L-arginine dihydrate - a nonlinear optical material*, Cryst. Res. Technol., **2006**, 41, (3), 280–284.

157 Mallik, T.; Kar, T., *Growth and characterization of nonlinear optical L-arginine dihydrate single crystals*, J. Cryst. Growth, **2005**, 285, 178–182.

158 Kalaiselvi, D.; Kurmar, R. M.; Jayavel, R., *Single crystal growth and properties of semiorganic nonlinear optical L-arginine hydrochloride monohydrate crystals*, Cryst. Res. Technol. **2008**, 43, (8), 851–856.

159 Zvonimir B. Maksić; Borislav Kovačević, *Neutral vs. zwitterionic form of arginine—an ab initio study*, J. Chem. Soc., Perkin Trans., **1999**, 2, 2623–2629.

160 Tanusri Pal; Tanusree Kar; Gabriele Bocelli; Lara Rigi, Synthesis, *Growth, and Characterization of L-Arginine Acetate Crystal: A Potential NLO Material*, Crystal Growth & Design, 3, (1), **2003**, 13–16.

161 Caitriona Cashell; David Corcoran; Kieran Hodnett, B., *Effect of Amino Acid Additives on the Crystallization of L-Glutamic Acid*, Crystal Growth & Design, **2005**, 5, (2), 504–597.

162 Mehdi Nematbakhsh; Shaghayegh Haghjooyjavanmard; Farzaneh Mahmoodi; Ali Reza Monajemi, T*he effect of L-arginine on serum lipids and nitrite levels, and the number of apoptotic cells, iNOS and eNOS expressions of aorta after the formation of fatty streaks in rabbit*, J. Appl. Biomed., **2008**, 6, 203–210.

163 S. Asadzadeh Vostakolaei, *Effect of L-Arginine on Neuromuscular Transmission of the Chick Biventer Cervicis Muscle*, World Academy of Science, Engineering and Technology, **2009**, 57, 429–432.

164 Eduardo Navarro1; Simeona J. Alonso1; Felipe A. Martin; Miguel A. Castellano, *Toxicological and Pharmacological Effects of D-Arginine*, Basic & Clinical Pharmacology & Toxicology, **2005**, 97, 149–154.

165 Klussmann, M.; Iwamura, H.; Mathew S. P.; Wells Jr, D. H.; Pandya, U.; Armstrong, A.; Blackmond, D. G., *Thermodynamic control of asymmetric amplification in amino acid catalysis*, Nature, **2006**, 441, 621–623.

168

166   Sidney M.; Morris, Jr., *Regulation of enzymes of urea and arginine synthesis*, Annu. Rev. Nutr., **1992**, 12, 81–101.

167   Wu, G.; Meininger, C. J., *Regulation of L-arginine synthesis from L-citrulline by L-glutamine in endothelial cells*, Am J Physiol., **1993,** 265, 1965–1971.

168   Pichat, L.; Guermont, J. P.; Phung Nhu Liem, *Synthèse de la DL- Arginine*, Journal of Labelled Compounds, **1968**, 4, (3), 251–255.

169   Jane Li, Z.; Mark T. Zell; Eric J. Munson; David J. W. Grant, *Characterization of Racemic Species of Chiral Drugs Using Thermal Analysis, Thermodynamic Calculation, and Structural Studies,* Journal of Pharmaceutical Sciences, **1999**, 88, (3), 337–346.

170   E.L. Charsley; P.G. Laye; V. Palakollu; J.J. Rooney; B. Joseph, *DSC studies on organic melting point temperature standards*, Thermochimica Acta, **2006**, 446, 29–32.

171   Etsuo Yonemochi; Yasuo Yoshihashi; Katsuhide Terada, *Quantitative Relationship Between Solubility, Initial Dissolution Rate and Heat of Solution of Chiral Drugs*, Pharmaceutical Research, **2000**, 17, (1), 90–93.

172   K. Khimeche; A. Dahmani, *Determination by DSC of Solid–Liquid Diagrams for Polyaromatic – 4,4'Diaminodiphenylmethane Binary Systems*, Journal of Thermal Analysis and Calorimetry, **2006**, 8,(1), 47–52.

173   David, W. I. F.; Shankland, K., *Structure determination from powder diffraction data*, Acta Cryst A, **2008**, 64, 52–64.

174   E. Kougoulos; A.G. Jones; K.H. Jennings; M.W: Wood-Kaczmar, *Use of focused beam reflectance measurement (FBRM) and process video imaging (PVI) in a modified mixed suspension mixed product removal (MSMPR) cooling crystallizer*, Journal of Crystal Growth, **2005**, 273, 529–534.

175   Norbert Kail; Wolfgang Marquardt; Heiko Briesen, *Estimation of particle size distributions from focused beam reflectance measurements based on an optical model*, Chemical Engineering Science, **2009**, 64, 984–1000.

176   Norbert Kail; Wolfgang Marquardt; Heiko Briesen, *Process Analysis by Means of Focused Beam Reflectance Measurements*, Ind. Eng. Chem. Res., **2009**, 48, 2936–2946.

177   Law, D.J.; Bale, A.J.; Jone, v, *Adaptation of focused beam reflectance measurement to in-situ particle sizing in estuaries and coastal waters*, Marine Geology, **1997**, 140, 47–59.

178   http://www.crystallizationsystems.com.

179   Sistla A; Wu Y; Khamphavong P; Liu J., *Medium-throughput hydrate screening using the Crystal 16™*, Pharm Dev Technol., **2011**, 16, (2), 102–109.

180   Jaroslav Nývlt, *Solid-liquid phase equilibria*, Praha, **1977**.

181   Barrett; B. Glennon, *Characterizing the metastable zone width and solubility curve using lasentec FBRM and PVM*, Trans IChemE Part A, **2002**, 80, 799–805.

182   Niall A. Mitchell; Patrick J. Frawley; Clifford T. Ó'Ciardhá, *Nucleation kinetics of paracetamol–ethanol solutions from induction time experiments using Lasentec FBRM®*, Journal of Crystal Growth, **2011**, 321, (1), 91–99.

183   Angela Alvarez Rodrigo; Heike Lorenz; Andreas Seidel-Morgenstern, *Online Monitoring of Preferential Crystallization of Enantiomers*, Chirality, **2004**, 16, 499–508.

184   Gilat, G.; Schulman, L. S., *Chiral interaction, magnitude of the effects and application to natural selection of L-enantiomer*, Chemical Physics Letters, **1985**, 121, (1, 2), 13–16.

185   Gilat, G., *Chiral interaction and thermodynamics*, Chemical Physics Letters, **1987**, 137, (5), 492–494.

186   Kaemmerer, H; Tulashie, S. K.; Lorenz, H.; Seidel-Morgenstern, A., *Solid – liquid phase equilibrium of N-Methylenphedrine enantiomers in two chiral solvents*, J. Chem. Eng. Data, **2010**, 55, 1131–1136.

187   Tulashie, S. K.; Kaemmerer, H; Lorenz, H.; Seidel-Morgenstern, A., *Solid – liquid phase equilibrium of mandelic acid enantiomers in two chiral solvents: Experimental determination and model correlaiton*, J. Chem. Eng. Data, **2010**, 55, 333–340.

188   Henri Renon; Prausnitz, J. M., *Estimation of Parameters for the NRTL Equation for Excess Gibbs Energies of Strongly Nonideal Liquid Mixtures*, Ind. Eng. Chem. Process Des. Dev., **1969**, 8, (3), 413–419.

189   Worlitscheka, J.; Boscoa, M.; Hubera, M.; Gramlichb, V.; Mazzotti, M., Solid-Liquid Equilibrium of Troeger's Base Enantiomers in Ethanol: Experiments and Modelling, Helvetica Chimica Acta, **2004**, 87, 279–291.

190   Kaemmerer, H.; Haida, H.; Lorenz, H.; Seidel-Morgenstern, A., Estimation of riliable parameters for SLE describtion of chiral systems, BIWIC 16th International workshop on Industrial Crystallization, **2006**, 1–8.

191   Lindenbeg, C.; Kraettli, M.; Cornel, J.; Matzzotti, M., *Design and optimization of a combineed cooling/antisolvent crystallization process*, Crystal Growth & Design, **2009**, 9, (2), 1124–1136.

192   O'Grady, D.; Marrett, M.; Casey, E.; Glennon, B., *The effect of mixing on metastable zone width and nucleation kinetics in the anti-solvent crystallization of benzoic acid*, Trans IchemE, Part A, Chemical Engineering Research and Design, **2007**, 85, (A7), 945–952.

193   Min-Woo Park; Sang-Do Yeo, *Antisolvent crystallization of carbamazepine from organic solutions*, Chemical Engineering Research and Design, **2012**, 90, (12), 2202–2208.

194 Nagy, Z.K.; Fujiwara, M.; Braatz, R.D., *Modelling and control of combined cooling and antisolvent crystallization processes*, Journal of Process Control, **2008**, 18, (9), 856–864.

195 Venkata S. Sistla; Jan von Langermann; Heike Lorenz; Andreas Seidel-Morgenstern, *Application of Classical Resolution for Separation of DL-Serine*, Chem. Eng. Technol. **2010**, 33, (5), 780–786.

196 Kaemmerer, Henning; Lorenz, Heike; Black, Simon N.; Seidel-Morgenstern, Andreas, *Study of System Thermodynamics and the Feasibility of Chiral Resolution of the Polymorphic System of Malic Acid Enantiomers and Its Partial Solid Solutions.* Crystal Growth and Design, **2009**, 9, (4), 1851–1862.

197 Le Minh, T.; von Langermann, J.; Lorenz, H.; Seidel-Morgenstern, A., *Enantiomeric 3-Chloromandelic Acid System: Binary Melting Point Phase Diagram, Ternary Solubility Phase Diagrams and Polymorphism.*, Journal of Pharmaceutical Sciences, **2010**, 99, (9), 4084–4095.

198 Ostwald, W., Z. Phys. Chem. (Leipzig), **1887**, 22, 289.

199 Imogen Foubert; Eveline Friedrick; Jeroen Vereecken; Maarten Sichien; Koen Dewettinck, *Stop-and-return DSC method to study fat crystallization*, Thermochimica Acta, **2008**, 471, 7–13.

200 Paris, S.; Gaffet, E.; Vrel, D.; Thiaudiere, D.; Gailhanou, M; Bernard, F., *Time-Resolved XRD Experiments for a Fine Description of Mechanisms Induced During Reactive*, Sintering Science of Sintering, **2005**, 37, 27–34.

201 Predel, B; Hoch, M.; Pool, M., *Phase diagram and heterogeneous equilibria: A practical introduction*, Springer, **2004**.

202 W. R. Burghardt, *Phase Diagrams for Binary Polymer Systems Exhibiting both Crystallization and Limited Liquid-Liquid Miscibility*, Macromolecules, **1989**, 22, 2482–2486.

203 Kai Kiesow; Feelly Tumakaka; Gabriele Sadowski, *Experimental investigation and prediction of oiling out during crystallization process*, Journal of Crystal Growth, **2008**, 310, 4163–4168.

204 Derdour, L., *A method to crystallize substances that oil out*, Chemical Engineering Research and Design, **2010**, 88, (9), 1174–1181.

205 Jie Lu; Yi-Ping Li; Jing Wang; Zhen Li; Sohrab Rohani; Chi-Bun Ching, *Study on the Oiling-out and Crystallization for the Purification of Idebenone*, Org. Process Res. Dev., **2012**, 16, (3), 442–446.

206 Perkampus, H.-H., *Raman/Infrared Atlas of Organic Compounds*, Nachrichten aus Chemie, Technik und Laboratorium, **1990**, 28, (2), 252–254

207 Singurel, GH., *Study of the hydrogen bond in the mandelic and 4-chloromandelic acids*, Revue Roumaine de Chimie, **1980**, 25, (11–12), 1469–1475.

208   Chocholousova, J.; Vacek, J.; Hobza, P., *Acetic acid dimmer in the gas phase, nonpolar solvent, microhydrated environment, and dilute and concentrated acetic acid: Ab Initio quantum chemical and molecular dynamic simulations*, J. Phys. Chem. A, **2003**, 107, 3086–3092.

209   Yanqing Tian; Xiaohe Xu; Yingying Zhao; Xinyi Tang; Tiejin Li; Jiazhong Sun; Chongwu Li; Ang Pan, *Temperature-dependent FTIR study on self-assembly chiral liquid crystals through intermolecular hydrogen bonding*, Thin Solid Films, **1996**, 284–285, 603–605.

210   Daniel Polenske; Heike Lorenz; Andreas Seidel-Morgenstern, *Potential of Different Techniques of Preferential Crystallization for Enantioseparation of Racemic Compound Forming Systems*, Chirality, **2009**, 21, 728–737.

211   Wilstroem, H.; Kakidas, C.; Taylor, L. S., *Determination of hydrate transition temperature using transformation kinetics obtained by Raman spectroscopy*, Jounal of Pharmaceutical and Biomedical Analysis, **2009**, 49, 247–252.

212   Pirttimaeki, J.; Lain, E., *The transformation of anhydrate and hydrate form of caffeine at 100% RH and 0% RH*, European Journal of Pharmaceutical Sciences, **1994**, 1, 203–208.

213   Luk, C. J.; Rousseau, R. W., *Solubilities of and transformation between the anhydrous and hydrated forms of L-serine in water-methanol solution*, Crystal Growth & Design, **2006**, 6, (8), 1808–1812.

214   Yilmaz, H, *Excess properties of alcohol – water systems at 298.15 K*, Turk J Phys, **2002**, 26, 243–246.

215   Peijun Ji; Jinxin Zoua; Wei Fenga, *Effect of alcohol on the solubility of amino acid in water*, Journal of Molecular Catalysis B: Enzymatic, **2009**, 56, 185–188.

216   Sapoundjiev, D.; Lorenz, H.; Seidel-Morgenstern, A. Thermochimica Acta. **2005**, 436, 1–9.

217   Somnath S. Kadam; Herman J. M. Kramer; Joop H. ter Horst, *Combination of a Single Primary Nucleation Event and Secondary Nucleation in Crystallization Processes*, Cryst. Growth Des., **2011**, 11, (4), 1271–1277.

218   Shanfeng Jiang; Joop H. ter Horst, *Crystal Nucleation Rates from Probability Distributions of Induction Times*, Cryst. Growth Des., **2011**, 11, (1), 256–261.

219   Kadam**, S. S.;** Kramer, H. J. M.; ter Horst, J. H., *The Combination of a Single Primary Nucleation Event and Secondary Nucleation in Crystallization Processes*, Cryst. Growth Des., **2011**, 11, (4), 1271–1277.

220   Le Minh, T.; Lorenz, H.; Seidel-Morgenstern, A., *Enantiomeric Purification of a Racemic Compound-Forming System Based on Different Hydrates*, ISIC 18th International Symposium on Industrial Crystallization, **2011**, 127–128.

Appendix

A. Quantitative description of Solid-Liquid equilibria

The well-known classical equation describing the solid-liquid equilibrium of a component i:

$$\ln\left(\frac{x_i \gamma_i}{x_i^s \gamma_i^s}\right) = -\ln\frac{f_i^0}{f_i^{0s}} = \frac{-\varDelta h_{m,i}}{RT}\left(\frac{T_{m,i} - T}{T_{m,i}}\right) + \frac{\varDelta c_{p,i}}{R}\left(\frac{T_{m,i} - T}{T}\right) - \frac{\varDelta c_{p,i}}{R}\ln\left(\frac{T_{m,i}}{T}\right) \tag{A1}$$

Assuming complete immiscibility in an ideal solid phase, Eq. (A1) can be simplified and rearranged to yield the following equation:

$$\ln(x_i \gamma_i) = \left(-\Delta h_{m,i} + \varDelta c_{p,i} T_{m,i}\right)\frac{1}{RT} + \frac{\varDelta c_{p,i}}{R}\ln T + \frac{1}{R}\left(\frac{\varDelta h_{m,i}}{T_{m,i}} - \varDelta c_{p,i} - \varDelta c_{p,i}\ln T_{m,i}\right) \tag{A2}$$

Summarizing the different terms with respect to the temperature, provide:

$$\ln\left(x_i \gamma_i\right) = a_i^{ideal}\frac{1}{T} + b_i^{ideal}\ln T + c_i^{ideal} \tag{A3}$$

with: $a_i^{ideal} = \frac{1}{R}\left(-\Delta h_{m,i} + \varDelta c_{p,i} T_{m,i}\right)$; $b_i^{ideal} = \frac{\varDelta c_{p,i}}{R}$; $c_i^{ideal} = \frac{1}{R}\left(\frac{\varDelta h_{m,i}}{RT_{m,i}} - \varDelta c_{p,i} - \varDelta c_{p,i}\ln T_{m,i}\right)$ (A4)

Eq. (A3) can be further rearranged:

$$\ln x_i = a_i^{ideal}\frac{1}{T} + b_i^{ideal}\ln T + c_i^{ideal} - \ln\gamma_i \tag{A5}$$

Thus, four parameters ($a_i^{ideal}, b_i^{ideal}, c_i^{ideal}, \gamma_i$) are needed to determine the equilibrium fraction x_i at a specific temperature T. Obviously, in general γ_i is a complex function of temperature and composition, *i.e.* $\gamma_i(x_i, T)$. However, in a limited concentration range, $\gamma_i(x_i, T)$ can be considered as a weak function of x_i and assumed to be expressed as a function of temperature only. Thus, Eq. (A5) is rewritten:

$$\ln x_i = a_i^{ideal}\frac{1}{T} + b_i^{ideal}\ln T + c_i^{ideal} - \ln\gamma_i(T) \tag{A6}$$

To express empirically the dependence $\gamma_i(T)$, it is suggested to use the following flexible function adapted to the structure provided by Eq. (A6):

$$\ln\gamma_i(T) = a_i^{\gamma}\frac{1}{T} + b_i^{\gamma}\ln T + c_i^{\gamma} \tag{A7}$$

Substituting Eq. (A7) into Eq. (A6) leads to

$$\ln x_i \left(T \right) = a_i \frac{1}{T} + b_i \ln T + c_i \qquad (A8)$$

with: $a_i = a_i^{ideal} - a_i^{\gamma}$, $b_i = b_i^{ideal} - b_i^{\gamma}$, $c_i = c_i^{ideal} - c_i^{\gamma}$

To evaluate the obtained parameters and the model, a second set of solubility measurements was carried out. The root-mean-square deviation (*RMSD*) and deviation (*Dev.*) defined by Eqs. (A9) and (A10) were used to characterize the model fit:

$$RMSD = \sqrt{\left[\frac{1}{N} \times \sum \left(x_{i,cal} - x_{i,exp} \right)^2 \right]} \qquad (A9)$$

$$Dev = \left| \frac{x_{i,cal} - x_{i,exp}}{x_{i,exp}} \right| \times 100, \% \qquad (A10)$$

B. Yield calculation from BPD
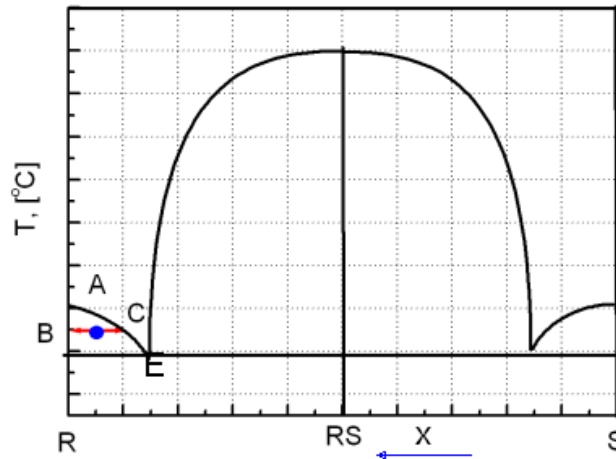
The considered system has composition at A (x_R^A, x_S^A). Based on thermodynamics, system at A will establish an equilibrium between B (x_R^B, x_S^B) and C (x_R^C, x_S^C).

Let consider 1 g mixture of R and S as in initial mixture A. m g pure enantiomer R will be obtained from B at equilibrium. Based on lever rule, m will be calculated as:

$$m\left(x_R^B - x_R^A \right) = \left(1 - m \right)\left(x_R^A - x_R^C \right) \qquad (B1)$$

In the optimal case, the system A is cooled down close to the eutectic line and, therefore, C close to E, obtain:

$$m\left(100 - x_R^A \right) = \left(1 - m \right)\left(x_R^A - x_R^{Eu} \right) \qquad (B2)$$

$$m = \frac{\left(x_R^A - x_R^{Eu} \right)}{\left(100 - x_R^{Eu} \right)} \qquad (B3)$$

The yield, therefore, is calculated as:

$$\eta = \frac{\left(x_R^A - x_R^{Eu}\right)100}{\left(100 - x_R^{Eu}\right)x_R^A},[\%]$$ (B4)

C. Yield calculation under guidance of TPDs

One point on the TPD will be represented by co-ordinates (x, y, z) in percentage. Let consider:

- The eutectic composition Eu: (x_E, y_E, z_E)

- The enantiomer R $(x_R, y_R, z_R) = (100, 0, 0)$

- The racemate RS $(x_{RS}, y_{RS}, z_{RS}) = (50, 50, 0)$

Let consider an initial system (x_0, y_0, z_0), it can be on the left or the right sides of the eutectic point. The enantiomeric excess of this mixture is define: $e.e_0 = \frac{x_0 - y_0}{x_0 + y_0}$,[-]

Starting with 1 g mixture of two enantiomers, amount of m [g] solvent has to be added to this mixture to reach the boundary line of two- and three-phase domains. There are two situations as presented at points Q and P. Amount of added solvent (in [g]) can be calculated from the lever rule. Consequently, comparing recoverable amount of the target enantiomer in the end mixture and total amount of that enantiomer in the initial mixture will obtain the yield of process. Results are presented as follows.
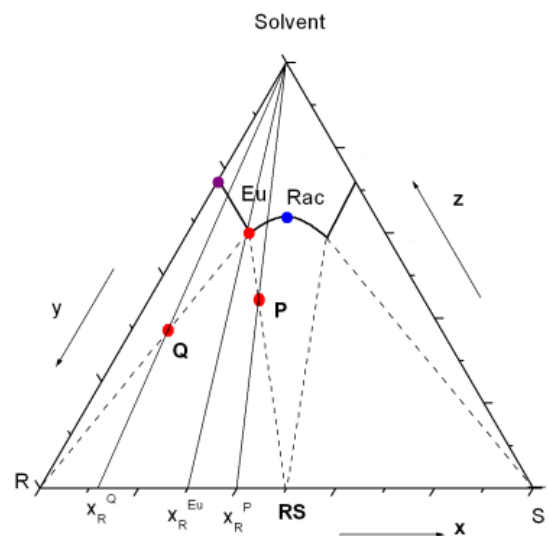
	P	Q
Added-solvent, m, [g]	$m_1 = \dfrac{e.e_0\left(100 - x_E - y_E\right)}{x_E - y_E}$	$m_2 = \dfrac{\left(1 - e.e_0\right)\left[50 - 0.5\left(x_E + y_E\right)\right]}{y_E}$
Yield, η, [%]	$\eta_1 = \dfrac{50\left(1 + e.e_0\right) - x_E\left(1 + m_1\right)}{\left(100 - x_E\right)\left(0.5 + 0.5ee_0\right)} \times 100$	$\eta_2 = \dfrac{\left(1 + m_2\right)\left[\dfrac{\left(0.5 + 0.5e.e_0\right)100}{0.5 + 0.5e.e_0 + m_2} - x_E\right]}{\left(100 - x_E\right)\left(0.5 + 0.5e.e_0\right)} \times 100$

D. Calibrations

a) Lactide system

- HPLC: $w_{enan} = 0.084A + 0.041$; $R^2 = 99.86$

- Refractive index : $w_t = 0.0034x + 0.8914$; $R^2 = 99.45$

b) 3-Chloromandelic acid system

- HPLC: $w_{enan} = 2.10^{-4}A + 0.037$; $R^2 = 99.99$

- Refractive index: $w_t = 0.0018x + 1.3326$; $R^2 = 99.94$

- Polarimeter:

$$w_t = 3.1395 \varrho - 3.1315; R^2 = 99.99$$

$$e.e = -4.9482 \alpha/w_t$$

c) Arginine system

- HPLC: $w_{enan} = 0.68209A - 61.884$; $R^2 = 99.67$

- Density: $w_t = 330.68 \varrho - 328.5$; $R^2 = 99.95$

- Polarimetry: $w_t = 4.2348 \varrho - 4.0132$; $R^2 = 99.99$

$$e.e = 2.3547 \alpha/w_t$$
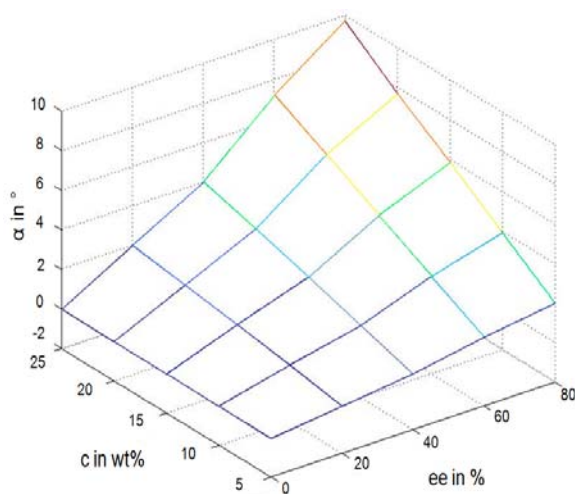
*HPLC: using suitable dilute factor k; ϱ-density; x-refractive index; $w_{t, enan}$- concentrations.

E. Materials

Compound	Company	Purity, [%]
L,L-lactide	ABCR GmbH & CO. KG	> 99%
D,D-lactide	Uhde GmbH	> 99%
D,L-lactide	ABCR GmbH & CO. KG; Uhde GmbH	> 99%
R-3ClMA	Sigma-Aldrich	97%
RS-3ClMA	Alfa Aesar	97
L-arginine	Sigma-Aldrich	> 99%
DL-arginine	Sigma-Aldrich	> 98%
R-2ClMA	AKScientific Inc	98%
R-4ClMA	Beta pharma Scientific Inc	95%
S-MA	Merck Schuchardt OHG	>99%
RS-MA	Merck Schuchardt OHG	>99%
Ethyl L-lactate	Sigma – Aldrich Chemie GmbH	> 99%
L-threonine	Sigma – Aldrich Chemie GmbH	> 98%
Isopropanol	Prolabo	(HPLC);>99.8 %
Toluene	Prolabo	(HPLC);>99.8 %
MTBE	Merck Darmstadt	(HPLC);>99.8%
Methanol	Merck KGa Damstadt	(HPLC);>99%
Ethanol	Merck KGa Damstadt	(HPLC);>99%
Ethylacetate	Merck KGa Damstadt	(HPLC);>99%
Acetone	Prolabo	(HPLC);>99%

F. Analytical equipments

1. Refractometer: Mettler Toledo RE40.

2. Density meter: Mettler Toledo DE40.

3. HPLC: Agilent Technology; DDR Chiral Advanced Laser Polarimeter.

4. Microscope: Axiocam.

5. Polarimeter: Perkin Elmer 341.

6. FBRM: Mettler Toledo 400S

7. DSC 131 Setaram

8. TG–DSC111, Setaram

9. XRPD: X'Pert Pro apparatus, PANanalytical GmbH

10. Themostat: Lauda

11. Crystal16™ Avantium.

G. Validation of the achieved model parameters.

Solid phase	Temp. ,[°C]	$w_{i,exp}$	$w_{i,cal}$	Dev., %
ϕ =0.00				
DL·1H$_2$O	32.60	21.80	21.79	0.004
DL·1H$_2$O	37.65	24.88	25.25	1.470
DL·1H$_2$O	41.77	28.09	28.27	0.656
L·2H$_2$O	24.93	15.21	15.02	1.228
L·2H$_2$O	27.84	16.35	16.58	1.407
L·2H$_2$O	28.79	16.91	17.11	1.192
ϕ =0.30				
DL·1H$_2$O	35.42	14.87	15.20	2.190
DL·1H$_2$O	24.38	9.59	9.57	0.185
L·2H$_2$O	44.23	21.18	21.23	0.210
L·2H$_2$O	26.34	10.27	10.42	1.427
ϕ =0.45				
DL·1H$_2$O	32.50	8.54	8.37	1.926
DL·1H$_2$O	21.11	4.65	4.78	2.850
L·2H$_2$O	48.57	18.70	18.51	1.026
L·2H$_2$O	23.62	6.02	6.23	3.627
L·2H$_2$O	19.99	5.08	5.21	2.730
ϕ =0.65				
DL·1H$_2$O	50.54	7.02	6.92	1.362
DL·1H$_2$O	63.95	13.95	13.69	1.832
L·2H$_2$O	39.52	5.09	4.97	2.310
L·2H$_2$O	60.97	14.90	14.43	3.203
ϕ =0.40 *				
DL·1H$_2$O	34.20	11.18	10.79	3.409
DL·1H$_2$O	44.30	16.41	16.555	0.881
DL·1H$_2$O	47.15	19.05	18.52	2.753
L·2H$_2$O	19.93	6.31	5.94	5.724
L·2H$_2$O	28.64	9.52	8.98	5.654
L·2H$_2$O	34.15	12.31	11.47	6.749

* validation experiments with "extra" solvent compositions

List of Figures

182

List of Tables

List of abbreviations and symbols

API	Active pharmaceutical ingredient
AS3PC	Auto-seeded polythermic preferential crystallization
BPD	Binary phase diagram
ButOH	Butanol
COSMO	Conductor-like Screening Model
COSMO-RS	Conductor-like Screening Model Real Solvents
COSMO-SAC	Conductor-like Screening Model Segment Activity Coefficient
DSC	Differential scanning calorimetry
DD-, LL- lactide	The enantiomers of lactide
DL-lactide	The racemate of lactide
D/L-arg	Enantiomers of arginine
DL-arg	Racemate of arginine
DL.1H_2O	Monohydrate of the racemate of arginine
DL.2H_2O	Dihydrate of the racemate of arginine
EA	Ethyl acetate
EtOH	Ethanol
e.e.	Enantiomeric excess
FBRM	Focused Beam Reflectance Measurement
HPLC	High Performance Liquid Chromatography
iPrOH	Isopropanol
L-met	L-methionine
L-thr	L-threonine
L.2H2O	Dihydrate of the enanatiomer of arginine
MSZW	Metastable zone width
MA	Mandelic acid
MeOH	Methanol
MTBE	Methyl tert-butyl ether
PC-SAFT	Perturbed-Chain Statistical Associating Fluid Theory
PLA	Polylactide

R/S	The enantiomers of 3ClMA
RS	The racemate of 3ClMA
R1 , R2	The stable form and the metastable form of enantiomer 3ClMA
RS1 , RS2	The stable form and the metastable form of racemate 3ClMA
SIPC	Seeded isothermal preferential crystallization
SLE	Solid-liquid equilibrium
S	Degree of Supersaturation
SMB	Simulating moving bed chromatography
TPD	Ternary phase diagram
T, P	Temperature and pressure
UNIFAC	Universal Quasichemical Functional Group Activity Coefficients
UNIQUAC	The universal quasichemical theory
XRD	Single-crystal X-ray diffraction
XRPD	X-ray powder diffraction
2, 3, 4-ClMA	2, 3, 4-chloromandelic acid derivatives
a_i, b_i, c_i	Model parameters
a, b, c	Mass of R, S and solvent
c_p	Heat capacity
F	Degrees of freedom
G	Gibb free energy
ΔG_{crit}	Critical Gibb energy change for nucleus formation
T^f	Melting temperature
r_{crit}	Critical Radius of nucleus
S	Entropy
x	Mole fraction between two enantiomers
w	Total mass concentration
f	Fugacity
i	Number of molecules in a critical nucleus
α	Solubility ratio between racemate/enantiomer

α_{ij}	Non-randomness factor
γ_i	Activity coefficient
η	Process yield
ϕ	Volume fraction EtOH/water
μ	Chemical potential
σ	Interfacial energy
Δg_{ij}	Interaction parameter between i-j
ΔH^{diss}	Enthalpy of dissolution
ΔH^{f}	Enthalpy of diffusion
ΔH^{mix}	Enthalpy of mixing